



# governmentattic.org

*"Rummaging in the government's attic"*

Description of document: Reports on the effects of neutrinos on radioactive decay rates, from Department of Energy (DOE) Contract DEDT0004091 (Techsource), 2016-2019

Requested date: 2019

Release date: 18-October-2019

2<sup>nd</sup> Release date; 21-November-2019

Posted date: 17-February-2020

Source of document: FOIA Request  
Department of Energy  
FOIA Requester Service Center  
1000 Independence Avenue, SW  
Mail Stop MA-46  
Washington, DC 20585  
Fax; (202) 586-0575

The governmentattic.org web site ("the site") is a First Amendment free speech web site, and is noncommercial and free to the public. The site and materials made available on the site, such as this file, are for reference only. The governmentattic.org web site and its principals have made every effort to make this information as complete and as accurate as possible, however, there may be mistakes and omissions, both typographical and in content. The governmentattic.org web site and its principals shall have neither liability nor responsibility to any person or entity with respect to any loss or damage caused, or alleged to have been caused, directly or indirectly, by the information provided on the governmentattic.org web site or in this file. The public records published on the site were obtained from government agencies using proper legal channels. Each document is identified as to the source. Any concerns about the contents of the site should be directed to the agency originating the document in question. GovernmentAttic.org is not responsible for the contents of documents published on the website.



**Department of Energy**  
Washington, DC 20585

OCT 18 2019

Via email

Re: HQ-2019-01408-F

This is a first response to the request for information that you sent to the Department of Energy (DOE) under the Freedom of Information Act (FOIA), 5 U.S.C. § 552. You requested:

Copy of the work product (reports, memos, studies, plans, etc.) received to date from Contract DEDT0004091 awarded to Techsource.

Your request was assigned to the DOE's Office of Management (MA-64) and the Office of Nuclear Energy (NE) to conduct a search of their files for responsive documents. The search started on November 14, 2018, which is the cutoff date for responsive records.

At this time, DOE has identified two (2) documents responsive to your request. The documents are being released to you in their entirety. DOE is continuing to process your request for additional responsive documents, which will be provided to you in subsequent response.

The adequacy of the search, may be appealed within 90 calendar days from your receipt of this letter pursuant to 10 C.F.R. § 1004.8. Appeals should be addressed to Director, Office of Hearings and Appeals, HG-1, L'Enfant Plaza, U.S. Department of Energy, 1000 Independence Avenue, S.W., Washington, D.C. 20585-1615. The written appeal, including the envelope, must clearly indicate that a FOIA appeal is being made. You may also submit your appeal by e-mail to [OHA.filings@hq.doe.gov](mailto:OHA.filings@hq.doe.gov), including the phrase "Freedom of Information Appeal" in the subject line. (This is the method preferred by the Office of Hearings and Appeals.). The appeal must contain all the elements required by 10 C.F.R. § 1004.8, including a copy of the determination letter. Thereafter, judicial review will be available to you in the Federal District Court either (1) in the district where you reside, (2) where you have your principal place of business, (3) where DOE's records are situated, or (4) in the District of Columbia.

You may contact DOE's FOIA Public Liaison, Alexander Morris, FOIA Officer, Office of Public Information, at 202-586-5955 or by mail at MA-46/Forrestal Building 1000 Independence Avenue, S.W. Washington, D.C. 20585 for any further assistance and to discuss any aspect of your request. Additionally, you may contact the Office of Government Information Services (OGIS) at the National Archives and Records Administration to inquire about the FOIA



mediation services they offer. The contact information for OGIS is as follows: Office of Government Information Services, National Archives and Records Administration, 8601 Adelphi Road-OGIS, College Park, Maryland 20740-6001, e-mail at ogis@nara.gov; telephone at 202-741-5770; toll free at 1-877-684-6448; or facsimile at 202-741-5769.

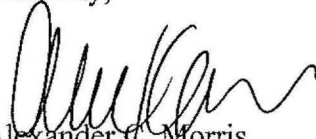
The FOIA provides for the assessment of fees for the processing of requests. See 5 U.S.C. § 552(a)(4)(A)(i); see also 10 C.F.R. § 1004.9(a). Your request was placed in the "other" category for fee purposes. Requesters in this category are entitled to two free hours of search time and 100 free pages. Since DOE did not exceed the two free hours of search time, no fees will be charged for processing your request.

If you have any questions about the processing of this request or this letter, you may contact me or Ms. Jeniffer Pérez Santiago at:

MA-46/ Forrestal Building  
1000 Independence Avenue, S.W.  
Washington, DC 20585  
(202) 586-4933

I appreciate the opportunity to assist you in this matter.

Sincerely,



Alexander C. Morris  
FOIA Officer  
Office of Public Information

Enclosures

## INDEX

Request #: HQ-2019-01408-F-F

### First response

**Copy of the work product (reports, memos, studies, plans, etc.) received to date from Contract DEDT0004091 awarded to Techsource.**

DOE has completed its search and has located two (2) documents responsive to your request.

- Two (2) document are *being released in its entirety*.

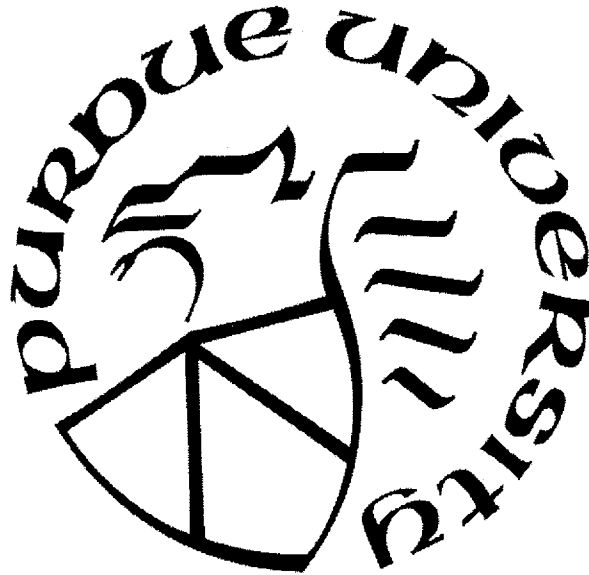
**TEST OF DECAY RATE PARAMETER VARIATION  
DUE TO ANTINEUTRINO INTERACTIONS**

by  
**Shih-Chieh Liu**

**A Dissertation**

*Submitted to the Faculty of Purdue University  
In Partial Fulfillment of the Requirements for the degree of*

**Doctor of Philosophy**



Department of Physics & Astronomy

West Lafayette, Indiana

December 2018



**THE PURDUE UNIVERSITY GRADUATE SCHOOL  
STATEMENT OF DISSERTATION APPROVAL**

Dr. David S. Koltick, Chair

Department of Physics and Astronomy, Purdue University

Dr. Robert S. Bean

Department of Nuclear Engineering, Purdue University

Dr. Martin M. Kruczenski

Department of Physics and Astronomy, Purdue University

Dr. Wei Xie

Department of Physics and Astronomy, Purdue University

**Approved by:**

Dr. John P. Finley

Head of Department of Physics and Astronomy, Purdue University

This dissertation is dedicated to my wife who encouraged me to pursue my dreams  
and finish my dissertation.



## ACKNOWLEDGMENTS

I would like to express my special appreciation and thanks to my advisor Professor David S Koltick. I thank David wholeheartedly, not only for his tremendous academic support but also for giving me so many excellent opportunities.

I am grateful to all of those with whom I have had the pleasure to work during this and other related projects. Each of the members of my Committee has provided me professional guidance in this research. I would also especially like to thank Dr. Haoyu Wang, Dr. Jonathan Nistor, and Dr. Jordan Heim for theoretical and technical support in this project.

In addition, I would like to thank the Physics Department for fully financial support during my graduate studies at Purdue. Also, this work would not have been possible without the financial support from Dr. Tom Ward, TechSource Inc.

Finally, I would like to thank my families, whose love and guidance are with me in whatever I pursue. They are the ultimate role models. Most importantly, I am grateful to my loving and supportive wife, Joling, and my two wonderful children, Alex, and Aiden, who provide unending inspiration.

## TABLE OF CONTENTS

	Page
LIST OF TABLES . . . . .	viii
LIST OF FIGURES . . . . .	x
ABSTRACT . . . . .	xiii
1 Overview . . . . .	1
2 Neutrinos . . . . .	7
2.1 Standard Properties of Neutrinos . . . . .	7
2.2 Neutrino Oscillations . . . . .	9
2.3 Solar Neutrino Flux . . . . .	10
2.4 Parity Invariance Violation . . . . .	11
2.5 Reactor Anomaly, and LSND Experiment . . . . .	12
3 Reported Results, and Phenomena . . . . .	15
3.1 Historical: Variation of Radioactive Decay Rate Parameters . . . . .	15
3.2 Cross Section Sensitivity to Variations of Decay Rate Parameter . . . . .	23
4 Experimental Configuration at High Flux Isotope Reactor . . . . .	31
4.1 High Flux Isotope Reactor (HFIR) . . . . .	31
4.2 Reactor-Generated Antineutrinos . . . . .	32
4.3 Flux of Antineutrinos at High Flux Isotope Reactor . . . . .	34
4.4 Experiment Layout at HFIR . . . . .	35
4.5 High Purity Germanium Detector (HPGe) . . . . .	39
4.6 Shielding Performance, and Background Stability of the HPGe Detector . . . . .	41
5 Energy Calibration of the $^{54}\text{Mn}$ , and the Background Spectra at HFIR . . . . .	47
5.1 Energy Calibration of Background Spectra . . . . .	48
5.2 Energy Calibration of $^{54}\text{Mn}$ $\gamma$ -Spectra . . . . .	52
6 Corrections to the $^{54}\text{Mn}$ Source, and Background Spectra . . . . .	65
6.1 Electronic Dead Time Correction . . . . .	66
6.2 Background Spectrum Correction . . . . .	69
6.2.1 Technical Process for Dead Time Correction . . . . .	70
6.2.2 Background Spectrum Energy Rescaling . . . . .	71
6.2.3 Background Spectrum Amplitude Rescaling . . . . .	73
6.2.4 Background Spectrum Subtraction . . . . .	75
6.3 Pile-up Correction by De-convolution Algorithm . . . . .	77
6.4 Region of Interest (ROI) of $^{54}\text{Mn}$ Spectrum . . . . .	81

	Page
6.5 Region of Interest(ROI) Measurement Limit Estimation . . . . .	84
7 Data Analysis of Corrected $^{54}\text{Mn}$ spectral . . . . .	87
7.1 Single Parameter Fitting to the Region of Interest . . . . .	87
7.2 Side Band Ambient Temperature Corrections . . . . .	91
7.3 Results After All Corrections (ROI) . . . . .	99
8 Conclusion . . . . .	105
VITA . . . . .	114

## LIST OF TABLES

Table	Page
2.1 Three known types of neutrinos, electron neutrino, muon neutrino, and tau neutrino. . . . .	8
2.2 The full neutrino flux production from each fusion reaction in the Sun. . .	11
2.3 Individual predicted cross section per fission per fissile isotope $k$ , $\sigma_k$ in units of $10^{-43} \text{ cm}^2/\text{fission}$ , and the error is represented as a percentage of the cross section[52] . . . . .	13
3.1 Summary of the $^{32}\text{Si}$ , and $^{36}\text{Cl}$ results. . . . .	16
3.2 Summary of the $^{152}\text{Eu}$ , $^{154}\text{Eu}$ , and $^{155}\text{Eu}$ results. . . . .	17
3.3 Summary of the $^3\text{H}$ results. . . . .	19
3.4 Summary of the $^{54}\text{Mn}$ results. . . . .	20
3.5 Summary of the $^{137}\text{Cs}$ results. . . . .	21
3.6 Summary of the $^{226}\text{Ra}$ results. . . . .	22
3.7 Summary of experiments that conclude time-dependence of radioactive decay rate parameters. . . . .	29
3.8 Summary of experiments that conclude <b>Null</b> evidence for radioactive decay rate parameter variation. . . . .	30
4.1 Antineutrino characteristics from $^{235}\text{U}$ , $^{238}\text{U}$ , $^{239}\text{Pu}$ , and $^{241}\text{Pu}$ [59]. . . . .	35
4.2 The yearly cycling of the humidity relative to the experiments starting date	39
4.3 The average background rate, and associated error during the reactor-on or reactor-off periods at HFIR. . . . .	46
5.1 Spectral lines used in the calibration of the background energy calibration.	48
5.2 Calibration coefficients of background spectra with reactor-off for linear, and nonlinear calibration. $\chi^2$ per degree of freedom significantly improves with the nonlinear calibration. . . . .	50
5.3 Accepted energy, and uncertainty of the calibration lines for the $^{54}\text{Mn}$ spectrum . . . . .	55

Table	Page
5.4 The yearly cycling of the humidity, temperature for the HPGe source detector, and linear term $b$ values relative to the experiments starting date.	62
6.1 Proprieties of the full $^{54}\text{Mn}$ spectrum. . . . .	69
6.2 Error analysis, and estimation per day in Region of Interest (ROI) of $^{54}\text{Mn}$ daily spectrum. . . . .	84
7.1 Comparison of in-phase, and out-of-phase ROI oscillation. . . . .	89
7.2 The $\chi^2$ per degree of freedom from fitting equal width energy regions in Figure 7.4. . . . .	94
7.3 Average residuals, and uncertainty of each reactor-on, and reactor-off period.	101
7.4 Residuals, and uncertainty of each reactor-on, and reactor-off period for segment analysis. . . . .	102
7.5 Size of effect, and uncertainty from a single constant term. . . . .	103
7.6 68% confidence upper limit on antineutrino interaction on $^{54}\text{Mn}$ . . . . .	103
8.1 Summary of measurements at HFIR of $^{54}\text{Mn}$ decay rate variations measurement. . . . .	105
8.2 Coefficients from four type of curve fitting with previous experiments. . .	107

## LIST OF FIGURES

Figure	Page
1.1 The logarithm cross section sensitivity of time-dependent variation results, no evidence results, and this HFIR result as a function of the logarithm mean lifetime. . . . .	5
2.1 Helicity of a neutrino, and antineutrino. . . . .	12
3.1 Using the estimates in this section shown is the cross section limit divided by the measuring time in units of mean lifetime. . . . .	26
4.1 High Flux Isotope Reactor at Oak Ridge National Lab . . . . .	31
4.2 The power as a function of time of High Flux Isotope Reactor at Oak Ridge National Lab during this experiment. . . . .	32
4.3 Mass distribution of $^{235}\text{U}$ fission fragments. . . . .	33
4.4 (Left) Nitrogen gas atmosphere to reduce reactor produced $^{40}\text{Ar}$ in the housing, and eliminate humidity to the detector. (Right) HPGe detector spectrometer system in operation at HFIR . . . . .	36
4.5 Experimental Layout at HFIR. . . . .	37
4.6 Ambient pressure, temperature, and humidity as a function of time at HFIR.	38
4.7 Daily average humidity fitted with in phase periodic function (Eq. 4.8), fixed at 1 year, as a function of time. . . . .	39
4.8 Configuration of High Purity Germanium Detector (HPGe). . . . .	40
4.9 (Left) The HPGe detector measured the background spectrum at HFIR. (Right) The HPGe source detector measured the source spectrum. . . . .	41
4.10 HFIR background spectra with, and without shielding in the reactor on or off status. . . . .	42
4.11 Full background spectrum rate as a function of time which includes reactor-on, and reactor-off cycles with the $^{54}\text{Mn}$ source removed. . . . .	44
5.1 Background spectrum with 19 identified lines at HFIR . . . . .	49
5.2 Background spectral line residuals for reactor-off, and reactor-on status. . . . .	51
5.3 Logarithm scale of the $^{54}\text{Mn}$ $\gamma$ -spectrum at HFIR. . . . .	53

Figure	Page
5.4 Differential Backscattered, and Compton Edges peaks from $^{54}\text{Mn}$ daily spectra at HFIR. . . . .	56
5.5 Independent $^{54}\text{Mn}$ spectrum measured in the Physics Building at Purdue University used to study systematic shift. . . . .	57
5.6 Differential Backscattered, and Compton Edges peaks from an independent measurement of the $^{54}\text{Mn}$ daily spectrum made in the Physics Building at Purdue University to study the energy peak shift. . . . .	58
5.7 Nonlinear energy calibration parameters, $a_r$ , $b_r$ , and $c_r$ , determined for each of the daily $^{54}\text{Mn}$ spectra. . . . .	60
5.8 Daily averages for the humidity, temperature of the HPGe source detector, and the linear term $b_r$ . . . . .	61
5.9 Energy of the $^{54}\text{Mn}$ primary photopeak as a function of time. The average energy of $^{54}\text{Mn}$ is $834.849 \pm 0.001$ KeV which shows stability after the nonlinear calibration. . . . .	63
6.1 Correction procedure flow for obtaining the true $^{54}\text{Mn}$ ROI count rate. . .	66
6.2 Illustration of electronic dead time from the DSPEC-50 spectrometer. . . .	67
6.3 DSPEC-50's Minimum, and Maximum Protection Times[64]. . . . .	68
6.4 Logarithm scale of the $^{54}\text{Mn}$ $\gamma$ -spectrum before background spectrum subtraction, and the background spectrum . . . . .	76
6.5 Logarithm scale of the $^{54}\text{Mn}$ $\gamma$ -ray spectrum after background subtraction. .	78
6.6 De-convolution algorithm used to determine pileup events to be removed from the $^{54}\text{Mn}$ spectrum. . . . .	79
6.7 Calculated pileup spectrum (blue) with the starting spectrum (red) demonstrating the fit achieved by the de-convolution algorithm. . . . .	80
6.8 The Region of Interest, from 820 to 900 KeV, is selected from the corrected daily $^{54}\text{Mn}$ spectrum. . . . .	82
7.1 Daily decay rate from the integration between 820 to 900 KeV of the $^{54}\text{Mn}$ spectra. . . . .	87
7.2 Daily residual fitted with a revised exponential decay function (Eq 7.3) which includes a single periodic function. . . . .	88
7.3 The oscillation term found by subtraction of the exponential term from the data (Eq. 7.3), and its fit shown in Red data points . . . . .	90
7.4 Residuals of equal width energy regions from the corrected $^{54}\text{Mn}$ spectrum. .	92

Figure	Page
7.5 Daily Decay rate of Region 740 KeV to 820 KeV of $^{54}\text{Mn}$ spectra . . . . .	95
7.6 (Upper) Daily residual of the side band energy region in the $^{54}\text{Mn}$ spectra. (Lower) Daily residual of the side band energy region of $^{54}\text{Mn}$ spectra after the exponential function correction. A significant fluctuations appear in Period, 1, 5, and 6. . . . .	96
7.7 (Upper)Daily residuals of the side band energy region as a function daily average Temperature.(Lower) Daily residual in Period 5, 6, and 7 dur- ing periods with stable temperature, of the side band energy region as a function of daily relative humidity. . . . .	97
7.8 Daily $\delta c_r$ , and corrected residual of Region 740 KeV to 820 KeV of $^{54}\text{Mn}$ spectra, and daily average Temperature. . . . .	99
7.9 Corrected ROI Residuals as a function of time. . . . .	100
8.1 The logarithm cross section sensitivity of time-dependent variation results, no evidence results, and this HFIR result as a function of the logarithm mean lifetime. . . . .	108

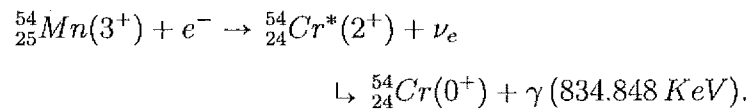


## ABSTRACT

Shih-Chieh Liu Ph.D., Purdue University, December 2018. Test of Decay Rate Parameter Variation due to Antineutrino Interactions. Major Professor: David S Koltick.

High precision measurements of a weak interaction decay were conducted to search for possible variation of the decay rate parameter caused by an antineutrino flux. The experiment searched for variation of the  $^{54}\text{Mn}$  electron capture decay rate parameter to a level of precision of 1 part in  $\sim 10^5$  by comparing the difference between the decay rate in the presence of an antineutrino flux  $\sim 3 \times 10^{12} \bar{\nu} \text{ cm}^{-2} \text{ sec}^{-1}$  and no flux measurements. The experiment is located 6.5 meters from the reactor core of the High Flux Isotope Reactor(HFIR) in Oak Ridge National Laboratory. The results show no effect during the antineutrino exposure. A measurement to this level of precision requires a detailed understanding of both systematic and statistical errors. Otherwise, systematic errors in the measurement may mimic fundamental interactions.

The  $\gamma$  spectrum has been collected from the electron capture decay of  $^{54}\text{Mn}$ ,



What differs in this experiment compared to previous experiments are, (1) a strong, uniform, highly controlled, and repeatable (Power  $\delta P/P \sim 10^{-3}$ ) source of antineutrino flux, using a reactor, nearly 50 times higher than the solar neutrino flux on the Earth, (2) the variation of the antineutrino flux from HFIR is 600 times higher than the variation in the solar neutrino flux on the Earth, (3) the extensive use of neutron and  $\gamma$ -ray shielding around the detectors, (4) a controlled environment for

the detector including a fixed temperature, a nitrogen atmosphere, and stable power supplies, (5) the use of precision High Purity Germanium (HPGe) detectors and finally, (6) accurate time stamping of all experimental runs. By using accurate detector energy calibrations, electronic dead time corrections, background corrections, and pile-up corrections, the measured variation in the decay rate parameter is found to be  $\delta\lambda/\lambda = (0.034 \pm 1.38) \times 10^{-5}$ . This measurement in the presence of the HFIR flux is equivalent to a cross section of  $\sigma = (0.097 \pm 1.24) \times 10^{-25} \text{ cm}^2$ . These results are consistent with no measurable decay rate parameter variation due to an antineutrino flux, yielding a 68% confidence level upper limit sensitivity in  $\delta\lambda/\lambda \leq 1.43 \times 10^{-5}$  or  $\sigma \leq 1.34 \times 10^{-25} \text{ cm}^2$  in cross section. The cross-section upper limit obtained in this null or no observable effect experiment is  $\sim 10^4$  times more sensitive than past experiments reporting positive results in  $^{54}\text{Mn}$ .

## 1. Overview

Unexplained periodic variation of the decay rate parameter measurement for weak interaction decays such as  $\beta^\pm$ -decay, and electron capture [1–18] as well as strong interaction  $\alpha$ -decay[5, 12] have been reported. Because the variation of the decay rate parameter has been presented by a number of groups, located at various locations, using various types of detectors, different isotopes, and over extended periods of time, some researchers have interpreted the source of these variations as not from ambient environmental factors such as temperature, pressure, and humidity but via an unexplained fundamental interaction. Some results show a correlation between an annual periodicity of the decay rate parameter variation, and the variable distance of the Earth from the Sun. The annual variation of the Earth-Sun distance causes a  $\sim 7\%$  variation of the total neutrino flux on the Earth. This flux variation as the source of the decay rate parameter variation is motivated by the large neutrino flux,  $6.5 \times 10^{10} \nu \text{ cm}^{-2} \text{ sec}^{-1}$ , on the Earth dominated by solar fusion. Also, some researchers suggest that decay rate parameters are affected by solar activity such as solar flares[19–22].

However, these conclusions are controversial. This research is focused on the possibilities that the reported variations are an extension of weak interactions. Conventional weak interaction neutrino-nucleon cross sections are 20 orders of magnitude smaller than the reported strong interaction level cross-sections being observed in

these experiments, if caused by neutrinos. The conventional neutrino interaction cross-section per nucleon ( $\nu + n \rightarrow p^+ + e^-$ ) is[23]

$$\begin{aligned}\sigma_{weak} &\sim \frac{4G_F^2 E_\nu^2 (\hbar c)^2}{\pi} \\ &\sim 9 \times 10^{-44} \text{ cm}^2 \left( \frac{E_\nu}{1 \text{ MeV}} \right)^2\end{aligned}\tag{1.1}$$

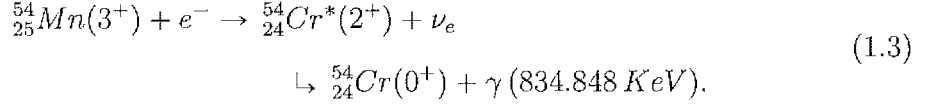
where  $G_F$  is the Fermi constant, and  $E_\nu$  is the neutrino energy. Because antineutrinos interact with protons ( $\bar{\nu} + p^+ \rightarrow n + e^+$ ), there is no significant difference between neutrino, and antineutrino interaction cross-section on target nuclei. That is neutron, and proton number are similar  $\sim A/2$ . If a typical neutrino or antineutrino energy is considered to be  $\sim 1$  MeV, Eq.1.1 leads to a nucleon cross section of

$$\sigma_{weak} \sim N^\beta \times 9 \times 10^{-44} \text{ cm}^2\tag{1.2}$$

where  $N \sim A/2$  is the number of neutrons or protons in the nucleus. The antineutrino cross section is proportional to  $N^\beta$ .  $\beta = 2$  if the antineutrino scattering is coherent from the nucleus, and  $\beta = 1$  if the scattering is incoherent. The largest possible conventional cross section occurs if the scattering is coherent.

The goal of this experiment is to maximize the sensitivity to the decay parameter variation caused by a possible extension to the weak interactions. The disadvantage of solar neutrinos as a test source is the low flux variation ( $\sim 10^9 \nu \text{ cm}^{-2} \text{ sec}^{-1}$ ) which demands long measurement time. Antineutrinos can be generated from a nuclear reactor having a stable antineutrino flux ( $\sim 3 \times 10^{12} \bar{\nu} \text{ cm}^{-2} \text{ sec}^{-1}$ ), and high flux variations due to the reactor off cycles ( $\sim 0 \nu \text{ cm}^{-2} \text{ sec}^{-1}$ )[24]. For this reason, the experiment was performed at the High Flux Isotope Reactor (HFIR) at Oak Ridge National Laboratory (ORNL). The HFIR provides reactor-on, and reactor-off cycles

of similar duration. Specifically, the experiment recorded the  $\gamma$  spectra from  $^{54}_{25}\text{Mn}$  electron capture decay



Even though the maximum possible weak cross section, coherent, for  $^{54}\text{Mn}(Z = 25$  with  $\beta = 2)$  is expected to be at the level of

$$\sigma_{weak} \sim 6 \times 10^{-41} \text{ cm}^2, \quad (1.4)$$

the cross-section sensitivity to decay parameter variation obtainable at HFIR is  $10^3$  to  $10^4$  more sensitive than the reported positive results having strong interaction level cross-section. The use of antineutrinos in no way invalids comparison between this, and previous experimental effects based on neutrinos.  $^{54}\text{Mn}$  was specially selected because the basic interaction involves a proton ( $p^+ + e^- \rightarrow n + \nu$ ) matching the inverse  $\beta^-$ -decay reaction on neutrons caused by neutrinos.

The  $^{54}\text{Mn}$  spectra were collected using a High Purity Germanium Detector (HPGe) Spectrometer system with background neutron, and  $\gamma$  radiation shielding, and well-monitored environmental factors to obtain the results. The shielding was effective in suppressing the backgrounds by a factors  $1.8 \times 10^{-4}$  (reactor-on), and  $6.7 \times 10^{-4}$  (reactor-off). The  $^{54}\text{Mn}$  spectra required corrections including dead time corrections, non-linear energy calibrations, background spectra subtraction, as well as pile-up effects correction using a de-convolution algorithm. While the entire spectrum was used in order to calculate the corrections, a Region of Interest (ROI) around the photopeak of  $^{54}\text{Mn}$  was carefully selected for optimal stability over time. No effect has been observed in the decay parameter at the level of

$$\frac{\delta\lambda}{\lambda} = (0.034 \pm 1.38) \times 10^{-5} \quad (1.5)$$

in the presence of an antineutrino flux  $F_{\bar{\nu}} \sim 3 \times 10^{12} \bar{\nu} \text{ cm}^{-2} \text{ sec}^{-1}$ , this measurement yields an equivalent cross-section

$$\begin{aligned} \sigma &= \frac{\delta\lambda/\lambda}{\tau \times \Delta F_{\bar{\nu}}} \\ &= (0.097 \pm 1.24) \times 10^{-25} \text{ cm}^2 \end{aligned} \quad (1.6)$$

where  $\tau$  is the mean lifetime of  $^{54}\text{Mn}$ . This results will be discussed in detail later in Chapters 7, and 8. The results are consistent with no measurable decay rate parameter variation due to an antineutrino flux yielding 68% confidence level upper limit of sensitivity  $\delta\lambda/\lambda \leq 1.43 \times 10^{-5}$  or  $\sigma \leq 1.34 \times 10^{-25} \text{ cm}^2$  in cross section. The significance of this limit needs a comparison to previous results as interpreted being due to solar neutrinos. Figure 1.1 summarizes the comparison showing this experiment to be previous experiments. In this comparison Figure, curve (a) is the temporal cross-section fit  $\sigma = A\tau^P$  to those experiments reporting decay rate parameter variations shown as triangles. Curve (b) compares experiments by cross-section only. This experiment is more sensitive than all previous experiments reporting positive decay rate parameter variations. Curve (c) connects this experiment, and a solar neutrino experiment using  $^{40}\text{K}$ [19]. The connection between these two experiments maps out an exclusion zone in the temporal cross-section space excluding decay rate parameter variations at a level  $10^4$  times more sensitive than any previously reported positive results. Curve (d) displays the temporal cross exclusion zone  $\sigma \sim \sigma_{limit}\tau^{-1}$  if extrapolated using only this experiment.

If the decay rate parameter variations had been detected in this experiment, the exact form of the interaction would need theoretical underpinning as at present no theoretical motivation exists. Such positive results would represent entirely new physics.

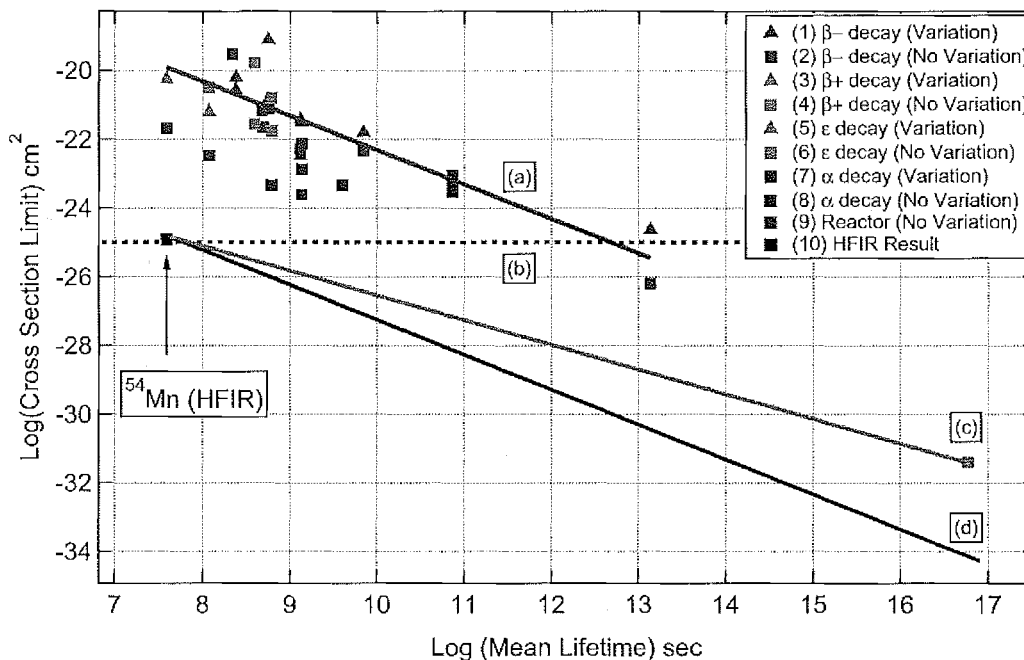


Figure 1.1. The logarithm cross section sensitivity of time-dependent variation results, no evidence results, and this HFIR result as a function of the logarithm mean lifetime. The data are based on Table 3.7, and 3.8. The data includes (1)  $\beta^-$  decay with variation results[1, 3, 6, 16, 18, 25–28], (2)  $\beta^-$  decay with no effect results[8, 12, 19, 29–32], (3)  $\beta^+$  decay with variation results[7], (4)  $\beta^+$  decay with no effect results[33], (5) Electron Capture decay with variation results[21], (6) Electron Capture decay with no effect results[8, 12, 19], (7)  $\alpha$  decay with with variation results[5], (8)  $\alpha$  decay with no effect results[12, 30, 34], and (9) reactor antineutrino as a test source with no effect results[35]. (10) The HFIR  $^{54}\text{Mn}$  experiment result. See the text for explanation of the curves (a), (b), (c), and (d).



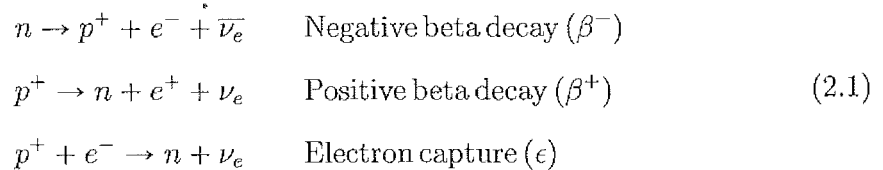


## 2. Neutrinos

In this chapter, the fundamentals of neutrinos relevant to this research are introduced.

### 2.1 Standard Properties of Neutrinos

From the moment of the neutrino hypothesis to the present, properties of the neutrino continue to be surprising, and strange. The original hypothesis of the neutrino was required because of the observed continuous energy distribution of the  $\beta$ -decay electrons. If beta decay were a two-body reaction, the  $\beta^-$  should be emitted at a fixed energy. However, the emitted particles had a continuous energy distribution. To solve this missing energy problem, Pauli assumed a second particle emitted in the  $\beta$ -decay process in 1930. It was assumed, and later measured to be highly penetrating radiation. This "second particle" is now known as the *Neutrino*, named by Fermi. The beta decay reactions are now understood to be



Some of the historical standard properties of neutrinos are as follows:

1. The neutrino is charge neutral, and its rest mass is near zero.
2. The neutrino was measured to have spin-1/2 making it a fermion.
3. The conservation of lepton number gives a rule to understand neutrino, and antineutrino interactions. Take  $\beta^-$ -decay as an example, the assignment of a lepton number of 1 to the electron, and -1 to the electron antineutrino explains the apparent lepton number conservation in weak interaction reactions.

4. Two different kind of neutrinos participate in  $\beta$  decay, *neutrinos*, and *antineutrinos*.
5. The neutrino is always observed to be a parity eigenstate. The helicity of an antineutrino is only observed parallel to its momentum while for the neutrino, it is anti-parallel to its momentum.
6. The neutrino discussed in  $\beta$ -decay is known as the "*Electron Neutrino*". In the Standard Model of particle physics, there are three kinds of charged leptons: electron, muon, and tau. The table below lists the known types of neutrinos.

Table 2.1.

Three known types of neutrinos, electron neutrino, muon neutrino, and tau neutrino.

Neutrino	$\nu_e$	$\nu_\mu$	$\nu_\tau$
Generation	First	Second	Third
Charged Partner	electron( $e$ )	muon( $\mu$ )	tau( $\tau$ )
First Exp. Discovery	1956	1962	2000

7. The first discovery of a particle fitting the expected characteristics of the neutrino was announced by Cowan, and Reines[36, 37]. In 1962, experiments at Brookhaven National Laboratory, and CERN, the European Laboratory for Physics, made surprising discoveries: neutrinos produced in association with muons do not behave the same as those produced in association with electrons[38]. Likewise, the tau neutrino was introduced after the tau had been discovered at Stanford Linear Acceleration Center. The DONUT experiment at Fermi Lab was built to specifically detect the tau neutrino, and reported the first detection in 2000[39].

In this study, the word *neutrino*, and *antineutrino* indicate the *electron neutrino*, and *electron antineutrino*.

## 2.2 Neutrino Oscillations

In contrast, initial studies of neutrinos assumed each neutrino type, electron, muon, and tau had separately conserved lepton numbers, and each was massless. Now neutrino lepton flavor oscillation experiments have changed these concepts. The concept of neutrino oscillations have a long history when as early as 1958, Bruno Pontecorvo mused over the possibility of neutrino-antineutrino oscillation in analogy with neutral Kaon mixing[40].

If neutrinos have mass, the particle mass eigenstate, and lepton flavor eigenstate of the particles may not be the same, allowing mixing. In this case, the neutrino can oscillate from one flavor to another while traveling through space. The observation of oscillations implies the neutrino flavor states are not mass eigenstate but are the superposition of such states. The neutrino flavour states  $|\nu_\alpha\rangle$  ( $\alpha = e, \mu, \tau$ ) are related to the mass state  $|\nu_j\rangle$ , ( $j = 1, 2, 3$ ) linearly,

$$\begin{bmatrix} \nu_e \\ \nu_\mu \\ \nu_\tau \end{bmatrix} = \begin{bmatrix} U_{e1} & U_{e2} & U_{e3} \\ U_{\mu1} & U_{\mu2} & U_{\mu3} \\ U_{\tau1} & U_{\tau2} & U_{\tau3} \end{bmatrix} * \begin{bmatrix} \nu_1 \\ \nu_2 \\ \nu_3 \end{bmatrix} \quad (2.2)$$

where  $U_{\alpha j}$  is the  $3 \times 3$  Pontecorvo–Maki–Nakagawa–Sakata(PMNS) unitary matrix. The probability of the three neutrino case is difficult to express explicitly. However, the two flavor mixing fully illustrates the effect. In this case, the unitary matrix  $U$  is given by

$$U = \begin{bmatrix} U_{\alpha1} & U_{\alpha2} \\ U_{\beta1} & U_{\beta2} \end{bmatrix} = \begin{bmatrix} \cos \theta & \sin \theta \\ -\sin \theta & \cos \theta \end{bmatrix} \quad (2.3)$$

where  $\theta$  is the mixing angle. By imputing this U matrix, and the  $\Delta m_{12}^2$  mass difference between the states, the probability of 2 neutrino mixing is

$$P(\nu_\alpha \rightarrow \nu_\beta) = \sin^2(2\theta) \sin^2\left(\frac{\Delta m^2 L}{4E}\right) \quad (2.4)$$

The mixing acts as a quantum mechanical phase factor in the wave function. If the neutrinos were zero mass particles,  $\Delta m_{12}^2$  is zero, and then  $P(\nu_\alpha \rightarrow \nu_{\alpha'}) = 0$ . Neutrino oscillations have been observed by a number of experiments showing lepton number is not conserved[41–46]. The observations of the neutrino oscillations conclude that at least one neutrino flavor has non-zero mass. Again, these surprising results are in sharp counterpoint to the neutrinos historical properties.

There are four different experimental confirmations of neutrino oscillations, (1) solar neutrino oscillations first observed by Davis[41], (2) atmospheric neutrino oscillations first observed by Fukuda[42], (3) reactor neutrino oscillations first observed by An, and Anh[43, 44], and (4) neutrino beam oscillations[45, 46] have been observed. Notably, the existence of neutrino oscillations has resolved the long-standing solar neutrino problem. That is the missing solar neutrino flux predicted by the solar model. Davis’s observations of solar neutrino oscillation open the door to the possibility of oscillation to other unpredicted weakly interacting particles within in the solar flux on the Earth as well in other neutrino sources.

### 2.3 Solar Neutrino Flux

Amazingly, during the course of a human lifetime approximately,  $10^{20}$  solar neutrinos will pass through each  $cm^2$  of our bodies. The source of solar neutrino production is the fusion reaction of hydrogen into helium. The nuclear fusion in the Sun occurs in the core at a temperature of about 15M Kelvin. 99% of the power is generated within 24% of the Sun’s radius, and by 30% of the radius, fusion has stopped entirely. The Sun’s energy is produced by nuclear fusion in the core region through a series of steps called the p–p (proton–proton) chain which produces > 91% of the solar neutrinos. Electron neutrinos are produced as steps in the fusion reaction from hydrogen to helium. For example, two protons fuse to produce  ${}^2\text{D}$  by jointly forming an unbound excited state of  ${}^2\text{He}^*$  which then  $\beta$  decays to  ${}^2\text{D}$ . This key step in the

Table 2.2.

The full neutrino flux production from each fusion reaction in the Sun. The average total solar flux on the Earth is  $6.5 \times 10^{10} \nu \text{ cm}^{-2} \text{ sec}^{-1}$ . Most of the solar neutrinos are from the pp(pronton--proton) chain(>91%). The  ${}^7\text{Be}$ , pep(proton-electron-proton), and  ${}^8\text{Be}$  chain are 7%, 0.2%, and 0.008%. The hep (helium3-electron-proton) chain can be neglected due to its relative small flux [47].

Reaction	Label	Flux ( $\text{cm}^{-2} \text{ sec}^{-1}$ )
$p + p \rightarrow {}^2\text{H} + e^+ + \nu_e$	<i>pp</i>	$5.95 \times 10^{10}$
$p + e^- + p \rightarrow {}^2\text{H} + \nu_e$	<i>pep</i>	$1.14 \times 10^8$
${}^3\text{He} + p \rightarrow {}^4\text{He} + e^+ + \nu_e$	<i>hep</i>	$9.30 \times 10^3$
${}^7\text{Be} + e^- \rightarrow {}^7\text{Li} + \nu_e$	${}^7\text{Be}$	$4.77 \times 10^9$
${}^8\text{Be} \rightarrow {}^8\text{Be} + e^+ + \nu_e$	${}^8\text{Be}$	$5.05 \times 10^6$

proton to helium fusion process has never been observed experimentally. On average, two  $\beta^+$  decays take place in the p–p chain to yield  ${}^4\text{He}$ . The total energy released by these reactions in turning 4 hydrogen atoms into 1 helium atom is 26.7 MeV.



The total solar neutrino flux on the Earth assuming no oscillations is  $6.5 \times 10^{10} \text{ cm}^{-2} \text{ sec}^{-1}$  [47]. Davis results indicates  $\sim 1/2$  these solar neutrino have oscillated before reaching the Earth[41].

## 2.4 Parity Invariance Violation

The mechanism, which generates neutrino oscillations is still under investigation, and the Standard Model may be changed due to this new physics reality. Because neutrinos always participate in weak interactions from a single parity eigenstate, the opposite non-participating state is called "sterile."

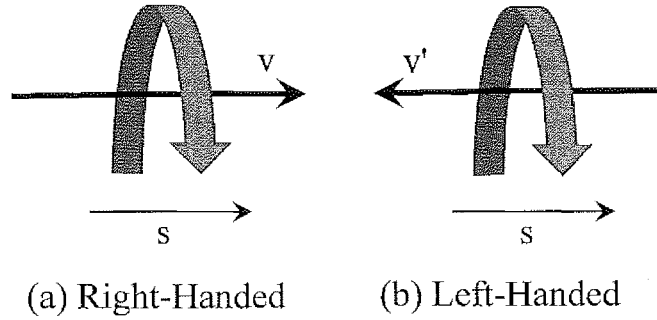


Figure 2.1. Helicity of Neutrino, and Antineutrino. (a) Right-handed (Antineutrino) the spin, and velocity are parallel. (b) Left-handed (Neutrino) represents the spin, and velocity are anti-parallel. The handedness (helicity) of the neutrino is consistent with the  $-1$ , and antineutrino is consistent with the  $+1$ .

Parity invariance had been considered a universal law of nature until the 1950s. Yang, and Lee proposed parity in  $\beta$ -decay (Weak Interactions) to be violated in 1956[48]. Wu's successful experiment soon confirmed their hypothesis by measuring  $^{60}\text{Co}$   $\beta$ -decay[49]. In the past, neutrinos were assumed to be produced in  $\pm 1$  helicity equally. However, Goldhaber's experiment proved all neutrinos to be left-handed, and all antineutrinos are right-handed[50]. The mirror images of neutrinos, and antineutrinos do not exist. Right-handed neutrinos, and left-handed antineutrinos have never been observed. If they were to exist, they would not interact via the weak interaction. Those hypothetical neutrinos are often referred to as "*sterile*" neutrinos. If sterile neutrinos do exist, they could explain not only the existence of neutrino masses but also the smallness of their mass scale[51]. Sterile neutrinos are also a candidate for dark matter.

## 2.5 Reactor Anomaly, and LSND Experiment

The three-neutrino framework has been extremely successful in explaining neutrino oscillation results in solar, atmospheric, accelerator, and reactor neutrino os-

cillation experiments. Their experiments are explained using only two oscillation frequencies. These frequencies correspond to two mass difference terms, each on the order of  $10^{-3}$  to  $10^{-5}$  eV. However, two experiments present results confronting this seemingly unified picture, the reactor anomaly experiment[52], and Liquid Scintillator Neutrino (LSND) experiment[41].

The reactor anomaly refers to the deficiency of observed antineutrinos from experiments performed at reactors compared with the theoretical predictions. The anomaly being that only about 94% of the expected antineutrinos are actually measured compared to the flux expected by theoretical models[52]. It is unknown whether this is due to new physics such as a fourth generation neutrino, a sterile neutrino, experimental error in the measurements, or errors in the theoretical flux calculations. Recently, some researchers have attempted to explain reactor anomalies as being caused by sterile neutrino production[52].

Table 2.3.

Individual predicted cross section per fission per fissile isotope  $k$ ,  $\sigma_k$  in units of  $10^{-43} \text{ cm}^2/\text{fission}$ , and the error is represented as a percentage of the cross section[52]. When the new cross-section estimates for the reactor fuel mix are compared to the experimentally measured flux, a significant 6% deficit is observed, possibility accounted for by production of new particles.

Predicted	Old(Bugey)[53]	New [52]
$\sigma(^{235}\text{U})$	$6.39 \pm 1.9\%$	$6.61 \pm 2.11\%$
$\sigma(^{239}\text{Pu})$	$4.19 \pm 2.4\%$	$4.34 \pm 2.45\%$
$\sigma(^{238}\text{U})$	$9.21 \pm 10\%$	$10.10 \pm 8.15\%$
$\sigma(^{241}\text{Pu})$	$5.73 \pm 2.1\%$	$5.97 \pm 2.15\%$
$\sigma(\text{Reactor Mix})$	$5.824 \pm 2.7\%$	$6.102 \pm 2.7\%$
$\sigma(\text{Exp})[53]$	$5.752 \pm 1.4\%$	
$\sigma(\text{Exp})/\sigma(\text{Reactor Mix})$	$0.987 \pm 1.4\% \pm 2.7\%$	$0.943 \pm 1.4\% \pm 2.7\%$

This view has also support from the LSND experiment started in the 1990s[41]. The LSND experiment reported an anomalous event excess in the  $\bar{\nu}_\mu \rightarrow \bar{\nu}_e$  appearance channel, which can be interpreted as an oscillation with  $\Delta m^2 \sim 1 eV$ [54, 55]. This  $\Delta m^2$  mass scale is clearly incompatible with the three-neutrino framework. The LSND anomaly, if true, indicates the existence at least an additional fourth neutrino family with  $\Delta m^2 \sim 1 eV$ . The antineutrino deficiency can be explained by a sterile neutrino with large  $\Delta m^2$ [52]. Therefore, resolving the question of the reactor anomaly's existence is an appropriate first step in determining whether sterile neutrinos exist.

### What Are Neutrinos?

In summary, with the above considerations, it is clear the "Story" of what is a neutrino is far from complete. The search for new, and novel neutrino interactions is worth pursuing.



### 3. Reported Results, and Phenomena

In this chapter, the experiments relevant to decay parameter variations are summarized. In addition, the observable effects of a decay parameter variation on the measuring sensitivity, and effective cross section are presented.

#### 3.1 Historical: Variation of Radioactive Decay Rate Parameters

Oscillation variations of the radioactive decay rate parameters have been investigated for several decades. A number of groups such as Alburger, Falkenberg, Veprev, and Jenkins *et. al.* observed time-dependent decay rate parameter variations[1–6, 21, 25]. Because the variation of the decay rate parameters has been reported (1) at various locations (2) with various type of detectors, (3) using different isotopes, and (4) over extend periods of time, these researchers believe the variations are not due to the ambient environmental factors such as temperature, pressure, and humidity. Some results show a correlation between an annual periodicity of the decay rate parameter variation, and the variable distance of the Earth from the Sun. These results motivate some researchers to conclude the solar neutrino flux variations cause the decay rate parameter variations[4–6, 21].

However, the correlation of the radioactive decay rate parameter variation, and solar neutrino flux has been challenged by Kossert, Semkow, Meijer, Bruhn , Schrader, and Bellotti *et. al.*[8, 9, 29–32, 35]. These "null evidence" experimental references attribute the decay rate parameter variation to ambient environmental factors or instrumental error, instead of the solar neutrino flux variation.

In this section, a summary of some key results will be discussed. The results are sorted by isotopes, and published date. A key comment, and a short summary table are presented at the beginning of each discussion. "Positive" represents those observation reporting time-dependent decay rate parameters, whereas "Negative" are those showing no variation results. The size of the observed effect or the experimental sensitivity( $\delta\lambda/\lambda$ ) in the case of null results are also displayed in the short summary table in each discussion. Where as Table 3.7, and Table 3.8 display the results of the full literature review, and cross-section sensitivities for each reported isotope.

- $^{32}\text{Si}$ , and  $^{36}\text{Cl}$

Table 3.1.  
Summary of the  $^{32}\text{Si}$ , and  $^{36}\text{Cl}$  results.

Source	Reference	Sensitivity (Size of Effect)	Variation
$^{32}\text{Si}/^{36}\text{Cl}$	Alburger <i>et. al.</i>	$5 \times 10^{-3}$	Positive
$^{36}\text{Cl}$	Kossert <i>et. al.</i>	$4 \times 10^{-4}$	Negative
$^{32}\text{Si}$	Semkow <i>et. al.</i>	$1 \times 10^{-3}$	Negative

- **Alburger *et. al.*** reported the first observation of decay rate parameter variations in 1986. Alburger worked on the half life measurement of  $^{32}\text{Si}$  with a gas proportional detector over the period 1982 through 1986 at Brookhaven National Lab(BNL)[1]. They unexpectedly observed small periodic annual deviations of the data points from an exponential decay. The authors reported that temperature, and humidity "*can not fully account*" for observed ratio  $^{32}\text{Si}/^{36}\text{Cl}$  decay rate variation during their measurement, as shown in Table 3.1. However, they do not have complete environment records, to backup these claims.
- **Kossert *et. al.*** reported no decay rate parameter variations of  $^{36}\text{Cl}$  measured using a custom-built triple-to-double coincident ratio detector (TDCR)

at Physikalisch-Technische Bundesanstalt (PTB)[31]. TDCR is an optical chamber with three photomultiplier tubes surrounding a liquid scintillation detector. The sample is placed in the center. A triple coincidence detector is much less sensitive to ambient environmental factors. Kossert measured much smaller variation of  $^{36}\text{Cl}$  as shown in Table 3.1 than observed by Alburger but Kossert attributes the small variation to instrumental effects, instead of variations of the decay rate parameter. This conclusion is much more reliable than Alburger's because Alburger used a single gas proportional detector which is sensitive to environmental variations.

- **Semkow** has written a review concerning decay rate parameter variations of  $^{32}\text{Si}$  from Alburger's results[30]. Semkow explained the variations of  $^{32}\text{Si}$  by the change of temperature causing the air density in the space between the source, and the gas proportional detector to change reducing, and increasing the count rate. The higher temperature in the summer causes lower air density in the space between the source, and the detector, and resulting in less absorption of the lower energy  $\beta$  particles in the air. Thus, the gas proportional detector collects more  $\beta$  particles at a higher temperature, generating a higher counting rate. The resulting limit is given in Table 3.1.

- $^{152}\text{Eu}$ ,  $^{154}\text{Eu}$ , and  $^{155}\text{Eu}$

Table 3.2.  
Summary of the  $^{152}\text{Eu}$ ,  $^{154}\text{Eu}$ , and  $^{155}\text{Eu}$  results.

Source	Reference	Sensitivity	Variation
$^{152}\text{Eu}$ , $^{154}\text{Eu}$ , and $^{155}\text{Eu}$	Siegert <i>et. al.</i>	$5 \times 10^{-4}$	Negative
$^{152}\text{Eu}$	Meijer <i>et. al.</i>	$1.4 \times 10^{-4}$	Negative

- **Siegert *et. al.*** studied the multi  $\beta$ -decay modes of Eu isotopes. Siegert used the strong interaction  $\alpha$ -particle  $^{226}\text{Ra}$  decay as a reference to de-

termine the half life of the weak interaction  $\beta$  decays of  $^{152}\text{Eu}$ ,  $^{154}\text{Eu}$ , and  $^{155}\text{Eu}$ , measured using two different kinds of detector systems; an ion chamber, and a solid state detector(Ge, Li) at Physikalisch-Technische Bundesanstalt (PTB)[12].  $^{152}\text{Eu}$  decays to  $^{152}\text{Gd}$  by electron capture with 72.1% branching ratio, and to  $^{152}\text{Sm}$  by  $\beta^-$ -decay with branching ratio 27.9%. Siegert reported that the oscillations of  $^{226}\text{Ra}$  have a maximum positive deviation in February, and minimum deviation in August. Siegert observed oscillations in  $^{226}\text{Ra}$  as well as in the other isotopes but explains the effect as follows:

*"A discharge effect on the charge collecting capacitor, the cables, and the insulator to the ionization chamber electrode caused by background radioactivity such as radon, and daughter products which are known to show seasonal concentration changes.*

Siegert concludes the oscillations are proportional to the ionization current. If the oscillations were due to solar neutrinos interacting with isotopes via the weak interactions, the  $^{226}\text{Ra}$  strong interaction decay oscillations should not depend on the ionization current. With these considerations, Siegert's observation are considered to be upper limits, as shown in Table 3.2.

- Meijer *et. al.* used reactor antineutrinos as a source. Meijer reported null evidence for the decay rate variation of  $^{152}\text{Eu}$  using reactor antineutrinos[35], as shown in Table 3.2. If the solar neutrino variations cause the decay rate parameter variation, Meijer should have observed a stronger effect compared to Siegert due to the factor of 10 higher antineutrino flux variation from the reactor cycling. No effect was observed.

- $^3\text{H}$

- Falkenberg is the first one to put forward the hypothesis that the variations of the  $\beta$ -decay rate parameters are due to the solar neutrino flux variations. Falkenberg measured the radioactive  $\beta$ -decay rate parameter of

Table 3.3.  
Summary of the  $^3\text{H}$  results.

Source	Reference	Sensitivity (Size of Effect)	Variation
$^3\text{H}$	Falkenberg	$3.7 \times 10^{-3}$	Positive
$^3\text{H}$	Bruhn	$2 \times 10^{-3}$	Negative
$^3\text{H}$	Veprev <i>et. al.</i>	$2 \times 10^{-1}$	Positive

tritium by a photodiode detector from 1980 to 1982[2], as shown in Table 3.3. To determine the significance of the data's periodic deviation, the residuals were first fit to a single periodic function. Falkenberg calculated the residuals as the differences between an aperiodic exponential form, and the data. Then, he included a cosine function in the fit with a period of 365 days in order to account for the variation away from the aperiodic function. Falkenberg concluded:

*"There is a positive correlation between the periodically changing solar neutrino flux, and the  $\beta$ -decay of tritium"*

– Bruhn re-analyzed Falkenberg's data, and criticized Falkenberg for not making corrections for any background effects in his tritium decay rate measurements [29]. In addition, Bruhn concludes Falkenberg's results are not sufficient for deducing a correlation between the tritium decay rate, and the orbital motion of the Earth because neither the period nor amplitude of the deviation coincides with the orbital motion of the Earth. Bruhn concludes:

*"By taking the deviation of the measurement data with respect to the optimal solution instead of the true solution (in the fits) E.D. Falkenberg cannot separate any (hypothetical) additional background effects in his data from the true solution."*

Bruhn's analysis of Falkenberg's data can be used to estimate a limit on the decay parameter variations in  $^3\text{H}$ . Both results are included in this review, as shown in Table 3.3.

- **Veprev *et. al.*** measured the high-energy region of the tritium beta decay spectrum using a liquid scintillation detector system viewed by three photomultipliers[25]. Veprev reported decay rate parameter oscillations which coincide with the solar neutrino flux variation distance from the Earth to the Sun, as shown in Table 3.3. Veprev concludes that the periodicity of the tritium decay rate parameter variations is due to the interactions of the tritium nuclei with solar neutrinos.

- $^{54}\text{Mn}$

Table 3.4.  
Summary of the  $^{54}\text{Mn}$  results.

Source	Reference	Sensitivity (Size of Effect)	Variation
$^{54}\text{Mn}$	Jenkins <i>et. al.</i>	$1 \times 10^{-3}$	Positive
$^{54}\text{Mn}$	Meijer <i>et. al.</i>	$4 \times 10^{-4}$	Negative

- **Jenkins *et. al.*** was the first to conclude there is a decay rate parameter variation due to the variable distance of the Earth from the Sun. The results are shown in Table 3.4. In addition, Jenkins *et. al.* reported the detection of a significant decrease in the decay rate parameter of  $^{54}\text{Mn}$  during a strong solar flare at the end of 2006. Jenkins measured the count rate of  $^{54}\text{Mn}$ , and compared it with the Solar X-ray data. The deviation is clearly visible on 12/12/06, through 12/17/06, which was coincident with a severe solar storm. Jenkins attributed the annual oscillations observed in

the data to the variations in solar neutrino flux due to the annual variation in the distance between the Sun, and the Earth[6, 21].

- **Meijer *et. al.*** used reactor antineutrinos as a source. Meijer reported null evidence of the  $^{54}\text{Mn}$  electron capture decay rate parameter to vary due to an antineutrino flux with improved sensitivity relative to Jenkins'[6, 21, 35], as shown in Table 3.4. The experiments were conducted comparing the  $\gamma$ -ray count rate during reactor on, and off periods at an antineutrino flux of  $\sim 5 \times 10^{10} \bar{\nu} \text{ cm}^{-2} \text{ sec}^{-1}$ . The results showed no variations of the  $^{54}\text{Mn}$  decay rate parameter. This challenges Jenkin's conclusions because the solar neutrino causes only  $\sim 7\%$  ( $4.6 \times 10^9 \nu \text{ cm}^{-2} \text{ sec}^{-1}$ ) variations on the Earth. Hence, Meijer should have observed an effect more than 10 times larger than Jenkin's, if Jenkin's hypothesis, were correct.

- $^{137}\text{Cs}$

Table 3.5.  
Summary of the  $^{137}\text{Cs}$  results.

Source	Reference	Sensitivity	Variation
$^{137}\text{Cs}$	Schrader	$4.6 \times 10^{-4}$	Negative
$^{137}\text{Cs}$	Bellotti <i>et. al.</i>	$8.5 \times 10^{-5}$	Negative

- **Schrader *et. al.*** observed variations in the decay rate measurements of  $^{137}\text{Cs}$  using an ionization chamber at Physikalisch-Technische Bundesanstalt (PTB)[8]. Schrader concludes the small yearly variations are from the measuring electronics, instead of decay rate parameter variations. The results are shown in Table 3.5.
- **Bellotti *et. al.*** measured the decay rate of  $^{137}\text{Cs}$  radioactive source using a NaI scintillation detector, and a Ge semiconductor detector[19]. The results are shown in Table 3.5. No significant yearly deviation from the

expectations was measured. In addition, the data exhibited no decay rate parameter variations in the presence of the two solar flares of the year 2011, and 2012.

- $^{226}\text{Ra}$

Table 3.6.  
Summary of the  $^{226}\text{Ra}$  results.

Source	Reference	Sensitivity (Size of Effect)	Variation
$^{226}\text{Ra}$	Siegert <i>et. al.</i>	$1 \times 10^{-3}$	Negative
$^{226}\text{Ra}$	Jenkins <i>et. al.</i>	$2 \times 10^{-3}$	Positive

- **Siegert *et. al.*** used  $^{226}\text{Ra}$ , having a strong interaction  $\alpha$ -particle decay, to study decay parameter variations. Siegert measured  $^{226}\text{Ra}$  decay rate with an ionization chamber at the PTB[12]. Siegert reported that the oscillations of  $^{226}\text{Ra}$  have a maximum positive deviation in February, and minimum deviation in August. He accounted for these oscillations as due to seasonal environmental variations. This conclusion meets the expectation of a null result if extensions to weak interactions were the source of parameter variations. The results are shown in Table 3.6.
- **Jenkins** re-analyzed Siegert's  $^{226}\text{Ra}$  decay rate data, and showed the observed variations have a correlation to the inverse squared distance between the Earth, and the Sun[5]. The results are shown in Table 3.6.

### In Summary

The literature does not report a consistent picture of decay rate parameter variations caused by neutrinos or antineutrinos. Moreover, most references do not discuss the cross section sensitivity in their reports. For this reason, the results are not di-



rectly comparable without such a framework. All authors except one report only the size of the effect relative to the decay rate. If the reported results claim interactions between the decay rate parameter variation, and a neutrino flux, they should show a meaningful cross-section sensitivity to account for the interaction. Therefore, this work places previous results into a unified framework expressed as an interaction cross section due to the neutrino flux. Furthermore, cross-section sensitivity provides an opportunity to examine further how to proceed in studies of possible decay rate parameter variations of radioactive isotopes.

### 3.2 Cross Section Sensitivity to Variations of Decay Rate Parameter

While the exact cause of decay rate parameter variation is not known, if the assumption is correct, the effect is proportional to the antineutrino flux from the reactor core or the neutrino flux in the case of the solar source. With this assumption, experimental cross section sensitivity represents the amount of exposure from the source.

To accomplish this the cross section needs to be framed in terms of the decay rate parameter variation. The standard decay rate is given by

$$\begin{aligned} R(t) &= N_0 \lambda \exp(-\lambda t) \\ &= \frac{N_0}{\tau} \exp\left(\frac{-t}{\tau}\right) \end{aligned} \tag{3.1}$$

where  $N_0$  is the constant of integration which gives the original number of nuclei present when exposure begins.  $\lambda$  is the decay constant, and  $\tau$  is the mean lifetime which also equals to  $1/\lambda$ . The variation of the radioactive decay rate parameter at time  $t$  results in

$$R'(t) = \frac{N_0}{\tau + \delta\tau} \exp\left(\frac{-t}{\tau + \delta\tau}\right) \tag{3.2}$$

where  $\delta\tau$  is the measured variation. The experimental cross-section expresses the reaction rate to the exposure from the source, and can be written as

$$\sigma = \frac{\text{Reaction Events per Unit Time per Nucleus}}{\text{Incident Flux of Neutrinos or Antineutrinos per Unit Area per Unit Time}} \quad (3.3)$$

This is equivalent to

$$\sigma = \left| \frac{\delta R(t)}{N(t)} \right| \times \frac{1}{\Delta F_{\nu \text{ or } \bar{\nu}}} \quad (3.4)$$

where  $\delta R(t)$  is the reaction events per unit time.  $N(t)$  is the number of nuclei at time  $t$ .  $\Delta F_{\nu \text{ or } \bar{\nu}}$  is the variation of the neutrino or antineutrino flux. Eq.3.4 can be written

$$\sigma = \frac{|\delta R(t)/R(t)|}{\tau \times \Delta F_{\nu \text{ or } \bar{\nu}}} \quad (3.5)$$

by definition  $N(t) = R(t)/\lambda$ .

To convert  $|\delta R(t)/N(t)|$  into the measuring limit  $\delta\lambda/\lambda$ , the reaction rate per unit time per nucleus is given by

$$\begin{aligned} \frac{\delta R(t)}{N(t)} &= \frac{R(t) - R'(t)}{N(t)} \\ &= \frac{N_0 [\tau^{-1} \exp(-t/\tau) - (\tau + \delta\tau)^{-1} \exp(-t/(\tau + \delta\tau))]}{N_0 \exp(-t/\tau)} \\ &= \frac{1}{\tau} - \frac{1}{(\tau + \delta\tau)} \exp\left(\frac{-t}{\tau + \delta\tau}\right) \exp\left(\frac{t}{\tau}\right) \end{aligned} \quad (3.6)$$

Because  $\delta\tau \ll \tau$ ,

$$\begin{aligned} \exp\left(\frac{-t}{\tau + \delta\tau}\right) &\sim \exp\left(-\frac{t}{\tau} \left(1 - \frac{\delta\tau}{\tau}\right)\right) \\ &= \exp\left(-\frac{t}{\tau}\right) \exp\left(\frac{\delta\tau t}{\tau^2}\right), \end{aligned} \quad (3.7)$$

and

$$\frac{1}{(\tau + \delta\tau)} \sim \frac{1}{\tau} \left(1 + \frac{\delta\tau}{\tau}\right)^{-1} \quad (3.8)$$

Using these approximations in Eq 3.6 results in

$$\frac{\delta R(t)}{N(t)} = \frac{1}{\tau} \left[ 1 - \left( 1 + \frac{\delta\tau}{\tau} \right)^{-1} \exp \left( \frac{\delta\tau t}{\tau \tau} \right) \right] \quad (3.9)$$

Even with significant decay ( $t \sim \tau$ ), the exponential term in Eq. 3.9 is still small because  $\delta\tau/\tau$  ranges from  $10^{-2}$  to  $10^{-5}$ . From this consideration

$$\begin{aligned} \frac{\delta R(t)}{N(t)} &= \frac{1}{\tau} \left[ 1 - \left( 1 - \frac{\delta\tau}{\tau} \right) \left( 1 + \frac{\delta\tau t}{\tau \tau} \right) \right] \\ &= \frac{1}{\tau} \left[ \frac{\delta\tau}{\tau} \left( 1 - \frac{t}{\tau} + \frac{\delta\tau t}{\tau \tau} \right) \right] \end{aligned} \quad (3.10)$$

In this experiment as well as all those reviewed the measurement time  $t \ll \tau$ , therefore,

$$\frac{\delta R(t)}{N(t)} \sim \frac{1}{\tau} \frac{\delta\tau}{\tau} \quad (3.11)$$

All the reviewed results as well as this experiment can be framed as a cross section for comparison by dividing by the neutrino flux variation. Inputting the variation decay rate, Eq. 3.11 into Eq. 3.4 yields,

$$\begin{aligned} \sigma &= \left| \frac{1}{\tau} \frac{\delta\tau}{\tau} \right| \times \frac{1}{\Delta F_{\nu \text{ or } \bar{\nu}}} \\ &= \frac{|\delta\tau/\tau|}{\tau \times \Delta F_{\nu \text{ or } \bar{\nu}}} \end{aligned} \quad (3.12)$$

where  $\Delta F_{\nu \text{ or } \bar{\nu}}$  is the variation of the neutrino or antineutrino flux. With  $\delta\tau = -\delta\lambda/\lambda^2$ , and  $\tau = 1/\lambda$ , Eq. 3.12 can be written

$$\sigma = \frac{|\delta\lambda/\lambda|}{\tau \times \Delta F_{\nu \text{ or } \bar{\nu}}} \quad (3.13)$$

From this it is observed there are two routes to improve the cross section sensitivity. The first method is to measure the isotope decay parameter as precisely as possible. The second is to get as close as possible to the reactor core to increase the antineutrino flux. This experiment has taken both approaches.

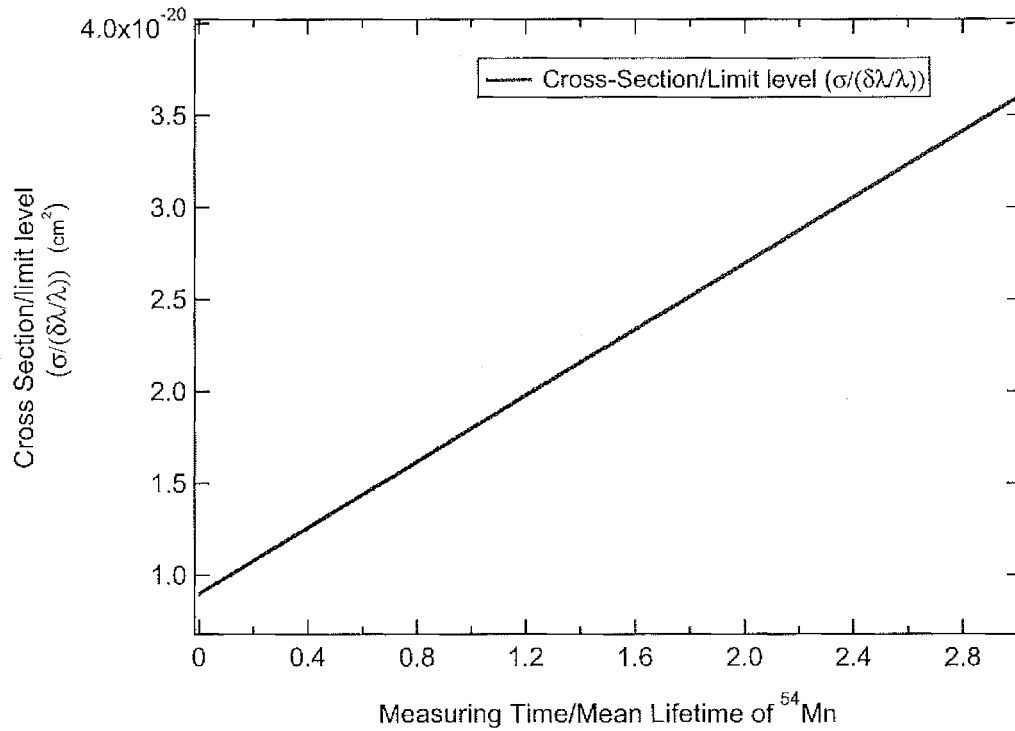


Figure 3.1. Using the estimates in this section shown is the cross section limit divided by the measuring time in units of mean lifetime. The cross section sensitivity is reduced as a function of experimental observation time due to the decay of the isotope.

### The HFIR Experiment Sensitivity Estimation

As will be shown, the flux ( $F_{\bar{\nu}}$ ) in HFIR is  $\sim 2.86 \times 10^{12} \bar{\nu} \text{ cm}^{-2} \text{ sec}^{-1}$  at 6.53 meters from the core. The reactor power is highly stable so the reactor-on antineutrino flux from HFIR is constant as a function of time in this experiment. A single reactor-on period is nearly 26 days compared to the  $^{54}\text{Mn}$  mean lifetime, 450.41 days, satisfying  $t \ll \tau$ , and as shown in Figure 3.1 no correction to Eq.3.13 is required. The cross section limit is effectively set by averaging individual reactor-on, and reactor-off measurements.

Eq. 3.13 shows that the cross-section sensitivity is related to the measuring error, is inversely related to the mean isotope lifetime, and the antineutrino flux. By using the  $^{54}\text{Mn}$  mean lifetime,  $\tau = 450.41$  days, setting the measuring error to  $\delta\lambda/\lambda \sim 10^{-5}$ , and using the neutrino flux at 6.53 meters away from the core, the expected cross-section sensitivity for this experiment is found using Eq. 3.13 to be

$$\sigma \sim 9.0 \times 10^{-26} \text{ cm}^2. \quad (3.14)$$

### Solar Neutrino Variation Estimation

Most of the references have used the Sun as a neutrino source. The total solar neutrino flux on the Earth is  $6.5 \times 10^{10} \nu \text{ cm}^{-2} \text{ s}^{-1}$ . The variation of the neutrino flux depends on the distance between the Earth, and the Sun. The Earth has an elliptical orbit with perihelion at 147.1M km, and aphelion at 152.1M km. The semi-major axis is 149.6M km. The solar neutrino flux is proportional to the inverse squared distance, thus

$$\frac{1/r_{\text{perihelion}}^2 - 1/r_{\text{aphelion}}^2}{1/r_{\text{semi-major}}^2} = \frac{(1/147.1)^2 - (1/152.1)^2}{(1/149.6)^2} \quad (3.15)$$

$$\sim 7\%$$

The result of the above equation yields a solar neutrino flux variation of nearly 7%. The amplitude of the variation of the solar neutrino flux is then  $\sim 4.6 \times 10^9 \nu \text{ cm}^{-2} \text{ sec}^{-1}$  on the Earth.

### Branching Ratio Cross-section Sensitivity

If an isotope has more than one decay mode, the branching fraction of the decay mode must be taken into consideration. The effective decay rate can be modified by multiplying with the branching fraction  $f$

$$\sigma_{effective} = \left| \frac{\delta R(t)}{N(t)} \right| \times \frac{1}{\Delta F_{\nu or \bar{\nu}}} \times f \quad (3.16)$$

The cross-section sensitivity defined by Eq.3.13 can then be modified to be

$$\sigma_{effective} = \frac{|\delta\lambda/\lambda|}{\tau \times \Delta F_{\nu or \bar{\nu}}} \times f \quad (3.17)$$

where  $\tau$  is the mean lifetime of the isotopes,  $\Delta F_{\nu or \bar{\nu}}$  is the flux variation of the neutrino or antineutrino source. Hence, the cross section sensitivity is improved by a factor of  $f$ , the branching fraction.

In conclusion, the cross-section sensitivity is obtained from the measuring error of the decay rate parameter, mean lifetime of the isotope, the variation in the neutrino or antineutrino flux. The cross-section sensitivity obtainable at HFIR is at the level of approximately  $10^3$  to  $10^4$  times more sensitive than past published results. If a decay parameter variation were detected due to antineutrino interactions, the neutrino-nucleus interaction would occur at the level of strong interaction nuclear cross sections. The cross-section sensitivity from all references in the literature has been calculated based on Eq.3.13. The references in Table 3.7, Table 3.8 provide a complete review of the literature. These cross-section limits are also displayed in Figure 8.1.

Table 3.7.

Summary of experiments that conclude time-dependence of radioactive decay rate parameters. Estimation of the interaction cross section is based on Eq. 3.13 by inputting the associated size of effect, mean lifetime as well as neutrino or antineutrino flux from each reference. The variation of the solar neutrino flux is taken to be  $4.6 \times 10^9 \nu \text{ cm}^{-2} \text{ sec}^{-1}$  on the Earth.

References That Conclude Time-dependence of Radioactive Decay Parameters							
Source	Reference	Mode	Detector Type	Measured Radiation	Size of Effect	$\nu$ or $\bar{\nu}$ Variations ( $\text{cm}^{-2} \text{sec}^{-1}$ )	Cross Section Sensitivity ( $\text{cm}^2$ )
$^3\text{H}$	Falkenberg (2001)[3]	$\beta^-$	Photodiodes	$\beta^-$	3.7E-03	4.6E+9	1.4E-21
$^3\text{H}$	Veprev(2012)[25]	$\beta^-$	Liq. Scintillation	$\beta^-$	2.0E-01	4.6E+9	7.8E-20
$^{22}\text{Na}/^{44}\text{Ti}$	O'Keefe(2013)[7]	$\beta^+, \epsilon$	Solid State (Ge)	$\gamma$	3.4E-04	4.6E+9	6.3E-22
$^{32}\text{Si}/^{36}\text{Cl}$	Alburger(1986)[1]	$\beta^-$	Gas proportional	$\beta^-$	5.0E-03	4.6E+9	1.6E-22
$^{36}\text{Cl}$	Jenkins(2012)[6]	$\beta^-$	Geiger-Muller	$\beta^-$	1.5E-02	4.6E+9	2.4E-25
$^{54}\text{Mn}$	Jenkins(2009)[21]	$\epsilon$	Scintillation	$\gamma$	1.0E-03	4.6E+9	5.6E-21
$^{60}\text{Co}$	Parkhomov (2005)[26]	$\beta^-$	Geiger-Muller	$\beta^-, \gamma$	3.0E-03	4.6E+9	2.7E-21
$^{60}\text{Co}$	Baurov(2007)[27]	$\beta^-$	Scintillation	$\gamma$	7.0E-03	4.6E+9	6.4E-21
$^{90}\text{Sr}/^{90}\text{Y}$	Parkhomov (2011)[28]	$\beta^-$	Geiger-Muller	$\beta^-$	2.3E-03	4.6E+9	3.8E-22
$^{90}\text{Sr}/^{90}\text{Y}$	Sturrock(2012) [16]	$\beta^-$	Geiger-Muller	$\beta^-$	2.3E-03	4.6E+9	3.8E-22
$^{90}\text{Sr}/^{90}\text{Y}$	Sturrock(2016)[18]	$\beta^-$	Liq., Scintillation(TDCR)	$\beta^-$	2.0E-04	4.6E+9	3.3E-23
$^{137}\text{Cs}$	Baurov(2007)[27]	$\beta^-$	Scintillation	$\gamma$	2.0E-03	4.6E+9	3.2E-22
$^{226}\text{Ra}$	Jenkins(2009)[5]	$\alpha$	Ion Chamber	$\alpha$	2.0E-03	4.6E+9	6.0E-24

Table 3.8.

Summary of experiments that conclude **Null** evidence for radioactive decay rate parameter variation. Estimation of the interaction cross section is based on Eq. 3.13 by inputting the associated size of the effect, mean lifetime as well as neutrino or antineutrino flux from each reference. The variation of the solar neutrino flux is taken to be  $4.6 \times 10^9 \nu \text{ cm}^{-2} \text{ sec}^{-1}$  on the Earth. \* indicates the reactor antineutrino flux at various locations.

References That Conclude Null Evidence of Radioactive Decay Rate Parameters Variation							
Source	Reference	Mode	Detector Type	Measured Radiation	Sensitivity	$\nu$ or $\bar{\nu}$ Variations ( $\text{cm}^{-2} \text{ sec}^{-1}$ )	Cross Section Sensitivity ( $\text{cm}^2$ )
$^3\text{H}$	Bruhn(2002)[29]	$\beta^-$	Photodiode	$\beta^-$	2.0E-03	4.6E+9	7.8E-22
$^{22}\text{Na}/^{44}\text{Ti}$	Norman(2009)[33]	$\beta^+, \epsilon$	Solid State (Ge)	$\gamma$	1.8E-03	4.6E+9	3.2E-21
$^{22}\text{Na}$	Meijer(2011)[35]	$\beta^+$	Solid State (Ge)	$\gamma$	2.0E-04	5.0E+10*	3.4E-23
$^{22}\text{Na}$	Meijer(2014)[56]	$\beta^+$	Solid State (Ge)	$\gamma$	5.1E-05	1.6E+13*	2.7E-26
$^{32}\text{Si}/^{36}\text{Cl}$	Semkow(2009)[30]	$\beta^-$	Gas proportional	$\beta^-$	1.5E-03	4.6E+9	4.7E-23
$^{36}\text{Cl}$	Kossert(2014)[31]	$\beta^-$	Liq. Scintillation(TDCR)	$\beta^-$	4.0E-04	4.6E+9	6.4E-27
$^{40}\text{K}$	Bellotti(2013)[19]	$\epsilon$	Scintillation(NaI)	$\gamma$	1.0E-04	4.6E+9	4.0E-32
$^{54}\text{Mn}$	Meijer(2011)[35]	$\epsilon$	Solid State (Ge)	$\gamma$	4.0E-04	5.0E+10*	2.1E-22
$^{90}\text{Sr}/^{90}\text{Y}$	Kossert(2015)[32]	$\beta^-$	Liq. Scintillation(TDCR)	$\beta^-$	3.0E-04	4.6E+9	5.0E-23
$^{85}\text{Kr}$	Schrader (2010)[8]	$\beta^-$	Ion Chamber	$\gamma$	5.0E-04	4.6E+9	2.2E-22
$^{108m}\text{Ag}$	Schrader (2010)[8]	$\epsilon$	Ion Chamber	$\gamma$	9.0E-03	4.6E+9	9.9E-23
$^{133}\text{Ba}$	Schrader (2010)[8]	$\beta^-$	Ion Chamber	$\gamma$	1.5E-03	4.6E+9	6.9E-22
$^{137}\text{Cs}$	Bellotti(2013)[19]	$\beta^-$	Scintillation	$\gamma$	8.5E-05	4.6E+9	1.4E-23
$^{137}\text{Cs}$	Schrader (2010)[8]	$\beta^-$	Ion Chamber	$\gamma$	4.6E-04	4.6E+9	7.4E-23
$^{137}\text{Cs}$	Meijer(2011)[35]	$\beta^-$	Solid State (Ge)	$\gamma$	1.7E-04	5.0E+10*	2.5E-24
$^{152}\text{Eu}$	Meijer(2011)[35]	$\beta^-, \epsilon$	Sol. St. (Ge)	$\gamma$	1.4E-04	5.0E+10*	4.5E-24
$^{152}\text{Eu}$	Siegert(1998)[12]	$\beta^-, \epsilon$	Ion Chamber	$\gamma$	5.0E-04	4.6E+9	1.8E-22
$^{152}\text{Eu}$	Siegert(1998)[12]	$\beta^-, \epsilon$	Sol. St. (Ge)	$\gamma$	3.0E-02	4.6E+9	1.6E-21
$^{152}\text{Eu}$	Schrader (2010)[8]	$\beta^-, \epsilon$	Ion Chamber	$\gamma$	5.0E-04	4.6E+9	1.8E-22
$^{154}\text{Eu}$	Siegert(1998)[12]	$\beta^-, \epsilon$	Ion Chamber	$\gamma$	5.0E-04	4.6E+9	2.8E-22
$^{154}\text{Eu}$	Siegert(1998)[12]	$\beta^-, \epsilon$	Sol. St. (Ge)	$\gamma$	3.0E-02	4.6E+9	1.7E-20
$^{154}\text{Eu}$	Schrader (2010)[8]	$\beta^-, \epsilon$	Ion Chamber	$\gamma$	5.0E-04	4.6E+9	2.8E-22
$^{155}\text{Eu}$	Siegert(1998)[12]	$\beta^-$	Sol. St. (Ge)	$\gamma$	3.0E-02	4.6E+9	3.0E-20
$^{226}\text{Ra}$	Siegert(1998)[12]	$\alpha$	Ion Chamber	$\alpha$	1.0E-03	4.6E+9	3.0E-24
$^{226}\text{Ra}$	Semkow(2009)[30]	$\alpha$	Ion Chamber	$\alpha$	3.0E-03	4.6E+9	9.1E-24
$^{238}\text{Pu}$	Cooper(2009)[34]	$\alpha$	Radioisotope Thermoelectric	$\alpha$	8.4E-05	4.6E+9	4.6E-24



## 4. Experimental Configuration at High Flux Isotope Reactor

The experiment used a 60% High Purity Germanium Detector Spectrometer (HPGe) system to test the variation of the decay rate parameter of  $^{54}\text{Mn}$ . The HPGe has an energy resolution  $\delta E/E \sim 1.67 \times 10^{-3}$  at  $E_\gamma = 1.33$  MeV measured using a  $^{60}\text{Co}$  button source placed at the center of the HPGe detectors face. The antineutrino source for the experiment is the High Flux Isotope Reactor (HFIR) located at Oak Ridge National Lab at Tennessee, USA. The HPGe system, and shielding house were designed, built, and tested at Purdue, and then shipped to HFIR for the experiment.

### 4.1 High Flux Isotope Reactor (HFIR)

High Flux Isotope Reactor (HFIR) is a light-water-cooled, and moderated, beryllium-reflected, and flux-trap type reactor[57]. The original purpose of HFIR is for the production of transuranic isotopes. The goal of HFIR includes materials irradiation,

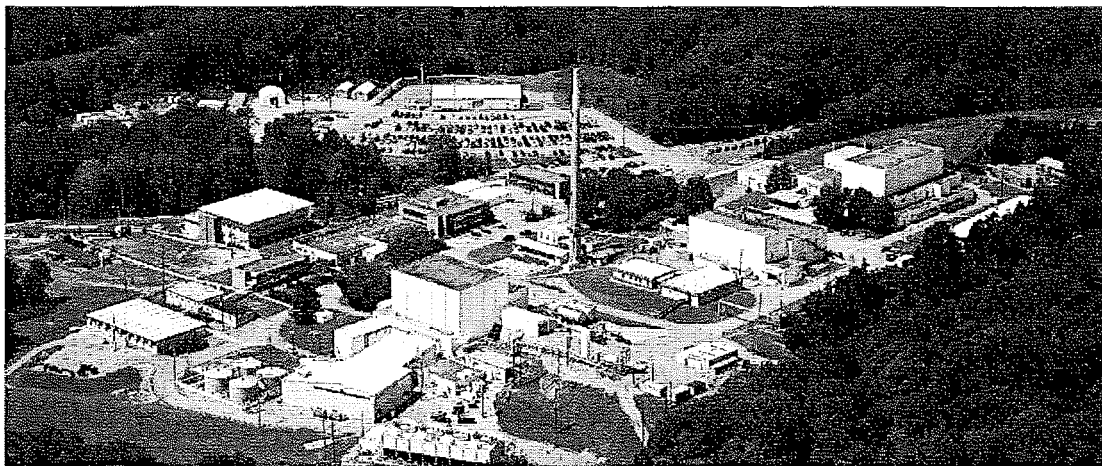


Figure 4.1. High Flux Isotope Reactor at Oak Ridge National Lab

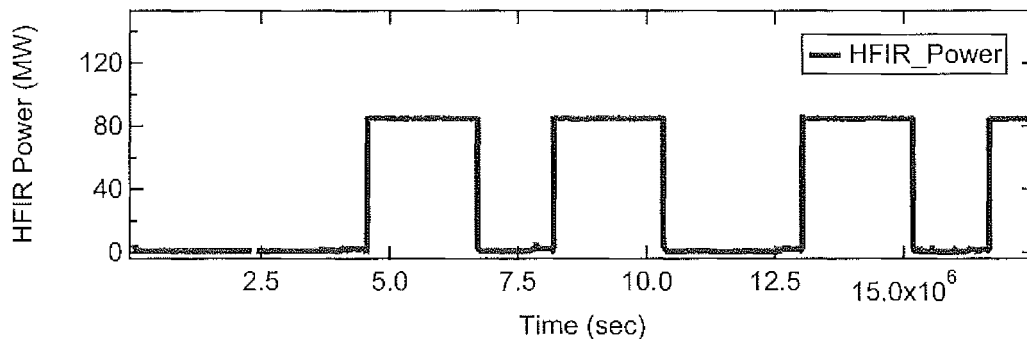


Figure 4.2. The power as a function of time of High Flux Isotope Reactor at Oak Ridge National Lab during this experiment. Three independent detectors are used to verify the stability of the reactor power. The average power was measured to be  $86.007 \pm 0.22$  MW.

neutron activation, and neutron scattering. It has a peak thermal neutron (25 meV) fluence of  $2.5 \times 10^{15} \text{ n cm}^{-2} \text{ sec}^{-1}$ . The thermal neutron flux of the HFIR core is  $\sim 100$  times higher than cores of commercial nuclear power plants ( $\sim 10^{13} \text{ n cm}^{-2} \text{ sec}^{-1}$ ). HFIR uses highly enriched  $^{235}\text{U}$  (HEU) as the fuel. The operating cycle normally consists of full-power operation for approximately 23-27 days at  $\sim 86$  MW. Figure 4.2 is the HFIR reactor power as a function of time during this experiment. The average operating power was calculated from the recorded reactor power data taken every second, and is  $86.007 \pm 0.22$  MW. The reactor power is very stable with a variance of  $\delta p / p_{\text{mean}} \sim 2.6 \times 10^{-3}$ , where  $\delta p$  is the standard deviation of the average power, and  $p_{\text{mean}}$  is the average power of HFIR in operation.

## 4.2 Reactor-Generated Antineutrinos

Nuclear power reactors are the brightest antineutrino sources. Antineutrinos are produced from the unstable fission fragments decay. The excess neutrons undergo  $\beta^-$

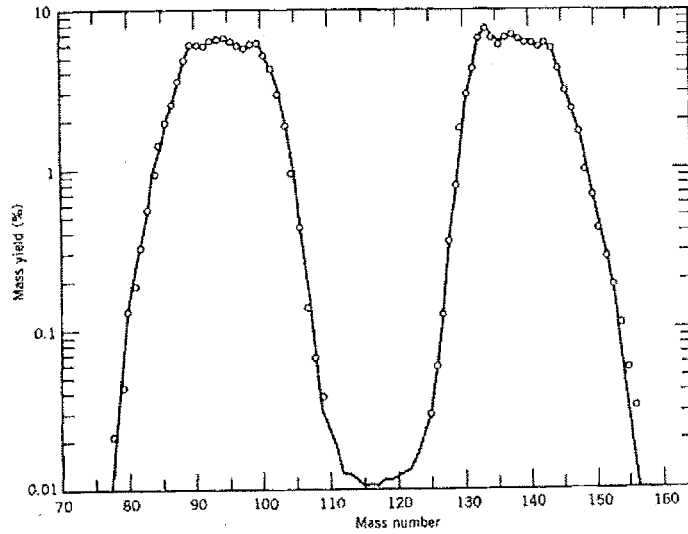
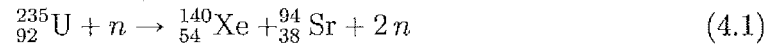
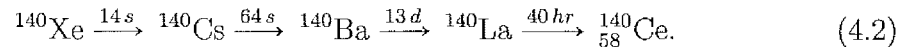


Figure 4.3. Mass distribution of  $^{235}\text{U}$  fission fragments[58]. The possible fission fragments are centered around  $A \sim 95$ , and  $A \sim 137$  which must share the original 92 protons. A typical pair of fragments from  $^{235}\text{U}$  fission are Xenon( $A=140$ ), and Strontium( $A=94$ ).

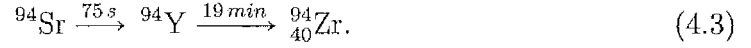
decay which produces protons, electrons, and antineutrinos as the fragments move towards stability. While the fission fragments are not unique, a possible reaction is



which illustrates the asymmetric mass distribution of the produced fragments shown in Figure 4.3. Most of these fission fragments are highly unstable (radioactive), and undergo further radioactive decays to stabilize. For example,  ${}_{54}^{140}\text{Xe}$  will decay to  ${}_{58}^{140}\text{Ce}$  via  $\beta^-$  decay, generating the possible decay chain



Likewise,  ${}^{94}_{38}\text{Sr}$  will decay to  ${}^{94}_{40}\text{Zr}$  via  $\beta^-$  decay, and follow the possible chain to stabilize,



In this example, the stable end chain nuclei have a total of 98 protons, and 136 neutrons. The fission fragments (parent nuclei) have together 92 protons, and 142 neutrons. Thus, 6 neutrons have  $\beta^-$ -decayed to protons. Similarly, for each  ${}^{235}\text{U}$  fission, the fission fragments have on average six negative beta decays (6 neutrons must decay to 6 protons) which results in six antineutrinos produced per each fission.

### 4.3 Flux of Antineutrinos at High Flux Isotope Reactor

The average antineutrino flux can be estimated by the fissile fuel composition,  ${}^{235}\text{U}$ , in the HFIR core, and the reactor's thermal power. Because the antineutrino flux is related to the reactor thermal power, the reactor antineutrino flux impinging on a detector can be accurately calculated. The antineutrino flux at HFIR is

$$\frac{dN_{\bar{\nu}}}{dt} = n_{\bar{\nu}} \times \frac{P_H}{E_F} \quad (4.4)$$

where  $P_H$  is the average thermal power output,  $E_F$  is average released thermal energy per fission, and  $n_{\bar{\nu}}$  is the average number of antineutrino generated per fission.

Table 4.1 displays the parameters needed to find the antineutrino flux for the most common reactor fuels. The thermal energy released per each fission of  ${}^{235}\text{U}$  is

$$\begin{aligned} E_f &= E_F - \langle E_{\bar{\nu}} \rangle \times n_{\bar{\nu}} \\ &= 201.7 - 1.46 \times 5.58 \\ &= 193.6 \text{ MeV} \end{aligned} \quad (4.5)$$

Table 4.1.  
Antineutrino characteristics from  $^{235}\text{U}$ ,  $^{238}\text{U}$ ,  $^{239}\text{Pu}$ , and  $^{241}\text{Pu}$ [59].

Type of Fuel	$^{235}\text{U}$	$^{238}\text{U}$	$^{239}\text{Pu}$	$^{241}\text{Pu}$
Released energy per fission ( $E_F$ )(MeV)	201.7	205	210	212.4
Mean energy of $\bar{\nu}$ ( $\langle E_{\bar{\nu}} \rangle$ )(MeV)	1.46	1.56	1.32	1.44
Number of $\bar{\nu}$ per fission ( $n_{\bar{\nu}}$ )( $E > 1.8$ MeV)	5.58	6.69	5.09	5.89

where  $E_F$  is the released energy per fission, and  $\langle E_{\bar{\nu}} \rangle$  is the mean energy of the antineutrinos. Hence, the typical rate of  $\dot{N}_{\bar{\nu}}$  from the HFIR reactor core is given by

$$\begin{aligned} \dot{N}_{\bar{\nu}} &= 5.58 \times \frac{86.007 \text{ MW}}{193.6 \text{ MeV}} \\ &= 1.53 \times 10^{19} \bar{\nu} \text{ sec}^{-1}. \end{aligned} \quad (4.6)$$

At a distance,  $d = 6.53 \text{ m}$  from the core, the antineutrino flux at the HPGe detector, assuming the core is a point source, is estimated to be

$$\begin{aligned} F_{\bar{\nu}(\text{HFIR})} &= \frac{1.53 \times 10^{19} \bar{\nu} \text{ sec}^{-1}}{4\pi(653)^2 \text{ cm}^2} \\ &= 2.86 \times 10^{12} \bar{\nu} \text{ cm}^{-2} \text{ sec}^{-1} \end{aligned} \quad (4.7)$$

which is nearly 50 times higher than the solar neutrino flux on the Earth, and more than 600 times higher than the variation in the solar neutrino flux on the Earth.

#### 4.4 Experiment Layout at HFIR

The HPGe spectrometer layout at HFIR is shown in Figure 4.5. The use of 5.5 tons of lead, as well as copper, aluminum, and borated poly shielding, reduced the background radiation activity by a factor of one thousand to the level of a few counts per second full spectrum (3 KeV to 3 MeV). Two ORTEC HPGe detectors are used for collecting the source, and background spectrum. The detectors are cooled by X-Cooler-3 mechanical Liquid-Nitrogen-Free chillers, and the signal processing is per-

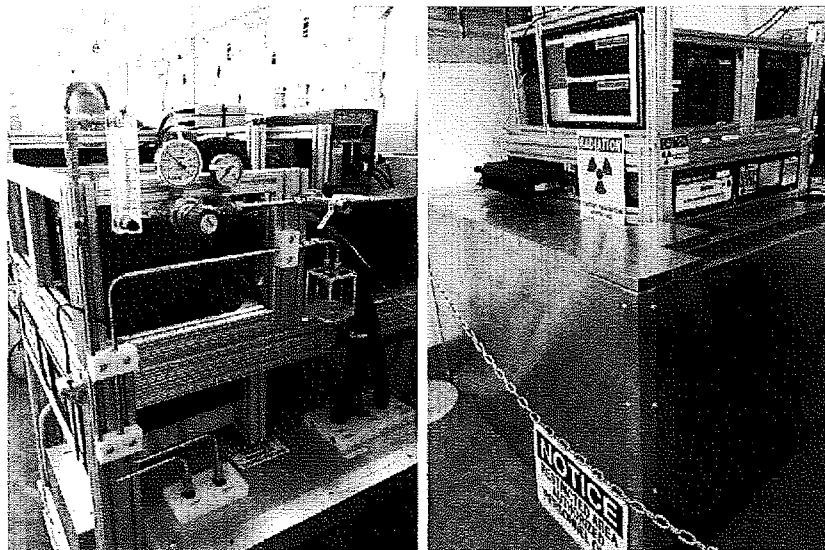


Figure 4.4. (Left) Nitrogen gas atmosphere to reduce reactor produced  $^{40}\text{Ar}$  in the housing, and eliminate humidity to the detector. (Right) HPGe detector spectrometer system in operation at HFIR

formed by a Digital Spectrometer (DSPEC-50) multichannel analyzers. The detectors are housed in a temperature controlled enclosure, which is continuously flushed with high purity nitrogen to eliminate condensation, and to isolate the detector from the reactor produced  $^{40}\text{Ar}$  radioactive background. The daily spectrum was saved into a computer which can be remotely controlled from off-site. The data was uploaded to an online storage service for further processing. The output spectra have been corrected, and produced by a 320 cores Intel Xeon E5450 cluster with MATLAB programming.

A well-known source for systematic error in counting experiments is a detector's response to ambient environmental factors such as temperature, pressure, and relative humidity. Variations in the ambient environmental factors can produce effects that mimic fundamental interactions if not accounted for. Figure 4.6 shows the ambient

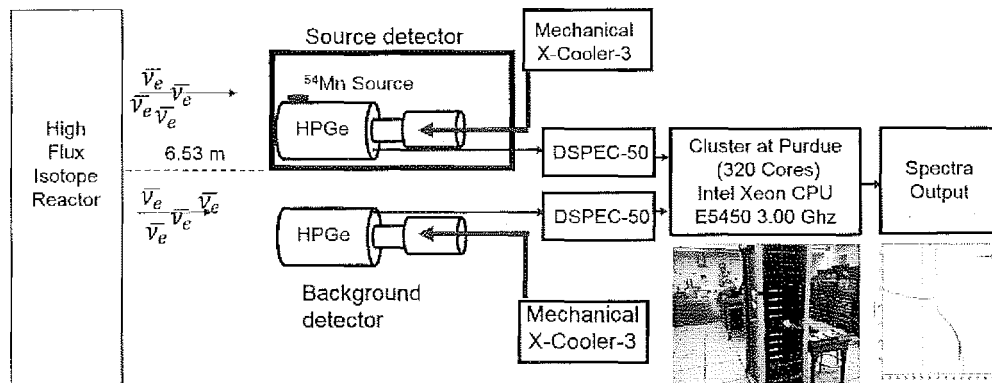


Figure 4.5. Experimental Layout at HFIR, The HPGe detector system is located 6.53 meter from the reactor core. The flux is  $2.86 \times 10^{12} \bar{v} \text{ cm}^{-2} \text{ sec}^{-1}$  when the reactor is in operation. One HPGe detector is to measure the  $^{54}\text{Mn}$  Source spectrum. The other HPGe detector is to monitor the background rate. A DSPEC collects, and analyzes the voltage pulses from the HPGe detector. Two mechanical cooler keep the HPGe detectors near liquid nitrogen temperature. Data Processing used a 320 cores Intel Xeon E5450 based cluster with MATLAB programming.

temperature, pressure, and relative humidity as a function of time.

The ambient pressure oscillations are limited to  $\delta P/P \sim 0.6\%$ , and behaves randomly as shown in Figure 4.6.

The ambient temperature shown in Figure 4.6 shows a  $\sim 27\%$  oscillation during the reactor-off Period 1. The ambient temperature also has some small  $\sim 10\%$  variation in Period 2, Period 3, and Period 4. The ambient temperature displays a significant  $\sim 20\%$  drop in the reactor-off Period 5, and reactor-on Period 6, caused by an outage of the air conditioning in the HFIR facility lasting about one month. These ambient temperatures variations are addressed as corrections by the study of variations in the relation between the ambient temperature, and the daily decay rate

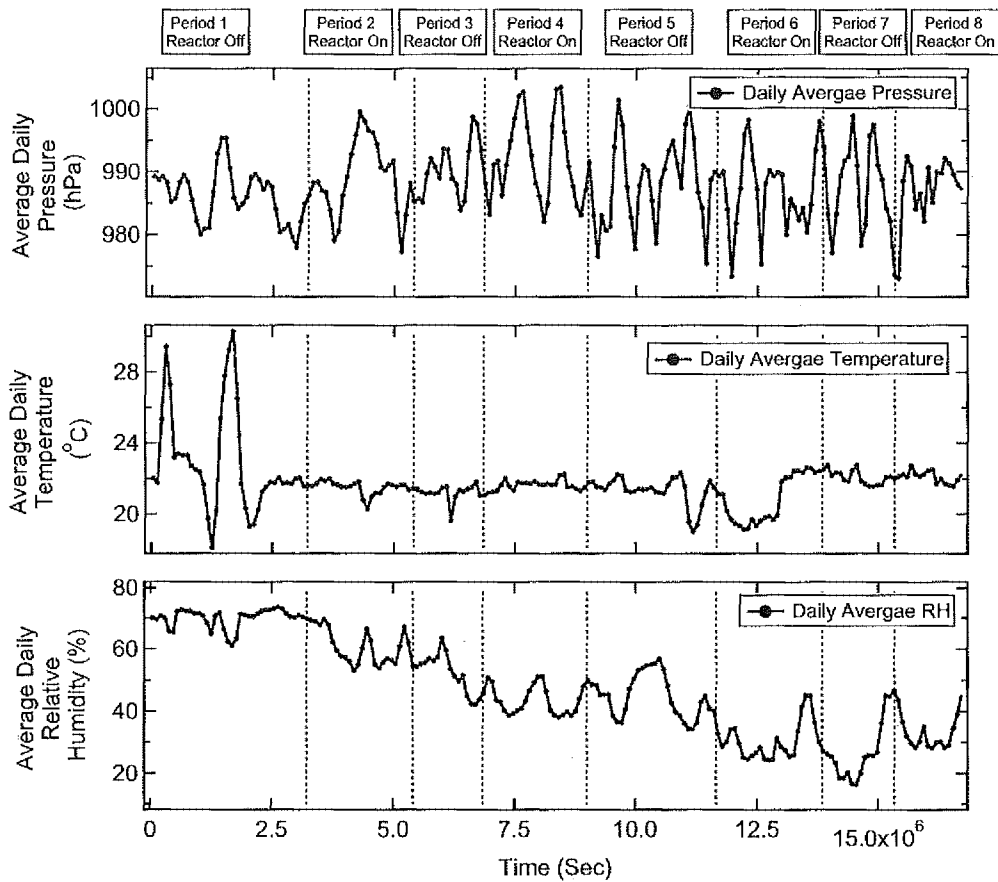


Figure 4.6. Ambient pressure, temperature, and humidity as a function of time at HFIR.

fitting residuals, using a side band method.

The relative humidity shown in Figure 4.6 has a decreasing trend due to the seasons; starting high at the start of the experiment in August, and decreasing towards spring at the experiment's end. The humidity has been fit to

$$h(t) = h_0 + A \sin(\omega t + \phi) \quad (4.8)$$



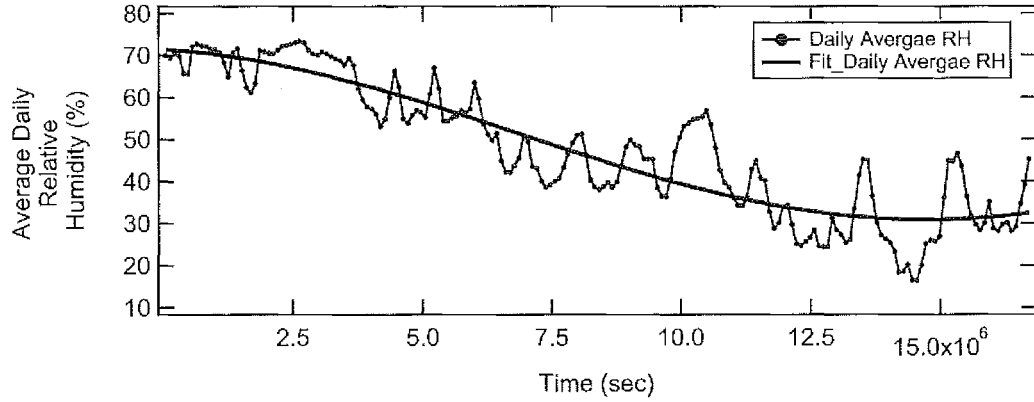


Figure 4.7. Daily average humidity fitted with in phase periodic function (Eq. 4.8), fixed at 1 year, as a function of time.

Table 4.2.

The yearly cycling of the humidity relative to the experiments starting date

Fixed $\omega=1$ year	Phase ( $\phi$ )
In Phase	$-79 \pm 1$ day
Out of Phase	$103 \pm 1$ day

and is shown in Figure 4.7, for the case,  $\omega$  is fixed at one year to match the cycling of the seasons. Two cases are fit, the data, and the negative of the data in order to compare with other in phase, and out of phase distributions. The results are shown in Table 4.2.

#### 4.5 High Purity Germanium Detector (HPGe)

An HPGe detector behaves in a way similar to a semiconducting diode detector. The incoming  $\gamma$  ray is absorbed by the crystal creating electron, and hole charge carriers generated proportional to the ratio  $E_\gamma/E_{Gap}(0.72eV)$ . The charge carriers are drawn to the inner, and outer contacts by the bias voltage. HPGe detectors are

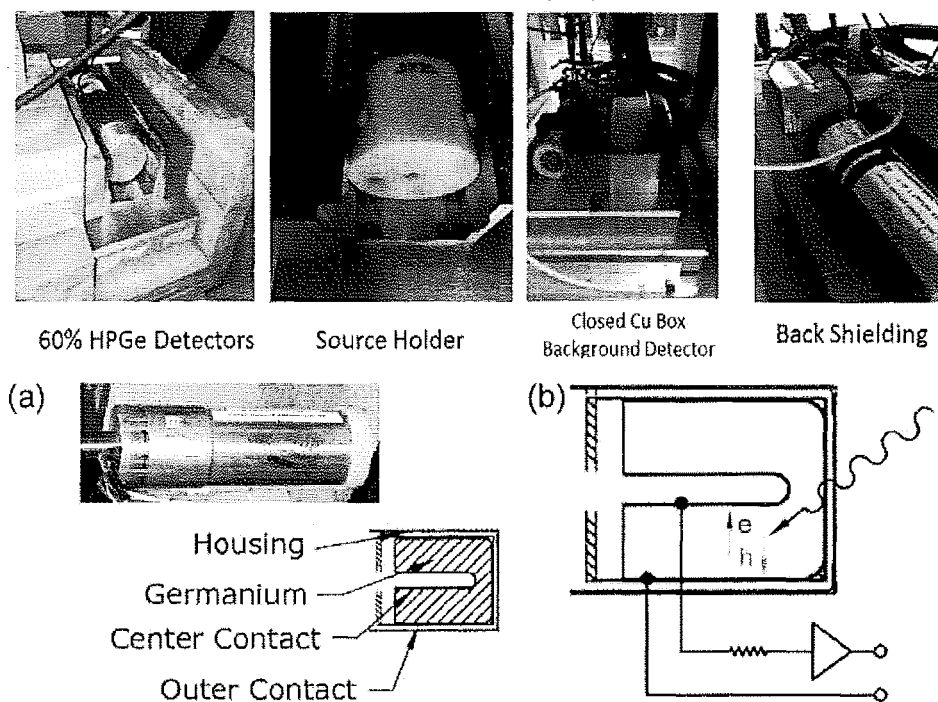


Figure 4.8. Configuration of High Purity Germanium Detector (HPGe). (a) The HPGe detector is encased in a vacuum housing. (b) The incoming gamma ray is absorbed by the crystal, and a proportional number of electron-hole charge carrier are generated. The current is sensed 1st by a cold pre-amplifier, and converted to an electric pulse.

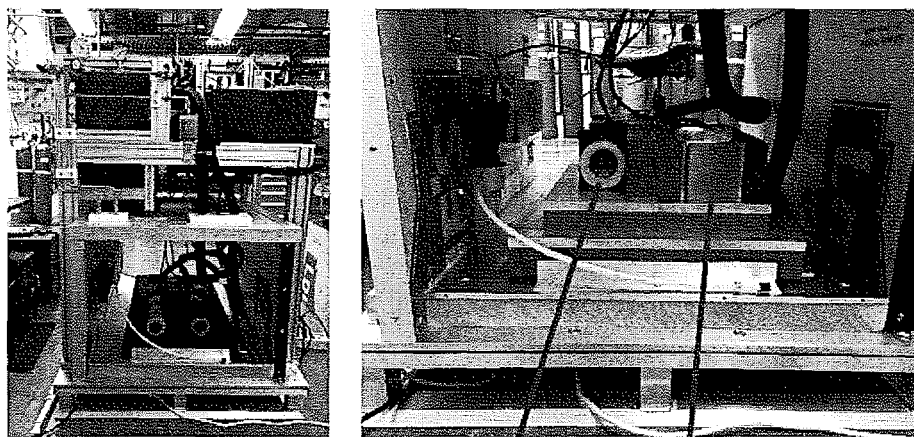
unable to operate at room temperature due to a large number of electrons able to cross the band gap of the Ge crystal. For this reason, the operational temperature of HPGe detectors was  $\sim 84^{\circ}\text{K}$  eliminating the probability of thermally excited electrons crossing the band gap into the conduction band of the crystal.

Charge carrier can be trapped on radiation-induced defects in the Ge crystal. This has the effect of broadening the line shape. For this reason, the line shape is not Gaussian, and in fact, no model can properly describe the trapping effects to the  $10^{-5}$  accuracy required in this experiment. Nonetheless, HPGe detectors have excellent

linearity as they are a gain-one device. An HPGe detector is to first order insensitive to low levels of external electric fields, magnetic fields, and ambient temperature variations.

#### 4.6 Shielding Performance, and Background Stability of the HPGe Detector

Background radiation is any radiation present in the environment which is not from the radiation source of interest. The background radiation in HFIR is due to (1) the neutrons, and gamma rays directly produced from the reactor operation, (2) cosmic radiation, (3) HPGe detector itself, (4) neutron activated building components, (5) scattered radiation from the nearby beamline operations, (6) shielding materials, (7) decay radiation from the nearby source storage room, and (8) natural



Two HPGe detectors, for *Background* and *Source* Radiations

Figure 4.9. (Left) The HPGe detector measured the background spectrum at HFIR. (Right) The HPGe source detector measured the source spectrum. Various material such as lead, aluminum, copper, and borated poly shielding have been utilized to reduce the background radiation. The complete shielding is not shown in these pictures.

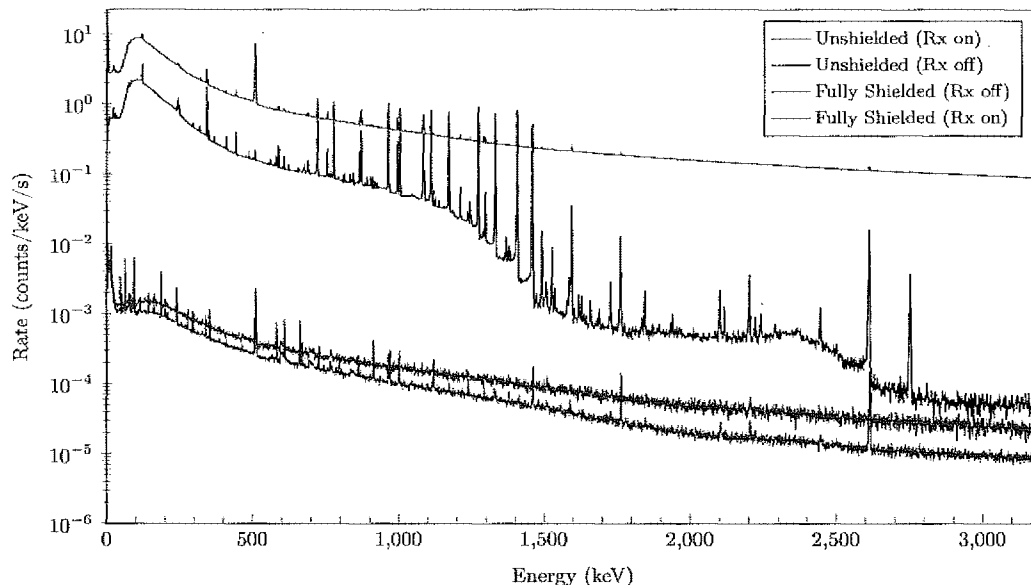


Figure 4.10. HFIR background spectra with, and without shielding in the reactor on or off status. The spectra show that the shielding was effective in suppressing the backgrounds by a factor greater than  $1.8 \times 10^{-4}$  (reactor-on), and  $6.7 \times 10^{-4}$  (reactor-off).

radioactivity within the building. As the detector is 6.53 meter from the HFIR core, the gamma rays, and neutrons produced during reactor operations are significant, and indeed become the dominant background source in the HPGe spectrometer. Various materials have been used to reduce the background based on absorption cross sections. Lead, copper, and aluminum are utilized for the  $\gamma$ -ray shielding. Borated-poly is for neutron shielding. The copper is to eliminate the fluorescence from lead, and the aluminum to eliminate the fluorescence from the copper. Figure 4.10 shows the background radiation with, and without shielding during reactor-on, and reactor-off periods. The spectra show that the shielding is effective in suppressing the backgrounds by a factor greater than  $1.8 \times 10^{-4}$  (reactor-on), and  $6.7 \times 10^{-4}$  (reactor-off).

The background spectra were collected in order to subtract the background from the  $^{54}\text{Mn}$  source spectra. The background data were collected for nearly 90 days con-

sisting of hourly, daily, and 10 days background runs after the  $^{54}\text{Mn}$  was removed on 03/09/2016. The full background measurement includes two reactor-on periods, and one reactor-off period. Before background subtraction, the time-dependence stability of the background rate is checked.

The total error in the channel by channel rate calculation in a single spectrum is given by

$$\sigma_i^2 = \frac{N_i}{(\Delta t)^2} + \frac{N_i^2}{(\Delta t)^2} \times \frac{(\delta t)^2}{(\Delta t)^2} \quad (4.9)$$

where  $N_i$  is the count for each channel of the background spectrum, and  $\Delta t$  is the live time of that background spectrum. The 1st term is the Poisson distributed statistical error, and the 2nd term is the timing error from the DSPEC-50. The DSPEC-50 reports out the live-times to an accuracy of 0.1 sec. The uncertainty due to the timing error in a uniform distribution is  $\delta t = 0.1\text{sec}/\sqrt{12} \sim 0.029$  sec.

Figure 4.11 shows the full background spectrum rate as a function of time after removing of the  $^{54}\text{Mn}$  source. Table 4.3 summarizes all the information during the background collection periods. Timing errors from the DSPEC-50 are below  $8.13 \times 10^{-7}$  cps which are negligible but tracked throughout the analysis. The rate distributions for the runs taken in Period 1, Period 2, and Period 3 are Gaussian (Figure 4.11). The width of the distributions are in agreement with the estimate found using the averaged error of the mean found for each run. As shown in Table 4.3, the statistical mean run error, and the width of the run rate distribution are in agreement. This means the calculated errors are correct as proven by the distributions.

The means of three reactor-off Periods 2, 3, and 4 are in excellent agreement with their individual variation from the averaged mean shown in the standard deviation row in Table 4.3. These results prove the background is exceptionally stable over the 74-days reactor-off period. All the reactor-off data are used for the background subtraction. The two reactor-on Period 1, and 5 are in disagreement at the level of

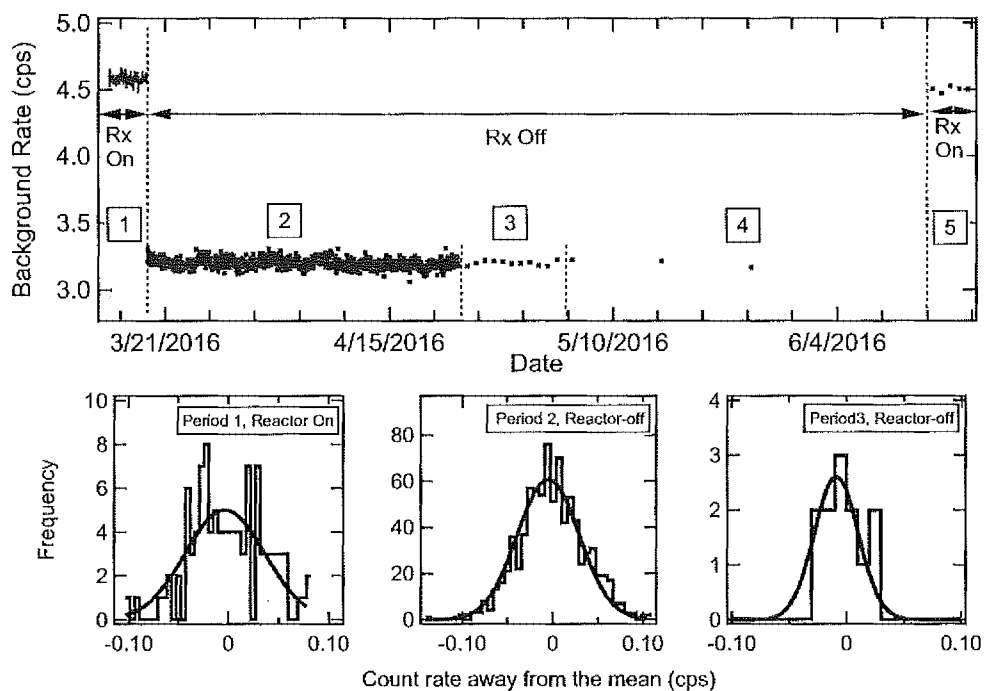


Figure 4.11. (Top) Full background spectrum rate as a function of time which includes reactor-on, and reactor-off cycles with the  $^{54}\text{Mn}$  source removed. (Left Lower) The distribution away from the mean in count rate for 1-hour runs in reactor-on Period 1. (Center Lower) The distribution away from the mean in count rate for 1-hour runs in reactor-off Period 2. (Right Lower) The distribution away from the mean in count rate for 1-day runs in reactor-off Period 3.

$0.04 \pm 0.005\text{cps}$  from the mean. While the disagreement is small, it is significant. The Period 1 data was discarded since Period 1 started just after removing the  $^{54}\text{Mn}$  source by deconstruction of the shielding, and reconstruction over a period of about a week. The 5-day Period 1 data is considered unstable as the detector system needed time to reach equilibrium. For this reason, the reactor-on background used for corrections only included Period 5, consisting of the average of 5 1-day runs.

The average full spectrum rate for the reactor-on background is  $4.502 \pm 0.003\text{cps}$  from Period 5. The average rate for the reactor-off background is  $3.2003 \pm 0.0007\text{cps}$

using Period 2, Period 3, and Period 4, that is the average of the 74 days of runs.

The average rate of  $^{54}\text{Mn}$  full spectrum is  $\sim 6500\text{cps}$ . From this, the estimated error level for the reactor-on background spectrum is  $\sim 6 \times 10^{-7}$ , and the reactor-off background error is  $\sim 1 \times 10^{-7}$ . Both are small enough to be neglected but are tracked throughout the analysis.

Table 4.3.

The average background rate, and associated error during the reactor-on or reactor-off periods at HFIR. The distribution error is not available in Period 4, and 5 due to lack of data points. S.D. means the standard deviation. The S.D from the mean is not available for reactor-on Period 1, and 5 because Period 1 data was dropped from the analysis (see text)

	Period 1	Period 2	Period 3	Period 4	Period 5
Reactor status	on	off	off	off	on
Duration (Days)	5	32	12	30	5
Single run time	1-hour	1-hour	1-day	10-day	1-day
Timing error(cps)	8.13E-07	6.77E-07	2.65E-08	2.66E-09	3.00E-08
Statistical mean run error(cps)	3.57E-02	2.99E-02	6.09E-03	1.93E-03	7.32E-03
Distribution error(cps)	3.95E-02	3.34E-02	1.80E-2	N/A	N/A
Mean rate(cps)	4.581±0.004	3.2001±0.001	3.199±0.002	3.201±0.001	4.501±0.003
Reactor-off S.D. from the mean	N/A	0.28	0.63	0.74	N/A
The average rate in all reactor-off periods :			3.2003 ± 0.0007 cps		
The average rate in all reactor-on periods :			4.502 ± 0.003 cps		



## 5. Energy Calibration of the $^{54}\text{Mn}$ , and the Background Spectra at HFIR

High Purity Germanium (HPGe) detector gamma-ray spectroscopy has wide-ranging applications. HPGe detector must be calibrated before proceeding with data correction, and analysis. That is, the relationship must be known between the energy deposited in the detector by a gamma ray, and the amplitude of the corresponding amplifier output pulse. The energy range sensitivity of commercial spectrometer systems ranges from 3 KeV to over 12 MeV. Because the Ge crystal is a gain-1 device, it is standard practice to use a linear relationship between the channel scale, and the energy scale. However, in this experiment, the electronics introduced a nonlinear term into the calibration.

To measure the calibration accurately, spectral lines are measured over the full energy range. For background spectra, 13 lines between 3 KeV, and 3 MeV were used in the calibration. These lines are produced by neutrons, neutron-induced ambient background, beta decay transitions induced by neutrons, atomic fluorescence, and natural environmental backgrounds. Because the  $^{54}\text{Mn}$  source overwhelms these background calibration lines, the  $^{54}\text{Mn}$  spectra have been calibrated using the Indium X-ray K-edge peak, the Compton edge, and back-scattered peak, the  $^{54}\text{Mn}$  photopeak, and a  $^{208}\text{Tl}$  gamma line. Both spectra type used a two-step calibration process. First, fitting the line shape for its centroid, and, second, combining all the fitting information into the non-linear detector calibration.

## 5.1 Energy Calibration of Background Spectra

Background spectra were collected in the HPGe detector with the source removed while the reactor was both in on, and off status. The background reactor-on data set was collected, from June 14, 2016, to June 19, 2016, consisting of approximately 120 hours of data. The data set consisted of 5 independent 24-hour spectra. Additional reactor-on data, consisting of 5 days of 1-hour runs, were discarded as discussed in Chapter 4. The reactor-off data set was collected from March 19, 2016, to June 04, 2016, consisting of 833 independent 1-hour spectra, 12 independent 1-day spectra, and 3 independent 10-days spectra. Figure 5.1, and Table 5.1 show the 13 spectral lines used in this calibration. The background data calibration process involves fitting the line shape for the centroid, and second combining all the fitted information into the detector calibration. The line shape was assumed to be a Gaussian distribution

Table 5.1.

Spectral lines used in the calibration of the background energy calibration. Accepted energies are from the National Nuclear Data Center, Brookhaven National Laboratory, based on ENSDF[60]. Accepted centroids are the fit bin number.

	Nuclide	Accepted Energy(KeV)	Accepted Centroid(No.)
1	<sup>210</sup> Pb	46.5390±0.0023	205.4116±0.0101
2	<sup>234</sup> Th	63.2900±0.0200	279.7169±0.0889
3	<sup>234</sup> Th	92.6000±0.0200	409.6237±0.0889
4	<sup>208</sup> Tl	583.1870±0.0091	2582.2496±0.0403
5	<sup>214</sup> Bi	609.3200±0.0090	2697.5935±0.0400
6	<sup>137</sup> Cs	661.6570±0.0073	2929.7250±0.0325
7	<sup>228</sup> Ac	911.2040±0.0129	4034.3824±0.0575
8	<sup>228</sup> Ac	968.9710±0.0206	4290.3542±0.0914
9	<sup>234m</sup> Pa	1001.0300±0.1000	4433.2512±0.4444
10	<sup>214</sup> Bi	1120.2940±0.0325	4960.8312±0.1445
11	<sup>40</sup> K	1460.8220±0.0324	6469.5223±0.1438
12	<sup>214</sup> Bi	1764.4910±0.0328	7815.7520±0.1460
13	<sup>208</sup> Tl	2614.5110±0.0224	11582.8926±0.0995

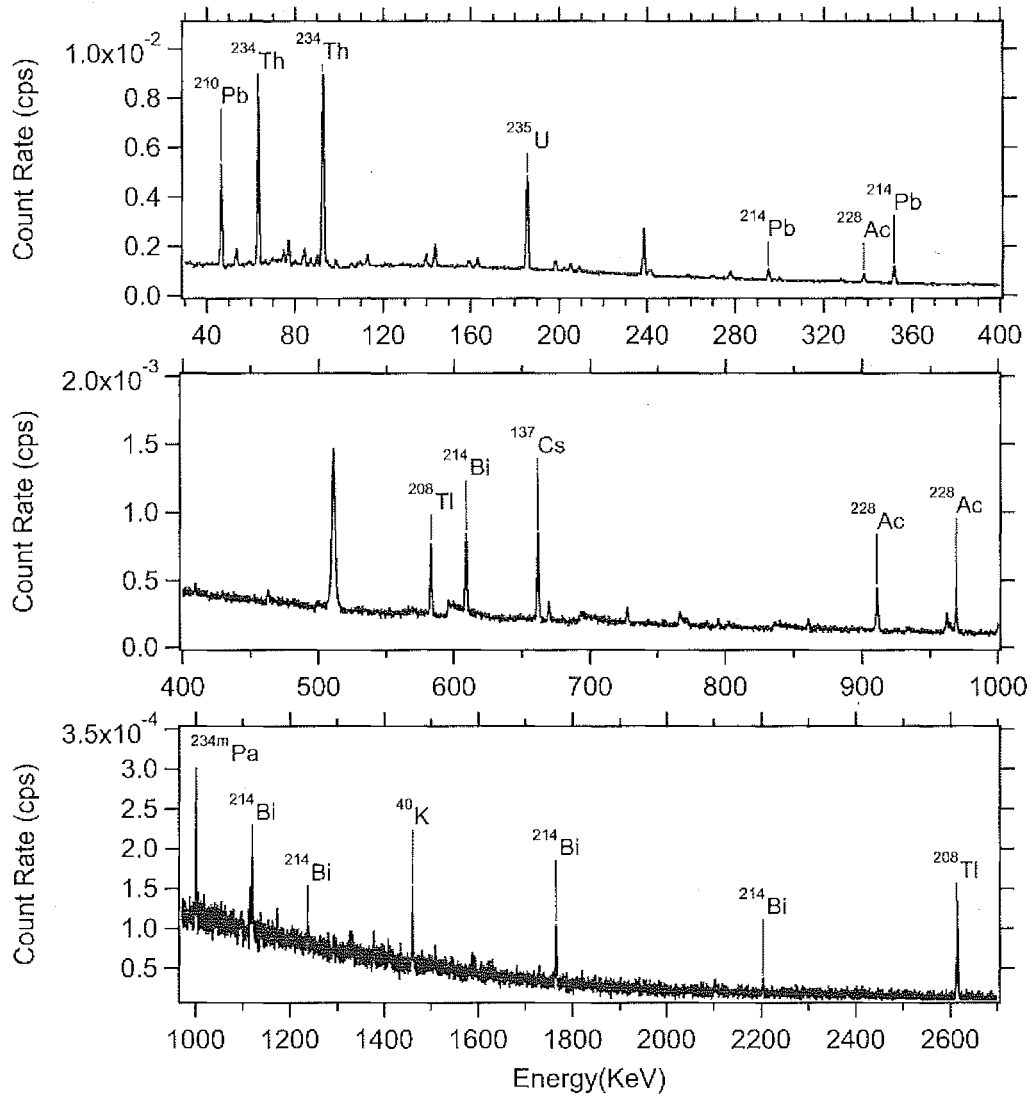


Figure 5.1. Background spectrum with 19 identified lines at HFIR. 13 spectral lines have been selected for the background spectrum energy calibration shown in Table 5.1.

with a continuous background,

$$f(x) = a + bx + cx^2 + \frac{A}{\sqrt{2\pi}\sigma} \exp\left(\frac{-(x - x_0)^2}{2\sigma^2}\right) \quad (5.1)$$

Table 5.2.

Calibration coefficients of background spectra with reactor-off for linear, and nonlinear calibration.  $\chi^2$  per degree of freedom significantly improves with the nonlinear calibration.

Background Spectral with Reactor Off Status				
Type of Calibration	$a_{back}$ (KeV)	$b_{back}$ (KeV/No.)	$c_{back}$ (KeV/No. <sup>2</sup> )	$\chi^2/DoF$
Linear	0.1824±0.0032	0.2257±1.7E-6	N/A	60.84
Non-linear	0.1466±0.0024	0.2258±2.4E-6	-1.1E-08±4.0E-10	6.46
Background Spectral with Reactor On Status				
Linear	0.1578±0.0094	0.2257±6E-6	N/A	6.61
Non-linear	0.1222±0.0072	0.2257±8E-6	-1.2E-08±1E-9	1.29

where  $a$ ,  $b$ , and  $c$  are the coefficients of the continuous background,  $A$  is the counts under the Gaussian distribution,  $x_0$  is the centroid, and  $\sigma$  is the energy resolution of the line shape. A  $\chi^2$  per degree of freedom minimization is performed using Poisson statistics weighting ( $\sqrt{N_i}$ ). The accepted line energies are from the National Nuclear Data Center(NNDC), Brookhaven National Laboratory, based on ENSDF[60]. However, the centroid resolution of the HPGe detector is not as well controlled as the uncertainty given by the standard values from the NNDC. The line shape in an HPGe detector is not well-known function if high accuracy is required. Because the measuring resolution is on the order of 1 keV, and the number of counts in each line varies considerably, it was decided to fix the error assigned to each reference line to the uncertainty listed by the NNDC or the measured error found from the fitting, whichever was larger. This method was selected so that no single line dominated the calibration fit, and the errors were dominated by the statistics, and the energy resolution of the measurements.

The Ge crystal in the HPGe detector is a gain-1 device, so it is standard practice

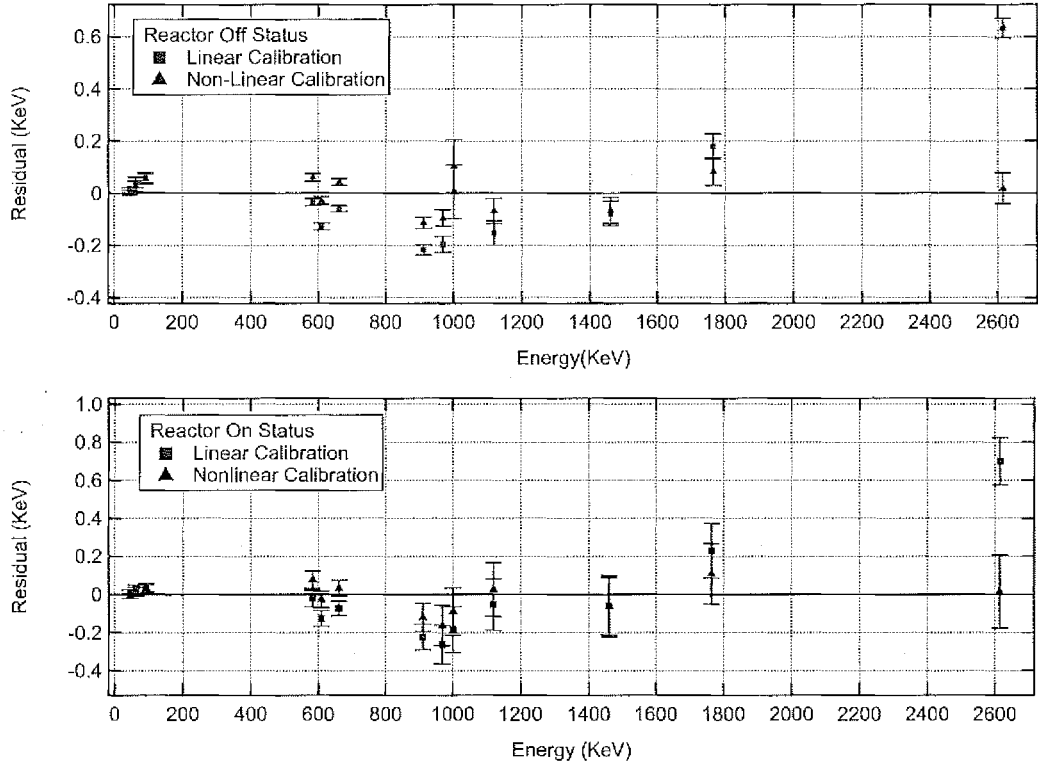


Figure 5.2. Background spectral line residuals for reactor-off, and reactor-on status. The nonlinear calibration for this experiment reduces standard deviation in the residuals of the background spectral lines.

to use a linear relationship between the channel scale, and the energy scale.

$$E_i = a_{back} + b_{back} \times i \quad (5.2)$$

The energy ( $E_i$ ) is equated to the channel number ( $i$ ) using two constants  $a_{back}$ , and  $b_{back}$  for the background calibrations. To check the goodness of the background calibration, Figure 5.2 shows the residual at each spectral line for the reactor-off, and reactor-on calibration using the linear conversion. The total  $\chi^2$  per degree of freedom ( $\chi^2_{DoF}$ ) for the linear calibration is 60.84 for the reactor-off data, and 6.61 for the reactor-on data. These results are not acceptable values. The residuals of the

background spectral lines with both reactor-on, and reactor-off are many standard deviations away from the fit. Because the experiment requires a high precision correction at the level of  $10^{-5}$ , further calibration of the background spectrum is necessary. While the HPGe detector response should be linear, the amplifier, and DSPEC-50 electronics are likely sources of the non-linear behavior. To improve the accuracy, a second-order nonlinear calibration is assumed,

$$E_i = a_{back} + b_{back} \times i + c_{back} \times i^2 \quad (5.3)$$

where  $a_{back}$ ,  $b_{back}$ , and  $c_{back}$  are the calibration coefficients. The  $\chi^2$  per degree of freedom significantly drops to 6.46 during the reactor-off period, and 1.29 during the reactor-on period. The nonlinear calibration significantly improves the standard deviation for spectral lines in the high energy range. Because the reactor-off background is a 74 days average spectrum, the  $\chi^2$  per degree of freedom for the reactor-off period is dominated by better statistical error without consideration to systematic errors. Temperature variations during this period, and the complex line shape for each spectral line causes systematic error, not taken into account in the  $\chi^2$ . It was desired to keep each lines importance related to its statistics, making the measured  $\chi^2$  acceptable. The nonlinear calibration coefficients,  $a_{back}$ ,  $b_{back}$ , and  $c_{back}$ , will be used for further background corrections to the spectral data.

## 5.2 Energy Calibration of $^{54}\text{Mn}$ $\gamma$ -Spectra

The  $^{54}\text{Mn}$  source spectra need to be converted from channel number to an energy scale so that the background energy scale can be matched to it, and subtracted. The high rate of the  $^{54}\text{Mn}$  source overwhelms all the background lines except for the high energy  $^{208}\text{Tl}$  line. For this reasons, a new set of calibration lines is required. The calibration lines are limited to 5-lines, the Indium atomic K-edge, the Backscattered Compton peak, the Compton edge peak, the  $^{54}\text{Mn}$  photopeak as well as the  $^{208}\text{Tl}$ , as shown in Figure 5.3. The pile-up lines above the photopeak cannot be used

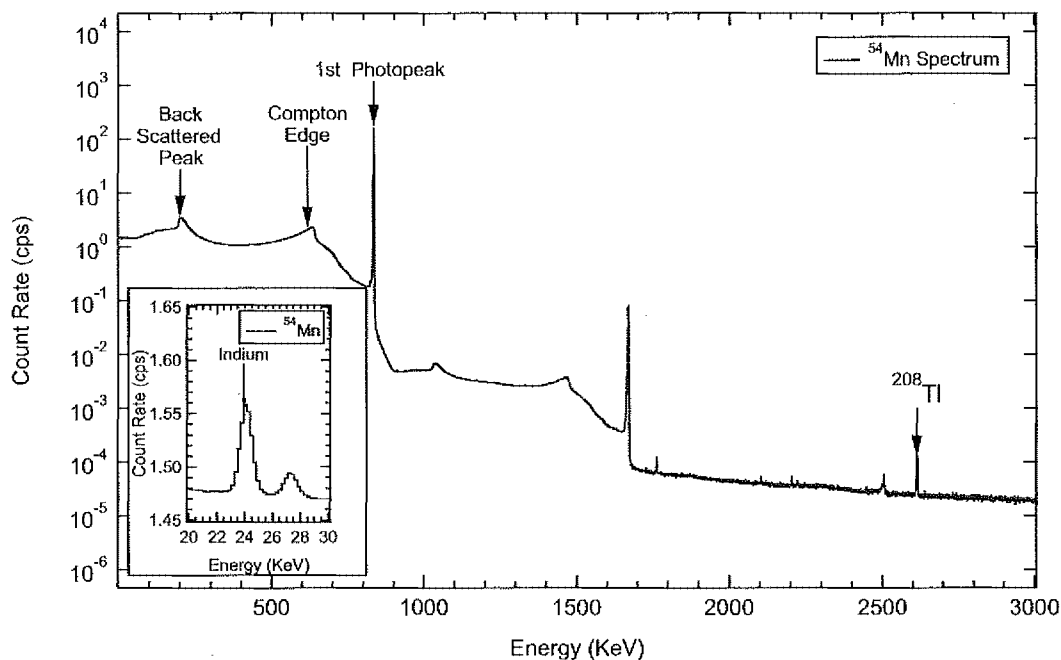


Figure 5.3. Logarithm scale of the  $^{54}\text{Mn}$   $\gamma$ -spectrum at HFIR. Indium atomic K-edge, Backscattered peak, Compton edge peak,  $^{54}\text{Mn}$  photopeak, and  $^{208}\text{Tl}$  have been used to calibrate the  $^{54}\text{Mn}$  spectra

because their precise energy is unknown. Each daily  $^{54}\text{Mn}$  spectrum is individually calibrated. The data is fit using a Gaussian distribution function which represents the complete energy deposition by the incident photon, and a second-order polynomial which represents the background spectrum,

$$f(x) = a + bx + cx^2 + \frac{A}{\sqrt{2\pi}\sigma} \exp\left(\frac{-(x - x_0)^2}{2\sigma^2}\right) \quad (5.4)$$

where  $a$ ,  $b$ , and  $c$  are the coefficients of the continuous background,  $A$  is the total count rate under the Gaussian distribution. The fit weighting of each channel is given by Poisson counting statistics. The centroid ( $x_0$ ), and energy resolution ( $\sigma$ ) are also obtained from this fitting. The energy for the  $^{54}\text{Mn}$  photopeak, and  $^{208}\text{Tl}$  are from the NNDC[60]. The energy of the Indium K-edge line is from X-ray Transition Energy

Database, Physical measurement, Laboratory, NIST[61].

The nonlinear energy calibration requires three parameters, and only three lines are usable in the  $^{54}\text{Mn}$  spectrum. This results in an unacceptable zero degree of freedom fit to the spectrum. For this reason, the Backscattered peak, and Compton edge peak were studied for this calibration. The Compton edge, and the Backscattered peak are due to incomplete absorption of the full energy of the incoming  $\gamma$ -ray. In Compton scattering, the gamma photon interacts with the electrons as if they were free or unbound. The Compton shift in energy at an angle  $\theta$  is given by

$$E_{\gamma'} = \frac{E_{\gamma}}{1 + \frac{E_{\gamma}}{m_0c^2}(1 - \cos \theta)} \quad (5.5)$$

As the incident photons are scattered, the Compton scattered electrons have a continuous distribution of energy from zero in the forward direction to a maximum when the photon is Backscattered. The Backscattered peak is due to  $^{54}\text{Mn}$  photons which first interact by a single Compton scattering with the shielding material surrounding the detector. The energy of the Backscattered photon ( $\theta = 180^\circ$ ) is

$$E_b = \frac{E_{\gamma}}{1 + 2\frac{E_{\gamma}}{m_0c^2}} \quad (5.6)$$

The Compton edge is the maximum energy of an electron from a single Compton scattering with in the detector,

$$\begin{aligned} E_{edge} &= E_{\gamma} - E_b \\ &= E_{\gamma} \left( 1 - \frac{1}{1 + 2\frac{E_{\gamma}}{m_0c^2}} \right) \end{aligned} \quad (5.7)$$

Based on the  $^{54}\text{Mn}$  photopeak energy 834.848 KeV, the predicted Backscattered energy is  $\sim 195.629$  KeV. The predicted Compton edge peak is  $\sim 639.220$  KeV. Table 5.3



Table 5.3.

Accepted energy, and uncertainty of the calibration lines for the  $^{54}\text{Mn}$  spectrum. The accepted energy, and uncertainty of Indium Atomic K-edge is from X-ray Transition Energy Database, NIST[61]. The accepted energy, and uncertainty of  $^{54}\text{Mn}$  photopeak, and  $^{208}\text{Tl}$   $\gamma$ -line are from NNDC[60]. The accepted energy of the Backscattered Peak, and Compton peaks are based on calculation in this Section. The estimated uncertainty of the Backscattered Peak, and Compton peaks are taken from the range of centroid values found by varying the fitting range.

Type of Spectral Lines	Accepted Energy (KeV)
Indium Atomic K-edge	24.002±0.017
Backscattered Peak	195.628±0.112
Compton Edge Peak	639.221±0.225
$^{54}\text{Mn}$ Photopeak	834.848±0.003
$^{208}\text{Tl}$ $\gamma$ -Line	2614.511±0.115

summarize the accepted energy, and uncertainty of each line in  $^{54}\text{Mn}$  spectrum.

The difficulty associated with these of Backscattered, and Compton edge peaks for energy calibration is to determine the centroid of those two peaks. To find the location of these peaks, a differential technique is used. The differential spectrum is give by

$$D_i = N_{i+1} - N_i \quad (5.8)$$

where  $N_i$  is the counts in the  $i$ th channel in the  $^{54}\text{Mn}$  spectra. Figure 5.4 shows the differential peaks of the Backscattered as well as Compton Edge Peak. After obtaining the centroids from the differential spectra for the Compton, and Backscattered peaks, a nonlinear function was used to calibrate the  $^{54}\text{Mn}$  daily spectrum

$$E_i^{Source} = a_r + b_r \times i + c_r \times i^2 \quad (5.9)$$

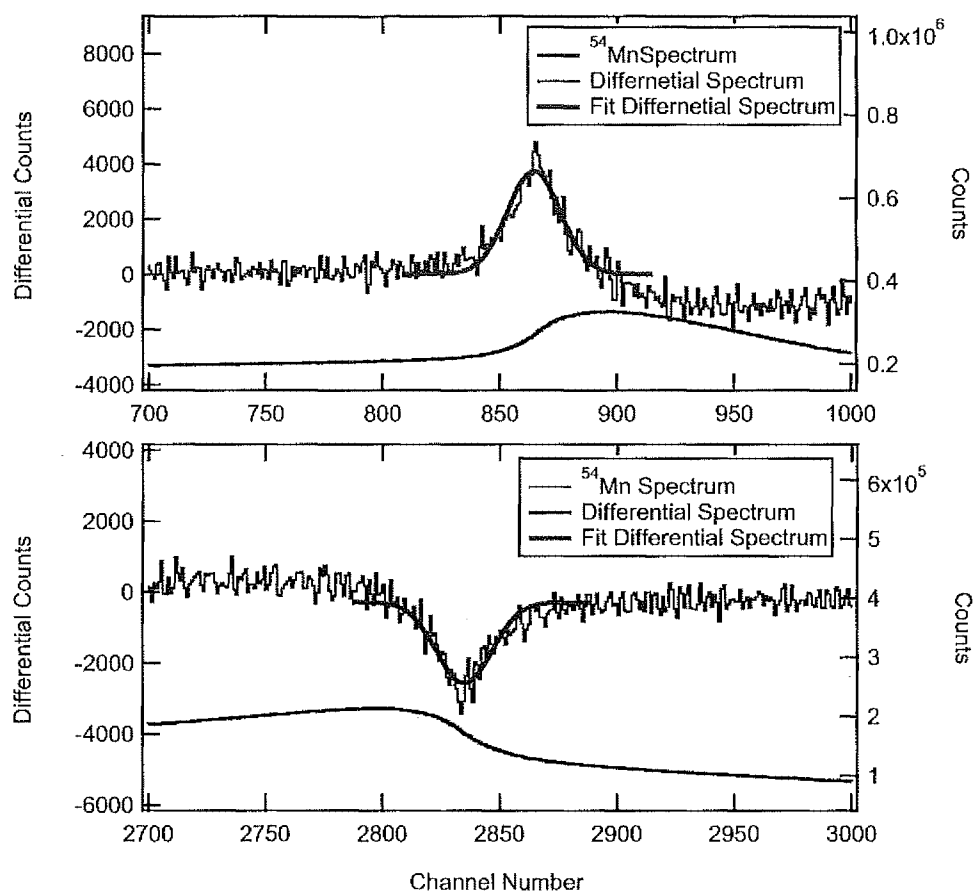


Figure 5.4. Differential Backscattered, and Compton Edges peaks from  $^{54}\text{Mn}$  daily spectra at HFIR.

where  $a_r$ ,  $b_r$ , and  $c_r$  are the coefficient of the nonlinear calibration.  $r$  represents the  $^{54}\text{Mn}$  spectrum of  $r$ th day. Unfortunately, the residuals for the Backscattered, and Compton Edge peaks were found to be unacceptable; causing unacceptable calibrations. The exact centroid value for the Backscattered, and the Compton Edge peaks depend on the source, detector, and shielding geometry. For this reason, the peak centroids of those peaks do not match the predicted energy of the Backscattered, and Compton edge peaks. In order to assign the correct centroid value of those peaks,

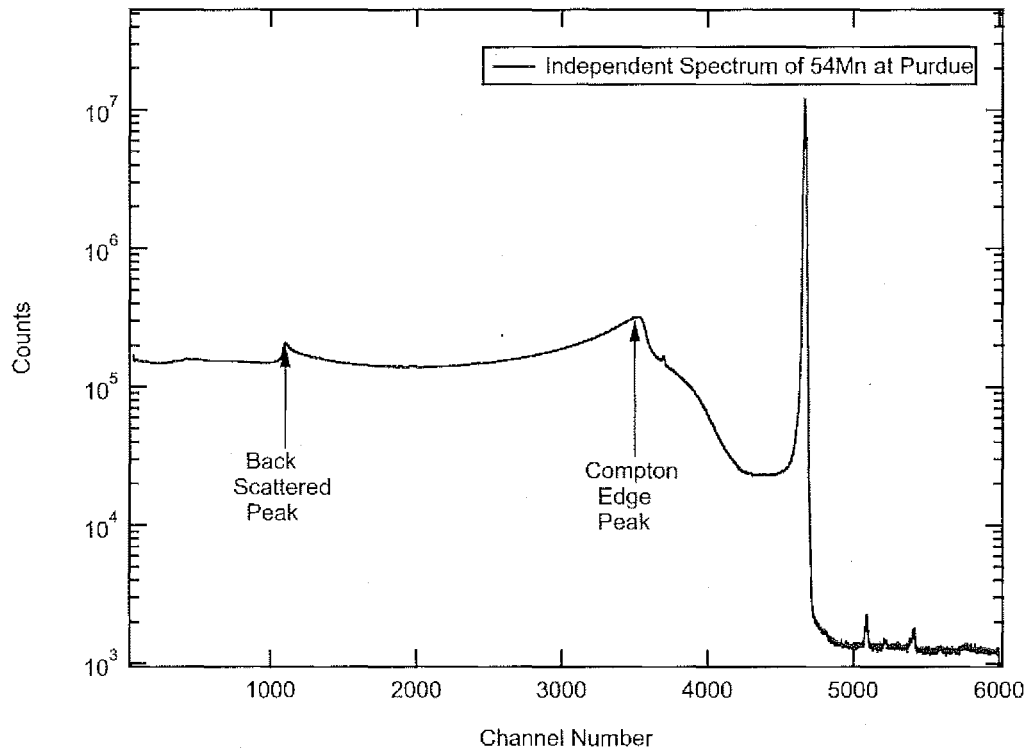


Figure 5.5. Independent  $^{54}\text{Mn}$  spectrum measured in the Physics Building at Purdue University used to study systematic shift.

the shift of the Backscattered ( $\delta E_{Back}$ ), and the Compton Edge ( $\delta E_{Compton}$ ) peaks are described as

$$E_{Back} + \delta E_{Back} + E_{Compton} + \delta E_{Compton} = E_{photopeak} \quad (5.10)$$

Because the sum of  $E_{Back}$ , and  $E_{Compton}$  is  $E_{photopeak}$ , based on the Eq.5.7, Eq. 5.10 can be simplified into

$$\delta E_{Back} = -\delta E_{Compton} \quad (5.11)$$

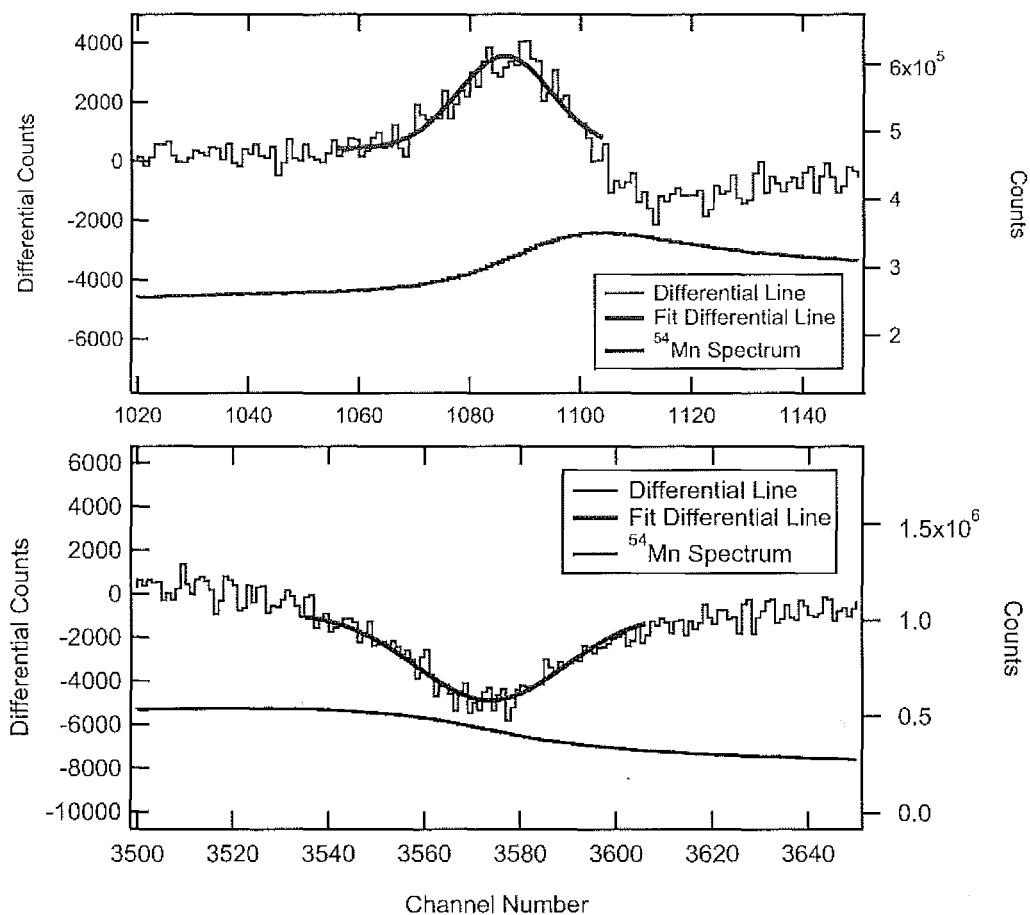


Figure 5.6. Differential Backscattered, and Compton Edges peaks from an independent measurement of the  $^{54}\text{Mn}$  daily spectrum made in the Physics Building at Purdue University to study the energy peak shift.

Eq. 5.11 shows the shift of the Backscattered Compton peak, and Compton edge peaks are equal, but of opposite sign.

$|\delta E|$  is found by taking the average shift from the nonlinear fit required to place the two differential peaks on to the fit. Only the residuals from the 1st day of the  $^{54}\text{Mn}$  data taking, the statistically most significant data, were used to calculate the

shift for all the experimental spectra. The shifted value of the Backscattered, and Compton edge peak for the HFIR data is measured to be  $\sim 0.2235$  KeV ( $\sim 1$  bin) with each peaks shifting in the opposite direction.

To verify this analysis, an independent  $^{54}\text{Mn}$  spectrum was taken using a different HPGe detector with similar geometry in the Physics Building at Purdue University. The results are shown in Figure 5.5. Figure 5.6 shows the Backscattered peak, Compton Edge peak, and their differential peaks from this measurement. Again, a nonlinear calibration was used, and the fit residuals of the Backscattered, and Compton Edge peaks from the independent spectrum were found to have the same value but with opposite sign, verifying Eq. 5.11. This method was used to optimize the calibration precision for every daily spectrum using only the first day's spectrum to find the centroid's shift value.

### Discussion of Calibration Coefficients

The results of the fitting are shown in Figure 5.7. Again, the calibration coefficient  $a_r$ ,  $b_r$ , and  $c_r$  are shown as a function of time found using the shifted centroids method.

#### Constant Terms $a_r$

The constant terms  $a_r$  vary about zero with a variance of  $\sim 0.02$  KeV or less than 10% of a single bins width at 0.225 KeV. The  $a_r$  parameters measure offsets in the energy scales.  $a_r$  is expected to be nearly zero in a low noise environment which is the case in this experiment. The stability of  $a_r$  yields a stable Region of Interest continuing the  $^{54}\text{Mn}$  photopeak.

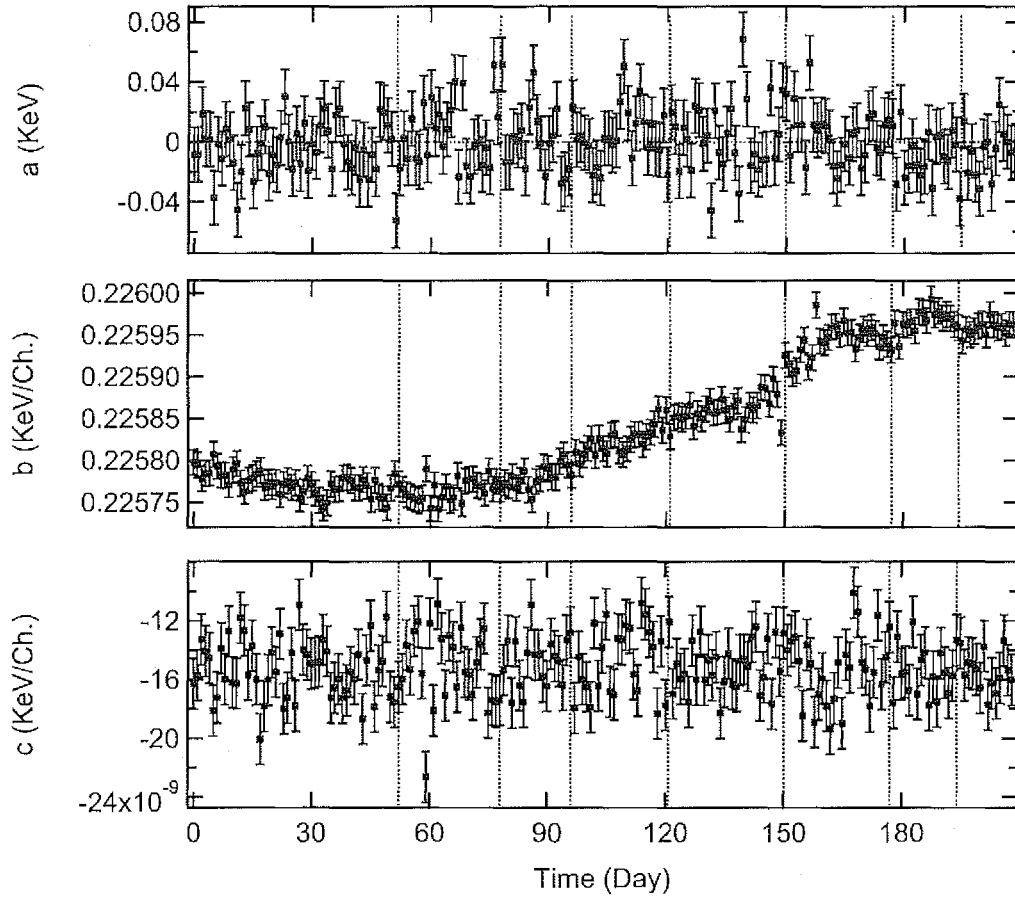


Figure 5.7. Nonlinear energy calibration parameters,  $a_r$ ,  $b_r$ , and  $c_r$ , determined for each of the daily  $^{54}\text{Mn}$  spectra.

### Linear Terms $b_r$

The linear parameter is well measured with an accuracy of  $\delta b/b \sim 7 \times 10^{-5}$ . Nonetheless, the  $b_r$  vary over the course of the experiment due to temperature variations driven by the X-cooler responding to variation in the humidity. To show this, the linear  $b_r$  parameters are fit to a periodic function,

$$b(t) = b_0 + A \sin(\omega t + \phi) \quad (5.12)$$

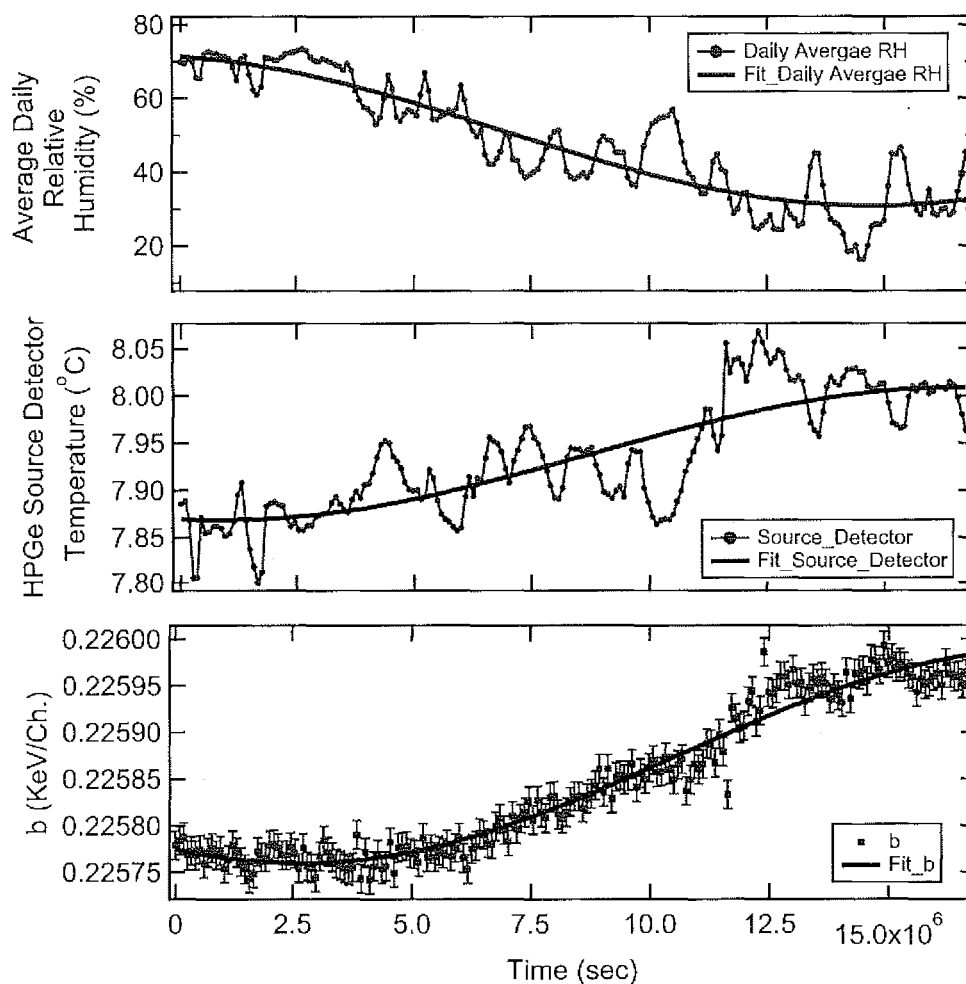


Figure 5.8. Daily averages for the humidity, temperature of the HPGe source detector, and the linear term  $b_r$ . Each is fitted with a periodic function fixed at 1 year, as a function of time.

in which  $\omega$  is fixed at 1-year. The resulting excellent fit,  $\chi^2/Dof = 1.14$ , is displayed in Figure 5.8, and the phase in Table 5.4.

Likewise, the detector temperature is fit as a function of time, with the fit shown in Figure 5.8, and Table 5.4. It should be noted that the magnitude of  $b_r$  is directly related to the detectors band gap which has a temperature dependence given

Table 5.4.

The yearly cycling of the humidity, temperature for the HPGe source detector, and linear term  $b$  values relative to the experiments starting date.

Fixed $\omega=1$ year	Negative phase ( $\phi$ )
Out of phase humidity	$103 \pm 1$ day
Source detector temperature	$101 \pm 6$ day
Linear term $b$	$122 \pm 2$ day

by Varshni's empirical form[62]. Varshni's form predicts that lower temperatures produce larger band gaps, and vice versa. Since lower  $b_r$  values represent larger band gaps,  $b$ , and the detector temperature should be in phase. As shown in Table 5.4, the phases are in reasonable agreement.

However, the temperature of the housing enclosure is held at a very stable temperature  $10.00 \pm 0.027^\circ\text{C}$ . Nonetheless, the detectors X-cooler is outside the housing. The X-cooler is affected by the humidity in the following manner, as the humidity increases the heat capacity of the air increases, allowing more efficiently cooling, lowering the temperature of the detector, and thus increasing the band gap. Likewise, as the humidity decreases, the heat capacity decreases, yielding less efficient cooling, and allowing the detector temperature to increase, narrowing the band gap. In this way, the humidity variation should be out of phase with the detector temperature, and  $b_r$  parameters as is the case shown in Figure 5.8, and Table 5.4, using the same fixed fit. While these effects are a small, they produce yearly oscillations in the data at the level of  $10^{-3}$ .

### Nonlinear Terms $c_r$

The  $c_r$  parameter is the nonlinear term, significant only for high energy spectral lines. It is due to temperature variations of the electronic outside the temperature



controlled housing specifically the DSPEC-50 spectrometer. While in the plot  $c_r$  appears stable, and small, at large channel number, for example,  $\sim 4000$  where the  $^{54}\text{Mn}$  photopeak is located, it accounts for a shifted of 1 full bin (0.225 KeV) in the spectrum. The  $c_r$  uncertainty is  $\delta c_r/c_r \sim 0.1$ , and requires further refinement. Higher accuracy in this parameter will be obtained using a "Side Band" analysis techniques as will be discussed later.

Finally, the result of the daily energy calibration shows, in Figure 5.9 the stability of the  $^{54}\text{Mn}$  photopeak using these calibration techniques. The average energy of the  $^{54}\text{Mn}$  photopeak is  $834.849 \pm 0.001$  KeV. The energy peak is exceptionally stable, and is within the uncertainty of the  $^{54}\text{Mn}$  standard error value  $\pm 0.003$  KeV[60]. The nonlinear calibration plays a critical role in the stability of the Region of Interest region, and the ability to make further accurate corrections to the spectrum.

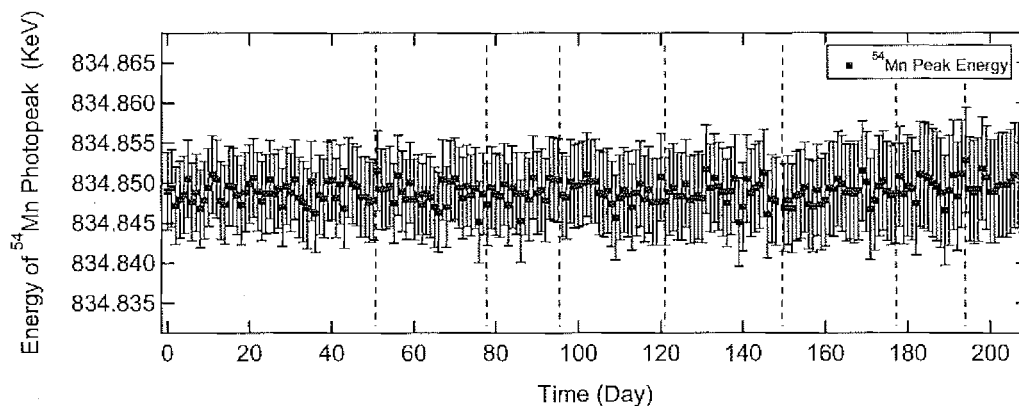


Figure 5.9. Energy of the  $^{54}\text{Mn}$  primary photopeak as a function of time. The average energy of  $^{54}\text{Mn}$  is  $834.849 \pm 0.001$  KeV which shows stability after the nonlinear calibration.



## 6. Corrections to the $^{54}\text{Mn}$ Source, and Background Spectra

The  $^{54}\text{Mn}$   $\gamma$  spectra were collected from August 14, 2015, at 23:58:22 to March 09, 2016 at 23:12:51 which includes four reactor-off, and four reactor-on periods. The total running period consisted of 95 reactor-on days, and 114 reactor-off days over 209 days of data collection. The data was collected using a 60% HPGe detector. The initial rate was 8.01 kcps with a dead time of  $\sim 13\%$ . The ending data rate was 5.05 kcps with a dead time of  $\sim 8\%$ .

Because the analysis of the HPGe spectrum requires mathematical manipulate on each channel, statistical, and systematic error must be considered channel by channel. Systematic error by definition is an error that causes a shift of the measurement away from its real value due to effects that are not entirely under the control of the experimenter. Thus, systematic error analysis requires a theory of its cause. There are three significant systematic errors associated with the measurement. (1) The Electronic Dead Time from the DSPEC-50 electronic spectrometer (2) Neutron, and natural background radiation cause an unwanted background spectrum (3) The Electronic pile-up due to the inability of the electronics spectrometer to distinguish two or more pulses occurring within a time window smaller than the electronics resolving time.

Correction procedures for obtaining the true count rate in the  $^{54}\text{Mn}$  *Region of Interest (ROI)* are summarized in Figure 6.1.

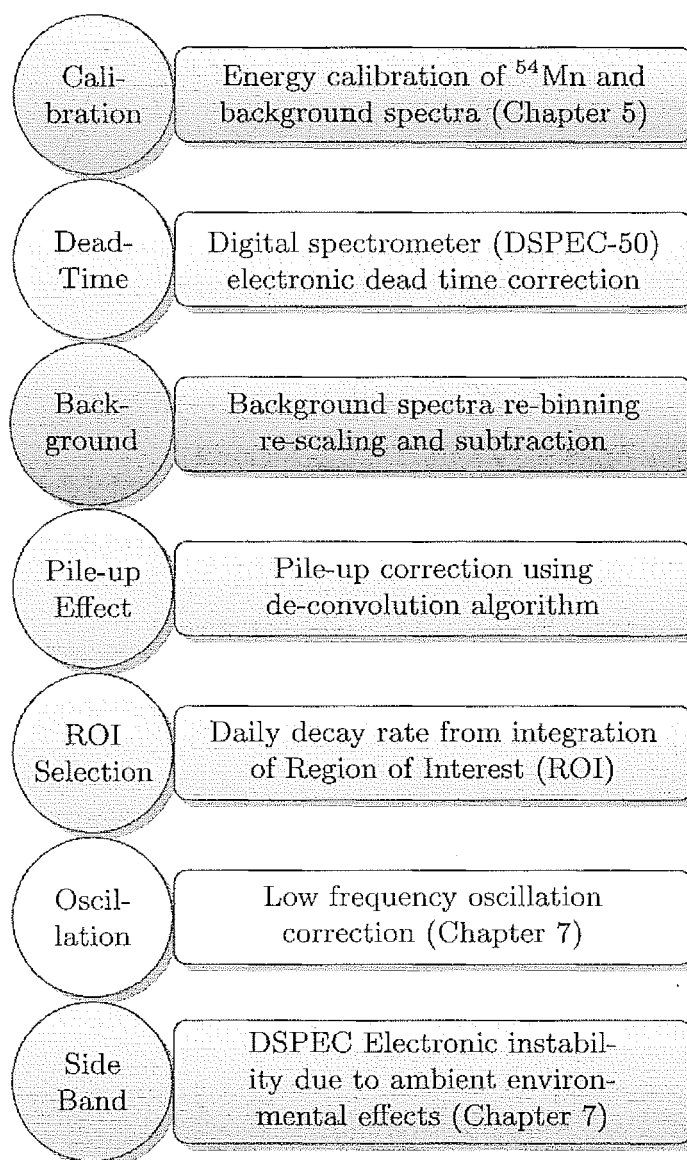


Figure 6.1. Correction procedure flow for obtaining the true  $^{54}\text{Mn}$  ROI count rate.

## 6.1 Electronic Dead Time Correction

Dead time is the integration of these periods in which the electronics do not give a response to detector pulses. The electronic spectrometer follows the non-paralyzable

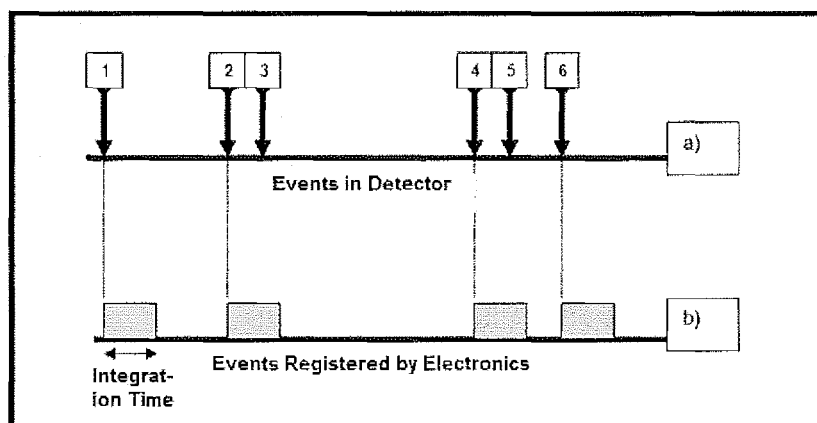


Figure 6.2. Illustration of electronic dead time from the DSPEC-50 spectrometer.

model as illustrated in Figure 6.2[63]. In this example, events 3, and 5 are not registered by the electronics because they come after the previous event before the pulse returns to the electronic baseline[64]. The ORTEC DSPEC-50 spectrometer is designed[64]

*"To optimally process an input pulse stream, and thereby obtain the best spectral resolution. (For this reason), the signal processing device..... (allows) the input signal to return to baseline before beginning to process the subsequent pulse.*

For this design approach[64],

*"The dead time for a conventionally processed pulse is the sum of the pulses rise time, flattop, and fall time."*

The DSPEC-50 has two different ways it processes the 2nd incoming pulse from the HPGe detector if the previous pulse has not returned to baseline. First, DSPEC-50 will reject the 2nd pulse if it is recognized. Second, if the 2nd pulse arrives unrecognized, that is within a shorter time than the electronic resolving time, the DSPEC-50 records the sum of two pulses which is called electronic pile-up. The dead time cor-

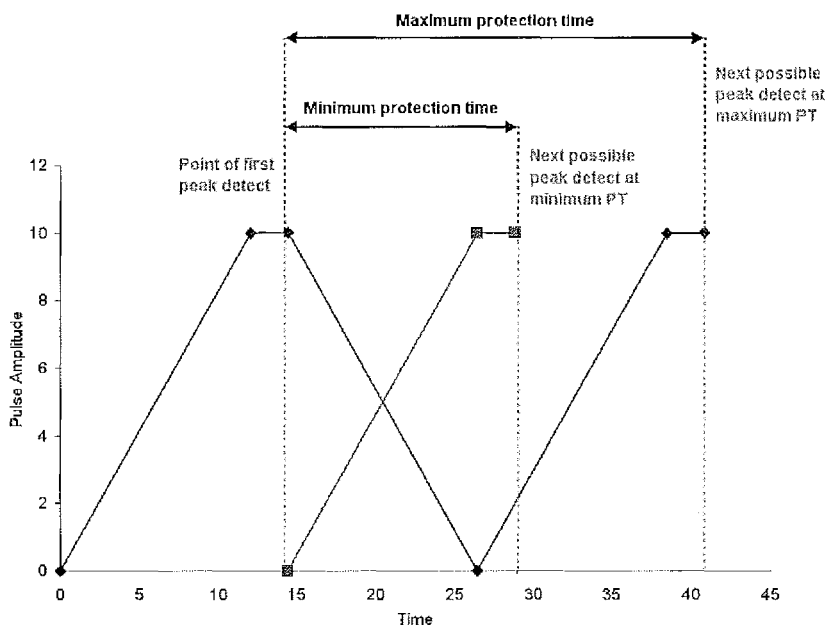


Figure 6.3. DSPEC-50's Minimum, and Maximum Protection Times[64]. At the maximum protection-time setting, the DSPEC-50 processes pulses in a conventional way. That is the dead time is the sum of the pulses rise time, flattop, and fall time. The dead time of an incoming pulse is nearly  $\sim 16 \mu\text{sec}$  for the HFIR experiment.

rection would be correct for the full spectrum if there were no electronic pile-up effect.

There are two types of pile-up effects, low energy, and high energy pile-up, defined with respect to the ROI region. The DSPEC-50 dead time correction is only correct when applied to the photopeak counts. However, the analysis uses an ROI not limited to the photopeak. The dead time correction does correctly account for the high energy pile-up, that is the loss of events out of the ROI region. However, the dead time correction does not take into account the lower energy pile-up effect. That is low energy events combining to an energy that places the combined event into the photopeak Region of Interest. Triple pile-up is also observed at the level of  $10^{-6}$  of

Table 6.1.

Properties of the full  $^{54}\text{Mn}$  spectrum. The 1st day spectrum is in a reactor-off period. The last day of the spectrum is in a reactor-on period.

Full Spectrum Daily Ratio	First Day (Reactor-off)	Last Day (Reactor-on)
Spectrum rate (cps)	8009.5	5054.5
Background rate (Fractional rate) (cps)	3.1(0.04%)	4.7 (0.09%)
Pile-up rate (cps)	33.5 (0.4%)	13.7 (0.04%)
Dead time for a day (sec)	11166.4	7235.9
Pulse generated dead time ( $\mu\text{sec}$ )	16	16
Double pulse time resolution ( $\mu\text{sec}$ )	0.5	0.5
Dead time rate for background rate (cps)	0.013	0.012

the photopeak rate, and is neglected in this analysis.

Table 6.1 gives the properties of the  $^{54}\text{Mn}$  spectrum using the corrections. While it may appear optimal to finalize the dead time corrections before moving on to other corrections, this is not possible. The pile-up correction is entangled with other corrections as will be shown later. The dead time correction is accurate to  $10^{-3}$  if pile-up is not taken into account. The pile-up correction can be untangled by first noting in Table 6.1 that the full spectrum background pile-up with the source is only 0.013 cps, calculated using the double pulse time resolution  $0.5 \mu\text{sec}$ . This, of course, is much smaller in the Region of Interest. For this reason, the background-source pile-up is negligible allowing the background to be first subtracted from the dead time corrected source spectrum.

## 6.2 Background Spectrum Correction

Before background subtraction can proceed, it must be noted the  $^{54}\text{Mn}$  source spectra, and background spectra have been calibrated using different nonlinear calibrations. As with this, and other corrections, the  $^{54}\text{Mn}$  spectrum is never energy

scale altered during correction. Corrections are always energy matched to the  $^{54}\text{Mn}$  calibration. In this way, the correction contributes to the minimum possible error to the analysis. For this reason, the background correction is a three-step process. (1) The dead time correction is made channel by channel. (2) The second step requires energy rescaling of the background data to match the difference in energy calibration parameters between the  $^{54}\text{Mn}$  data, and the background data. (3) The third step is to adjust for the difference in the background rate between the  $^{54}\text{Mn}$  data, and the collected background data. The collected background is normalized to the daily rate above the triple  $^{54}\text{Mn}$  pile-up of the photopeak, in the range  $E_{low} = 2515$  to  $E_{high} = 3680$  KeV, using a single scaling parameter. This region has no pile-up effects. The total number of counts must match in the  $^{54}\text{Mn}$  source, and background histograms in this comparison region. After completing all the correction to the background, the resulting background spectrum is subtracted from the  $^{54}\text{Mn}$  source spectrum.

### 6.2.1 Technical Process for Dead Time Correction

The dead time correction is made channel by channel each day, requiring the timing errors reported out by the DSPEC-50 to be included for each channel calculation. The channel by channel correction must be made as other corrections require channel by channel accounting. The  $^{54}\text{Mn}$  spectrum from the DSPEC-50 includes 16384 channels. The channel by channel correction is accomplished as follows. First, the rate in each channel of the spectrum is found

$$R_i = \frac{N_i}{\Delta t} \quad (6.1)$$

where  $N_i$  is the raw counts of  $i$ th channel, and  $\Delta t$  represents the live time of the spectrum. The live time is the period the detector electronics respond to the detector pulses. In another word, it is the real-time minus the dead time for each spectrum.



The variance associated with the  $i$ th channel of the spectrum is

$$\sigma_i^2 = \frac{N_i}{(\Delta t)^2} + \frac{(N_i)^2}{(\Delta t)^2} \times \frac{(\delta t)^2}{(\Delta t)^2} \quad (6.2)$$

The 1st term is from the statistical uncertainty of the Poisson distributed for the  $i$ th channel counts in the spectrum. The second term is the DSPEC-50 timing error which reports out the live times ( $\Delta t$ ) to an accuracy of 0.1 sec. The timing error is a uniform squared distribution, yielding a variance of  $\delta t = 0.1 \text{ sec}/\sqrt{12} = 0.029 \text{ secs}$ . The dominate error in the HPGe spectrum is the statistical error. The timing error from the DSPEC-50 is at the level of  $10^{-7}$ , and it is negligible but tracked in the total error estimation.

### 6.2.2 Background Spectrum Energy Rescaling

The 2nd step in the energy rescaling process is to assign the energy value associated with a background spectrum bin to a location within the  $^{54}\text{Mn}$  bin taking into account the different calibration values of the  $^{54}\text{Mn}$  source, and background spectra. During calibration, each gamma-ray line is fit using channel number which is an integer. The fitting program assigns an integer value channel number bin ( $i$ ) to an integer number of counts ( $N_i$ ) associated with that bin ( $i$ ). Thus, each pair [ $B(i)$ ,  $N(i)$ ] is what the fitting programs operate on. The assumption is that  $N(i)$  is associated with the central value of the bin. That is  $B(i)$ , and  $N(i)$  are located at the center of the bin.

The energy calibration of each daily spectrum

$$E_r^{\text{Source}}(i) = a_r + b_r \times i + c_r \times i^2 \quad (6.3)$$

where  $r$  is the run number, and  $i$  represents the index for each bin for the  $^{54}\text{Mn}$  source spectrum.  $a_r$ ,  $b_r$ , and  $c_r$  is the daily calibration coefficient which is shown in

Figure 5.7. Likewise, the reactor-on, and reactor-off background data were calibrated using the spectral lines shown in Table 5.1. These yield two calibrations,

$$\begin{aligned} E_{off}^{back}(j) &= a_{off}^{back} + b_{off}^{back} \times j + c_{off}^{back} \times j^2 \\ E_{on}^{back}(j) &= a_{on}^{back} + b_{on}^{back} \times j + c_{on}^{back} \times j^2 \end{aligned} \quad (6.4)$$

where  $j$  represents the index for each bin for each background spectrum.  $a_{off}^{back}$ ,  $b_{off}^{back}$ , and  $c_{off}^{back}$  are the calibration coefficients of reactor-off background spectrum, and  $a_{on}^{back}$ ,  $b_{on}^{back}$ , and  $c_{on}^{back}$  are the calibration coefficients of reactor-on background spectrum, as shown in Table 5.2. Because both the  $^{54}\text{Mn}$ , and the background spectra have nonlinear calibrations, it is convenient to use the calculated energy scale directly in the energy rescaling process. The background spectra were re-scaled to match the energy scaling in each  $^{54}\text{Mn}$  spectrum. The new background value  $V_i^*$  is the estimated background associated with the  $i$ th bin in the  $^{54}\text{Mn}$  source data histogram, that is

$$\begin{aligned} V_{background}^*(i) &= \frac{E_r^{source}(i+1) - E^{back}(j)}{E^{back}(j+1) - E^{back}(j)} \times V^{back}(j) \\ &+ \frac{E^{back}(j+1) - E_r^{source}(i+1)}{E^{back}(j+2) - E^{back}(j+1)} \times V^{back}(j+1) \end{aligned} \quad (6.5)$$

where  $V^{back}(j)$ , and  $V^{back}(j+1)$  are the original background values in the  $j$ , and  $(j+1)$  background spectrum bins. If the  $^{54}\text{Mn}$  source spectrum was collected in the reactor-off period, the  $E^{back}(j)$ , and  $V^{back}(j)$  will be  $E_{off}^{back}(j)$ , and  $V_{off}^{back}(j)$  for the  $j$  index of the reactor-off background spectrum. Similarly, if the  $^{54}\text{Mn}$  source spectrum was collected in the reactor-on period, the  $E^{back}(j)$ , and  $V^{back}(j)$  will be  $E_{on}^{back}(j)$ , and  $V_{on}^{back}(j)$  for  $j$  index of the reactor-on background spectrum. The new uncertainty value  $\sigma^*(i)$  in the estimated background associated with the  $i$ th bin in the source data histogram

$$\begin{aligned} (\sigma_{background}^*(i))^2 &= \left( \frac{E_r^{source}(i+1) - E^{back}(j)}{E^{back}(j+1) - E^{back}(j)} \right)^2 \times (\sigma^{back}(j))^2 \\ &+ \left( \frac{E^{back}(j+1) - E_r^{source}(i+1)}{E^{back}(j+2) - E^{back}(j+1)} \right)^2 \times (\sigma^{back}(j+1))^2 \end{aligned} \quad (6.6)$$

where  $\sigma^{back}(j)$ , and  $\sigma^{back}(j+1)$  are the original background values in  $j$ , and  $(j+1)$  bins. After the energy rescaling process for the reactor-on, and the reactor-off background spectra, the background, and  $^{54}\text{Mn}$  source spectral histograms have been aligned. No additional error is assigned to the energy rescaling process as the number of counts is conserved. After the daily  $^{54}\text{Mn}$  source spectrum, and background spectrum are aligned, the background spectrum is ready for amplitude rescaling.

### 6.2.3 Background Spectrum Amplitude Rescaling

To re-scale the background amplitude, the  $^{54}\text{Mn}$  spectrum, and the reactor-on or reactor-off background spectrum is summed above the third photopeak for comparison. Because the comparison region is above the triple pile-up of the photopeak, the  $^{54}\text{Mn}$  source contributes negligibly to counts within this region. Thus, the summation of the rate in this region represents the background rate during the 24-hour measurement.

The  $^{54}\text{Mn}$  calibration parameters vary day to day for each spectrum. For this reason, the edge of the energy band of the comparison region can fall between the bin boundaries. The low, and high comparison band boundary have been set to  $E_{low} = 2515$  keV, and  $E_{high} = 3680$  keV above the 3rd photopeak which contains only background. The bin integration extends from

$$\begin{aligned} k_{low} &= \frac{-b_r + \sqrt{b_r^2 - 4c_r(a_r - E_{low})}}{2c_r} \\ k_{high} &= \frac{-b_r + \sqrt{b_r^2 - 4c_r(a_r - E_{high})}}{2c_r} \end{aligned} \quad (6.7)$$

where  $k$  is not an integer number in the above equations. It must be remembered that integer values of  $k$  represent the bin center. The fractional part of the first bin to be summed, and the sum start index is determined by

$$V_{\text{Fraction}}^{\text{Start}} = (1 - F[k_{\text{low}}]) \times V_{I[k_{\text{low}}]}^* \quad (6.8)$$

where  $F$  is a fraction that takes the fractional part of the number, and  $I$  is a fraction that takes the integer part of the number. The fractional part of the last bin, and the sum end index is determined from,

$$V_{\text{Fraction}}^{\text{End}} = F[k_{\text{high}}] \times V_{I[k_{\text{high}}]}^*. \quad (6.9)$$

From these evaluations the total rate sum,  $S$  is then found

$$S = V_{\text{Fraction}}^{\text{Start}} + \sum_{k=I[k_{\text{low}}]+1}^{I[k_{\text{high}}]} V(k) + V_{\text{Fraction}}^{\text{End}}. \quad (6.10)$$

Notice that the start, and end indices need to be calculated for every days run as the calibration coefficients vary each day. Because no counts have been lost during this process, the statistical error associated with the sum is  $\sim \sqrt{S}$ . The other contributions to the error, such as the dead time corrections have already been taken into account before this calculation. Because the error associated with this correction is so much smaller than the errors already calculated for each bin in the  $^{54}\text{Mn}$  spectrum, no error will be assigned to this correction.

The amplitude of the background spectra is shifted to match the estimated background found in the  $^{54}\text{Mn}$  spectrum by comparing the energy region above the 3-event pileup photopeak with the background data observed in that same region. Every bin of the background spectrum is scaled by

$$V(i)^{**}_{\text{background}} = \frac{S_{\text{source}}}{S_{\text{background}}} V^*(i)_{\text{background}}, \quad (6.11)$$

and the associated error is simply scaled

$$\sigma(i)_{background}^{**} = \frac{S_{source}}{S_{background}} \sigma^*(i)_{background} \quad (6.12)$$

As has been stated the parameters, and binning of the collected  $^{54}\text{Mn}$  source spectra are not altered in this process. All background spectra subtractions to the  $^{54}\text{Mn}$  source data sets are accomplished by altering the parameters, and binning of the near zero error of the background data set.

#### 6.2.4 Background Spectrum Subtraction

After completion of the energy rescaling, and amplitude rescaling for background spectrum, the resulting background spectrum can be subtracted from the  $^{54}\text{Mn}$  source spectrum. Figure 6.4 compares the 1st day of the  $^{54}\text{Mn}$  spectrum before background correction, and the background spectrum after the matching correction. The process is channel by channel (bin by bin) subtraction using either the reactor-on background or reactor-off background spectra. The corrected  $V(i)_{corrected}$  at the  $i$ th bin is

$$V(i)_{corrected} = V(i)_{source} - \frac{S_{source}}{S_{background}} V^*(i)_{background} \quad (6.13)$$

where  $V(i)_{source}$  is the value at the  $i$ th bin from the  $^{54}\text{Mn}$  source spectrum.

The corrected uncertainty  $\sigma(i)_{corrected}$  for the  $i$ th bin is

$$\sigma(i)_{corrected} = \sqrt{(\sigma(i)_{source})^2 + (\sigma(i)_{amplitude})^2 + (\sigma(i)_{background}^{**})^2} \quad (6.14)$$

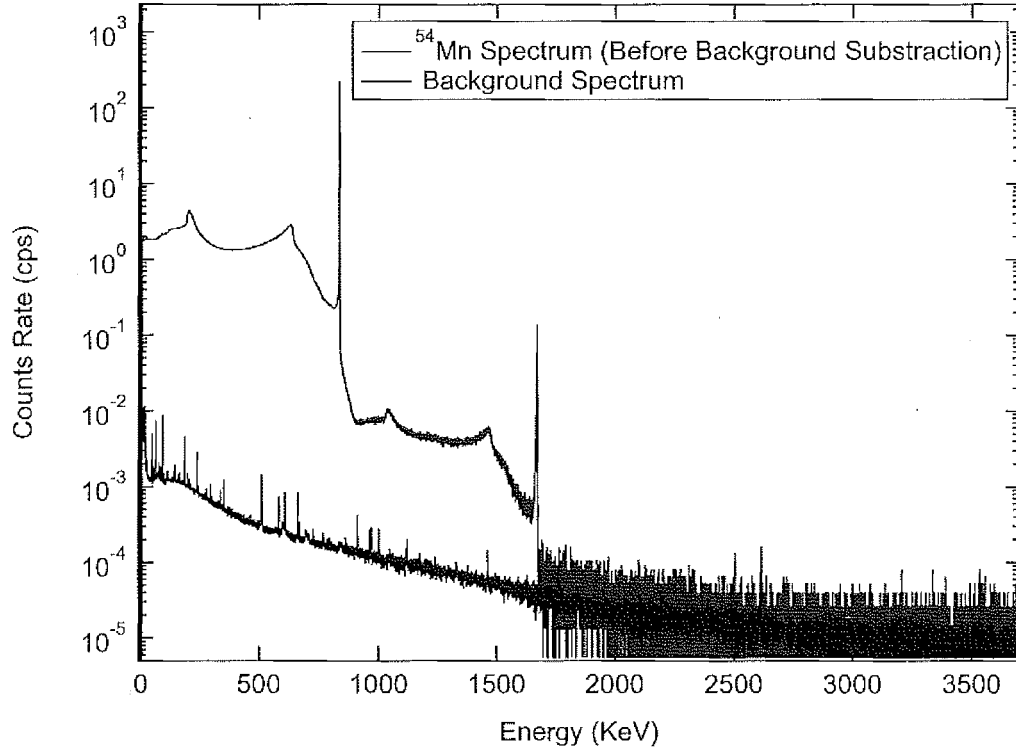


Figure 6.4. Logarithm scale of the  $^{54}\text{Mn}$   $\gamma$ -spectrum before background spectrum subtraction, and the background spectrum

where  $\sigma(i)_{source}$  is the uncertainty in the  $i$ th bin of the  $^{54}\text{Mn}$  source spectrum.  $\sigma(i)_{amplitude}$  considers the errors in  $S_{background}$ . The ratio of the  $^{54}\text{Mn}$  spectrum's error to the error caused by amplitude scaling of the background is

$$\frac{\sigma(i)_{amplitude}}{\sigma(i)_{source}} = \frac{\delta S_{source} \times V(i)_{background}^*}{S_{background} \times V(i)_{source}} \sim \left\{ \begin{array}{l} 2 \times 10^{-3} \text{ In the Compton Region} \\ 1 \times 10^{-4} \text{ In the ROI Region} \end{array} \right\} \quad (6.15)$$

where  $S_{background} \sim 0.06$  cps, and the values of  $\delta S_{source}$ ,  $V(i)_{background}^*$ , and  $V(i)_{source}$  are taken from Figure 6.4. The background  $\sigma(i)_{background}$ , and the amplitude scaling

error  $\sigma(i)_{amplitude}$  are extremely small compared to the statistical error in the  $^{54}\text{Mn}$  spectrum, and are dropped. The corrected  $\sigma(i)_{corrected}$  uncertainty in the  $i$ th bin is

$$\sigma(i)_{corrected} \sim \sigma(i)_{source} \quad (6.16)$$

Thus, the background subtraction contributes no error to the  $^{54}\text{Mn}$  spectrum.

### 6.3 Pile-up Correction by De-convolution Algorithm

With the background correction completed, the pile-up correction can be made. Figure 6.5 shows the full  $^{54}\text{Mn}$   $\gamma$ -ray spectrum after background subtraction. The  $^{54}\text{Mn}$  spectrum consists of a "Compton" region in which the full energy of the  $\gamma$ -ray was not completely absorbed. This region is labelled Region 1 in Figure 6.5. The full-energy peak or the photopeak is produced by the complete absorption of the  $\gamma$ -energy, as shown in Region 2. The ratio of events in Region 1 to Region 2 is nearly 3. One of the major systematic errors in the  $^{54}\text{Mn}$  spectrum is the electronic pile-up. The pile-up, shown in Region 3, and 4, is caused by two independent nuclear decay photons which interact with the detector within a time period shorter than the resolving time of the detector. Because the primary photopeak can be treated as a  $\delta$ -function, the pile-up Region 3, and 4 appears as an integration of the "Compton" Region 1, with the photopeak, Region 2, yielding a mirror-like image of the lower energy single,  $\gamma$ -ray region, but at higher energy. Region 3, and 4 is called the first pile-up of the  $^{54}\text{Mn}$  spectrum that has the ratio of  $10^{-2}$  to the 1st photopeak. Region 5, and 6 are called the second pile-up of the  $^{54}\text{Mn}$  spectrum in which 3  $\gamma$ -rays interact with the detector in a time shorter than the resolving time. This region has a ratio to the primary photopeak of nearly  $10^{-5}$ . The expected measuring sensitivity in the experiment is to be 1 part in  $10^5$ , so the pile-up corrections play a key role to improve the measuring sensitivity.

To obtain a highly accurate single-events  $^{54}\text{Mn}$  spectrum, the piled-up events are removed through an iterative de-convolution algorithm. This procedure is per-

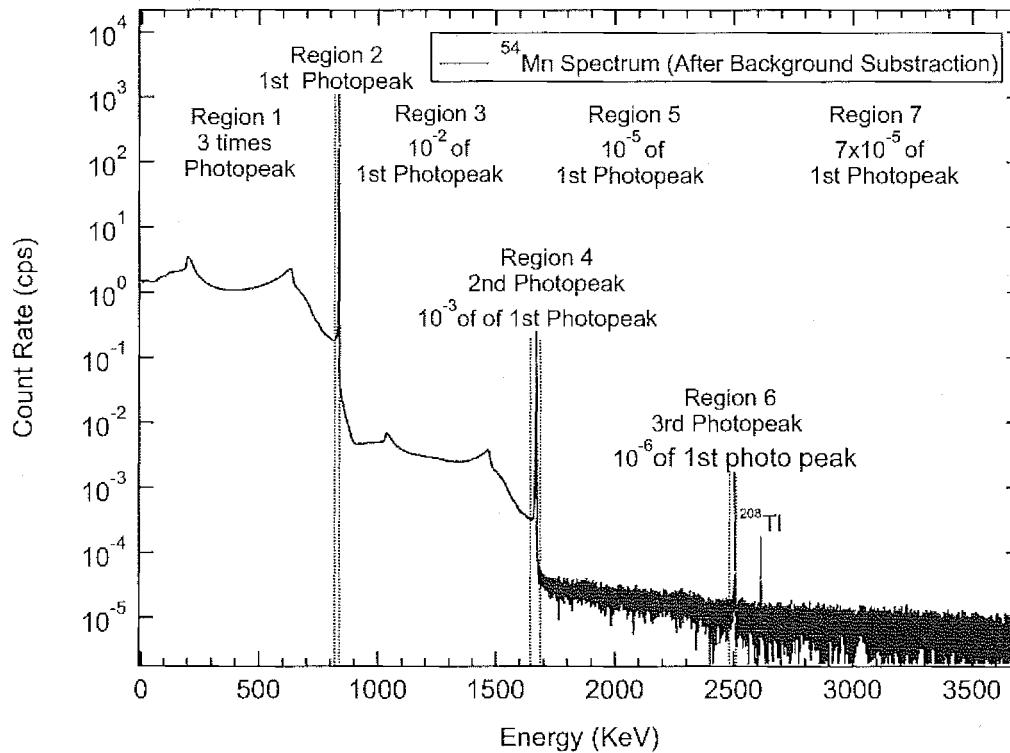


Figure 6.5. Logarithm scale of the  $^{54}\text{Mn}$   $\gamma$ -ray spectrum after background subtraction. The  $^{54}\text{Mn}$  photopeak is at 834.848 KeV. The second coincident photopeak shows at  $\sim 1665$  KeV, and the third coincident photopeak shows at  $\sim 2497$  KeV.

formed for the energy-calibrated spectra, and background subtracted spectra. Each de-convolution cycle starts with only the energy region containing the photopeak, and below. It proceeds by calculating destination bin of any two events residing in the single-events region, and as a metric computes the reduced S-value of the residuals between the input spectrum to the resulting de-convolution in the first-order pileup region[65]. The de-convolution spectrum is generated in the following way,

$$P_k(E_i + E_j) = \sum_{k=i+j} P_i(E_i) * P_j(E_j) \quad (6.17)$$



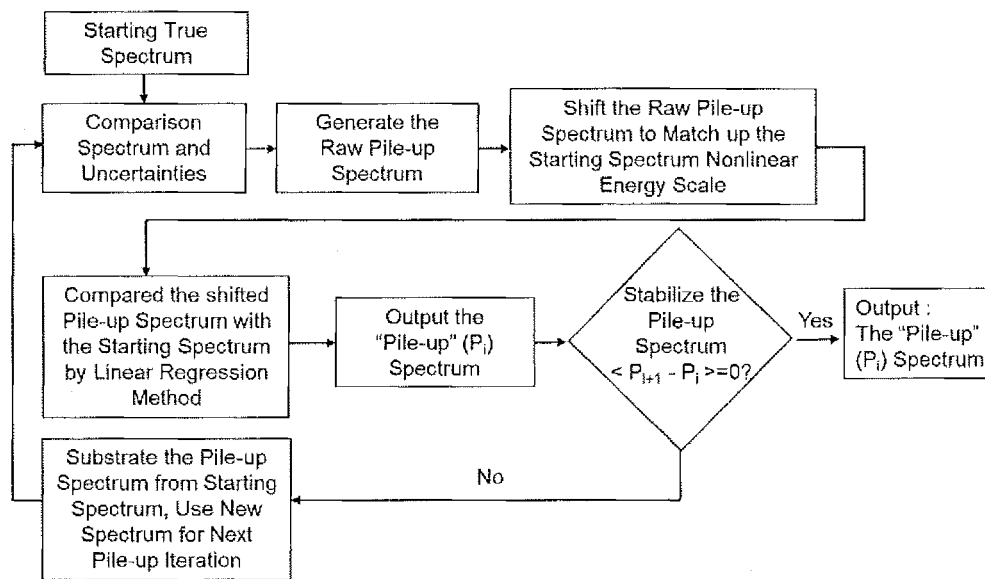


Figure 6.6. De-convolution algorithm used to determine pileup events to be removed from the  $^{54}\text{Mn}$  spectrum.

where it is assumed that the energy value refers to the bin center. Unfortunately, the energy associated with the convoluted bin  $k$  does not match the energy bins associated with the original energy spectrum because of the nonlinear calibration. The de-convolution spectrum must be appropriately energy scaled before it can be subtracted from the original energy spectrum. Thus, the energy scale of the pile-up spectrum must be corrected to match the original spectrum energy scale. Because the energy scale of the  $^{54}\text{Mn}$  spectra is non-linear, it is convenient to match up energy scales directly for this subtraction process. Again, only the pile-up spectrum is manipulated. This procedure is similar in the previous background correction process.

Once the pile-up spectrum is generated, and appropriately energy matched to the  $^{54}\text{Mn}$  spectrum, the pile-up spectrum is then compared with the 1st pile-up region input the spectrum for amplitude rescaling. The comparison region for the source, and the pileup spectrum is the energy region between the end of the primary photo-

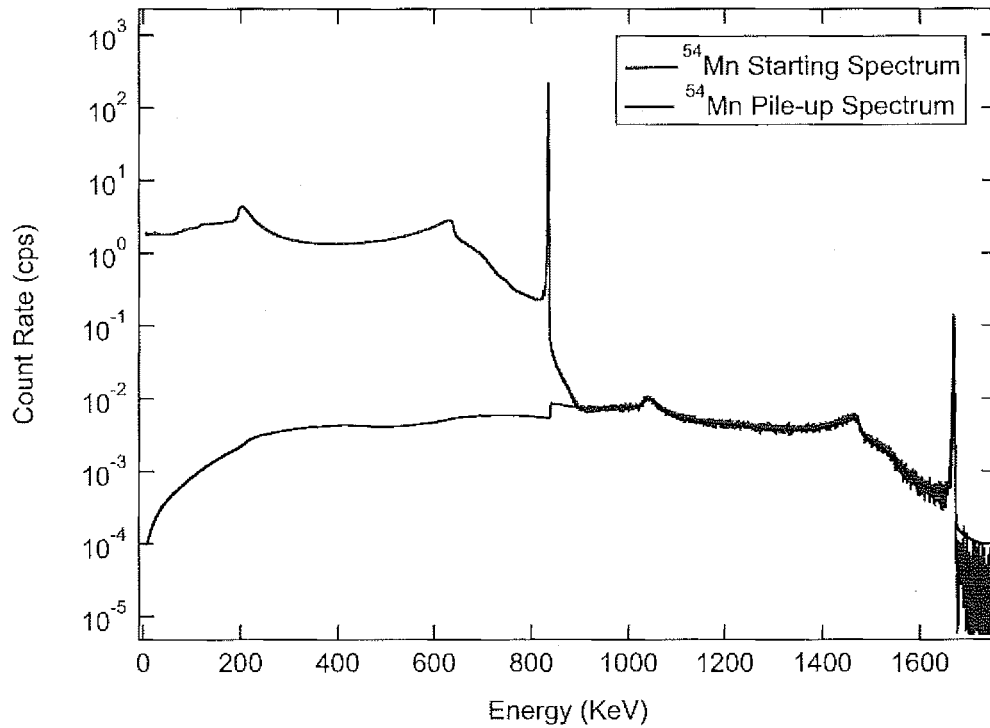


Figure 6.7. Calculated pileup spectrum (blue) with the starting spectrum (red) demonstrating the fit achieved by the de-convolution algorithm.

peak (1st), and the end of the pileup photopeak (2nd) which is within the boundaries of Region 2 to Region 4 in Figure 6.5. A linear regression method with uncertainties in 2-dimension is utilized to obtain the scaling factor[65]. After the pile-up spectrum amplitude scaling, the pileup spectrum is subtracted from the original starting energy spectrum that served as the first guess to generate the pileup spectrum. This process is then iterated until the starting spectrum, and the generated pileup spectrum stabilize. A reduced S-value test is used to stabilize the pile-up spectrum[65]. Each iteration requires reconstruction of the de-convolution or pileup spectrum to correctly compare it to, and subtract it from its generating spectrum. The de-convolution algorithm flowchart is shown in Figure 6.6. Figure 6.7 shows the starting spectrum, and

the results pile-up spectrum. As shown the method compares well in the comparison region, however, the pile-up photopeak's width is underestimated because the energy resolution is not a linear function of energy. Nonetheless, this effect does not alter the estimate of the pile-up within the region of the single event spectrum due to its smoothness in this region.

The  $\chi^2_{Dof}$  of the difference between the convolution, and the data in the match region is 1.26 indicating an acceptable convergence. Using the first day's data in which the pileup is largest, the rate difference between the convolution spectrum, and the  $^{54}\text{Mn}$  spectrum in the match region is  $\Delta R = 8 \times 10^{-6}$  cps. Again, showing an excellent match for the convolution, as the total rate in this region is  $15.176 \pm 0.014$  cps. Because the total rate difference is so much smaller than the regions total rate error, this indicates that the error generated by the convolution method is dominated by the statistics in the  $^{54}\text{Mn}$  spectrum.

The accuracy of the background match region rate is known to  $\sim 10^{-3}$ . Assuming a similar background pileup rate in the region including, and below the photopeak in the  $^{54}\text{Mn}$  spectrum means the pileup correction is at the level of  $2 \times 10^{-3}$ , given the rate in the same region of the  $^{54}\text{Mn}$  spectrum is  $\sim 8 \times 10^3$  cps. With these considerations, it is shown that the error generated by the convolution process is order  $2 \times 10^{-6}$  which can be neglected in this analysis.

After energy scaling, and convergence, the pileup spectrum is subtracted from the starting spectrum generating the true  $^{54}\text{Mn}$  pile-up corrected spectrum.

#### 6.4 Region of Interest (ROI) of $^{54}\text{Mn}$ Spectrum

The daily decay rate from the  $^{54}\text{Mn}$  corrected spectrum can be determined using two different techniques. One technique is to fit the photopeak shape. The drawback

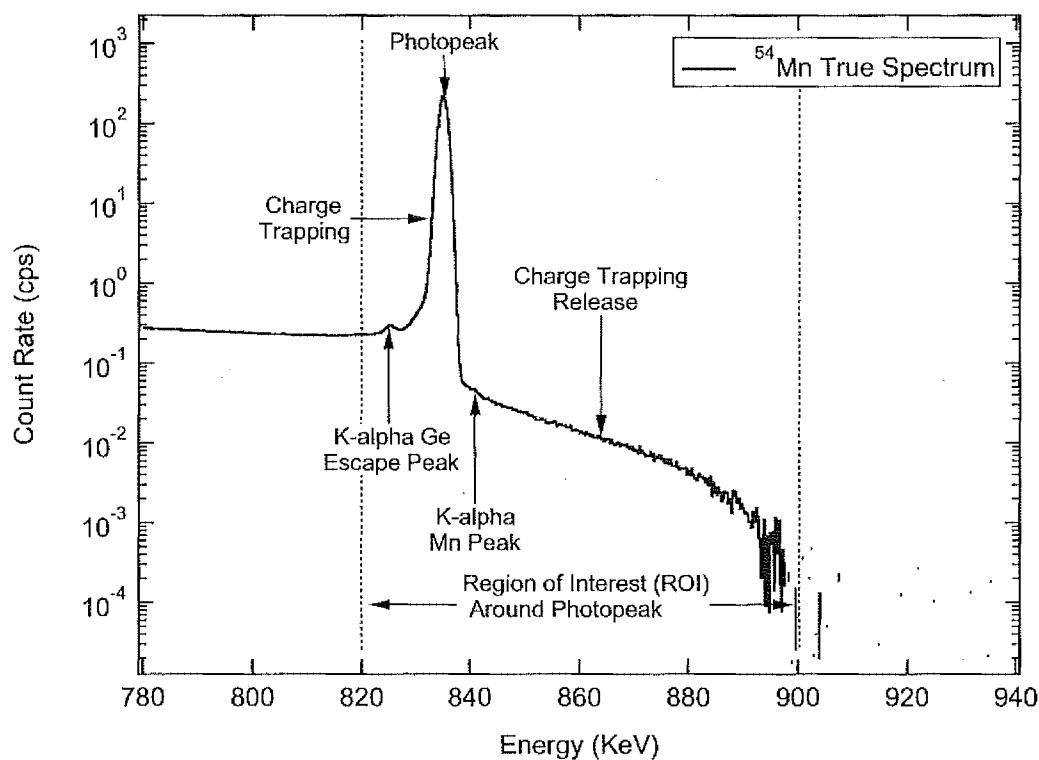


Figure 6.8. The Region of Interest, from 820 to 900 KeV, is selected from the corrected daily  $^{54}\text{Mn}$  spectrum.

of this method is the photopeak is too complicated to model to the level of accuracy required. For example, charge trapping, and charge trapping release occur in the HPGe detector during the  $\gamma$ -ray interaction process. These effects alter the HPGe line shape, as shown in Figure 6.8, and may cause reduced or excess energy to be measured in the HPGe detector that is deposited by the  $\gamma$ -ray. As is shown in Figure 6.8, the line shapes are far from having a Gaussian distribution, and no simple model can properly describe there trapping effects.

In this experiment source detector charge trapping release alters the measured  $\gamma$ -ray energy by up to 60 keV. This effect is due to the detectors previous exposure to neutrons causing defects in the crystal. Another effect due to radiation damage

is due to charge trapping on defects. In this case, the collected charge from the  $E_\gamma$  deposition is reduced. The trapping is typically 1 to 2 keV. While this detector had previously been exposed to a significant neutron flux, in evaluating the detector the only measure of merit used was a  $^{54}\text{Mn}$  Gaussian line width fit for  $\sigma_E$  measured to be very acceptable at  $\sim 1\text{keV}$ .

As it is known to degrade as a function of radiation damage,  $\sigma_E$  is the figure of merit for such damage. However, because of the very high precision required in this experiment,  $10^{-5}$ , the additional damage effects of charge trapping release were only observable after background, and pileup corrections were made to the spectra. This effect has not been reported in the literature. This effect has been studied[66], and its observation is due to the strength of the photopeak. This feature is understood as follows; Using the first days spectrum in which the effect is largest, the total rate of charge release events is 3.5 cps. This is a fractional rate of  $2 \times 10^{-3}$  when compared to the photopeak. The side band region of equal energy width below the ROI has a total rate of 0.1 cps yielding a charge release rate of  $2 \times 10^{-4}$  cps, which is not measurable in this experiment. Thus, the observation of the effect is due totally to the strength of the photopeak. For this reason, the ROI has been selected to fully include it as the upper end of the ROI energy band. Note that after the background, and pileup corrections, there are effectively zero events above the ROI energy band. In addition, the low energy band has been selected to include charge trapping as well as the k-alpha escape peak in the Ge crystal. These escape events occur when a surface Ge atom radiates a k-alpha photon away from the crystal. Thus, its energy is lost. Likewise, the k-alpha pileup from the  $^{54}\text{Mn}$  source, and the photopeak have not been removed, because these are photopeak events, while energy shifted, are not lost out of the ROI region as is shown in Figure 6.8.

By selection of the ROI band instead of what is an ill-defined, and elusive definition of photopeak, the effects of charge trapping, and charge trapping release, and

other effects do not impact the sensitivity of the measurement. Thus, the ROI in this measurement extends from 820 KeV to 900 KeV.

In addition, the ROI is a fixed energy region, instead of a fixed channel range. Selecting a fixed energy region eliminates the effects of calibration drift, and is accounted for by the time-dependent energy spectrum calibration coefficients.

### 6.5 Region of Interest(ROI) Measurement Limit Estimation

The goal of this experiment is to search for possible extensions to the weak interaction due to decay rate parameter variation caused by a flux of antineutrinos. The electronic dead time correction, the background spectrum subtraction, and pile-up spectrum correction have been used to correct each  $^{54}\text{Mn}$  daily spectrum. The error estimation of the measurement in the ROI per day includes statistical error from counting, and systematic error from instruments. Table 6.2 is the summary of the count rate, and error from each correction to the ROI per day. The total error estimation in the ROI per day for this measurement is 0.022 cps. Averaging the

Table 6.2.  
Error analysis, and estimation per day in Region of Interest (ROI) of  $^{54}\text{Mn}$  daily spectrum.

Type of Corrections per Day in ROI	Count Rate in ROI (cps)	Error Rate in ROI (cps)
Statistical (Average 20 days) with 8 periods	1431.43	1.0E-02
Dead time Poisson (0.029 sec/day)	1431.43	9.7E-03
Average ROI uncertainty (2.2E-2 KeV)	0.18	1.8E-02
Background with reactor-off	0.056	1.4E-05
Background with reactor-on	0.086	2.4E-05
Pile-up Effect from HPGe	1.70	3.4E-05
Total error per day estimation in rate (cps)		2.2E-02
Total error per day estimation in the level of		1.5E-05

daily measured decay rate in the ROI over the full length of the experiment yields on average count rate using this average a **per day** sensitive in  $\delta\lambda/\lambda \sim 1.5 \times 10^{-5}$ .





## 7. Data Analysis of Corrected $^{54}\text{Mn}$ spectral

### 7.1 Single Parameter Fitting to the Region of Interest

The  $^{54}\text{Mn}$  daily decay rate as a function of time, which is taken as the Region of Interest (ROI), is shown in Figure 7.1. The rate was calculated for each daily spectrum starting August 30, 2015, at 23:58:22, and ending March 09, 2016 at 23:12:51. The time period includes four reactor-off, and four reactor-on periods. Those daily runs which cover the transition time of the reactor-on or reactor-off period have been removed to reduce possible error. The data collection consists of a continuous period including 87 reactor-on days, and 105 reactor-off days over 192 days of data collection.

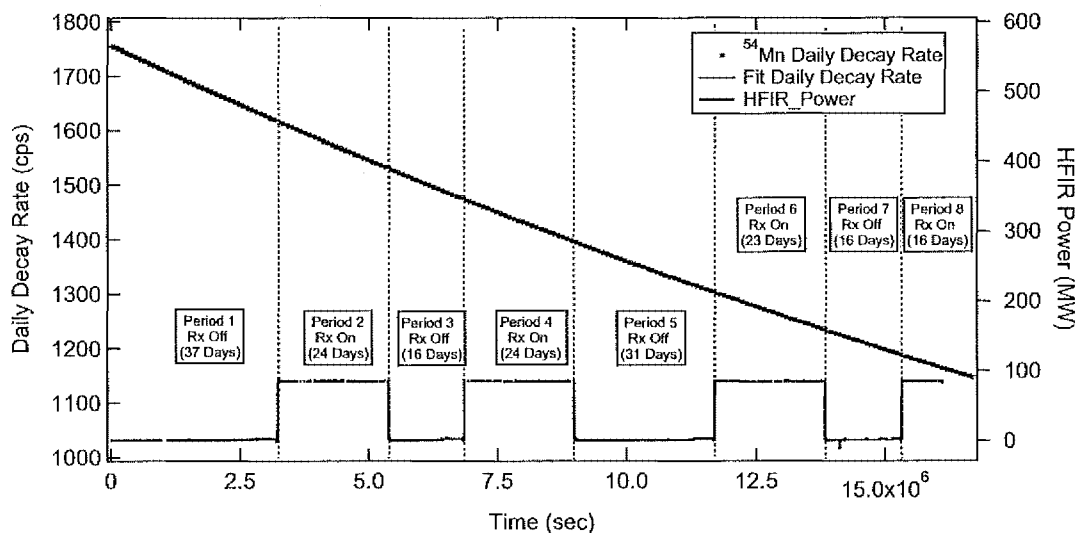


Figure 7.1. Daily decay rate from the integration between 820 to 900 KeV of the  $^{54}\text{Mn}$  spectra. Error bars are too small to be shown. The HFIR reactor power is also shown in this Figure. The Periods 1, 3, 5, and 7 are the reactor-off periods. The Periods 2, 4, 6, and 8 are reactor-on periods.

The count rate of the ROI continuing the  $^{54}\text{Mn}$  photopeak was initially  $1754.31 \pm 0.15$  cps but decayed to approximately  $1146.37 \pm 0.12$  cps at the end of the experiment. The data point for each day is plotted at the average time weighed by an exponential function calculated using the standard  $^{54}\text{Mn}$  mean lifetime  $\tau$  ( $450.41 \pm 0.29$  days)[60]. The average time is then calculated as

$$t_{ave} = \frac{\int t \exp(t/\tau) dt}{\int \exp(t/\tau) dt}, \quad (7.1)$$

integrated over the days real time period of 86,400 seconds.

Once the average time is found, and the daily rate in the ROI is obtained, the daily decay rate is then fit to an exponential decay function,

$$R(t) = ae^{-t/\tau} \quad (7.2)$$

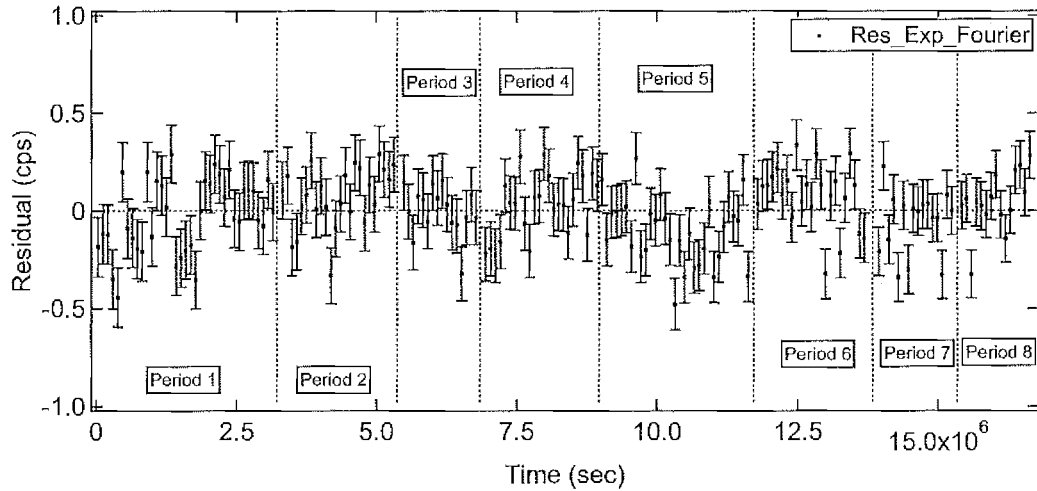


Figure 7.2. Daily residual fitted with a revised exponential decay function (Eq 7.3) which includes a single periodic function. The residuals show the oscillation significantly reduced the fit  $\chi^2$  per degree of freedom.

where  $a$  is the amplitude variable, and again  $\tau$  is fixed at the standard mean lifetime of  $^{54}\text{Mn}$ [60]. The  $\chi^2$  per degree of freedom is  $\sim 100$  which is unacceptable. The correct approach is to fit for the decay simultaneously with a revised decay function including a single periodic function with a phase to take into account the known yearly environmental oscillations already observed in the data,

$$R(t) = ae^{-t/\tau} + A\sin(\omega t + \phi). \quad (7.3)$$

Figure 7.2 shows the residuals of the revised fit(Eq. 7.3). Again,  $\tau$  is fixed at the mean lifetime of  $^{54}\text{Mn}$ [60],  $\omega$  is the periodicity fixed at one year, and  $\phi$  is the phase relative to the start of the experiment. Including the yearly environmental effects in the fit reduces the  $\chi^2$  per degree of freedom to an acceptable 1.54. As expected the oscillation has a good match to the  $b_r$  parameters oscillation, and has a good out of phase match to the humidity considering the complexity of there interactions. These are shown in Table 7.1. This is as expected if the oscillation is driven by the yearly variations in the humidity acting on the X-cooler. The amplitude of the oscillation is  $1.55 \pm 0.01$  cps. When compared to the average rate in the ROI,  $1431.43 \pm 0.18$  cps the fractional effect is at the level of  $1.1 \times 10^{-3}$ .

The revised fitting function successfully removes the oscillation behavior. The minimum value occurs on Sep/20/2015 which is nearly 21 days from the starting date Aug/30/2015. This date is not associated with the Earth's perihelion or the aphelion which occurred Jan/02/2016 17:49 (EST), and Jul/06/2015 14:40 (EST)[67], as

Table 7.1.  
Comparison of in-phase, and out-of-phase ROI oscillation.

ROI Oscillation	Phase ( $\phi$ )	In phase factors	Phase ( $\phi$ )
In phase	$-111 \pm 0.5$ day	Linear terms $b_r$	$-122 \pm 2$ day
Out of phase	$71 \pm 0.5$ day	Humidity	$79 \pm 1$ day

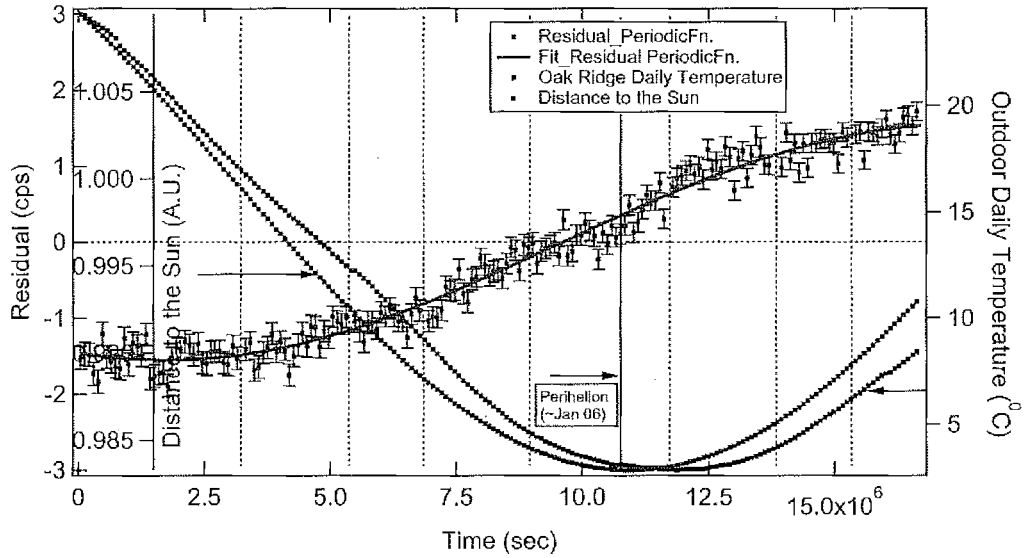


Figure 7.3. The oscillation term found by subtraction of the exponential term from the data (Eq. 7.3), and its fit shown in Red data points. For comparison, the daily outdoor temperature, and the Earth's distance from the Sun are not in phase with the environmental oscillations in HFIR.

shown in Figure 7.3. If the periodicity is allowed to vary, the  $\chi^2/DoF$  is unchanged, and yields an oscillation of 363.6 days, in agreement within error, with the 1-year fixed value. Therefore, the oscillation of the decay rate does not correlate to the solar neutrino flux variation due to the Earth's motion.

As an aside, The subtraction of this low-frequency term in no way affects the sensitivity of the search for decay rate parameter variations in this experiment, but instead demonstrates the ability to reject environmental effects, as the HFIR characteristic on-time period is 30 days a much higher frequency than the 1-year environmental frequency being filtered-out in this search.

## 7.2 Side Band Ambient Temperature Corrections

The DEPEC-50 spectrometer electronics are located outside the controlled environmental housing. For this reason, it is influenced by environmental factors such as temperature, pressure, and humidity. These variations are the cause of the nonlinear energy scale calibrations. The use of nonlinear calibrations has been presented in Chapter 5 for both the source, and background spectra. The nonlinear energy scale correction is given by,

$$E = a_r + b_r x + c_r x^2 \quad (7.4)$$

where  $a_r$ ,  $b_r$ , and  $c_r$  are the calibration coefficient of  $r$ th daily spectrum, and  $x$  is the channel number of the spectrum. The data is analyzed using the counts per second (cps) in a fixed energy band  $\Delta E$  which includes the photopeak. For illustration using fixed bins, this band is given by

$$\begin{aligned} \Delta E &= b_r(x_{i+n} - x_i) + c_r(x_{i+n}^2 - x_i^2) \\ &= [b_r + c_r(x_{i+n} + x_i)] \times (x_{i+n} - x_i) \end{aligned} \quad (7.5)$$

The error in the bands energy width generates an error in the counts associated with that band. The error in the width is

$$\delta(\Delta E) = [\delta b_r + \delta c_r(x_{i+n} + x_i)] \times (x_{i+n} - x_i) \quad (7.6)$$

$b_r$  is well measured to a fractional accuracy of  $7 \times 10^{-5}$ , as shown in Figure 5.7.  $c_r$  is measured only to a fractional accuracy of order  $10^{-1}$ , and requires more accurate evaluation. At low bin number the non-linear term has no effect on the energy band width. However, as the bin number increases, and in the ROI band where  $x_i \sim 4000$ , the error in the band width is dominated by the non-linear term

$$(\delta c_r \cdot 2x_i)^2 \geq (\delta b_r)^2 \quad (7.7)$$

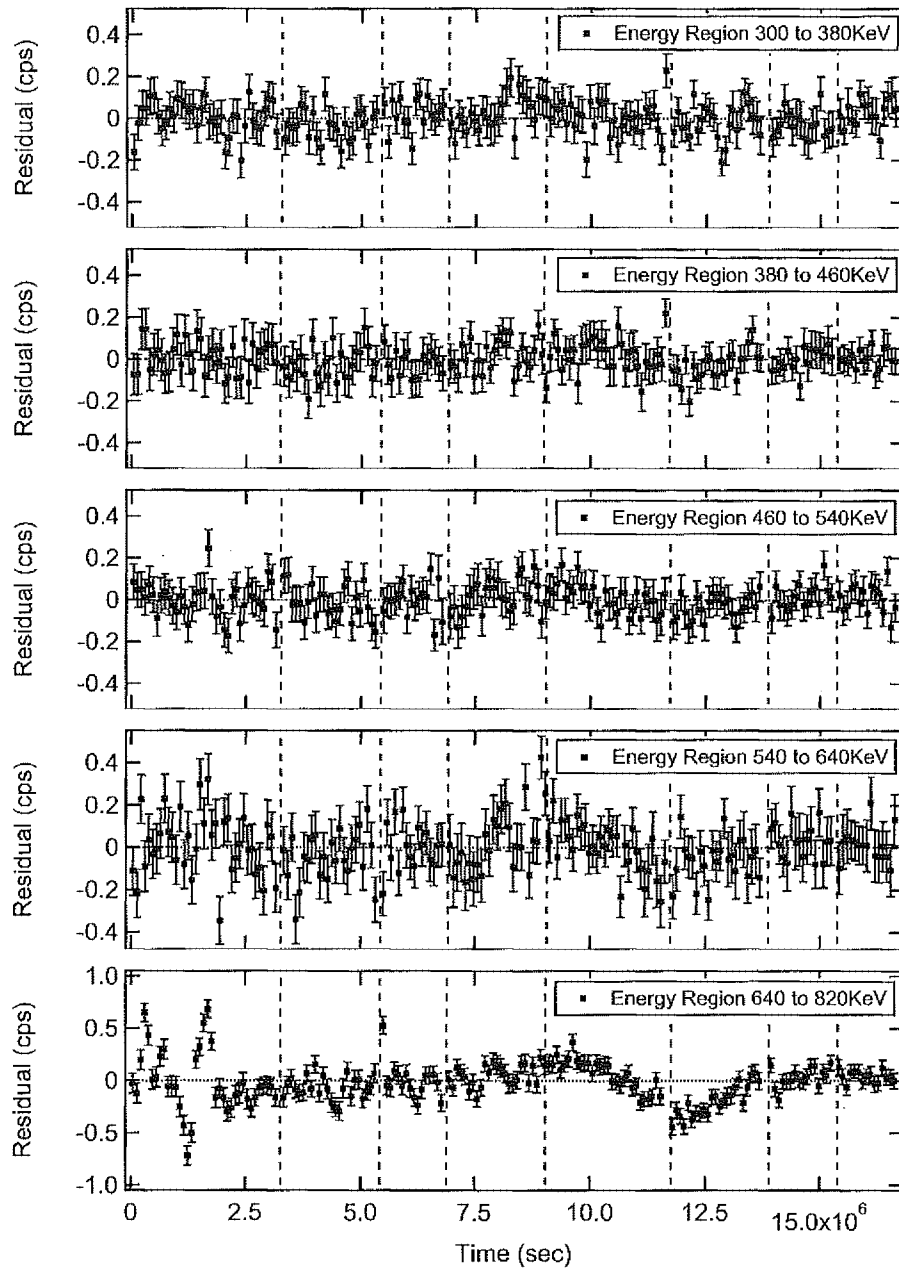


Figure 7.4. Residuals of equal width energy regions from the corrected  $^{54}\text{Mn}$  spectrum. The residuals show the environmental effects strongly correlate with the strength of the nonlinear term  $c_r x^2$ .

so that the error on the width is given approximately by

$$\delta(\Delta E) \sim \delta c_r (x_{i+n}^2 - x_i^2) \quad (7.8)$$

The knowledge of  $c_r$ -term motion as a function of the environmental parameters can be improved by study of the side band residuals. In addition, the motion of the error in the  $b_r$ -term is expected to be random as  $b_r$ 's dominant source of motion is due to the inherent linearity of the HPGe detectors temperature dependence where as the motion of the  $c_r$  term error is coming from the DSPEC-50 located outside the controlled environmental housing.

These expectations concerning  $\delta c_r$  are verified in the spectral data by study of the energy regions below the ROI. Regions of equal energy width were selected starting from 300 to 380 KeV, 380 to 460 KeV, 460 to 540 KeV, 540 to 640 KeV as well as 640 to 820 KeV all below the ROI. The daily decay rate for each of these energy regions is fit to the same function as the ROI, that is

$$R(t) = ae^{-t/\tau} + A\sin(\omega t + \phi) \quad (7.9)$$

where only  $a$ , and  $A$  are variable in this fitting.  $\omega$ ,  $\tau$ , and  $\phi$  are the same fitted coefficients found for the ROI; the fitting function from Eq. 7.3. Figure 7.4 shows the residual of these energy regions, and Table 7.2 gives the  $\chi^2$  per degree of freedom for each energy region.

As expected the  $\chi^2$  per degree of freedom for the lower energy bands is  $\sim 1$ . However, because the uncertainty in  $c_r$  has a significant effect at high bin numbers, this error is clearly observed in the side band region just below the photopeak. The  $\chi^2$  per degree of freedom is  $\sim 12$ , demonstrating a lack of knowledge in the parameter  $c_r$ .

Table 7.2.

The  $\chi^2$  per degree of freedom from fitting equal width energy regions in Figure 7.4.

Energy Region (KeV)	$\chi^2$ per degree of freedom
300 to 380	0.98
380 to 460	0.86
460 to 540	0.87
540 to 640	1.24
640 to 820	12.02

The error in  $c_r$  contributes a significant effect that increases with the channel number (energy scale). An incorrect assignment of the energy width of the ROI, as will be shown is a function in time of the environmental parameters. This correction causes events to be lost or gained as a function of the environmental changes measured through the motion of the non-linear term. The gain or loss of events due to this error is measured by the difference in the error in the energy width of the edge bins. These effects can be calculated from

$$R_L(f(E_L)) - R_U(f(E_U)) = \delta R \quad (7.10)$$

where  $f(E_L)$ , and  $f(E_U)$  are the fractional variation in the edge bins of the side band at the lower, and upper edge.  $R_L$ , and  $R_U$  are the rates in the side band edge channels of the  $^{54}\text{Mn}$  spectrum.  $\delta R$  is the residual in that energy band. The side band rate variation is caused by the poor measurement of  $c_r$ . This causes residual motion away from the fit. Because events enter or leave the band only through the edges, the knowledge of  $c_r$  can be improved by relating the correction in  $c_r$  to the residuals. Eq. 7.10 can be rewritten into

$$R_L \frac{\delta c_r(x_L^2)}{\Delta E_L} - R_U \frac{\delta c_r(x_U^2)}{\Delta E_U} = \delta R \quad (7.11)$$



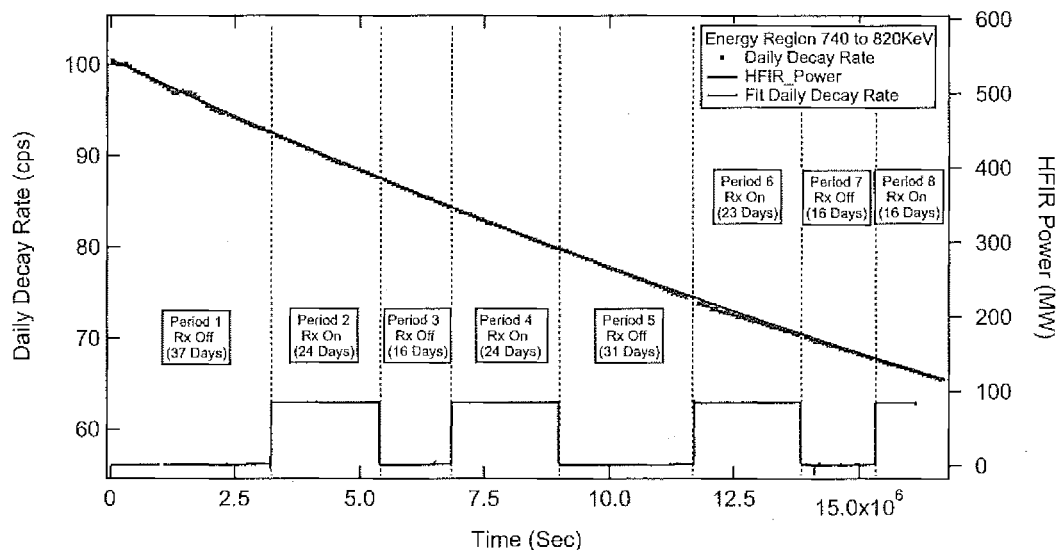


Figure 7.5. Daily Decay rate of Region 740 KeV to 820 KeV of  $^{54}\text{Mn}$  spectra

where  $\delta c_r$  is the correction to the  $c_r$  found using the side band residuals where the residuals are dominated by  $\delta c_r$ , the error in  $c_r$ . This correction provides a unique way to correct effects due to the electronic instability from the DSPEC-50.

Once the corrections are found to the non-linear calibration term using the side band, this improved knowledge is used to correct the ROI band. In order to find the correction in the ROI, the same energy width band has been selected starting from 740 KeV to 820 KeV which is the lower side band of the ROI. The upper edge of this energy region connects to the lower edge of the ROI.

Before the  $\delta c_r$  corrections can be found, an additional correction must be made to the side band. The residuals for the side band are shown in Figure 7.6. The  $\chi^2$  per degree of freedom is unacceptable  $\sim 12$ . Ambient environmental factors will be shown to correlate to these variations. These same environmental variations in the photopeak lower side band caused the fit given in Section 7.1 to fail. To correct for

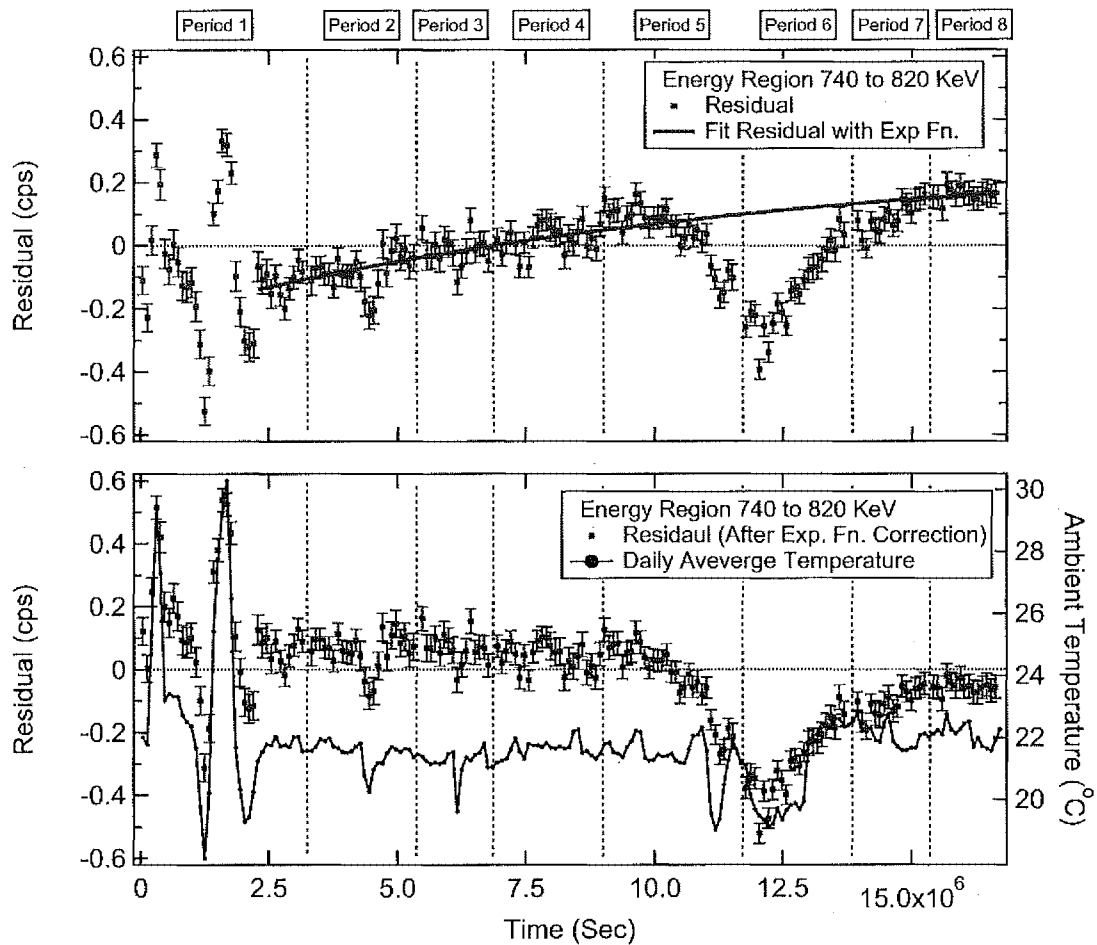


Figure 7.6. (Upper) Daily residual of the side band energy region in the  $^{54}\text{Mn}$  spectra. (Lower) Daily residual of the side band energy region of  $^{54}\text{Mn}$  spectra after the exponential function correction. A significant fluctuations appear in Period, 1, 5, and 6.

this, an additional exponential decay function, used only on this side band region, has been used to optimize the  $\chi^2$  per degree of freedom of these side band residuals found using the fit in Eq.7.9

$$\delta R(t) = C + D \times \exp(-t/\tau_1) \quad (7.12)$$

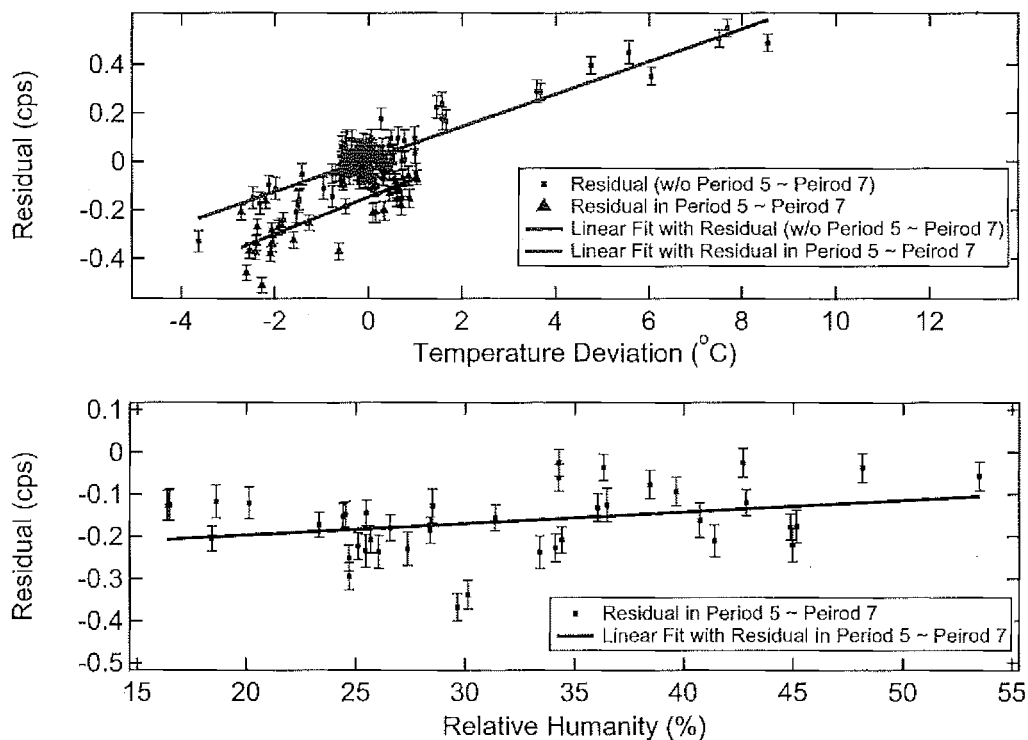


Figure 7.7. (Upper) Daily residuals of the side band energy region as a function daily average Temperature. (Lower) Daily residual in Period 5, 6, and 7 during periods with stable temperature, of the side band energy region as a function of daily relative humidity.

where  $C$ ,  $D$ , and  $\tau_1$  are the fitting coefficients of this function. Once fit the residuals in the energy region 740 to 820 KeV successfully drop the  $\chi^2$  per degree of freedom from 12 to 1.49, which is acceptable.  $\tau$  is found to be the low frequency at 139 days showing this correction is not related to reactor operations.

After correcting the lower side band residuals by Eq. 7.12, the correlation between the residuals, and the ambient temperature is clear. Figure 7.7(Upper) displays the daily residuals after exponential correction as a function of daily average temperature. The red squares in Figure 7.7 include all side band residual data points. The blue triangles only include the end of Period 5 to 7 which is related to a significant drop in

temperature. It is clear there are  $\pm 0.6$  cps variations with temperature deviations of  $-4$  to  $8$  °C. Two linear fittings have been applied to the data set independently. The fitting coefficients from the red data point are different compared with the blue data points. The residual variations with temperature prove that environmental effects are causing the motion. However, the length of the time-dependent temperature variations also plays a role causing the difference between the red, and blue data points. Because the variations of blue data points include both reactor-off, and reactor-on periods, they are not caused by the reactor status. That is, antineutrino exposure is not the reason for this effect.

Likewise, the residuals motion is correlated with humidity as shown in Figure 7.7 (Lower) during a period with unstable temperature. It should be noted that the residual shifts displayed in Figure 7.6 do not coincide with reactor-on, and reactor-off cycles. Because of the strong correlation of the side band residuals with environmental factors, these residual shifts are taken as environmental, to be used to correct for environmental factors in the ROI. That is, the residuals from the lower side band, with energy width equal to the ROI region, are set to zero as a measure of the environmental factors. This pre-assumes that not measurable antineutrino effects are measurable in the side band. This is reasonable as the data rate ratios between the side band  $\sim 0.1$ cps compared to the photopeak ROI of 1800cps is  $5.6 \times 10^{-5}$ . It is assumed that any effect due to antineutrino interactions is proportional to the number of decays or this ratio.

It is noted the lower edge of the Region of Interest is the same as the upper edge of the side band edge. The upper edge of the Region of Interest is zero after the pile-up correction. After using Eq.7.11 to find  $\delta c$  from the side band, the resulting effect on the residuals in the ROI is given by

$$\delta R_{ROI} = R_U \frac{\delta c_r x_U^2(Side\ Band)}{\Delta E_U(Side\ Band)} \quad (7.13)$$

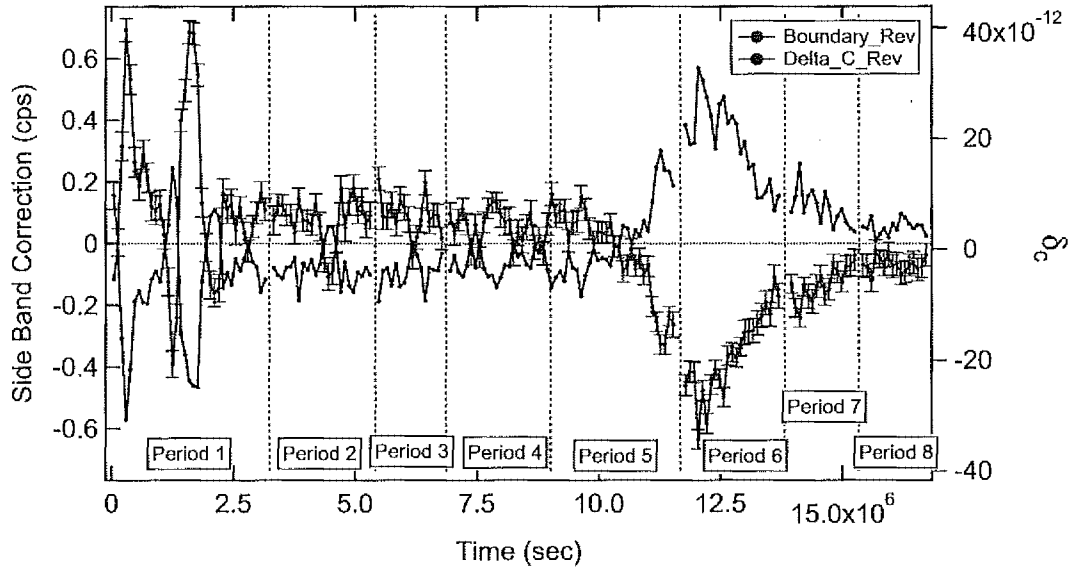


Figure 7.8. Daily  $\delta c_r$ , and corrected residual of Region 740 KeV to 820 KeV of  $^{54}\text{Mn}$  spectra, and daily average Temperature.

where  $R_{U(\text{Side Band})} = R_{L(\text{ROI})}$ , and  $x_{\text{Sideband}}^2 = x_{\text{ROI}}^2$ . Note the sign changes for the correction. The rate from the upper side band edge is the lower edge of the ROI. This occurs because events lost from one band edge is a gain to the other band. The corrected daily decay rate for the ROI is then,

$$R_{\text{Corrected ROI}}(t) = R_{\text{ROI}}(t) + R_U \frac{\delta c_r(x_U^2)}{\Delta E_U} \quad (7.14)$$

### 7.3 Results After All Corrections (ROI)

The corrected daily decay rate from the  $^{54}\text{Mn}$  ROI was used to search for antineutrino interactions through decay parameter variations. The corrections made to the ROI are (1) Background Correction. (2) Pile-up Correction. (3) The exponential fit (Eq. 7.2) (4) A periodic fit with periodicity of one-year. (Eq. 7.3) (5) Side band environmental correction. Figure 7.9 shows the final residuals for the ROI as

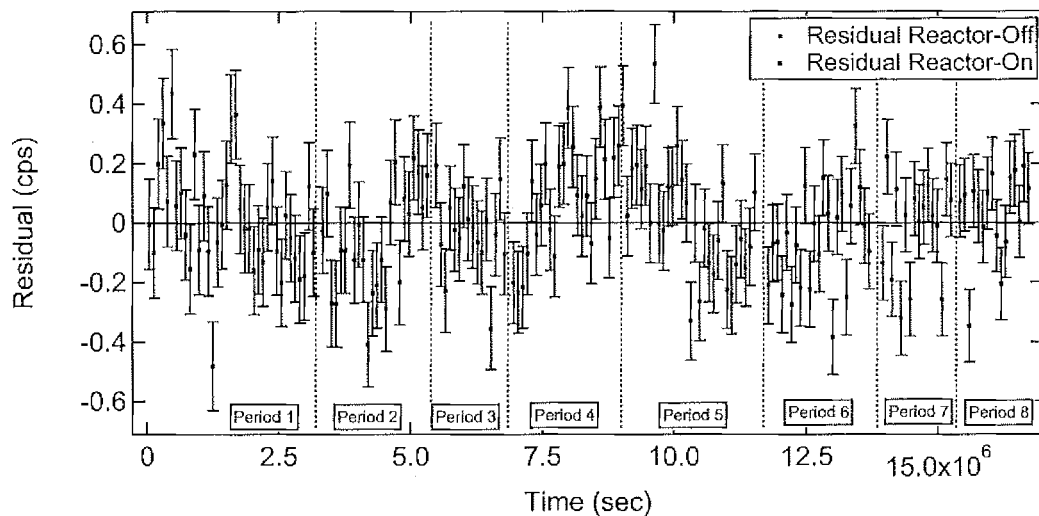


Figure 7.9. Corrected ROI Residuals as a function of time. The red data points indicate the residuals in reactor-off periods, and blue data points indicate the residuals in reactor-on periods.

a function of time, and reactor status. The red data points indicate the residuals in reactor-off periods, and blue data points indicate the residuals in reactor-on periods. Three different methods were used to search for an effect, and estimate sensitivity, including (1) A simple average of the residual form each period without regard to reactor status. (2) Segment analysis by checking 3 consecutive reactor cycles (3) Step search, by comparing all reactor-on residuals to all reactor-off residuals.

### Average Residual Analysis

The first method is to calculate the average residuals in each reactor-on period, and reactor-off period. This average analysis is to test consistency with the flatness of the residuals. Table 7.3 shows the average residual of each period yielding the size of its motion away from zero,  $\delta R(\text{cps})$ . Averaging all the periods without regard to reactor status yields  $\delta R = (0.52 \pm 1.08) \times 10^{-2} \text{cps}$ , and  $\delta R/R = (3.62 \pm 7.53) \times 10^{-6}$  where  $R$  is taken as the experimental average rate. This test shows the residuals are

Table 7.3.

Average residuals, and uncertainty of each reactor-on, and reactor-off period. The averaged results without regards to reactor status. The mean of all the data is less than 1-standard deviation. This is one test showing the data's consistency indicating no effect during the antineutrino exposure.  $R$  is taken as the experimental average rate in ROI.

Average Residual Analysis			
Period	Reactor Status	Residual (cps)	Uncertainty (cps)
1	Off	9.35E-03	3.02E-02
2	On	-5.01E-02	3.07E-02
3	Off	-3.24E-02	3.57E-02
4	On	7.52E-02	2.92E-02
5	Off	2.24E-03	2.48E-02
6	On	-5.81E-02	2.73E-02
7	Off	-1.90E-02	3.28E-02
8	On	3.41E-02	3.22E-02
Average Size of Effect in $\delta R$ (cps)		5.18E-03	1.08E-02
Average Size of Effect in $\delta R/R$		3.62E-06	7.53E-06

consistent with an origin having a single value, zero, indicating no effect during the antineutrino exposure.

### Segment Analysis

The second method is called the segment analysis. The approach to this data analysis is to use a walking window technique, taking advantage of the alternating reactor cycle pattern for the antineutrino flux. The two like reactor status periods are averaged into a single data point, and compared to the average of the opposite reactor status they guard.

Table 7.4.

Residual, and uncertainty of each reactor-on, and reactor-off period for segment analysis. The sign of the residuals in on-off-on test are flipped relative to the off-on-off test. The average size of effect is within one standard deviation.  $R$  is taken as the experimental average rate in ROI.

Segment Analysis			
Period	Reactor Status	Residual (cps)	Uncertainty (cps)
1-2-3	off-on-off	-3.86E-02	3.31E-02
2-3-4	on-off-on	4.49E-02	3.00E-02
3-4-5	off-on-off	8.02E-02	3.07E-02
4-5-6	on-off-on	-1.38E-02	2.83E-02
5-6-7	off-on-off	5.98E-02	2.91E-02
6-7-8	on-off-on	6.98E-03	2.99E-02
Average Size of Effect in $\delta R$ (cps)		2.11E-2	2.13E-2
Average Size of Effect in $\delta R/R$		1.48E-5	1.49E-5

The Periods 1-2-3 off-on-off, Periods 2-3-4 on-off-on, Periods 3-4-5 off-on-off, Periods 4-5-6 on-off-on, Periods 5-6-7 off-on-off, and Periods 6-7-8 on-off-on have been used to search for an effect. This comparison is highly correlated as each measurement is used 3 times. For this reason, the calculated residual is increased by  $\sqrt{3}$  accounting for the correlation. Table 7.4 shows the segment analysis average residual of each group of periods as well as the final size of the effect. That is  $\delta R = (2.11 \pm 2.13) \times 10^{-2}$  cps, and  $\delta R/R = (1.48 \pm 1.49) \times 10^{-5}$ . The results are within one standard deviation, and again consistent with no effect during the antineutrino exposure.

### Linear Fitting Analysis

The strongest test of the data is to combine all the reactor-on data, and compare to all the reactor-off data in search of a step. This is the method



Table 7.5.  
Size of effect, and uncertainty from a single constant term.

Linear Fitting Analysis				
Fitting Period	Reactor Status	Residual (cps)	Uncertainty (cps)	$\chi^2/DoF$
All	N/A	1.49E-05	9.89E-03	1.68
1,3,5,7	Off	2.49E-04	1.38E-02	1.63
2,4,6,8	On	-2.33E-04	1.42E-02	1.79
Size of Effect in $\delta R$ (cps)		4.83E-04	1.98E-02	
Size of Effect in $\delta R/R$		3.37E-07	1.38E-05	

## Summary

For this analysis, the nuclear decay rate parameter of  $^{54}\text{Mn}$  is found not to be effected when exposed to an antineutrino flux. These results are consistent with no measurable decay rate parameter variation due to an antineutrino flux yielding a 68% confidence level upper limit sensitivity, as shown in Table 7.6.

Table 7.6.  
68% confidence upper limit on antineutrino interaction on  $^{54}\text{Mn}$

Measured Variation	$\frac{\delta\lambda}{\lambda} \leq 1.43 \times 10^{-5}$
Cross Section Sensitivity	$\sigma \leq 1.34 \times 10^{-25} \text{ (cm}^2\text{)}$



## 8. Conclusion

The original goal of the experiment is to measure decay rate parameter variation with sensitivity at 1 part of  $10^5$  by measuring the  $\gamma$  spectra from the  $^{54}\text{Mn}$  electron capture decay. The experiment has achieved its sensitivity goal at the level of  $\delta\lambda/\lambda \sim 10^{-5}$ . Table 8.1 gives the result of the  $^{54}\text{Mn}$  decay rate variation as measured at HFIR. The result is consistent with no observed effect at the level of the measuring sensitivity of  $1.38 \times 10^{-5}$ . The 68% confidence level upper limit on the cross section is 0.13 barns, on the order of a nuclear or strong interaction cross-section.

Figure 8.1 compares the full data available in the literature as discussed in Chapter 3, and these final results. The logarithm cross-section or sensitivity as a function of logarithm mean lifetime of the decay parameter, is display for all experiments reporting both observed effects, and null observations. The reported decay modes include (1) the negative  $\beta$ -decay with time-dependent variation results (Red

Table 8.1.  
Summary of measurements at HFIR of  $^{54}\text{Mn}$  decay rate variations measurement.

Antineutrino Flux	$F_{\bar{\nu}} = 2.86 \times 10^{12} \text{ (sec}^{-1}\text{cm}^{-2}\text{)}$
Measured Variation	$\frac{\delta\lambda}{\lambda} = (0.034 \pm 1.38) \times 10^{-5}$
68% Upper Limit Confidence Level	$\frac{\delta\lambda}{\lambda} \leq 1.43 \times 10^{-5}$
Measured Cross Section Sensitivity	$\sigma = (0.097 \pm 1.24) \times 10^{-25} \text{ (cm}^2\text{)}$
68% Upper Limit Confidence Level	$\sigma \leq 1.34 \times 10^{-25} \text{ (cm}^2\text{)}$

Triangles)[1, 3, 6, 16, 18, 25–28], (2)the negative  $\beta$ -decay with "Null" variation results (Red Squares)[8, 12, 19, 29–32] (3) the positive  $\beta$ -decay with time-dependent variation results (Orange Triangles)[7] (4)the positive  $\beta$ -decay with "Null" variation results (Orange Squares)[33] (5) the electron capture  $\beta$ -decay with time-dependent variation results (Green Triangles)[21] (6) the electron capture  $\beta$ -decay with "Null" variation results (Green Squares)[8, 12, 19] (7) the  $\alpha$ -decay with time-dependent variation results (Purple Triangles)[5] (8) the  $\alpha$ -decay with "Null" variation results (Purple Squares)[12, 30, 34], are by exposing the solar neutrino. (9) The reactor antineutrino "Null" variation results [35]. (10) The HFIR  $^{54}\text{Mn}$  experiment result.

It is expected that the cross section sensitivities for neutrino, and antineutrino interactions at a fixed measuring sensitivity should follow the curve.

$$\sigma = A \tau^P \quad (8.1)$$

where  $A$ , and  $P$  are the fitting coefficients. In this comparison Figure 8.1, curve (a) is the temporal cross-section fit  $\sigma = A \tau^P$  to those experiments reporting decay rate parameter variations. Curve (b) compares experiments by cross-section only. This experiment is more sensitive than all previous experiments reporting positive decay rate parameter variations, and thus it is in disagreement with all positive result experiments on this basis. Curve (c) connects this experiment, and a solar neutrino experiment using  $^{40}\text{K}$ [19]. The connection between these two experiments maps out an exclusion zone in the temporal cross-section space excluding decay rate parameter variations at a level  $10^4$  times more sensitive than any previously reported positive result. Curve (d) displays the temporal cross exclusion zone  $\sigma \sim \sigma_{limit} \tau^{-1}$  if extrapolated using only this experiment, and again is in disagreement with all positive result experiments.

The properties of these curve are displayed in Table 8.2. From these data, a

Table 8.2.  
Coefficients from four type of curve fitting with previous experiments.

Curve	$A$	$P$
(a) Observed variation	-12.31	-1
(b) Cross section only comparison	-24.87	0
(c) Exclusion Region	-19.54	-0.71
(d) This experiment temporal exclusion	-17.28	-1

convincing case is made that those measurements reporting decay rate parameter variations are not consistent with the source of the variations being caused by neutrino or antineutrino interactions.

As displayed in Figure 8.1, isotopes with longer mean lifetime can obtain better cross-section sensitivity. Data in the same experimental configuration at HFIR using  $^{137}\text{Cs}$  a  $\beta^-$ -decay process, and  $^{108}\text{Ag}$  an electron capture decay process, having nearly 30, and 400 years mean lifetime, has been collected, and are under analysis for decay rate parameter variations.

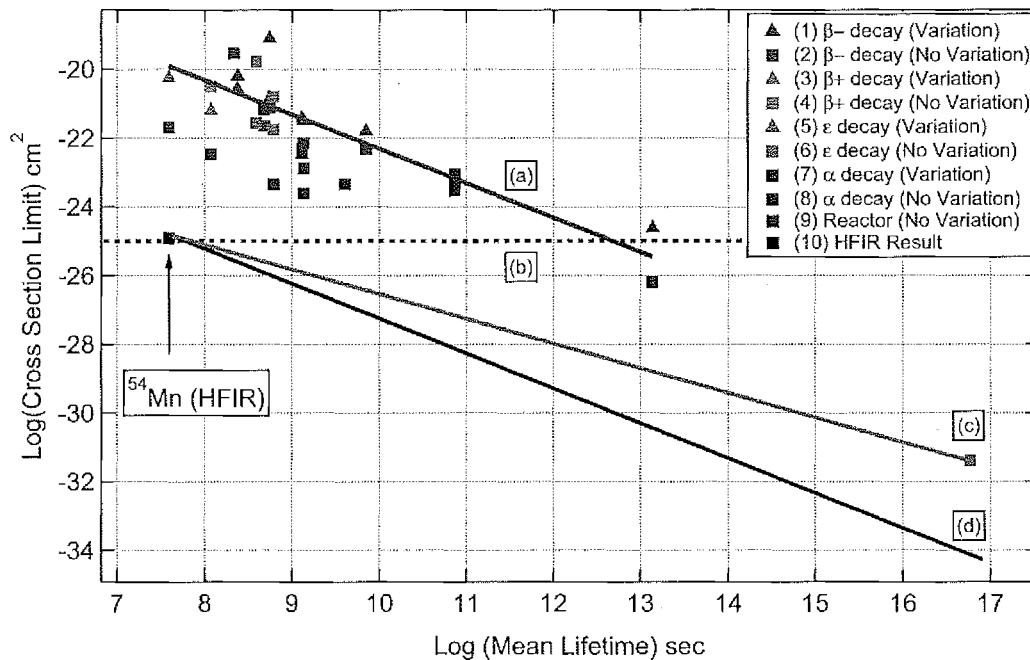


Figure 8.1. The logarithm cross section sensitivity of time-dependent variation results, no evidence results, and this HFIR result as a function of the logarithm mean lifetime. The data are based on Table 3.7, and 3.8. The data includes (1)  $\beta^-$  decay with variation results[1, 3, 6, 16, 18, 25–28], (2)  $\beta^-$  decay with no effect results[8, 12, 19, 29–32], (3)  $\beta^+$  decay with variation results[7], (4)  $\beta^+$  decay with no effect results[33], (5) Electron Capture decay with variation results[21], (6) Electron Capture decay with no effect results[8, 12, 19], (7)  $\alpha$  decay with with variation results[5], (8)  $\alpha$  decay with no effect results[12, 30, 34], and (9) reactor antineutrino as a test source with no effect results[35]. (10) The HFIR  $^{54}\text{Mn}$  experiment result. See the text for explanation of the curves (a), (b), (c), and (d).

## Bibliography

- [1] D. Alburger, G. Harbottle, and E. Norton, *Earth and Planetary Science Letters* **78**, 168 (1986).
- [2] E. Falkenberg, *Apeiron* **8**, 32 (2001), 12.
- [3] E. Falkenberg, *Apeiron* **9**, 41 (2002), 3.
- [4] J. Jenkins, E. Fischbach, D. J. II, R. Lee, and P. Sturrock, *Applied Radiation and Isotopes* **74**, 50 (2013).
- [5] J. H. Jenkins et al., *Astroparticle Physics* **32**, 42 (2009).
- [6] J. H. Jenkins et al., *Astroparticle Physics* **37**, 81 (2012).
- [7] D. O’Keefe et al., *Astrophysics and Space Science* **344**, 297 (2013).
- [8] H. Schrader, *Applied Radiation and Isotopes* **68**, 1583 (2010), *Proceedings of the 17th International Conference on Radionuclide Metrology and its Applications (ICRM 2009)*.
- [9] H. Schrader, *Applied Radiation and Isotopes* **114**, 202 (2016).
- [10] S. E. Shnoll et al., *Physics-Uspekhi* **41**, 1025 (1998).
- [11] S. E. Shnoll et al., *Physics-Uspekhi* **43**, 205 (2000).
- [12] H. Siegert, H. Schrader, and U. Schtzig, *Applied Radiation and Isotopes* **49**, 1397 (1998).
- [13] P. A. Sturrock, E. Fischbach, and J. H. Jenkins, *Solar Physics* **272**, 1 (2011).
- [14] P. Sturrock et al., *Astroparticle Physics* **42**, 62 (2013).

- [15] P. Sturrock et al., *Astroparticle Physics* **59**, 47 (2014).
- [16] P. Sturrock, A. Parkhomov, E. Fischbach, and J. Jenkins, *Astroparticle Physics* **35**, 755 (2012).
- [17] P. Sturrock, G. Steinitz, E. Fischbach, D. J. II, and J. Jenkins, *Astroparticle Physics* **36**, 18 (2012).
- [18] P. Sturrock, G. Steinitz, E. Fischbach, A. Parkhomov, and J. Scargle, *Astroparticle Physics* **84**, 8 (2016).
- [19] E. Bellotti, C. Brogini, G. D. Carlo, M. Laubenstein, and R. Menegazzo, *Physics Letters B* **720**, 116 (2013).
- [20] E. Fischbach et al., *Space Science Reviews* **145**, 285 (2009).
- [21] J. H. Jenkins and E. Fischbach, *Astroparticle Physics* **31**, 407 (2009).
- [22] D. Krause et al., *Astroparticle Physics* **36**, 51 (2012).
- [23] J. A. Formaggio and G. P. Zeller, *Rev. Mod. Phys.* **84**, 1307 (2012).
- [24] K. S. Krane, *Introductory Nuclear Physics*, John Wiley & Sons, Inc., 1988.
- [25] D. Veprev and V. Muromtsev, *Astroparticle Physics* **36**, 26 (2012).
- [26] A. G. Parkhomov, *International Journal of Pure and Applied Physics* **1**, 119 (2005).
- [27] Y. A. Baurov, Y. G. Sobolev, Y. V. Ryabov, and V. F. Kushniruk, *Physics of Atomic Nuclei* **70**, 1825 (2007).
- [28] A. Parkhomov, *Journal of Modern Physics* **2**, 1310 (2011).
- [29] G. Bruhn, *Apeiron* **9**, 28 (2002), 2.
- [30] T. Semkow et al., *Physics Letters B* **675**, 415 (2009).



- [31] K. Kossert and O. J. Nhle, *Astroparticle Physics* **55**, 33 (2014).
- [32] K. Kossert and O. J. Nhle, *Astroparticle Physics* **69**, 18 (2015).
- [33] E. B. Norman, E. Browne, H. A. Shugart, T. H. Joshi, and R. B. Firestone, *Astroparticle Physics* **31**, 135 (2009).
- [34] P. S. Cooper, *Astroparticle Physics* **31**, 267 (2009).
- [35] R. de Meijer, M. Blaauw, and F. Smit, *Applied Radiation and Isotopes* **69**, 320 (2011).
- [36] C. L. Cowan, F. Reines, F. B. Harrison, H. W. Kruse, and A. D. McGuire, *Science* **124**, 103 (1956).
- [37] F. REINES and C. L. C. JUN., *Nature* **178**, 446 (1956).
- [38] G. Danby et al., *Phys. Rev. Lett.* **9**, 36 (1962).
- [39] K. Kodama et al., *Physics Letters B* **504**, 218 (2001).
- [40] B. Pontecorvo, *Journal of Experimental and Theoretical Physics* **33**, 549 (1958).
- [41] R. Davis, D. S. Harmer, and K. C. Hoffman, *Phys. Rev. Lett.* **20**, 1205 (1968).
- [42] Y. Fukuda et al., *Phys. Rev. Lett.* **81**, 1562 (1998).
- [43] F. P. An et al., *Phys. Rev. Lett.* **108**, 171803 (2012).
- [44] J. K. Ahn et al., *Phys. Rev. Lett.* **108**, 191802 (2012).
- [45] N. Agafonova et al., *Physics Letters B* **691**, 138 (2010).
- [46] K. Abe et al., *Phys. Rev. D* **88**, 032002 (2013).
- [47] A. BELLERIVE, *International Journal of Modern Physics A* **19**, 1167 (2004).
- [48] T. D. Lee and C. N. Yang, *Phys. Rev.* **104**, 254 (1956).

- [49] C. S. Wu, E. Ambler, R. W. Hayward, D. D. Hoppes, and R. P. Hudson, *Phys. Rev.* **105**, 1413 (1957).
- [50] M. Goldhaber, L. Grodzins, and A. W. Sunyar, *Phys. Rev.* **109**, 1015 (1958).
- [51] R. N. Mohapatra and G. Senjanović, *Phys. Rev. Lett.* **44**, 912 (1980).
- [52] G. Mention et al., *Phys. Rev. D* **83**, 073006 (2011).
- [53] Y. Declais et al., *Physics Letters B* **338**, 383 (1994).
- [54] C. Athanassopoulos et al., *Phys. Rev. Lett.* **75**, 2650 (1995).
- [55] A. Aguilar et al., *Phys. Rev. D* **64**, 112007 (2001).
- [56] S. S. R.J. de Meijer, arXiv (2014).
- [57] High Flux Isotope Reactor, Oak Ridge National Laboratory (ORNL), <https://neutrons.ornl.gov/hfir>.
- [58] G. J. Dilorio, *Direct Physical Measurement of Mass Yields in Thermal Fission of Uranium 235*, New York: Garland, 1979.
- [59] G. Kessler, *Proliferation-Proof Uranium / Plutonium Fuel Cycles Safeguards and Non-Proliferation*, KIT Scientific Publishing, 2011.
- [60] National Nuclear Data Center (NNDC), Brookhaven National Laboratory, <http://www.nndc.bnl.gov/chart/>.
- [61] X-ray Transition Energy Database, Physical Measurement Laboratory, National Institute of Standards and Technology, <https://www.nist.gov/pml/x-ray-transition-energies-database>.
- [62] Y. Varshni, *Physica* **34**, 149 (1967).
- [63] G. E. Knoll, *Radiation Detection and Measurement*, John Wiley & Sons, Inc., 2000.

- [64] *DSPEC 50 /50A DSPEC 502/502A Standard / Advanced Digital Gamma-Ray Spectrometer Hardware Users Manual.*
- [65] D. York, N. M. Evensen, M. L. Martinez, and J. De Basabe Delgado, *American Journal of Physics* **72**, 367 (2004).
- [66] Energy calibration of hpge detector using neutrons, neutron induced ambient background and natural background, in *24th International Conference on the Application of Accelerators in Research and Industry (CAARI 2016)*, 2016.
- [67] Astronomical Applications Department, The United States Naval Observatory (USNO), <http://aa.usno.navy.mil/data/docs/EarthSeasons.php>.

VITA

## VITA

Shih-Chieh Liu was born in Taipei, Taiwan. He attended National Chung Cheng University from 2003 to 2007, graduated in 2007 with a Bachelor of Science in Physics. He then attended National Tsing Hua University from 2007 to 2009 and graduated in 2009 with a Master of Science in Physics. He pursued his research in condensed matter and X-ray physics under the direction of Professor Di-Jing Huang. He received a 2-year Advanced Light Source Scholarship from National Synchrotron Radiation Research Center from 2007 to 2009.

He came to Purdue University in the Fall of 2012 and began graduate studies in Physics. He received fully financial support, Research and Teaching Assistantships, from 2012 to 2018 as well as a summer research grant in 2017. He pursued his research in nuclear physics under the direction of Professor David S. Koltick and received the Doctor of Philosophy from Purdue University in 2018. He is now working at Intel as a PTD Module and Integration Yield Engineer in Oregon.



# Advanced Reactors by 2030

---

## Challenges and Opportunities

**DRAFT**

Robert R. Price  
December 30, 2016



## Table of Contents

<b>EXECUTIVE SUMMARY .....</b>	<b>1</b>
<b>INTRODUCTION .....</b>	<b>3</b>
Questions to be Answered .....	3
Context .....	4
Decarbonization .....	4
Lowering Electricity Demand.....	6
Natural Gas Supply and Price .....	7
Light Water Reactor Retirements.....	11
Solar and Wind Energy Costs.....	14
Advanced Reactors.....	15
When Available?.....	17
When To Start Construction?.....	21
Barriers to Advanced Reactors .....	22
Economics.....	23
<b>COMPETITION FROM NATURAL GAS.....</b>	<b>26</b>
Length and Cost of Regulatory Approval.....	28
Waste Management.....	29
Utility Acceptance .....	31
Summary of barriers.....	33
<b>POTENTIAL ENERGY MIXES.....</b>	<b>34</b>
2016 Annual Energy Outlook.....	34
DOE Fuel Cycle Options Campaign Analysis .....	38
Base Case with no Subsidies for any technology .....	39
Business As Usual Case (existing subsidies continue for renewables).....	40
Expanded Subsidies Case.....	42
Alternate Expanded Subsidies Case .....	46
Alternate Expanded Subsidy Case 1 – Renewable Subsidies plus carbon taxes to achieve CPP goal.....	46
<b>R&amp;D PROGRAM .....</b>	<b>51</b>
Advanced Reactor Technologies (ART) subprogram.....	52
Material Recovery and Waste Form Development (MRWFD) .....	52
Advanced Fuels.....	53
Systems Analysis and Integration.....	53
Fuel Resources.....	53
Used Nuclear Fuel Disposition R&D .....	53
Analysis of the NE R&D Programs .....	53
A Word on Innovation and Technology Transfer .....	55
<b>SUMMARY AND CONCLUSIONS .....</b>	<b>56</b>
<b>RECOMMENDATIONS.....</b>	<b>58</b>
1. EMBRACE AND ENABLE NATIONAL ADVOCACY .....	58
2. CONDUCT DEMONSTRATION(S).....	59
3. FACILITATE COMMERCIAL EFFORTS .....	60
a. Construct and operate a fast neutron test reactor .....	60

- b. Modifications to the Gateway for Accelerated Innovation in Nuclear initiative ..... 61
- c. Establish the Correlation of Heavy Ion Irradiation and Neutron Irradiation, if possible ..... 62
- d. Waste Management R&D on advanced reactor used fuels ..... 62
- 4. BECOME ECONOMICALLY COMPETITIVE..... 63
  - a. AIM HIGH; GENERATION V ..... 63
  - b. ENHANCED ELECTRICTY GRID MODELING..... 64
  - c. ENHANCED ANALYSIS CAPABILITIES..... 65
  - d. RELATIONSHIPS WITH OTHER ORGANIZATIONS ..... 66
- REFERENCES ..... 67

### List of Figures

- Figure 1. US Electricity Generation in Base Case with No Subsidies..... 39
- Figure 2. US Electricity Generation with Renewable Energy Subsidies (Business as Usual)..... 41
- Figure 3. Electricity Generation in Expanded Subsidies Case ..... 43
- Figure 4. Nuclear Electricity Generation in Expanded Subsidy Case ..... 44
- Figure 5. CO2 Emissions from Electricity Generation in Expanded Subsidy Case..... 45
- Figure 6. Carbon Taxes Needed to Achieve CPP Goals ..... 46
- Figure 7. Electricity Generation with Carbon Tax to Achieve CPP Goal..... 47
- Figure 8. CO2 Emissions with Carbon Taxes ..... 48
- Figure 9. Carbon Taxes to Achieve CPP with (red) and without (blue) a Nuclear Subsidy ..... 49
- Figure 10. Electricity Generation with Carbon Tax and Nuclear Subsidy to Achieve CPP Goal ..... 49
- Figure 11. CO2 Emissions with Carbon Taxes and Nuclear Subsidy..... 51

### List of Tables

- Table 1. Assumed Capital Costs for Electricity-generating Technologies in PNNL GCAM Model..... 38
- Table 2. Electricity Generation in Base Case (2015 and 2050) ..... 40
- Table 3. Subsidies Used in Business as Usual Case ..... 41
- Table 4. Electricity Generation in Business as Usual Case (2015 and 2050)..... 42
- Table 5. Electricity Generation in Expanded Subsidies Case (2015 and 2050) ..... 43
- Table 7. Electricity Generation in Alternate Expanded Subsidies Case 1 – Carbon Taxes to Meet CPP (2015 and 2050)..... 47
- Table 8. Electricity Generation in Alternate Expanded Subsidies Case 2 – Carbon Taxes and Nuclear Subsidy to Meet CPP (2015 and 2050)..... 50



## Executive Summary

As the United States (US) looks to reduce carbon emissions from the energy sector, as proposed in the Environmental Protection Agency's Clean Power Plan, nuclear energy and advanced reactors are seen as natural components in the future energy mix, because they emit no carbon. However, over the next several decades it appears that nuclear energy and specifically advanced reactors will face significant headwinds that will minimize or even prevent widespread commercial deployment of new nuclear reactors even if the US moves to decarbonize its energy sector. Three major issues are identified with analysis and recommendations.

**COMPETITIVENESS:** Even considering that nuclear energy emits zero carbon, current energy market realities means that nuclear energy will likely remain a declining element of US electricity generating technologies. Retirements of current generation LWR will likely be preferentially replaced with natural gas, solar, and wind, not light water reactors (LWR) or advanced reactors; in part because low prices for domestic natural gas are expected to continue over the next several decades. These factors will result in the economics of current advanced reactors being insufficiently attractive to drive widespread adoption unless they are subsidized by some means to account for the social costs of carbon or to achieve policy goals like: security of supply, sustainability, or maintenance of technological advantage. Unless it can be monetized at the utility level, it will not be done by the utility. A production tax credit is one policy tool that can effectively influence technology decision makers. The override of competitive forces that exists in other countries with strong national policies supporting nuclear energy does not exist in the US where there is no strong government advocacy function or policy-push for nuclear energy.

**READINESS:** The next issue is whether advanced reactor concepts could be ready for widespread commercial deployment by 2030. A review of advanced reactors being developed commercially indicates that several light water-based small and medium-sized reactor concepts could be ready for commercial deployment in 2030. However, it is unlikely that any non-LWR advanced reactor concepts will be ready by 2030. The most mature technologies (VHTR and SFR) will not likely be available until 2035-2040, at the earliest. Other, less mature concepts, e.g. MSR or LFR, will need more time for demonstration before being available for commercial deployment, likely near 2050. Other aspects of readiness include regulatory, supply chain, and waste management readiness, each of which has its own challenges to be ready to support commercial deployment of advanced reactors.

**"We're moving faster than anybody ever has in that space, but that's about a 30-year period, assuming things go really well."**

– Bill Gates

**CHALLENGES:** There are non-economic barriers to commercial deployment of advanced reactors that include: length and cost of regulatory approval, waste management, utility acceptance, and public acceptance and national will. Taken together, there is a high bar to the widespread commercial deployment of advanced reactors. Fundamentally the question is: what is the compelling case for changing to a new nuclear energy technology in the US? At present, there appears little to answer this question positively given the large uncertainties, competitive forces, and risks involved.

**OPPORTUNITIES:** Yet, the promise of advanced reactors remains unchanged; a source of clean energy that provides the US with an affordable, sustainable, and reliable driver for economic growth and competitiveness. Generation IV advanced reactors maturing for deployment represent improvements to the light water reactor technology in terms of safety, security, and reliability. Future generations need to go further, especially in terms of economic competitiveness. When seen as a component of a complementary mix of electricity generating technologies, advanced reactors have the potential to bring the nation closer to the vision of clean, economic, reliable, sustainable, safe and secure energy.

The commercial deployment of advanced reactors in the US requires a significant national effort akin to the commercial deployment of LWR at the beginning of the atomic age. Looking to this past we can discern the essential elements that led to successful deployment of a new, complex, unproven energy technology. These essential elements include: Strong National Advocacy, Adequate Demonstration, Support for Industry, and Economic Competitiveness.

The Office of Nuclear Energy (NE) has a major role to play in creating and sustaining these essential elements in order to enable the commercial deployment of advanced reactors. Therefore, it is recommended that NE devise an improved research and development framework that will allow advanced reactors to fully compete in the all-important arena of economics, including construction and operation of appropriate test and demonstration reactors. These and other recommendations are given at the end of the report.

## Introduction

On 21 Oct 2016 at DOE/NE offices in Germantown, MD a meeting was held with Dr. John Herczeg, William McCaughey, Bhupinder Singh, and Robert Price. At that meeting recent events and reports (e.g., SEAB report to S-1, recent work by Third Way, Clean Power Plan) were reviewed and discussions held on the potential role of advanced reactors in achieving US carbon reduction goals. Subsequently, a task was developed to govern an independent review:

*“Conduct a quick, independent review of the R&D portfolio of the Office of Nuclear Technology Research and Development (NE-4) and provide an assessment that can be used to as input for prioritization of the Office’s R&D that is needed to meet the goals of the office in support of the Department of Energy’s mission to achieve climate change objectives.”*

To accomplish this task, the following activities were conducted:

- Obtain background information
- Obtain Information on Current NE-4 Advanced Reactor R&D program activities.
- Conduct an assessment that can be used as input for prioritization of the Office’s R&D.

## Questions to be Answered

Using the information gathered and developed, answer the following questions:

1. What does the mix of electricity supply sources look like in 2050 to obtain national security and carbon reduction goals in a competitive market?
  - a. This would be done by evaluating a series of four cases working with NE/FCO staff. To the extent possible efforts will be made to differentiate between LWR, SMR, and Advanced Reactor technologies.
    - i. Base case with no subsidies for any technology
    - ii. Business as usual (existing subsidies continue for renewables)
    - iii. Expanded subsidies (current subsidies for renewables plus a \$0.027/kWe-hr production credit for carbon-free energy as recommended by SEAB)
    - iv. Alternate expanded subsidies (current subsidies and/or a carbon tax sized to achieve 2050 carbon reduction goal)
2. What type(s) of nuclear reactor technologies can be expected to be available in the 2030 timeframe to support meeting the US carbon reduction goal?
3. When do we need to start their deployment (construction, operation) if we are to meet the carbon reduction goal?
4. What barriers need to be overcome to enable advanced reactors to be ready in time?
5. Are there modifications to the current R&D program that could be made to improve alignment with the goal to support deployment of advanced reactors by 2030 timeframe to support carbon reduction goals?

## Context

The energy sector in US is being shaped by several significant forces and trends that will impact choices on energy technology in the coming decades. These are decarbonization; natural gas supply; lowering energy demand; light-water reactor (LWR) retirements, and solar and wind energy costs.

## Decarbonization

For over two decades there has been a growing push to reduce emissions of man-made carbon because of its potential role in affecting global climate.

The United Nations Framework Convention on Climate Change (UNFCCC) was negotiated at the Earth Summit in Rio de Janeiro in June 1992 and entered into force on 21 March 1994. The ultimate objective of the UNFCCC was agreed to be *“stabilization of greenhouse gas concentrations in the atmosphere at a level that would prevent dangerous anthropogenic interference with the climate system.”*<sup>1</sup>

This eventually led most recently to the Paris Agreement of 2015, an agreement within the UNFCCC dealing with greenhouse gases emissions mitigation, adaptation and finance starting in the year 2020:

*“Adopted in Paris by the 196 Parties to the UN Framework Convention on Climate Change (UNFCCC) at a conference known as (COP21) last December, the Agreement’s objective is to limit global temperature rise to well below 2 degrees Celsius, and to strive for 1.5 degrees Celsius.”*<sup>2</sup>

As of 2 Nov 2016, 192 UNFCCC members have signed the treaty, 92 of which have ratified it. After the European Union ratified the agreement in October 2016, there were enough countries that had ratified the agreement that produce enough of the world's greenhouse gases for the agreement to enter into force; the agreement took effect on 4 November 2016. The US Government signed the Paris Agreement on 22 April 2016 and formally accepted it on 3 Sep 2016, but has yet to formally approve it.<sup>3</sup>

While the US Government has not formally approved the Paris Agreement, the Obama Administration has already taken steps to implement its intent. In June 2014, the Environmental Protection Administration (EPA) released the Clean Power Plan (CPP); which was formally unveiled by President Obama on 3 Aug 2015. The overarching goal of the CPP is, for the first time, to limit the amount of carbon emissions from electricity generating power plants, specifically to reduce carbon emissions from power plants by 32 percent from the 2005 level by 2030. The intent of the CPP is to influence change to the energy technologies used in the US, away from coal and toward lower carbon-emitting options:

---

<sup>1</sup>[http://unfccc.int/files/essential\\_background/background\\_publications\\_htmlpdf/application/pdf/conveing.pdf](http://unfccc.int/files/essential_background/background_publications_htmlpdf/application/pdf/conveing.pdf), Article 2.

<sup>2</sup> [www.un.org/apps/news/story.asp?NewsID=53756#.WBnFUjXQfcd](http://www.un.org/apps/news/story.asp?NewsID=53756#.WBnFUjXQfcd), retrieved 2 Nov 2016

<sup>3</sup> [http://unfccc.int/paris\\_agreement/items/9444.php](http://unfccc.int/paris_agreement/items/9444.php)

---

### Background: Clean Power Plan

- On April 2, 2007, in a landmark decision in *Massachusetts v. EPA*, the Supreme Court determined that greenhouse gases, including carbon dioxide, are air pollutants under the Clean Air Act and EPA must determine if they threaten public health and welfare.
- On December 15, 2009, the EPA Administrator found that the current and projected concentrations of greenhouse gases endanger the public health and welfare of current and future generations.
- In June 2013, President Obama directed EPA to reduce carbon pollution from power plants as part of a Climate Action Plan.
- On September 20, 2013, EPA announced proposed standards to limit carbon pollution from new power plants – the agency's first step under the President's Climate Action Plan to reduce GHGs from the power sector.
- On June 2, 2014, EPA announced proposed standards to limit carbon pollution from modified and reconstructed power plants.

(source:  
[www.epa.gov/sites/production/files/2015-11/documents/fs-cps-overview.pdf](http://www.epa.gov/sites/production/files/2015-11/documents/fs-cps-overview.pdf)

*“Specifically, the EPA assumes that the required emission reductions may be achieved by 1) heat rate improvements at individual plants; 2) increased use of natural gas instead of coal for electricity generation, and 3) increased use of renewable energy. The EPA also hopes that states will use their SIPs [State Implementation Plans] to encourage energy conservation and increased efficiency as well...”<sup>4</sup>*

With respect to nuclear energy, the EPA's fact sheet “*Clean Power Plan - Opportunities for Nuclear Power*” envisions that nuclear energy will provide 19 percent of electricity in the US in 2030; essentially unchanged from its role today.<sup>5</sup> The fact sheet states:

*“EPA expects nuclear power to be a key partner in achieving the goals of the CPP. States can use new nuclear generation to help meet their Clean Power Plan goals. This includes new nuclear reactors that come on-line, including those under construction, and existing facilities that expand their capacity (uprates)...*

*“The CPP creates incentives for nuclear energy. Nuclear energy accounts for nearly 20 percent of the power produced in the U.S., and is a reliable, carbon free generation source (see chart below). The CPP provides multiple pathways and approaches for leveraging the value of clean energy in state plans, and creates incentives for clean energy technologies, including nuclear power. There are incentives to continue operation of existing nuclear units so that emissions from affected fossil-fuel fired sources will not increase from today's levels. There are incentives to upgrade equipment and increase a unit's capacity through an uprate, which can further offset carbon emissions from affected power plants. And there are incentives for investment in new nuclear capacity to help states meet their goals. In addition, if existing units receive operating license extensions that are accompanied by an eligible capacity uprate as a result of the relicensing process, the capacity uprate will be eligible for credit towards compliance under the Clean Power Plan.”<sup>6</sup>*

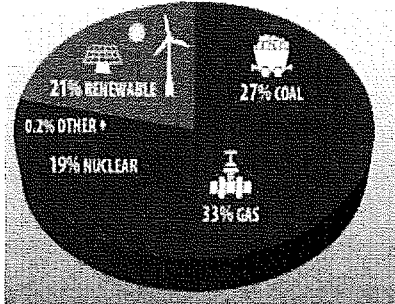
---

<sup>4</sup> [www.washingtonpost.com/news/volokh-conspiracy/wp/2016/02/10/placing-the-clean-power-plan-in-context/](http://www.washingtonpost.com/news/volokh-conspiracy/wp/2016/02/10/placing-the-clean-power-plan-in-context/), retrieved 2 Nov 2016

<sup>5</sup> [www.epa.gov/sites/production/files/2015-11/documents/fs-cpp-nuclear.pdf](http://www.epa.gov/sites/production/files/2015-11/documents/fs-cpp-nuclear.pdf), retrieved 2 Nov 16

<sup>6</sup> [www.epa.gov/sites/production/files/2015-11/documents/fs-cpp-nuclear.pdf](http://www.epa.gov/sites/production/files/2015-11/documents/fs-cpp-nuclear.pdf), retrieved 2 Nov 16

With CPP, Nuclear Power Remains Nearly 20% of the Energy Mix in 2030

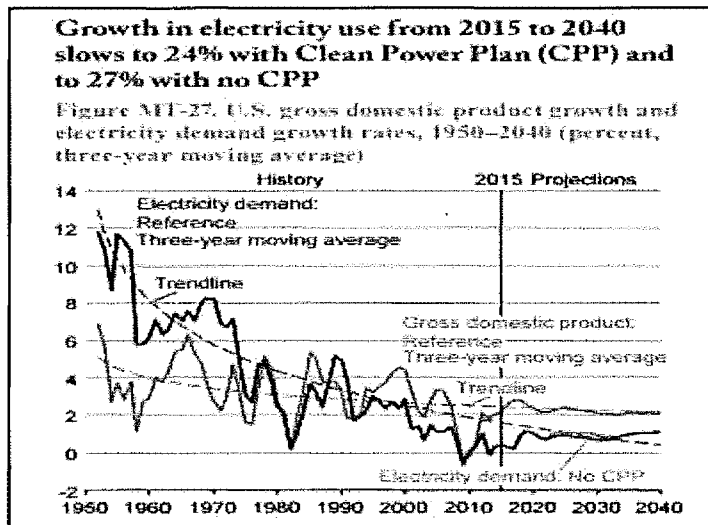


Given that the driver for decarbonization stems from a 2007 Supreme Court decision that classifies greenhouse gases, including CO<sub>2</sub>, as pollutants there is a significant barrier to overturning the push to limit greenhouse gases and thus it remains likely that the drive to decarbonize electricity-generating technologies in the US will remain, irrespective of the political party controlling the White House and/or Congress. As it is targeted at reducing the number of coal and natural-gas generating facilities, it appears that nuclear technologies could benefit from its imposition and enforcement, due to nuclear energy's zero carbon-emission.

### Lowering Electricity Demand

Another long-term trend that will affect future decisions on electricity generation capacity is the continued de-industrialization of the US coupled with increasing energy efficiency of remaining industry and everyday life (see Figure MT-27). This is important because it places an upper limit on the amount of capacity additions can be expected in the US through 2040 and beyond and that new plant construction will mainly take place as replacements for retiring coal capacity as those plants close in response to age and carbon restrictions. This portends a highly competitive market for construction of new electricity-generation plants, heightening the differences in economic competitiveness between technology choices.

According to the EIA forecast low electricity demand growth over the next 25 years due to a number of strategic factors:



Source: EIA annual Energy Outlook 2016, page MT-15.

*“Electricity demand growth (including retail sales and direct use) has slowed in every decade since the 1950s, from 9.8%/year from 1949–59 to 0.5%/year from 2000–2015. In the AEO2016 Reference case and No CPP case, electricity demand growth remains relatively slow, as rising demand for electric services is offset by efficiency gains from new appliance standards and investments in energy-efficient equipment. Total electricity demand grows by 24% (0.9%/year) from 2015–40 in the Reference case, which includes the effects of the Clean Power Plan (CPP).”*

<sup>7</sup> U.S. Energy Information Administration, Annual Energy Outlook 2016, page MT-15

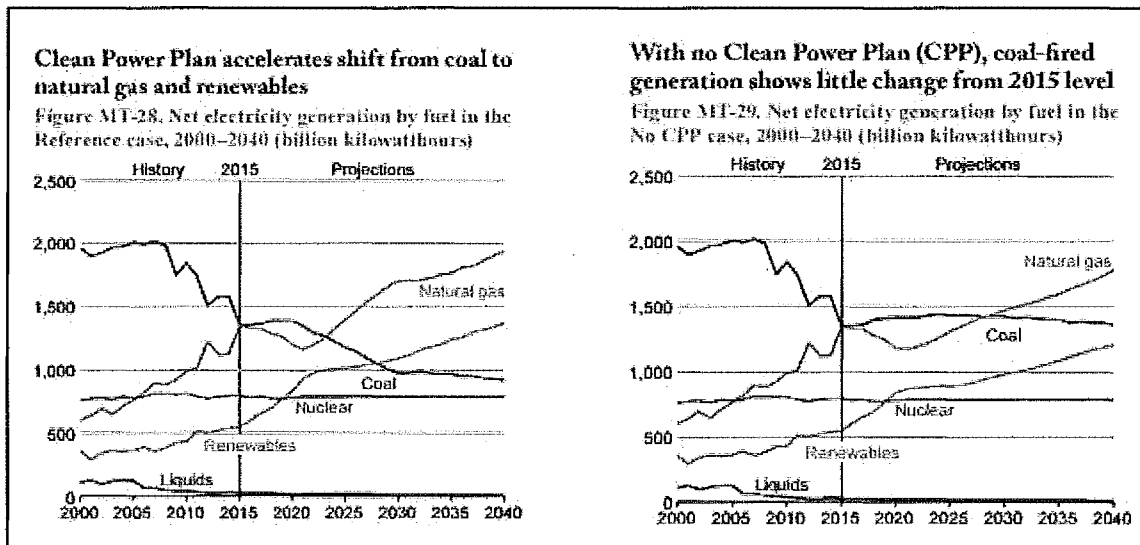
### Natural Gas Supply and Price

Natural gas abundance in the US and corresponding low prices have had a dramatic effect on electricity generating technology decision-making in the US. The US has considerable resources of domestic natural gas, of which the recovery efficiency and cost continue to improve. This has driven a significant increase in the use of natural gas for electricity generation due to its low cost and ready availability (see charts MT-28 and MT-29 below). Due to its low cost, natural gas is the current go-to technology to replace coal. As can

*“The fact that this is the largest assessment of continuous oil we have ever done just goes to show that, even in areas that have produced billions of barrels of oil, there is still the potential to find billions more”*

*Walter Guidroz, USGS Energy Resources Program, 15 Nov 2016.*

be seen, renewables are also competitive economically, due to production tax credits and the Clean Energy Incentive Plan that supports the CPP. Note, however, that even without the CPP the EIA forecast continued growth in renewables, mainly due to state-level actions, e.g., renewable portfolio standards (RPS), to reduce carbon emissions (See Figure MT-29 below).

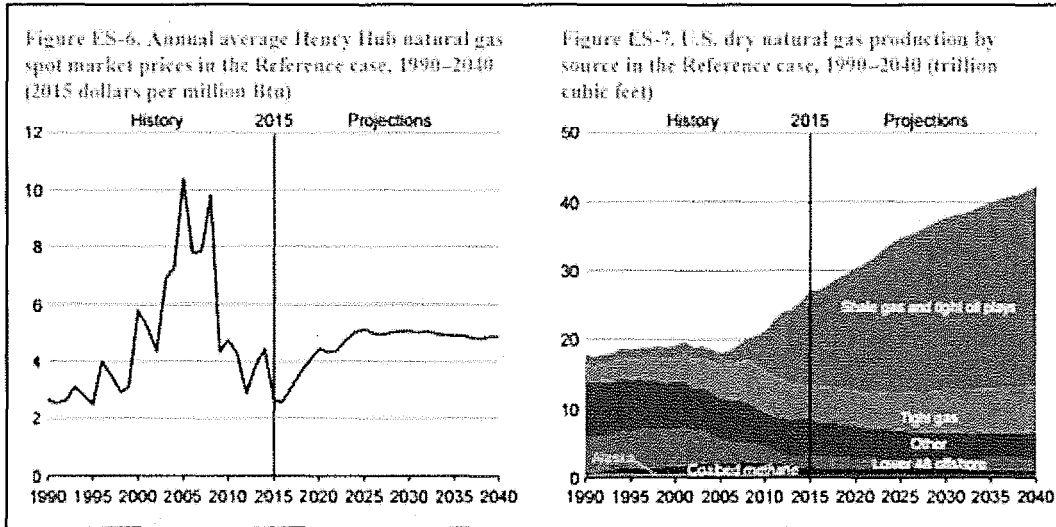


Source: EIA annual Energy Outlook 2016, page MT-15.

Despite the expected significant growth in natural gas generating capacity the EIA forecasts that the price for this fuel will remain fairly constant through 2040 (see charts ES-6 and ES-7 below). This is because increases in domestic production are expected to more than match increased demand from natural gas electricity generation with the net result being a fairly constant and low price of natural gas. For example, in November 2016, the US Geological Survey just announced: *“the largest estimate of continuous oil that USGS has ever assessed in the United States.”*<sup>8</sup> There is no reason to believe that this is the last new

<sup>8</sup> [www.usgs.gov/news/usgs-estimates-20-billion-barrels-oil-texas-wolfcamp-shale-formation](http://www.usgs.gov/news/usgs-estimates-20-billion-barrels-oil-texas-wolfcamp-shale-formation)

discovery of oil and natural gas in the US. This means that the economic pressure on nuclear energy from low gas prices and low-cost natural gas produced electricity can be expected to continue for the next few decades.



Source: EIA annual Energy Outlook 2016, page ES-5.

It is hard to comprehend the magnitude of the revolution that hydraulic fracking has caused in the supply of natural gas. The impact of the technological advances of hydraulic fracking and horizontal drilling has led to a massive shift in the availability of inexpensive natural gas in the US. For example:

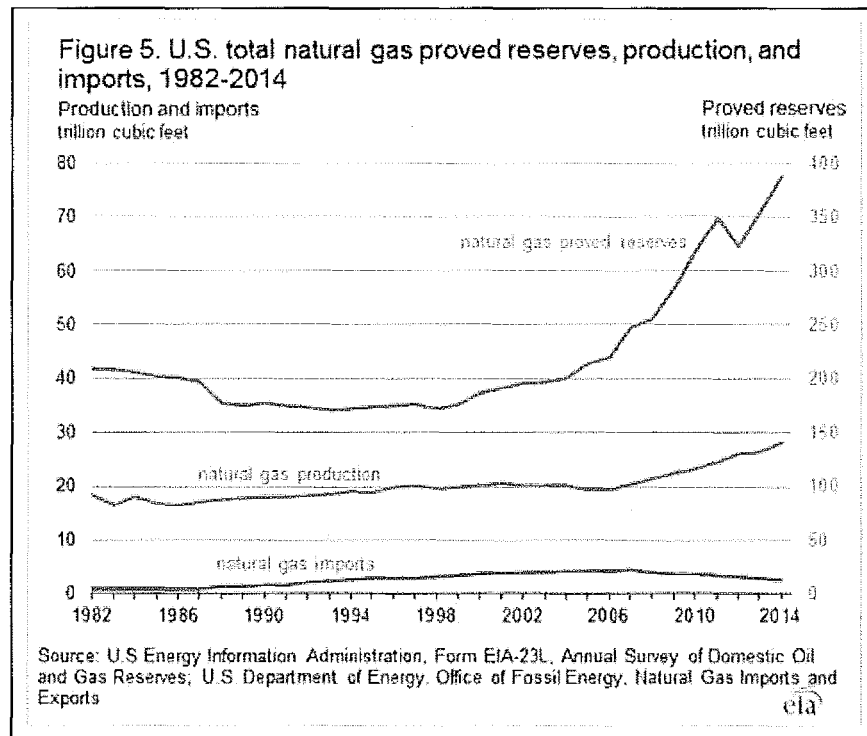
*"...when prices fell, many thought that it might be the end of the shale revolution because shale resources can be more expensive to produce than conventional oil and natural gas resources. However, innovation has led to much lower production costs than previously believed possible. This is great news for Americans because it means that oil and natural gas prices will likely continue to remain affordable for years to come."<sup>9</sup>*

Domestic production has soared and there has been a steady increase in estimates of resources and reserves as existing and potential well-fields and geologies are reassessed in light of improvements in extraction technology. In 2014, conventional natural gas reserves were estimated at about 388 TCF by the EIA; the largest ever recorded conventional gas reserves in the US, even as production has increased (see Figure 5).<sup>10</sup>

<sup>9</sup> Institute for Energy Research, New Oil Finds in Texas and Alaska, 12 Oct 2016, <http://instituteforenergyresearch.org/analysis/new-oil-finds-texas-alaska/>, retrieved 12 Dec 2016

<sup>10</sup> [www.eia.gov/naturalgas/crudeoilreserves/](http://www.eia.gov/naturalgas/crudeoilreserves/), retrieved 13 Dec 2016





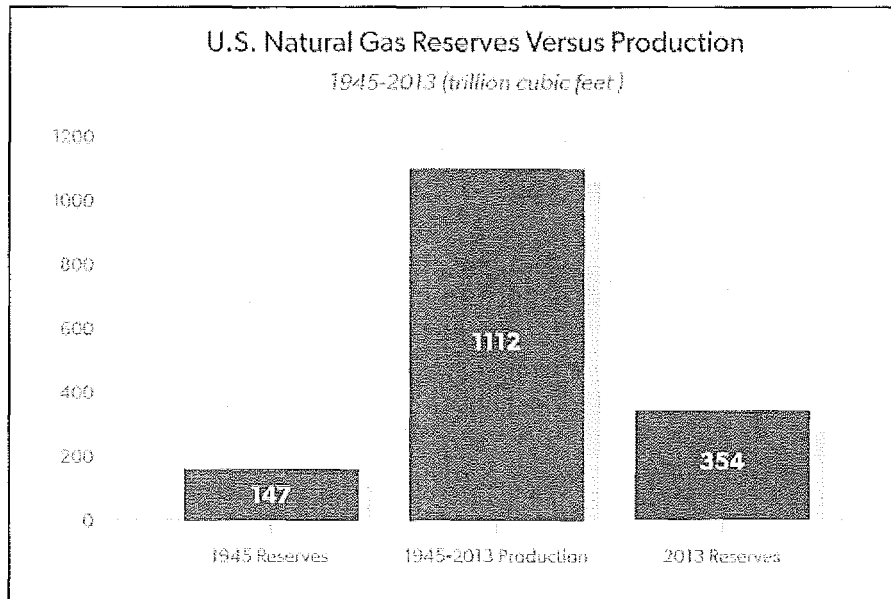
The unlocking of shale-based natural gas has been mainly a US-phenomenon but these resources exist around the world and are beginning to be tapped. In 2013, The US Energy Information Administration conducted a major assessment of worldwide technically recoverable shale-based natural gas resources and should be considered as a conservative lower bound, because it did not assess significant areas of the world and it only considered shale-based resources and no other tight gas geologies like sandstone.<sup>11</sup> It should also be noted that they did not include the Middle East, Central Africa, and other significant countries in the study. They concluded:

*“...that the world shale gas and shale oil resource is vast. Overall, for the 41 countries assessed in the EIA/ARI study, we identified a total risked shale gas in-place of 31,138 Tcf. Of this total, approximately 6,634 Tcf is considered the risked, technically recoverable shale gas resource, not including the U.S. Adding the U.S. shale gas resource increases the assessed shale gas in-place and technically recoverable shale gas resources of the world to 35,782 Tcf and 7,795 Tcf, respectively.”<sup>12</sup>*

<sup>11</sup> Technically recoverable resources can be discovered, developed, and produced using current technology.

<sup>12</sup> EIA/ARI “World Shale Gas and Shale Oil Resource Assessment Technically Recoverable Shale Gas and Shale Oil Resources,” June 2013, page 4.  
[www.eia.gov/analysis/studies/worldshalegas/pdf/overview.pdf](http://www.eia.gov/analysis/studies/worldshalegas/pdf/overview.pdf)

The study shows that the US has an estimated 1,161 TCF of technically recoverable shale gas, about 15 percent of the assessed world total. For the sake of context, the total demand for natural gas in 2015 was about 27.3 TCF in the US.<sup>13</sup> Thus, there are about 40 years of supply at current rates of usage for the resources already identified. Not an indefinite period but two things must be considered. One, as shown above, resource estimates have steadily increased along with increasing production as they are reassessed in light of new exploration, technical advances, and the price for the gas. The following chart shows this to be true over a considerable period of time.<sup>14</sup>



Second, there are other significant sources of natural gas not yet economic or accounted for. A potentially massive source of unconventional natural gas are the vast amounts of methyl hydrates increasingly being discovered around the world; on land under the permafrost of the Arctic and Antarctic as well as offshore in all of the world's oceans. The most recent assessment by the US Bureau of Ocean Energy Management in 2012 concluded that there are over 51,000 TCF of in-place natural gas resources in the oceans surrounding the lower 48 states.<sup>15</sup> Gas hydrates portend an energy future with significant natural gas participation as these resources are researched and developed in order to make them economically available.

<sup>13</sup> [www.eia.gov/dnav/ng/ng\\_sum\\_lsum\\_dcu\\_nus\\_a.htm](http://www.eia.gov/dnav/ng/ng_sum_lsum_dcu_nus_a.htm), retrieved 13 Dec 2016

<sup>14</sup> [http://instituteeforenergyresearch.org/wp-content/uploads/2015/04/IER\\_HardFacts\\_2015\\_3.pdf](http://instituteeforenergyresearch.org/wp-content/uploads/2015/04/IER_HardFacts_2015_3.pdf), page 24, retrieved 19 Dec 2016

<sup>15</sup> US BOEM, Assessment of In-Place Gas Hydrate Resources of the Lower 48 United States Outer Continental Shelf, [www.boem.gov/uploadedFiles/BOEM/Oil\\_and\\_Gas\\_Energy\\_Program/Resource\\_Evaluation/Gas\\_Hydrates/BOEM-FactSheetRED\\_2012-01.pdf](http://www.boem.gov/uploadedFiles/BOEM/Oil_and_Gas_Energy_Program/Resource_Evaluation/Gas_Hydrates/BOEM-FactSheetRED_2012-01.pdf), retrieved 12 Dec 2016

Not too long ago, the idea of economic recovery of unconventional gas resources was ridiculous. Yet, shale gas accounted for over 50 percent of US natural gas production in 2015.<sup>16</sup> This move from concept to economic reality came about over a period of about 40 years. The concept of hydraulic fracking was patented in 1949. The hydraulic fracturing process was used in conventional limestone and sandstone reservoirs for decades before the onset of the shale revolution. But it was not until the 1970s that significant attempts to apply the technology to shale-based resources were made, pioneered by DOE research and demonstration project cost-sharing with industry in such ventures as the Eastern Gas Shales Project (1976-92).<sup>17</sup> When fracking was combined with horizontal drilling techniques in shale formations these resources became economic and caused the renaissance of US natural gas production in the US; the effects we see today manifested in very low prices for natural gas.

For gas hydrates, US government-sponsored research began in the 1990s, so it may be a couple of decades yet before these resources can be economically recovered. Whether or not they can be economically recovered is unknown, but if the history of shale gas in the US is any indication, it is not unreasonable to believe that the likelihood is high that they will eventually become economically available. This point is important as emphasized in a recent Institute for Energy Research report:

*“Needless to say, the world’s natural gas industry would be radically transformed even if we were to recover just a very small share of all of the hydrates in shallow sediments. Tapping just 1% of the resource would yield more methane than is currently stored in the known reserves of natural gas.”<sup>18</sup>*

Therefore, it should be presumed that low-cost natural gas will remain a key factor in the US energy landscape for many decades to come. The continued availability and low price of domestic natural gas produces a significant economic advantage for gas-fired electricity generation plants, which by their nature have their generation cost dominated by their fuel costs.

### **Light Water Reactor Retirements**

While the importance and value of existing Light Water Reactor (LWR) is recognized by many, the facts are that they are aging and coming under increasing economic pressure resulting from low prices of natural gas as well as regulations that dictate how electricity is priced and dispatched to the marketplace by the Independent Service Organizations (ISO) in the “deregulated” portions of the US. Over the past several years these difficult market conditions have led to a number of closures or planned closures (e.g., Kewaunee in Wisconsin). Most recently, Entergy announced on 8 Dec 2016 that it will be

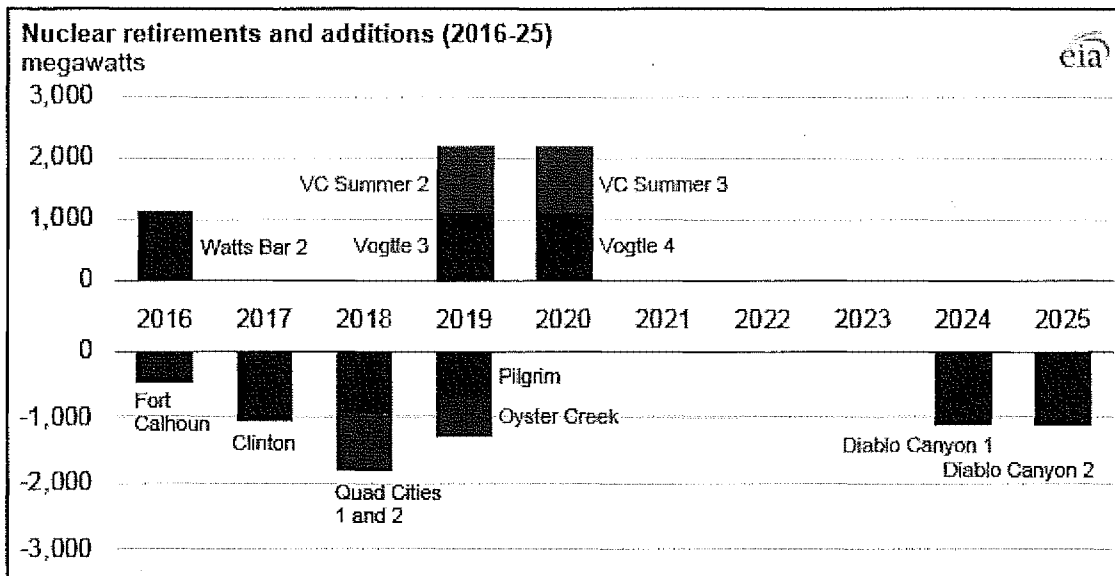
---

<sup>16</sup> [www.eia.gov/naturalgas/crudeoilreserves/](http://www.eia.gov/naturalgas/crudeoilreserves/), figure 12, retrieved 13 Dec 2016

<sup>17</sup> [http://energy.gov/sites/prod/files/2013/04/f0/how\\_is\\_shale\\_gas\\_produced.pdf](http://energy.gov/sites/prod/files/2013/04/f0/how_is_shale_gas_produced.pdf), retrieved 13 Dec 2016

<sup>18</sup> [http://instituteforenergyresearch.org/wp-content/uploads/2015/04/IER\\_HardFacts\\_2015\\_3.pdf](http://instituteforenergyresearch.org/wp-content/uploads/2015/04/IER_HardFacts_2015_3.pdf), page 37, retrieved 19 Dec 2016.

permanently closing the Palisades plant on 1 Oct 2018.<sup>19</sup> Also, technical issues and public pressure have affected decisions to close or announce closure of other units (e.g., Diablo Canyon in California). At the same time nearly all reactor operating companies have applied or plan to apply for license extensions. Taking these factors into consideration, the EIA produced a graphic to visualize the expected changes in LWR capacity in the US over the next decade (see below).



Source: US Energy Information Administration, *Electric Power Monthly*, [www.eia.gov/todayinenergy/detail.php?id=28572](http://www.eia.gov/todayinenergy/detail.php?id=28572) retrieved 2 Nov 2016

However, given that reasons stated for the closings range from economics to technical issues, it is unclear if these announced closures will be the last.

*“The Kewaunee and Vermont Yankee nuclear power plants were retired early for economic and financial reasons. The owners of the Crystal River and San Onofre units chose to retire those units early, rather than invest in needed plant repairs. Early retirement has been announced or proposed for Clinton and Quad Cities in Illinois, FitzPatrick and Ginna in New York, and Fort Calhoun in Nebraska. Other nuclear power plants, including Palisades, Davis-Besse, Prairie Island, and Three Mile Island Unit 1, have been identified as facing financial stress that might lead to early retirement.”<sup>20</sup>*

<sup>19</sup> [www.palisadespower.com/palisades-power-purchase-agreement-to-end-early-nuclear-plant-to-close-in-2018/](http://www.palisadespower.com/palisades-power-purchase-agreement-to-end-early-nuclear-plant-to-close-in-2018/), retrieved 14 Dec 2016

<sup>20</sup> Idaho National Laboratory, *Economic and Market Challenges Facing the U.S. Nuclear Commercial Fleet*, September 2016, INL/EXT-16-39951,

The DOE's recent Summit on Improving the Economics of America's Nuclear Power Plants highlights this potential:

*"If current market conditions persist, it is plausible that 50% or more of the current nuclear fleet could be at risk of retirement before 2030, making it much more difficult for the United States to meet its clean-energy, national-security, and economic objectives."<sup>21</sup>*

The Nuclear Energy Institute echoes this in its Advanced Reactor Strategy: "By 2030, a significant portion of the existing generation capacity will likely need to be replaced."<sup>22</sup>

However, despite all the uncertainty, at least through 2030, it appears likely that the LWR fleet will remain stable after a wave of already announced closures has passed. This is the assumption of the EIA and others. However, beginning in 2030 as older reactors pass 60 years in life, it is likely that a trend will develop of increasing numbers of reactors being retired due to technical and economic issues if there are no changes in market conditions and regulation. This opens the door for new build advanced reactors to take their place as part of national efforts to minimize carbon emissions from power generation, taking advantage of their established workforce, prior regulatory approval of the site, and familiarity with the technology, vendors, and suppliers.

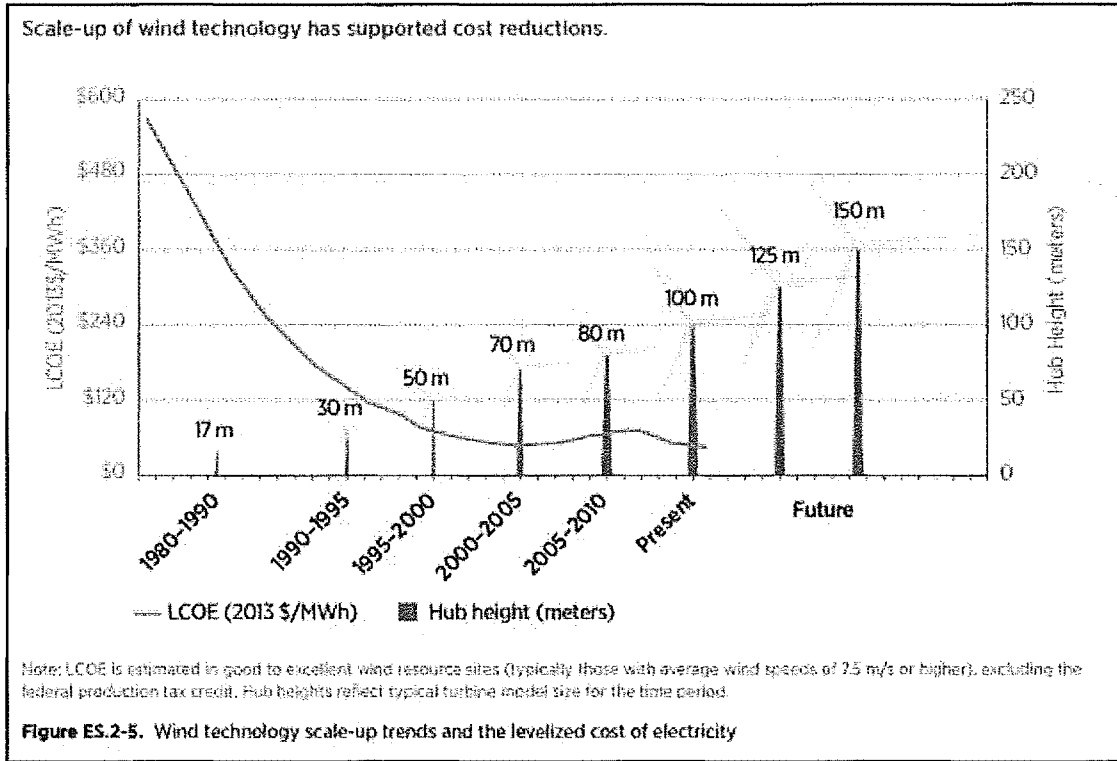
---

<sup>21</sup> Idaho National Laboratory, Summit on Improving the Economics of America's Nuclear Power Plants, INL/EXT-16-39257, September 2016, page 2.

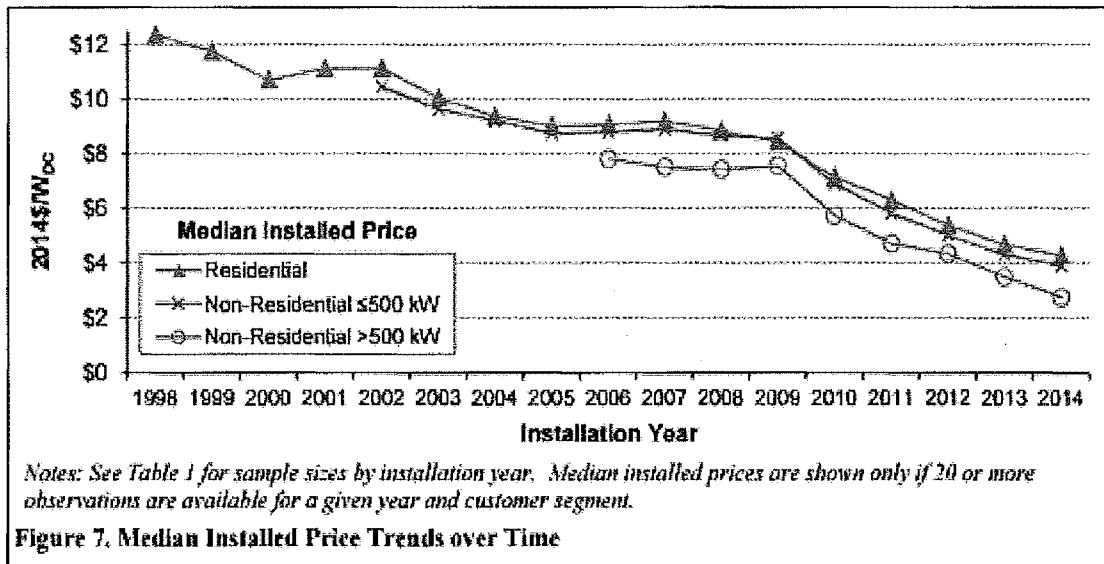
<sup>22</sup> Nuclear Energy Institute, Strategic Plan for Advanced Non-Light Water Reactor Development and Commercialization, May 2016, page 1.

### Solar and Wind Energy Costs

A significant trend in the US has been the continuous declines in costs for solar and wind technologies. Data from the DOE show significant reductions in costs for both technologies over time:



Source: Department of Energy, 2015 Wind Vision, page xxxviii



Source: Lawrence Berkeley National Laboratory, Tracking the Sun VIII, page 15.

It is not unreasonable to believe that continued progress will be made. For example the DOE 2015 Quadrennial Technology Review highlighted:

*“Solar will become economically competitive nationally when the unsubsidized LCOE of solar energy reaches roughly \$0.06/kilowatt-hours (kWh) at the utility scale (PV and CSP), \$0.08/kWh at the commercial scale, and \$0.09/kWh at the residential scale.... This outcome would require installed costs to reach roughly \$1/W for utility-scale PV systems, \$1.25/W for commercial rooftop PV, and \$1.50/W for residential rooftop PV, and \$3.60/W for CSP (including thermal energy storage). Since 2010, the industry has progressed by more than 60% of the way toward these targets, and costs continue to drop year after year.”<sup>23</sup>*

Similarly, for wind technology, the 2015 Wind Vision report concludes that continued cost reductions are likely:

*“Wind cost reductions do not depend on disruptive technological breakthroughs, but do rely on continued cost improvements, including rotor scale-up; taller towers to access higher wind speeds; overall plant efficiency improvements achieved through advanced controls; improved plant designs enabled by deepened understanding of atmospheric physics; installation of both intra-region and inter-region transmission capacity to high quality wind resource locations; and collaboration and co-existence strategies for local communities and wildlife that support the timely and cost-effective installation of wind power plants.”<sup>24</sup>*

Continued costs reductions for solar and wind technologies portend a lowering of the economic target that advanced reactor technologies will have to compete against for selection to meet future capacity additions. To summarize, there are several long-term trends affecting US energy markets that appear likely to continue through the 2030 timeframe that will have an impact on electricity-generating technology choices. These include decarbonization; natural gas supply; lowering energy demand; LWR retirements; and solar and wind energy costs.

### **Advanced Reactors**

Over the decades since the 1950s, dozens of different types of advanced reactors have been designed, researched, tested, and/or demonstrated worldwide representing tens of billions of dollars in R&D. But, except for a few early attempts at commercializing advanced reactors, almost every reactor in operation around the world today is light-water based, either boiling water reactors or pressurized water reactors. Yet, research continues around the world to develop new designs some of which may be ready for deployment by 2030. The main types being investigated currently are sodium fast reactors (SFR), high temperature gas-cooled reactors (HTGR), lead-cooled fast reactors (LFR), molten salt reactors (MSR), and light-water reactors that are small and medium sized (LWR SMR).

---

<sup>23</sup> DOE 2015 Quadrennial Technology Review, page 126.

<sup>24</sup> DOE 2015 Wind Vision, page xxv

The promise of advanced reactors has long been that they offer advantages over LWR in terms of safety, security, economics, efficiency, reliability, and sustainability. The draft DOE Vision and Strategy for Advanced Reactors captures this succinctly:

*“Advanced reactor concepts offer significant potential advantages relative to current light water reactor technology in terms of enhanced safety, lower cost, greater resource utilization, reduced waste management challenges, co-production of process heat for industrial operations, improved proliferation resistance, and easier operation.”<sup>25</sup>*

The focus in the US has mainly been on SFR and HTGR with minor efforts on lead fast reactors and molten salt-cooled reactors. Several major test programs, e.g., the Experimental Breeder Reactor II and the Fast Flux Test Facility, provided significant operating experience and performance data on sodium fast reactors in the US. US efforts also included design of a sodium-cooled fast breeder reactor as part of the Clinch River Breeder Reactor project funded from 1972 – 1983. Numerous other countries also have developed and demonstrated SFR, notably China, France, India, Japan, and Russia. Within the Generation IV International Forum China, the European Union, France, Japan, Korea, Russia, and the US remain engaged in joint development efforts.<sup>26</sup> Given this wealth of operational experience with sodium-cooled reactors, SFR technology is arguably the most mature advanced reactor technology available.

This significant experience base, representing billions of dollars in R&D and years of operating experience, has allowed private companies to develop advanced reactor designs with a view to commercial deployment, including Areva, GE-Hitachi, and Terrapower.

Significant experience with HTGR has been developed in the US from the 1950s to the present. The Peach Bottom Nuclear Generating Station served as a technology demonstration plant and produced electricity from 1966-1974. Similarly, the gas-cooled reactor at Fort St. Vrain provided similar experience and data from 1969-1979. More recently, the Next Generation Nuclear Plant project sought to develop, license, build, and operate a prototype modular high temperature gas-cooled reactor from 2006 – 2011.<sup>27</sup> Additionally, there has been a sustained TRISO fuel development program that continues with positive results. Internationally, China, Germany, Russia, and Japan have experience with HTGR and the United Kingdom operated a fleet of gas-cooled reactors for decades. Within the Generation IV International Forum, Canada, China, France, Japan, Korea, and the US are supporting continued development.<sup>28</sup>

Private companies have emerged to leverage this knowledge base and develop designs for commercial deployment including Areva and X-Energy. In January 2016, DOE awarded X-Energy partnering with BWX Technology, Oregon State University, Teledyne-Brown Engineering, SGL Group, Idaho National

---

<sup>25</sup> DOE Vision and Strategy for the Development and Deployment of Advanced Reactors (Draft), page 2.

<sup>26</sup> [https://www.gen-4.org/gif/icms/c\\_9343/system-arrangements-mou](https://www.gen-4.org/gif/icms/c_9343/system-arrangements-mou), retrieved 14 Nov 2016

<sup>27</sup> [www.nrc.gov/reactors/advanced/ngnp.html](http://www.nrc.gov/reactors/advanced/ngnp.html), retrieved 4 Nov 2016

<sup>28</sup> [https://www.gen-4.org/gif/icms/c\\_9343/system-arrangements-mou](https://www.gen-4.org/gif/icms/c_9343/system-arrangements-mou), retrieved 14 Nov 2016



Laboratory, and Oak Ridge National Laboratory, up to \$80 million to solve design and fuel development challenges of the Xe-100 Pebble Bed Advanced Reactor.<sup>29</sup>

Lead-cooled reactors have been designed and evaluated for decades at a low level in the US, e.g., the Small Secure, Transportable, Autonomous Reactor of LLNL. No lead-cooled test or demonstration reactors were ever built in the US though material test loops have been built and operated, e.g., LANL. The main experience base for this type of advanced reactor has been Russia where they have operated lead-cooled reactors for decades in a series of naval nuclear propulsion designs. This experience base has been made available and has resulted in commercial interest to develop a reactor for commercial deployment, i.e., Gen4 Energy. An effort by the European Union to develop a European lead-cooled reactor system has existed since the early-2000s. Within the Generation IV International Forum China, the European Union, Japan, Korea, Russia remain engaged in joint development efforts with the US accorded observer status.<sup>30</sup>

Molten salt reactors (MSR) were evaluated in the US during the 1950s-1970s resulting in construction of the Aircraft Reactor Experiment and the Molten Salt Reactor Experiment (MSRE) at Oak Ridge National Laboratory. Later, the Molten Salt Breeder Reactor program (1970-1976) developed advanced designs for MSR, though it was never built. All of these efforts used liquid fuels with fissile material in solution with a molten salt. More recently, efforts in the US have focused on molten-salt cooled reactors with more traditional solid fuel elements. In January 2016, DOE awarded up to \$80 million to Southern Company Services, partnering with TerraPower, Electric Power Research Institute, Vanderbilt University, and Oak Ridge National Laboratory, to perform integrated effects tests and materials suitability studies to support development of a Molten Chloride Fast Reactor.<sup>31</sup>

Another category of reactors that may be available in the 2030 timeframe comprises a number of small and medium-sized light-water reactors. Because these represent designs that build on and take advantage of the decades of experience in light water reactor design and operation, they are already very mature. Research and development is mainly needed to test and gather data on specific aspects of performance or in specific components. A number of commercial firms are developing designs ranging in size from a Attachment 2 for a list of commercial SMR and advanced reactor companies).

### **When Available?**

When any of these advanced reactor designs could be ready for commercial deployment is a difficult question to answer as it depends on funding, availability of research facilities, resolution of technical challenges, and development of regulatory processes; all with uncertain timing.

---

<sup>29</sup> [www.energy.gov/articles/energy-department-announces-new-investments-advanced-nuclear-power-reactors-help-meet](http://www.energy.gov/articles/energy-department-announces-new-investments-advanced-nuclear-power-reactors-help-meet), retrieved 5 Nov 2016.

<sup>30</sup> Technology Roadmap Update for Generation IV Nuclear Energy Systems, January 2014, [www.gen4.org/gif/icms/c\\_60729/technology-roadmap-update-2013](http://www.gen4.org/gif/icms/c_60729/technology-roadmap-update-2013), retrieved 5 Nov 2016

<sup>31</sup> [www.energy.gov/articles/energy-department-announces-new-investments-advanced-nuclear-power-reactors-help-meet](http://www.energy.gov/articles/energy-department-announces-new-investments-advanced-nuclear-power-reactors-help-meet), retrieved 5 Nov 2016

There do not appear to be any technical or regulatory reasons why any or all of the LWR SMR designs could not be ready for commercial deployment by 2030. NuScale, a private company founded to develop and deploy a LWR SMR, plans for "... the first NuScale Power Module™ to achieve commercial operation in 2024, with the full 12-module plant doing so in 2025."<sup>32</sup> However, no LWR SMR has yet to apply for a design certification or construction and operating license, though NuScale is expected to submit an application for Design Certification in December 2016.<sup>33</sup>

No matter the concept, development of any new reactor and advancing it to the point where it is ready for commercial deployment is a complicated, long-term, and expensive endeavor. Bill Gates, the multi-billionaire philanthropist, has made it a personal goal to try and reduce greenhouse gas emissions through the expanded use of advanced nuclear energy. His privately-funded efforts to develop advanced reactors are viewed as multi-decade efforts:

**"We're moving faster than anybody ever has in that space, but that's about a 30--year period, assuming things go really well."**

— Bill Gates

*"We're moving faster than anybody ever has in that space, but that's about a 30-year period, assuming things go really well."<sup>34</sup>*

The Terrapower TWR is a fully-funded, commercial advanced SFR design. It is arguably free of any and all of the bureaucratic and funding delays usually associated with government-funded design efforts. If any Generation IV-based advanced reactor development effort will succeed as soon as possible, it should be this one. Yet, starting from scratch in 2008 they expect a prototype only in late-2020s and commercial FOAK only in early-2030s at the earliest.

*"The first TWR will demonstrate key plant equipment, qualify the fuel and materials for longer term use, and provide the technical, licensing and economic basis for commercial TWRs. This prototype is expected to be constructed between 2018 and 2023. After a suitable period of testing and optimization, commercial plants are expected to be licensed with start up in the late 2020s or early 2030s. This will be 10 to 20 years earlier than other Generation IV technologies."<sup>35</sup>*

---

<sup>32</sup> [www.nuscalepower.com/our-technology/technology-validation/program-win/uamps](http://www.nuscalepower.com/our-technology/technology-validation/program-win/uamps), retrieved 7 Nov 2016

<sup>33</sup> [www.nuscalepower.com/our-technology/nrc-interaction](http://www.nuscalepower.com/our-technology/nrc-interaction), retrieved 4 Nov 2016

<sup>34</sup> [www.scientificamerican.com/article/the-nuclear-option-could-be-best-bet-to-combat-climate-change/](http://www.scientificamerican.com/article/the-nuclear-option-could-be-best-bet-to-combat-climate-change/), retrieved 3 Nov 2016

<sup>35</sup> [http://terrapower.com/uploads/docs/The TWR Bringing Nuclear Technology to Its Fullest Potential\\_030713.pdf](http://terrapower.com/uploads/docs/The_TWR_Bringing_Nuclear_Technology_to_Its_Fullest_Potential_030713.pdf), retrieved 2 Nov 2016

Several potential barriers exist to achieving this aggressive schedule based on the need to develop and qualify in-core materials that can perform under neutron irradiation to levels never before achieved (i.e., ~550 dpa).<sup>36</sup> First, there exists the challenge to develop materials that can withstand these high levels of irradiation damage. Terrapower's efforts to accomplish this involve the use of heavy ion irradiations and it appears that progress is being made. However, even if the technical challenges of developing a new material are overcome, the correlation of heavy ion and neutron irradiation results has not yet been widely established and there remains uncertainty as to whether and how this data could be utilized in the NRC licensing process.

The recent draft study by Idaho National Laboratory "Advanced Demonstration and Test Reactor Options Study" highlights the long times needed to mature advanced reactor designs. According to this study, the most mature advanced reactor, the GE-Hitachi PRISM, a sodium fast reactor, will only be available for commercial deployment after it has been demonstrated in the 2035 timeframe and this because of previous experience gained through the design and operations of the EBR-II and FFTF.<sup>37</sup> In other words, the advanced reactor design with arguably the highest technology readiness level will require almost 20 years of steady funding and effort in order to get a design to the point where it could be available for commercial deployment.

Similarly, the HTGR is the other mature advanced reactor concept that could potentially be available for commercial deployment in the 2035 timeframe, but only after a period of operation by a yet-to-be built commercial demonstration reactor.<sup>38</sup> The DOE 2015 Quadrennial Technology Review foresees a longer term developmental period for HTGR reactors:

*"Major technical challenges still must be overcome and thus the overall technology readiness is low (about a technology readiness level [TRL] of 3). A 25 to 30 year development time is estimated as needed to reach commercial deployment status with a vigorous R&D effort."*<sup>39</sup>

---

<sup>36</sup> [www.sciencedirect.com/science/article/pii/S2095809916301527](http://www.sciencedirect.com/science/article/pii/S2095809916301527), retrieved 23 Nov 16

<sup>37</sup> Idaho National Laboratory, Advanced Demonstration and Test Reactor Options Study (Draft), March 2016, INL/EXT-16-37867, Revision 0, page 34.

<sup>38</sup> Idaho National Laboratory, Advanced Demonstration and Test Reactor Options Study (Draft), March 2016, INL/EXT-16-37867, Revision 0, page 33.

<sup>39</sup> 2015 Quadrennial Technology Review, Appendix 4J High Temperature Reactors, p 5, [www.energy.gov/sites/prod/files/2016/03/f30/QTR2015-4J-High-Temperature-Reactors.pdf](http://www.energy.gov/sites/prod/files/2016/03/f30/QTR2015-4J-High-Temperature-Reactors.pdf), retrieved 7 Nov 2016

For less mature advanced reactor concepts the road to commercialization will take even longer, becoming available after 2050, because of the need for additional research and development to resolve technical challenges and to develop the data and information essential for design certification and licensing:

*"The less-mature technologies, FHR and LFR, are facing a longer technology development path...to commercial offerings because they need a combination of both the engineering demonstration step and the performance demonstration step through 2040 prior to commercial offerings in ~2050."*<sup>4041</sup>

As part of the review on which this paper is based, an independent analysis of publically-available information on commercial advanced reactor companies and associated designs was conducted to identify those companies and designs that were most likely to be credibly ready for commercial deployment by the 2030 timeframe (See Attachment 3). Criteria used to assess these reactors were the size of company and staffing committed to the effort; whether or not they are actively hiring; the number and quality of partners; if they are actively engaged with the NRC; the financial strength and/or funding available for the effort (private or government); the technical maturity of the design; whether or not there has been prior experience with the technology in the US; the amount of R&D needed to obtain a license which is tied to the innovativeness of the proposed design; and whether or not there is active R&D work underway. Based on the review it was concluded that about a dozen different companies could potentially have designs available for commercial deployment by the 2030 timeframe. But, of those thirteen, it is judged that only five (5) are actively and aggressively engaged in development with a view to having a design available for commercial deployment in the 2030 timeframe, with 2035 being the likely earliest opportunity for deployment. It should be noted that some of these designs will be matured for commercial deployment using private resources and international demonstrations and not require significant US government support or resources.

Of course, existing Generation III+ LWR reactors will be available for commercial deployment because of their current worldwide deployment; for example, Westinghouse's AP1000 in China and the US and Areva's EPR in China, Finland, France and the UK.

Therefore, given current plans and funding levels, it is likely that only Generation III+ LWR designs (e.g., AP1000, EPR) and LWR SMR concepts (e.g., NuScale, Holtec, mPower, Westinghouse) will be available for commercial deployment by 2030. Advanced reactor concepts, e.g., Terrapower, PRISM, will likely only be available in 2035-2040 timeframe at the earliest.

---

<sup>40</sup> Idaho National Laboratory; Advanced Demonstration and Test Reactor Options Study (Draft), March 2016, INL/EXT-16-37867, Revision 0, page 76.

41

### When To Start Construction?

A review of EIA projections for electricity generation through 2040 reveals some interesting factors. Chief among them is that the greatest retirement of coal and natural gas plants will occur from 2015-2025.<sup>42</sup> EIA projects a cumulative retirement of 100GW in coal capacity and 85 GW in oil and natural gas through 2040. Of this, 80 GW (80 percent) of coal retirements and 60 GW (70 percent) of oil and natural gas retirements will occur before 2025. With advanced LWR SMR only becoming available for construction around 2025, and the Terrapower SFR only becoming available around 2035, there is little likelihood that advanced reactors will be able to contribute to this significant shift in generation capacity.

Another interesting factor is that EIA projects that with nuclear capacity remaining essentially constant through 2040, that nuclear energy will only represent about 15.6 percent of electricity generating capacity in 2040, decreasing from 19.5 percent in 2015. In order for nuclear to maintain its historic position of generating about 20 percent of US electricity in 2040, assuming that advanced reactors were built to achieve this, would require about 22 Terrapower SFR or about 500 NuScale LWR SMR. Presuming that Terrapower reactors become available in 2035 this would require the construction of about four (4) Terrapower SFR reactors per year. Assuming NuScale reactors become available in 2025 means that about 33 NuScale reactors per year would need to be built.

Third, in 2015 nuclear energy represented about 59 percent of the carbon-free generation in the US.<sup>43</sup> In 2040, nuclear is projected to only represent 36 percent. If nuclear were to stabilize its decline at a 40 percent share of carbon-free generation in 2040, it would require building about 220 Nuscale SMR beginning in 2025 (~14.5 reactors per year) or 10 Terrapower SFR beginning in 2035 (~2.5 reactors per year). To re-attain a 60 percent share in carbon-free electricity generation would require over 1,300 Nuscale SMR beginning in 2025 (~90 reactors per year) or about 60 Terrapower SFR beginning in 2035 (~12 reactors per year).

For a new technology like the Terrapower SFR, without an established supply chain or experienced human capital base, it seems a bit unrealistic to expect to go from zero to build four *per year* and sustain that over a period of years. For the NuScale LWR SMR, it is possible that they could ramp up production over the period of 15 years but this would require a significant investment in production capabilities and infrastructure, akin to establishing a Boeing aircraft-sized production capability over that timeframe. For example, in 2015 Boeing delivered 762 commercial aircraft, using on the order of 80,000 employees to do so.<sup>44</sup> To achieve 33 or up to 90 LWR reactors *per year* would this scale of production capability and to finance this would require them to have firm orders on the books as well as prospects of continued orders to develop. Given that the costs of the SMR are on the order of a Generation III+ LWR it appears unlikely that these levels of orders will be achieved because other options exist at lower cost; provided there are

---

<sup>42</sup> U.S. Energy Information Administration, Annual Energy Outlook 2016, Table CP-4, page CP-7.

<sup>43</sup> Carbon-free generation was taken as hydro, nuclear, solar, and wind.

<sup>44</sup> [www.seattletimes.com/business/boeing-aerospace/boeing-2015/](http://www.seattletimes.com/business/boeing-aerospace/boeing-2015/), retrieved 3 Dec 2016

no changes to law to monetize policy objectives or to create more substantial economic disincentives for carbon.

The number of utilities that can afford to procure reactors is another factor. With the Terrapower SFR costing about the same as a Generation III+ LWR and being about the same capacity (1,150 MWe), there are only a small number of utilities in the US that could afford to procure a Terrapower SFR. And two of them have already purchased the AP-1000. It is unlikely that they would commit to the procurement of a new type of reactor, even if they would consider new nuclear build going forward; more likely they would choose additional AP-1000.

One of the advantages of the NuScale LWR SMR is that it can add capacity in smaller tranches and thus reduce the capital requirements at any given moment. Utilities looking to replace coal-powered plants or natural gas units would need reactors plants on the order of 300 MWe or 600 MWe. This equates to a six or twelve NuScale reactors at a site. NuScale estimates that it will cost about \$3 billion to construct a 570 MWe plant.<sup>45</sup> This sized plant would require 12 reactors to be built and delivered. To achieve a build-rate of 33 reactors a year would mean having three different utilities committing to procure new nuclear reactors per year for 15 years. Given that there is no cost advantage to doing so, this appears unlikely.

### Barriers to Advanced Reactors

Decisions by utilities to deploy advanced reactors will be made considering economic and other factors beyond technical readiness, so availability for deployment does not automatically infer that deployment will follow.

Presuming that the technical challenges to timely development of advanced reactors are overcome there still remain significant barriers to their widespread commercial deployment. Barriers to deployment include: economics, length and cost of regulatory approval, waste management, utility acceptance, and public perception and national will.

Ultimately, there will need to be adequate demonstration of performance of any advanced reactor design that is sufficiently long in duration in order to reduce the uncertainties and risks to the extent that a risk-adverse utility will contract to purchase an advanced reactor. The DOE's 2015 Quadrennial Technology Review highlights this:

*“Decisions to build new nuclear capacity, uprate existing reactors, or extend their operating lifetimes depend on the cost-competitiveness of nuclear generation in electric power markets.”*

-2016 EIA Annual Energy Outlook

<sup>45</sup> [www.nuscalepower.com/smr-benefits/economical/construction-cost](http://www.nuscalepower.com/smr-benefits/economical/construction-cost)

*"In addition to capital cost reduction, future commercialization of fast reactor technology will require low technical risk and high system reliability."<sup>46</sup>*

## Economics

The most significant barrier to commercial deployment of advanced reactors is their economics and the uncertainties of costs to construct, operate, maintain, and decommission an advanced reactor, including fuel and waste management.

This point is emphasized in the 2016 EIA Annual Energy Outlook:

*"Decisions to build new nuclear capacity, uprate existing reactors, or extend their operating lifetimes depend on the cost-competitiveness of nuclear generation in electric power markets."<sup>47</sup>*

All of these aspects will be uncertain until there is adequate demonstration of a design to reduce these uncertainties to an acceptable level. The demonstration of economic certainty must also be undertaken within the wider context of other competing electricity generating technologies to include natural gas, solar, and wind; it is not enough to demonstrate equivalence or even marginal improvement over current LWR technologies. **The US EIA in its 2016 Annual Energy Outlook forecasts no advanced reactor deployments through 2040** primarily because of its assumption that costs of advanced nuclear systems will remain above natural gas and certain renewables.<sup>48</sup>

Other aspects of economics need to be considered including financing arrangements. It is important to note that financing arrangements are an important element in the economics for any reactor construction. To establish a workable financing arrangement, the project must have some "collateral" to assure lenders that the loans will be repaid. In the past this has meant having a long-term power purchase agreement for the new plant. Such agreements are not available for potential plants in ISO (unregulated) areas that cover much of the US. Therefore, plant location will affect its potential for construction potential due to its impact on the economics of the project.

Similarly, in the recent past the US government has structured loan guarantees to assist in easing the financing hurdles for new build plants, for example through the Energy Policy Act of 2005. Unfortunately, while such guarantees give assurances to 3<sup>rd</sup> party financing entities, there are no guarantees to protect stockholders of the companies that actually purchase/operate the plant. The purchasing company in most cases is "betting the farm" on the project since the cost of one or a pair of Generation III+ LWR represents a significant fraction of the company's capitalization so that the company would fail if the project failed.

---

<sup>46</sup> 2015 Quadrennial Technology Review, Appendix 4H Fast Reactors, p 4,  
[www.energy.gov/sites/prod/files/2016/01/f28/QTR2015-4H-Fast-Spectrum-Reactors.pdf](http://www.energy.gov/sites/prod/files/2016/01/f28/QTR2015-4H-Fast-Spectrum-Reactors.pdf)

<sup>47</sup> EIA Annual Energy Outlook 2016, page MT-19, [www.eia.gov/forecasts/aeo/pdf/0383\(2016\).pdf](http://www.eia.gov/forecasts/aeo/pdf/0383(2016).pdf),  
retrieved 2 Nov 2016

<sup>48</sup> EIA Annual Energy Outlook 2016, Table 8.2: Cost and performance characteristics of new central station electricity generating technologies,  
[www.eia.gov/forecasts/aeo/assumptions/pdf/table\\_8.2.pdf](http://www.eia.gov/forecasts/aeo/assumptions/pdf/table_8.2.pdf), retrieved 7 Nov 2016

This presents an unacceptable risk to stockholders in deregulated areas and is one of the reasons why all new construction in the US is occurring in regulated markets.

Information gathered for this report indicates that no current advanced reactor concept is expected to provide an economic case that is significantly better than current LWR technologies, as exemplified by the construction of AP1000s in Georgia and South Carolina. The apparent parity with existing LWR systems coupled with the large uncertainties in these cost estimates present a significant hurdle for advanced reactors to overcome. Several recent studies make these points:

#### For Sodium Fast Reactors

- *"Large variations are observed in the estimated cost of commercial fast reactor systems; for current designs, these range from -10% to +40% compared to advanced LWR costs. However, modern large power reactors being developed in national programs (e.g., Japan SFR [JSFR] and BN-1200 in Russia) claim capital costs similar to advanced LWRs.... Near-term demonstration plants can be considered as an indicator of current technology status. It is claimed that the BN-800 plant has a capital cost 20% higher than its Russian LWR counterpart, VVER-1200, with operating costs only 15% higher."<sup>49</sup>*
- *"TerraPower expects to make the traveling wave reactor (TWR) cost-competitive with existing light water reactors."<sup>50</sup>*

#### For High Temperature Gas Reactors

- *"...based on detailed NGNP estimates [3], the first-of-a-kind cost for four 600 MW HTGRs is ~\$6.5 billion and the overnight cost is ~\$6200/kWeh. For the nth-of-a-kind, the corresponding values are ~\$4.6 billion and ~\$4365/kWeh."<sup>51</sup>*

#### For Light Water Small and Medium-sized Reactors

- *"The estimated construction cost for the first NuScale 570 MWe (net) plant is less than \$3 billion" (see table below).<sup>52</sup>*

---

<sup>49</sup> 2015 QTR Appendix 4H Fast Reactors, p 4.

<sup>50</sup> <http://terrapower.com/pages/cost>, retrieved 7 Nov 2016

<sup>51</sup> Idaho National Laboratory, Advanced Demonstration and Test Reactor Options Study (Draft), March 2016, INL/EXT-16-37867, Revision 0, page 58.

<sup>52</sup> [www.nuscalepower.com/smr-benefits/economical/construction-cost](http://www.nuscalepower.com/smr-benefits/economical/construction-cost), retrieved 7 Nov 2016



## Overall EPC Overnight Plant Costs (\$1,000,000)

ITEM	2014 Dollars
Power Modules (FOAK Cost plus Fee, Transportation, & Site Assembly)	\$ 848
Home Office Engineering and Support	\$ 144
Site Infrastructure	\$ 60
Nuclear Island (RXB, RWB, MCR)	\$ 538
Turbine Island (2 buildings with 6 turbines each)	\$ 350
Balance of Plant (annex, cooling towers, etc)	\$ 225
Distributables (Temp. Bldgs., Field Staff, Const. Equip., etc.)	\$ 545
Other Costs	\$ 185
<b>Total Overnight Price</b>	<b>\$ 2,895</b>

**\$ 5,078 per kWe net**

Bottom line, two of the companies most actively engaged in advanced reactor development, i.e., Nuscale and Terrapower, both estimate that their costs will likely only be competitive with advanced LWR costs. At some level this makes sense given that nuclear electricity generating systems will always need significant containment systems and safety systems, safeguards and security, highly trained workforce, regulatory overhead, specialized quality assurance including counterfeit part assurance, specially qualified materials, etc. All improvements in current advanced reactor systems offer evolutionary variations of these factors, not breakthroughs. Recent work by Ganda shows that "engineering" costs for AP-1000 are nearly the same as historic costs for Gen II reactors, indicating a remarkable continuity based on these similarities absent considerations for project management and other management-related costs.<sup>53</sup> So, it is unlikely we can expect any miracles from Generation IV advanced reactors in terms of economics.

This economic reality can be overcome in several ways:

1. Reduce the costs of nuclear energy through technical breakthroughs;
2. Account for and monetize the social costs of carbon and methane as a way of leveling the playing field; or
3. Account for and/or monetize other government policy objectives like energy security, waste management, non-proliferation, or maintenance of knowledge.

First, a fairly small reduction in capital costs, for example, can have significant effect and thus it is critical to aim for improvements in this area. A recent Fuel Cycle Options campaign study found: "Efforts to target and limit nuclear capital cost to 4,000 \$/kW could ensure the growth in nuclear energy shares, even

---

<sup>53</sup> Ganda, et al, "Economic Evaluation of Promising Options," FCRD-FCO-2015-000013, September 30, 2015, section 2

*without the relative cost benefit of carbon penalties.*"<sup>54</sup> Thus, efforts to help reduce capital costs of advanced reactors could be very influential in the commercial deployment of advanced reactors.

Second, if, in the near-term, nuclear energy cannot compete economically on its own, it could become more attractive if support is provided to account for the social costs of carbon. This could come in the form of Production Tax Credits, carbon credits, or other mechanisms (that are available to renewable sources) in order to reduce the economic barrier to deployment. As it stands now, until there is a policy driver through law or regulation that monetizes environmental costs, nuclear will not likely grow.

Third, barring an unlikely revolution in economics of advanced reactors or the imposition of taxes/fees that account for the social costs of carbon, the only other way for advanced reactors to compete economically will be, at least initially, through imposition and/or monetization of other, non-economic policy-driven factors, e.g., security of supply, sustainability, improved safety and security, reduced risk for proliferation. In other words, the initial value of advanced reactors may not be to provide economic, reliable, carbon-free electricity; but rather to support other objectives; i.e., waste management, sustainability, energy security, or non-proliferation goals. A government-funded program to build and operate advanced reactors for these other objectives could be the driver to prove these technologies. This experience will in turn provide the economic, operational, and performance information that will then reduce uncertainties and risk and thus facilitate commercial deployment for electricity generation purposes.

### **Competition from Natural Gas**

Traditional analyses concerning nuclear energy have long cited commercial nuclear power's relative competitiveness against fossil fuel prices for coal, natural gas, and oil. Such analyses observed the stability of nuclear power's costs as contrasted to the volatility of fossil fuel prices, particularly gas, and highlighted the market conditions in which nuclear energy is economically competitive. In recent years, competing fossil fuels have seen dramatic changes in prices, especially for natural gas because supplies have dramatically increased and prices have decreased with forecasts for stable low-prices for years to come. This results in nuclear energy being non-competitive economically with natural gas-generated electricity.

Many nuclear advocates persist in believing that nuclear power's economic advantage will be restored when natural gas prices inevitably increase or typical volatility reasserts itself. Certainly, they argue that lower prices help account for the rise of using natural gas for electricity production over coal and nuclear. Certainly too, they agree that in "unregulated" power markets, at least, these low prices negatively affect nuclear compared to natural gas because the current markets fail to reward generators for reliability and stability. But over the long-run, they argue that gas prices will inevitably rise to levels that make nuclear again the fuel of choice.

Three sets of factors suggest their hopes that nuclear power will become a cost leader with respect to natural gas are unfounded: 1) the quickly increasing supply of natural gas and related transportation

---

<sup>54</sup> Nuclear Energy, Renewable Energy with Storage, and Climate Change Mitigation, Son H. Kim, Pacific Northwest National Laboratory, September 16, 2016, FCRD-FCO-2016-000501, page 11.

infrastructure, 2) the greater ease of construction, financing, operation, and decommissioning of natural gas plants compared to nuclear plants, and 3) the technological advantage of gas turbines over nuclear turbines.

In the **first category** is the growing distribution of production of domestic natural gas and associated increase in resources. Coupling those new production sources with an increasing number of new pipelines assures gas supply can reach new gas turbines and other gas markets as needed, at competitive prices. Consequently, abundant gas supplies at stable, low prices will be enduring. A recent EPRI Journal article buttresses this point:

*"...large, lower cost shale and other unconventional gas supplies, with many active wells, can be brought to market much more quickly—within months instead of years. This reduced the lag between price signals and availability of new supply and decreased the need for longer term price increases to drive out demand. Periods of price volatility will be shorter than in the past. As a result, electric utilities that rely more on natural gas have lower supply and price risks now than they did 10–15 years ago."<sup>55</sup>*

The **second category** includes not only economic risk factors, but more favorable public acceptance of natural gas over nuclear fuel. Watt for watt, the construction of a new gas turbine is one fifth the cost of a new nuclear plant. In addition, it can be built in one third of the time. And when it is no longer needed it can quickly be dismantled, sold for scrap, and the location returned for another use in a short time. These differences greatly affect shorter-run economics and politics and overall project risk; against which nuclear energy's longer-run benefits become a tough sell.

The **third category** is possibly nuclear power's biggest threat. Technological advances in turbine technologies provide natural gas generating plants with an enduring competitive advantage. Combined Cycle Gas Turbine (CCGT) power plants can now achieve over 60 percent efficiency whereas current LWR nuclear plants only achieve about 33 percent efficiency. Some of the advanced reactors expected to be ready for deployment by 2050 anticipate using advanced steam cycles and hope to achieve about 44 percent and some anticipate using Brayton cycles and achieve over 50 percent. So, while technical advances will raise overall efficiencies in advanced reactors they will still remain below that of CCGT. Therefore, even if natural gas prices increase, natural gas turbines will continue to remain more attractive relative to nuclear power.

---

<sup>55</sup> Vello Kuuskraa, President of Advanced Resources International, 'FROM "MOONBEAM GAS" TO SHALE REVOLUTION TO WHAT'S NEXT' published in EPRI Journal, 17 Oct 2016, <http://eprijournal.com/from-moonbeam-gas-to-shale-revolution-to-whats-next/>, retrieved 12 Dec 2016

In short, do not bet on rising gas prices to fuel hopes for a nuclear renaissance, given current or foreseeable reactor technologies and economic and market conditions. It is unlikely that current advanced reactor designs can improve sufficiently to overcome the substantial, obvious factors that favor gas: technically, operationally, flexibly, financially, and preferentially. These factors are summarized by the OECD/IEA:

*"CCGT plants offer many advantages, including high efficiency, lower CO2 emissions, relatively quick and cheap construction, modularity and less local resistance to the siting of new plants than for coal and nuclear plants. Moreover, when the distinctive economic and financial characteristics of CCGTs are taken into account, they reveal their critical advantages for new entrants in liberalised markets... Finally, CCGT investments take place with a lower capital expenditure than coal or nuclear plants (IEA, 2010)."*<sup>56</sup>

Until costs of nuclear electricity are competitive with all other electricity sources it is unlikely to be widely adopted. Given the advantages described above, natural gas will likely remain an attractive technology option for utilities and a significant challenge for nuclear energy. Compounding this is the likelihood that the economics of renewable energy sources and other technologies will likely continue to improve, making the economic target for advanced reactors even harder to match going forward.

### **Length and Cost of Regulatory Approval**

The long time and large costs associated with obtaining NRC Design Certification and licenses to construct and/or operate a nuclear reactor are barriers to commercial deployment of advanced reactors. Almost all experience and regulation in the US is based on LWR technology. Shifting to a new technology will require new data, new training, new models, new regulations, guidelines, and standards. It is not a trivial undertaking and it will be an expensive and lengthy process for the first several advanced reactor designs given the 95 percent cost-recovery requirement of the NRC. Consider the following:

- "Current cost estimates to complete licensing work and design finalizations for light water reactors can vary widely – anywhere between \$600 million and \$1 billion per design. While the cost structure for advanced reactor designs is currently less certain, it is imperative to plan to address financial challenges similar to those facing the LWR community."<sup>57</sup>
- "Start-ups and even large companies with first-of-a-kind reactors cannot raise the hundreds of millions of dollars in private capital needed today to pay for licensing or engage in a decade or longer review process.... The longer the U.S. goes without a timely, predictable, affordable, and safe licensing path for the companies that emerge and are ready to commercialize their advanced reactors, the more likely it is that another country will be the home to this technology."<sup>58</sup>

---

<sup>56</sup> Coal to Gas Competition in the U.S. Power Sector, OECD/IEA, 2013, page 7, [www.iea.org/publications/insights/insightpublications/CoalvsGas\\_FINAL\\_WEB.pdf](http://www.iea.org/publications/insights/insightpublications/CoalvsGas_FINAL_WEB.pdf)

<sup>57</sup> Nuclear Energy Institute, "Advanced Reactor Strategy," page 15.

<sup>58</sup> [www.thirdway.org/report/advanced-nuclear-101](http://www.thirdway.org/report/advanced-nuclear-101), retrieved on 29 Oct 2016

- "The Government Accountability Office's July 28, 2015 Technology Assessment Report on Nuclear Reactors (GAO-15-652) clarified the extent of NRC's fees by stating that:  
*'Designing and certifying a new type of nuclear reactor design can cost up to \$1 billion to \$2 billion, with much of the cost going to R&D and reactor design work, and around \$50 million to \$75 million paying for NRC's fees for design certification.' NRC fees are less than 10% of the cost of the R&D and design work.*"<sup>59</sup>
- "The United States' licensing process is the global gold standard for rigorous attention to reducing accident risks. However, the cost burden is substantial; licensing involves a formidable front-end investment and can approach \$1 billion because of the required submission of extensive confirming data to support the performance of the safety systems."<sup>60</sup>

This potential barrier to commercial deployment of new reactor technologies has been recognized and steps have been taken to address this with a series of joint DOE/NRC workshops in 2015 and 2016, the Multinational Design Evaluation Program managed by the OECD/NEA, etc. But, much more will need to be done and it remains an uncertainty as to whether any of the commercial advanced reactor designs will obtain design certifications and construction and operating licenses given the time and costs involved.

### Waste Management

The inability of the US to commit to and follow a path for the disposal of used nuclear fuel remains a barrier for the deployment of advanced reactors. The SEAB report states:

*"Progress on waste management is important for public acceptability of nuclear power. The Task Force makes certain observations about these vital fuel-cycle and waste management activities but acknowledges that its analysis is incomplete, especially for new, advanced technologies for which there is little or no practical field experience."*<sup>61</sup>

The official quest for a spent fuel disposal site in the US began in 1982 when Congress passed the Nuclear Waste Policy Act. This law directed the Department of Energy to build and operate a repository for used nuclear fuel and other high-level radioactive waste. The act set a deadline of 1998 for the Energy Department to begin moving used fuel from nuclear energy facilities.

In 1987, Congress amended the Nuclear Waste Policy Act, directing the Energy Department to exclusively study Nevada's Yucca Mountain as the site for a potential repository for geologic disposal of used nuclear fuel.

---

<sup>59</sup> Comment from NRC response to SEAB report

[http://energy.gov/sites/prod/files/2016/09/f33/NRC\\_Comments\\_on\\_SEAB\\_Report\\_0.pdf](http://energy.gov/sites/prod/files/2016/09/f33/NRC_Comments_on_SEAB_Report_0.pdf)

<sup>60</sup> Secretary of Energy Advisory Board "Final Report of the Task Force On the Future of Nuclear Power," page 38.

<sup>61</sup> Secretary of Energy Advisory Board "Final Report of the Task Force On the Future of Nuclear Power," page 7, [http://energy.gov/sites/prod/files/2016/10/f33/9-22-16\\_SEAB%20Nuclear%20Power%20TF%20Report%20and%20transmittal.pdf](http://energy.gov/sites/prod/files/2016/10/f33/9-22-16_SEAB%20Nuclear%20Power%20TF%20Report%20and%20transmittal.pdf), retrieved 8 Nov 2016

On June 3, 2008, the U.S. Department of Energy (DOE) submitted a license application to the U.S. Nuclear Regulatory Commission (NRC), seeking authorization to construct a high-level waste geologic repository at Yucca Mountain, Nevada. In 2010, the Obama Administration stopped work and funding for work on Yucca Mountain. Several states challenged this in court.

The NRC resumed work on its technical and environmental reviews of the Yucca Mountain application using available funds in response to an August 2013 ruling by the U.S. Court of Appeals for the District of Columbia Circuit. The staff completed and published the final volumes of the safety evaluation report in January 2015. The staff completed and issued an Environmental Impact Statement supplement in May 2016. The adjudicatory hearing, which must be completed before a licensing decision can be made, remains suspended.<sup>62</sup>

So, some 34 years after a legal requirement was put in place, the US remains without an operating repository. According to the DOE Strategy for the Management and Disposal of Used Nuclear Fuel and High-Level Radioactive Waste, a repository is not anticipated to be operational any earlier than 2048, another 32 years from now, at least.<sup>63</sup>

Currently more than 68,000 metric tons heavy metal (MTHM) of used nuclear fuel are stored at 72 commercial power plant sites around the country with approximately 2,000 MTHM added to that amount every year.<sup>64</sup> Given that the legal limit for commercial spent fuel in Yucca Mountain was set at 63,000 metric tons of heavy metal, there is already a need for a second repository or an amendment to the law to accommodate the fuel from existing reactors.

Moreover, how to address fuels from different advanced reactor technologies has not yet been defined. There are issues that would need to be addressed on each new fuel and waste type that would arise through the use of new technologies. For example, each new fuel type will require waste acceptance criteria to be developed and approved by the NRC; a process that will require experimental data collected over a lengthy period. It is unclear if costs for fuel treatment have been incorporated in cost estimates of advanced reactors and what impact they may have on the already difficult economic competitiveness of advanced reactors.

Just as there is inertia to a change in regulation that is based on LWR technology and experience there will also be inertia to change spent fuel transportation, storage, and disposal as we move away from LWR fuel types. How long this will take and how costly it will be have not yet been defined. Since this is partly driven by the geological environment that the waste will be subjected to there is considerable uncertainty about how to even begin to develop an understanding of this issue, since the US is focused solely on

---

<sup>62</sup> [www.nrc.gov/waste/hlw-disposal.html](http://www.nrc.gov/waste/hlw-disposal.html), retrieved 6 Dec 2016

<sup>63</sup> DOE, "Strategy for the Management and Disposal of Used Nuclear Fuel and High-Level Radioactive Waste," January 2013, page 7.

<sup>64</sup> DOE, "Strategy for the Management and Disposal of Used Nuclear Fuel and High-Level Radioactive Waste," January 2013, page 3.

opening a single repository, and there is little progress yet evident on its opening. Given the history to date, this may require a long time to address.

These issues are not insurmountable, by any means, but they represent an uncertainty that will require time and money to resolve. The continued lack of a route to disposal remains a significant uncertainty for any utility to build an advanced reactor. This uncertainty represents a liability that electricity producers may be unwilling to assume by themselves without adequate Federal policy, facilities, operations, and funding.

### Utility Acceptance

Electric utilities or electricity-generating companies are by their nature risk-averse enterprises because of their mandate to provide economic and reliable electricity. Thus, there is a high bar to prove that a new generating technology can meet these requirements.

Unless it can be demonstrated over an adequate period of time that a new technology is safe, reliable, and economic it is unlikely to be chosen, absent a significant cost incentive. Consider the decision to deploy the Generation III+ AP1000s at Summer and Vogtle. Their construction was spurred by loan guarantees and production tax credits set up through the Energy Policy Act of 2005. Even with these incentives for tried and true LWR technology, only two utility consortia chose to go forward and both in regulated markets. To date, these Generation III+ LWR, the first new reactors in decades, are beset with schedule delays and cost overruns. Similarly, construction of the EPR, a Generation III+ LWR, in China, Finland, and France has also been subject to cost and schedule overruns. Any company considering construction of an advanced reactor will likely weigh the difficulties being experienced with construction of these advanced LWR heavily as they represent the most recent experience in reactor construction.

All advanced reactor designs reviewed for this study require fuels with >15 percent enrichment. Therefore, in addition to proving that the reactor technology will function reliably and economically, it will also be essential to prove that the entire supply chain of equipment and services is functional and available, including demonstration that new fuels with higher enrichments can be provided reliably, at the necessary quality, on time, and at a reasonable price. This means demonstration of all the new infrastructure that will be required to support operation and maintenance of a new reactor technology; another source of uncertainty. Building new capability to deliver fuel will be an extensive and expensive undertaking. Identifying mechanisms to provide an incentive for first movers will be a challenge.

Further, a utility with a choice of two economically competitive options will likely choose the one with the lower technical, regulatory, and human resources overheads and that provides the greatest flexibility to respond to changing market conditions. With nuclear energy, a utility has a significant burden to maintain safety with strict compliance to regulations while it is engaged in validating the long-term performance of a new generating technology.

***"[A] Reactor and its fuel ... must promise a significant reduction in cost as compared to once-through fuel LWRs to have any industrial interest."***

Dr. Rita Baranwal, Director,  
Technology Development &  
Application, Westinghouse Global  
Technology Development

Additionally, the experience of utilities that have shut down and decommissioned a LWR shows that a utility/owner must maintain positive controls over spent nuclear fuels indefinitely. Contrast that with natural gas or wind or solar where they can rapidly decommission a site and return it to greenfield reuse with no long-term commitments. All things considered, vendors of advanced reactors have a strong need for demonstration plants to be operational well in advance of commercial deployment to serve as proof that all of these risks have been satisfactorily addressed.

The significant overhead associated with nuclear energy is a barrier to commercial deployment of advanced reactors particularly in light of the availability of other cost-competitive options. That said, if the strengths of nuclear – high capacity factor baseload, carbon-free – can be monetized it is likely that it will be considered attractive. Key to this is a demonstration reactor operated over a sufficiently long period to reduce uncertainty.

### **Public Acceptance and National Will**

Every nation that has deployed nuclear energy has done so with sovereign support that provided the driving force to overcome the numerous challenges, not least of which is public acceptance. The commercial deployment of advanced reactors in the US represents the deployment of a new technology akin to the commercial deployment of LWR at the beginning of the atomic age. Therefore, to successfully deploy this new technology will require an expression of sovereign support that can provide the driving force needed to overcome the many challenges it will face, not the least of which is public acceptance.

Adverse public opinion will undoubtedly exist for advanced nuclear technologies. Responses to the Fukushima events have done nothing to ease public concerns about nuclear energy. The public opposition to nuclear energy will likely be exacerbated by media highlighting opposition and hostility, which likely stir political opposition, at least in the local area. Easy nucleation points would be fear of the new and unknown, the lack of a path to disposal for new fuels and waste types, and the unproven nature of the economics. To counter this and successfully deploy advanced reactors will require a long and difficult struggle to win the hearts and minds of the public; to create a national will to move forward as a nation. The increasing view of nuclear as an environmentally friendly zero carbon emission technology may help but absent a solid widespread belief that advanced nuclear reactors are safe, secure, reliable and economic, this may not be enough. To create the national will to move forward will require a significant and sustained effort and require strong sovereign support. Objective, informed, and persuasive advocates, one of which must be the DOE Office of Nuclear Energy, will be needed to generate and focus this sovereign support.



## Summary of barriers

This short overview of the potential barriers to commercial deployment of advanced reactors shows a very challenging environment. The 2015 Quadrennial Technology Review summarizes this concisely:

*"In addition to technology development, institutional challenges for commercial demonstration and deployment of future nuclear technology options (not just fast reactors) include the following:*

- *The establishment of a licensing framework for advanced reactors*
- *Sustained R&D infrastructure for training of the next generation of scientists and engineers*
- *Establishment of mechanisms for financially recognizing the environmental and waste management benefits of nuclear energy options*
- *Creation of the industrial infrastructure (i.e., supply chain) to produce fast reactors and fuel*
- *The retention and transfer of essential institutional knowledge and specialized expertise as senior scientists and engineers retire*<sup>65</sup>

What is needed to address many of the barriers is a demonstration reactor that would focus efforts to resolve technical and institutional issues such as licensing framework and regulations, create and mature a supply chain, allow for education and training of personnel, establish the economics, reliability, and safety of the technology, and create familiarity with the buyers and public. Only through demonstration will a new reactor concept transition from a technology-push deployment model driven by government and/or vendors to a technology pull model driven by users.

Any demonstration reactor will likely be too expensive for industry to undertake alone, so its purpose will also need to include support for achieving US policy objectives such as demonstration of a sustainable fuel cycles thereby ensuring a public-policy objective. The recent DOE study on the need for a demonstration reactor also makes this point:

*"These costs and the associated financial and deployment schedule uncertainties at this stage are high enough that private industry in the U.S. will most likely not deploy these systems without government assistance."*<sup>66</sup>

Also needed is a high-level systems view of the deployment of any advanced reactor to identify any waste management concerns. It would be useful to extend the Fuel Cycle Options campaign's Evaluation and Screening of Fuel Cycles to include technology-specific evaluations of how different advanced reactor types would perform in their associated fuel cycles.<sup>67</sup> This would allow issues related to fuel treatment, storage, and disposal to be evaluated. This would inform NE of gaps that need to be addressed by DOE

---

<sup>65</sup> DOE 2015 QTR Appendix 4H Fast Reactors, p 4-5.

<sup>66</sup> Idaho National Laboratory, Advanced Demonstration and Test Reactor Options Study (Draft), March 2016, INL/EXT-16-37867, Revision 0, page 58.

<sup>67</sup> Nuclear Fuel Cycle Evaluation and Screening – Final Report, October 8, 2014, INL/EXT-14-31465

policy and R&D. It could also inform DOE of the type of demonstration reactor technology would be most beneficial to aim for.

In summary, in addition to technical challenges facing advanced reactors there are a number of other barriers to their commercial deployment. All are surmountable if there is will and incentive to do so. None represent fundamentally different challenges than those faced by LWRs as they were being deployed at the beginning of the atomic age. Key to any success will be adequate demonstration well in advance of any commercial deployment.

### Potential Energy Mixes

Analysis of the potential role of advanced reactors in helping the US meet its carbon goals is now considered. First a review of the EIA 2016 Annual Energy Outlook is given which addressed the Clean Power Plan. Then, results of specific analyses done by the Office of Nuclear Energy's Fuel Cycle Options campaign will be provided. Specifically, four scenarios were analyzed to provide a counterpoint to the EIA's analysis. The four scenarios are:

- a. Base case with no subsidies for any technology
- b. Business as usual (existing subsidies continue for renewables)
- c. Expanded subsidies (current subsidies for renewables plus a \$0.027/kWe-hr production credit for carbon-free energy as recommended by SEAB)
- d. Alternate expanded subsidies (current subsidies and/or a carbon tax sized to achieve 2050 carbon reduction goal)

### 2016 Annual Energy Outlook

The EIA 2016 Annual Energy Outlook took a focused look at implementation of the Clean Power Plan (CPP). Concisely, the result of their analysis is a forecast that nuclear energy will remain level through 2040 after reactors currently under construction come on line (see charts MT-28 and MT-31 below):

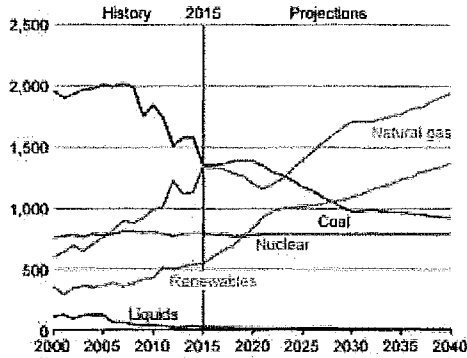
*"Decisions to build new nuclear capacity, uprate existing reactors, or extend their operating lifetimes depend on the cost-competitiveness of nuclear generation in electric power markets. Independent power producers have faced financial losses in recent years on their nuclear capacity as a result of competition from lower-cost energy sources—including natural gas and wind—and declining electricity demand and reduced capacity payments in some regions. Low natural gas prices reduce the competitiveness of newly built nuclear capacity relative to natural gas-fired combined-cycle plants, and they reduce wholesale market prices for electricity from existing nuclear power plants. **As a result, no uprates or new builds of nuclear capacity beyond those already underway occur in any of the AEO2016 cases.** (highlight added) ...The Reference case addresses near-term accelerated nuclear retirements but assumes that subsequent license renewals will allow for long-term operation up to 80 years."<sup>68</sup>*

---

<sup>68</sup> EIA Annual Energy Outlook 2016, page MT-19, [www.eia.gov/forecasts/aeo/pdf/0383\(2016\).pdf](http://www.eia.gov/forecasts/aeo/pdf/0383(2016).pdf) retrieved 2 Nov 16

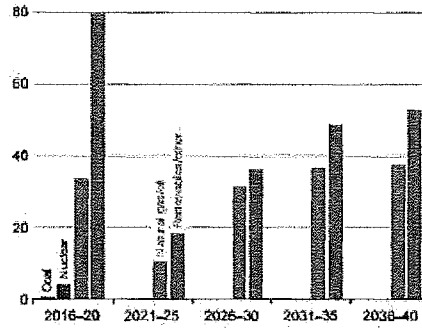
**Clean Power Plan accelerates shift from coal to natural gas and renewables**

Figure MT-28. Net electricity generation by fuel in the Reference case, 2000–2040 (billion kilowatt-hours)



**In the No CPP case, most new electricity generation capacity uses natural gas and renewables**

Figure MT-31. Cumulative additions to electricity generation capacity by fuel in the No CPP case by period (gigawatts)



Source: MT-28 EIA annual Energy Outlook 2016, page MT-15, MT-31 page MT-19.

As can be seen, the EIA forecasts that nuclear electricity generation will remain stable through 2040 with no new capacity deployed after the reactors currently under construction come on line. Even in an extended policies scenario where further carbon reductions drive technology changes, nuclear does not increase. Also, in the case that the CPP is not implemented, natural gas and renewables remain the technologies of choice. A look at their assumptions shows that this is because the National Energy Model assumes that the costs of advanced nuclear higher than natural gas, photovoltaic solar and wind (See Table 8.2 below).<sup>69</sup>

<sup>69</sup> Cost and Performance Characteristics of New Generating Technologies, Annual Energy Outlook 2016, [www.eia.gov/forecasts/aeo/assumptions/pdf/table\\_8.2.pdf](http://www.eia.gov/forecasts/aeo/assumptions/pdf/table_8.2.pdf), retrieved 3 Nov 2016

Table 8.2. Cost and performance characteristics of new central station electricity generating technologies

Technology	First Available Year <sup>1</sup>	Size (MW)	Lead time (years)	Base Overnight Cost in 2015 (2015 \$/kW)	Contingency Factors		Total Overnight Cost in 2015 <sup>2,3</sup> (2015 \$/kW)	Variable O&M <sup>4</sup> (2015 \$/MWh)	Fixed O&M (2015 \$/kW/yr.)	Heatrate <sup>5</sup> in 2015 (Btu/kWh)	nth-of-a-kind Heatrate (Btu/kWh)
					Project Contingency Factor <sup>2</sup>	Technological Optimism Factor <sup>3</sup>					
Coal with 30% carbon sequestration (CCS)	2019	650	4	4,649	1.07	1.03	5,098	6.95	68.49	9,750	9,221
Conv Gas/Oil Comb Cycle	2018	702	3	911	1.05	1.00	956	3.42	10.76	6,600	6,350
Adv Gas/Oil Comb Cycle (CC)	2018	429	3	1,000	1.08	1.00	1,080	1.96	9.78	6,300	6,200
Adv CC with CCS	2018	340	3	1,898	1.08	1.04	2,132	6.97	32.69	7,525	7,493
Conv Comb Turbine <sup>7</sup>	2017	100	2	1,026	1.05	1.00	1,077	3.42	17.12	9,960	9,600
Adv Comb Turbine	2017	237	2	632	1.05	1.00	664	10.47	6.65	9,800	8,550
Fuel Cells	2018	10	3	6,217	1.05	1.10	7,181	44.21	0.00	9,500	6,960
Adv Nuclear	2022	2,234	6	5,288	1.10	1.05	6,108	2.25	98.11	10,449	10,449
Distributed Generation - Base	2018	2	3	1,448	1.05	1.00	1,520	7.98	17.94	9,004	8,900
Distributed Generation - Peak	2017	1	2	1,739	1.05	1.00	1,826	7.98	17.94	10,002	9,880
Biomass	2019	50	4	3,498	1.07	1.01	3,765	5.41	108.63	13,500	13,500
Geothermal <sup>8,9</sup>	2019	50	4	2,559	1.05	1.00	2,687	0.00	116.12	9,541	9,541
MSW - Landfill	2018	50	3	7,954	1.07	1.00	8,511	9.80	403.97	14,360	18,000
Conventional Hydropower <sup>5</sup>	2019	500	4	2,191	1.10	1.00	2,411	2.62	14.70	9,541	9,541
Wind <sup>10</sup>	2018	100	3	1,516	1.07	1.00	1,644	0.00	45.98	9,541	9,541
Wind Offshore	2019	400	4	4,605	1.10	1.25	6,331	0.00	76.10	9,541	9,541
Solar Thermal <sup>6</sup>	2018	100	3	3,895	1.07	1.00	4,163	0.00	69.17	9,541	9,541
Photovoltaic <sup>11</sup>	2017	150	2	2,362	1.05	1.00	2,480	0.00	21.33	9,541	9,541

Further, EIA calculations of levelized costs of electricity (LCOE) and levelized avoided costs of electricity (LACE) show advanced nuclear remains non-competitive economically through 2040 (See Table 8.4b).<sup>70</sup> According to the EIA:

*“...LACE provides an estimate of the cost of generation and capacity resources displaced by a marginal unit of new capacity of a particular type, thus providing an estimate of the value of building such new capacity. This is especially important to consider for intermittent resources, such as wind or solar, that have substantially different duty cycles than the baseload, intermediate, and peaking duty cycles of conventional generators... When the LACE of a particular technology exceeds its LCOE at a given time and place, that technology would generally be economically attractive to build. While the build decisions in the real world, and as modeled in the AEO, are somewhat more complex than a simple LACE to LCOE comparison, including such factors as policy and non-economic drivers, the net economic value (LACE minus LCOE, including tax credits, for a given technology, region and year) shown in Table 4a and Table 4b provide a reasonable point of comparison of first-order economic competitiveness among a wider variety of technologies than is possible using either LCOE or LACE tables individually.... a negative difference indicates that the cost of the marginal new unit of capacity exceeds its value*

<sup>70</sup> Levelized Cost and Levelized Avoided Cost of New Generation Resources in the Annual Energy Outlook 2016, [www.eia.gov/forecasts/aeo/pdf/electricity\\_generation.pdf](http://www.eia.gov/forecasts/aeo/pdf/electricity_generation.pdf), page 20.

to the system, as measured by LACE; a positive difference indicates that the marginal new unit brings in value in excess of its cost by displacing more expensive generation and capacity options.”<sup>71</sup>

Table B4b: Difference between levelized avoided costs of electricity (LACE) and levelized costs of electricity (LCOE), plants entering service in 2040

**Comparison of LCOE with tax credits and LACE (2015 \$/MWh)**

Plant Type	Average LCOE	Average LACE	Average Net Difference <sup>1</sup>	Range of Non-Weighted Differences <sup>2</sup>	
				Lower Bound	Upper Bound
<b>Dispatchable Technologies</b>					
Advanced Coal with CCS <sup>3</sup>	125.8	63.6	-62.1	-81.6	-50.3
<b>Natural Gas-fired</b>					
Conventional Combined Cycle	57.6	64.0	6.4	-1.7	11.0
Advanced Combined Cycle	56.0	64.0	8.0	0.0	12.9
Advanced CC with CCS	81.1	64.0	-17.1	-26.3	-10.3
Advanced Nuclear	93.0	63.5	-29.4	-34.6	-25.8
Geothermal	53.3	60.5	7.2	-14.7	27.7
Biomass	78.7	64.1	-14.5	-36.6	-2.1
<b>Non-Dispatchable Technologies</b>					
Wind	58.8	58.8	0.0	-14.2	20.8
Wind – Offshore	133.7	64.6	-69.1	-117.4	-48.1
Solar PV <sup>4</sup>	65.5	70.7	5.2	-16.2	17.7
Solar Thermal	189.4	69.9	-119.6	-214.4	-66.7
Hydroelectric <sup>5</sup>	65.3	62.1	-3.2	-11.7	2.4

<sup>1</sup>The “Average Net Difference” represents the average of the (LACE – LCOE) calculation, where the difference is calculated for each of the 22 regions based on the cost with tax credits for each technology, where tax credits are applicable.

<sup>2</sup>This “range of differences” is not based on the difference between the minimum values shown in Table B2 and Table B3 but represents the lower and upper bound resulting from the LACE minus LCOE calculations for each of the 22 regions.

<sup>3</sup>Due to new regulations (CAA 111b), conventional coal plants cannot be built without CCS because they are required to meet specific CO<sub>2</sub> emission standards. The coal with CCS technology modeled is assumed to remove 30% of the plant’s CO<sub>2</sub> emissions. Coal plants have a 3 percentage-point adder to their cost-of-capital.

<sup>4</sup>Costs are expressed in terms of net AC power available to the grid for the installed capacity.

<sup>5</sup>As modeled, hydroelectric is assumed to have seasonal storage so that it can be dispatched within a season, but overall operation is limited by resources available by site and season.

Source: U.S. Energy Information Administration, Annual Energy Outlook 2016, April 2015, DOE/EIA-0383(2016).

Taken together, this data shows that according to the Energy Information Administration and its National Energy Model that advanced nuclear reactors will not be economically competitive with other widely available generating technologies through 2040. With or without the CPP in full effect they forecast that advanced reactors will not be deployed primarily due to the higher costs for advanced nuclear compared with other available technologies.

<sup>71</sup> Levelized Cost and Levelized Avoided Cost of New Generation Resources in the Annual Energy Outlook 2016, [www.eia.gov/forecasts/aeo/pdf/electricity\\_generation.pdf](http://www.eia.gov/forecasts/aeo/pdf/electricity_generation.pdf), pages 4-5.

### DOE Fuel Cycle Options Campaign Analysis

Four scenarios were analyzed using Office of Nuclear Energy's Fuel Cycle Options campaign staff to provide a counterpoint to the EIA's analysis. The four scenarios are:

- a. Base case with no subsidies for any technology
- b. Business as usual (existing subsidies continue for renewables)
- c. Expanded subsidies (current subsidies for renewables plus a \$0.027/kWe-hr production credit for carbon-free energy as recommended by SEAB)
- d. Alternate expanded subsidies (current subsidies and/or a carbon tax sized to achieve 2050 carbon reduction goal)

The analyses below are derived from work done by Dr. Sonny Kim of Pacific Northwest National Laboratory (PNNL). The scenarios were analyzed using an enhanced version of PNNL's Global Change Assessment Model (GCAM) that simulates alternative futures of nuclear and renewable energy use in the US within the context of US and global emissions mitigation efforts including representations of energy storage systems and integration costs of intermittent energy use. In the PNNL GCAM model, technology choice uses an approach called Discrete Choice Method. It is a statistical approach where a distribution of costs for each technology is assumed and is based on the use of a Logit function. This approach shares out the electricity demand to the entire set of available technologies, where the cheaper option takes greater share but not necessarily all of the market. Even relatively expensive technologies will maintain some penetration in the energy technology mix. In the analyses, overnight capital costs are assumed as given in Table 1. Additional detail on the model can be found in reference 15.

**Table 1. Assumed Capital Costs for Electricity-generating Technologies in PNNL GCAM Model**

Technology	2015 (2010\$)	2050 (2010\$)
Coal (steam plant)	2,900	2,685
Coal (steam plant CCS)	5,800	4,618
Coal (IGCC)	4,000	3,213
Coal (IGCC CCS)	6,600	4,946
Natural Gas (CC)	1,050	972
Natural Gas (CC CCS)	2,100	1,672
Nuclear	5,500	5,092
Solar (PV large scale)	2,800	1,607
Solar (PV rooftop)	4,200	3,776
Solar (CSP)	4,800	3,199
Wind (on-shore)	2,000	1,607

### Base Case with no Subsidies for any technology

A base case was defined to provide a basis for comparative analysis between the scenarios. The base case for this report is a look into the future absent policy-driven subsidies for any electricity-generating technology. In this case the main driver for technology decisions is the relative economics represented by levelized costs of electricity (LCOE). In the base case, total electricity generation grows from 15.6 EJ/yr in 2015 to 20.4 EJ/yr in 2050 (see Figure 1).

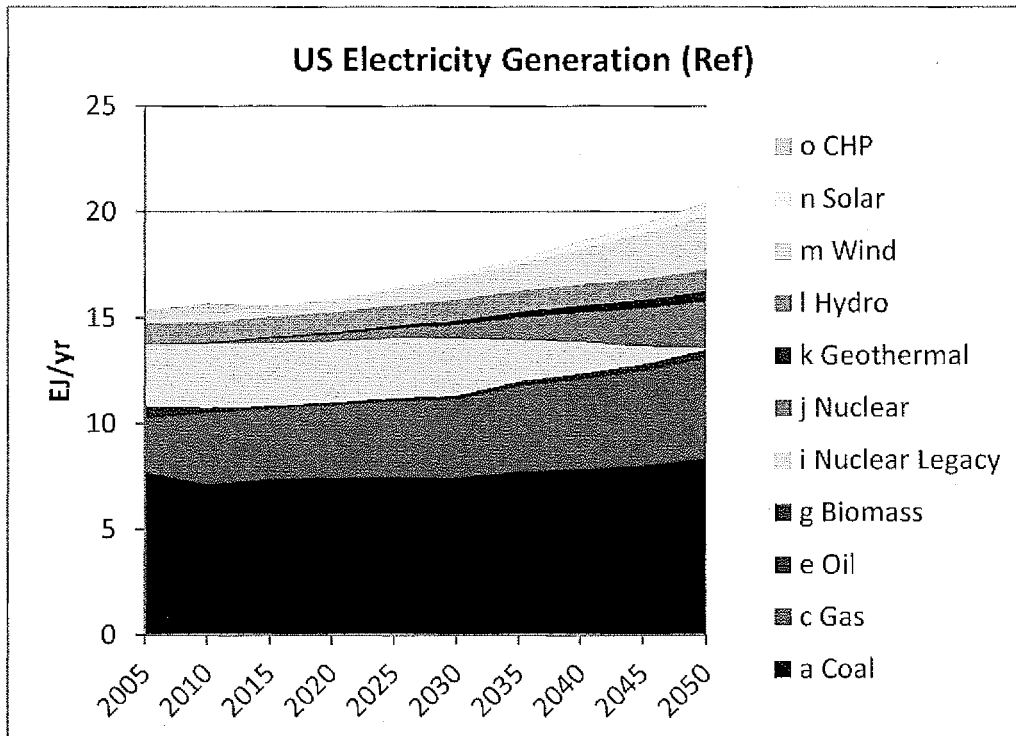


Figure 1. US Electricity Generation in Base Case with No Subsidies

In the base case coal remains the largest electricity generation technology. Natural gas increases by over 42 percent; increasing from 3.3 EJ/yr in 2015 to 4.7 EJ/yr in 2050. In the base case wind energy makes a significant impact, increasing from 3.2 percent share of electricity generation in 2015 to almost 13 percent in 2050. Conversely, nuclear energy decreases from over 20 percent share in 2015 to just over 11 percent in 2050 (See Table 2 below).

Table 2. Electricity Generation in Base Case (2015 and 2050)

Technology	2015		2050	
	Electricity Generation (EJ/Yr)	Share (%)	Electricity Generation (EJ/Yr)	Share (%)
Coal	7.4	47.4	8.4	41.2
Natural Gas	3.3	21.2	4.7	23.0
Nuclear	3.2	20.5	2.3	11.3
Solar	0.0	0	0.6	2.9
Wind	0.5	3.2	2.6	12.7
<b>Total</b>	<b>15.6</b>	<b>100</b>	<b>20.4</b>	<b>100</b>

Absent subsidies, fossil-fueled electricity generation would continue to dominate the electricity generation landscape in 2050; nuclear energy will decline, and wind energy will take third place as technology of choice, according to the PNNL model. The base case supports the argument that the economics of nuclear do not support widespread use absent subsidies to monetize other less tangible, policy-oriented benefits of nuclear energy.

**Business As Usual Case (existing subsidies continue for renewables)**

The first scenario looks at the impacts of continue existing subsidies for renewable energy. This case is a look into the future essentially continuing business as usual with respect to subsidies for renewable electricity-generating technologies. In this case, as with the reference case, total electricity generation grows from 15.6 EJ/yr in 2015 to 20.4 EJ/yr in 2050 (see Figure 2). The subsidies modeled based on existing values are given in Table 3.



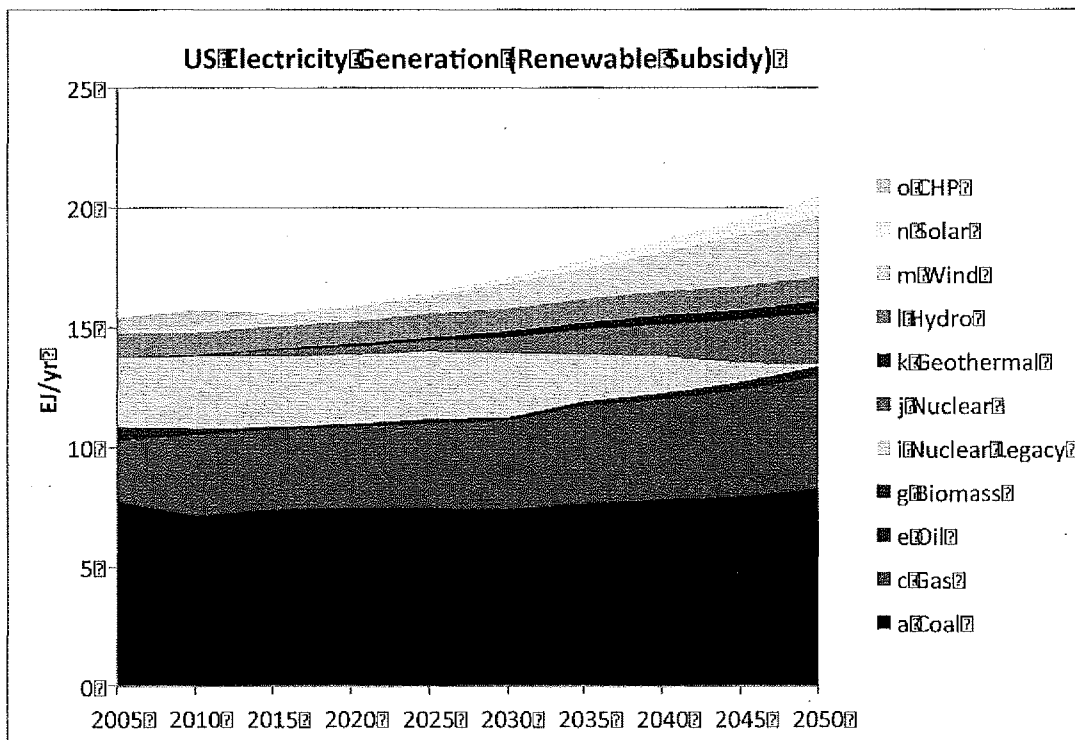


Figure 2. US Electricity Generation with Renewable Energy Subsidies (Business as Usual)

Table 3. Subsidies Used in Business as Usual Case

Production Tax Credit (93\$/kWh)										
Technology	2016	2017	2018	2019	2020	2021	2022	2023	2024	Future Years
Wind – Onshore	\$0.015	\$0.015	\$0.015	\$0.015	\$0.012	\$0.009	\$0.006	-	-	-
Geothermal	\$0.015	\$0.015	\$0.015	\$0.015	\$0.015	-	-	-	-	-
Landfill Gas	\$0.008	\$0.008	\$0.008	\$0.008	-	-	-	-	-	-
Hydro	\$0.008	\$0.008	\$0.008	\$0.008	\$0.008	-	-	-	-	-
Investment Tax Credit (% of overnight capital cost)										
Technology	2016	2017	2018	2019	2020	2021	2022	2023	2024	Future Years
Utility PV	30%	30%	30%	30%	30%	30%	26%	22%	10%	10%
CSP	30%	30%	30%	30%	30%	30%	30%	26%	22%	10%
Wind – Offshore	30%	30%	30%	30%	30%	24%	18%	12%	0%	0%
Biomass	30%	0%	0%	0%	0%	0%	0%	0%	0%	0%
Fuel Cells	30%	0%	0%	0%	0%	0%	0%	0%	0%	0%
Resid. PV	30%	30%	30%	30%	26%	22%	0%	0%	0%	0%
Comm. PV	30%	30%	30%	30%	26%	22%	10%	10%	10%	10%

In the business as usual case, coal remains the largest electricity generation technology providing over 40 percent of electricity in the US in 2050. Natural gas increases from 3.3 EJ/yr in 2015 to 4.7 EJ/yr in 2050; about 23 percent of electricity generated in 2050. In the business as usual case, solar energy begins to make a significant impact, increasing from essentially 0 percent share of electricity generation in 2015 to almost 4.0% in 2050. In this case, wind grows substantially to about 12.7 percent of electricity generation in 2050. In contrast, nuclear energy significantly declines; generating only about 11 percent of electricity in 2050; down from over 20 percent in 2015 (See table 4 below).

Table 4. Electricity Generation in Business as Usual Case (2015 and 2050)

Technology	2015		2050	
	Electricity Generation (EJ/Yr)	Share (%)	Electricity Generation (EJ/Yr)	Share (%)
Coal	7.4	47.4	8.3	40.7
Natural Gas	3.3	21.2	4.7	23.0
Nuclear	3.2	20.5	2.3	11.3
Solar	0.0	0.0	0.8	3.9
Wind	0.5	3.2	2.6	12.7
<b>Total</b>	<b>15.6</b>	<b>100</b>	<b>20.4</b>	<b>100</b>

In the business as usual case, even with subsidies for renewable sources of electricity, fossil-fueled electricity generation continues to dominate the landscape in 2050; nuclear will decline, and wind energy will take third place as technology of choice, according to the PNNL model. Solar energy is a major beneficiary of subsidies and makes its gains at the expense of coal.

#### Expanded Subsidies Case

This case is a look into the future assuming current subsidies for renewables plus a \$0.027/kWe-hr production tax credit for carbon-free energy as recommended by the Secretary of Energy Advisory Board final report on The Future of Nuclear Power.<sup>72</sup> This expanded subsidies case seeks to understand if a nuclear-focused subsidy would spur deployment of nuclear energy and what impact an expanded role for nuclear could have on carbon emissions from the electricity-generation sector as sought by the Clean Power Plan. The production tax credit serves to improve the economics of nuclear relative to other technologies and seeks to create a demand-pull for the technology by technology users.

In this expanded subsidies case, total electricity generation grows from 15.6 EJ/yr in 2015 to 21.2 EJ/yr in 2050 (see Figure 3). Slightly more electricity is generated in this case in 2050 than the reference case because a lower price for electricity caused by the carbon-free subsidy reduces the overall price for electricity and spurs demand.

<sup>72</sup> Secretary of Energy Advisory Board (SEAB) Task Force Final Report on The Future of Nuclear Power, <https://energy.gov/seab/downloads/final-report-task-force-future-nuclear-power>

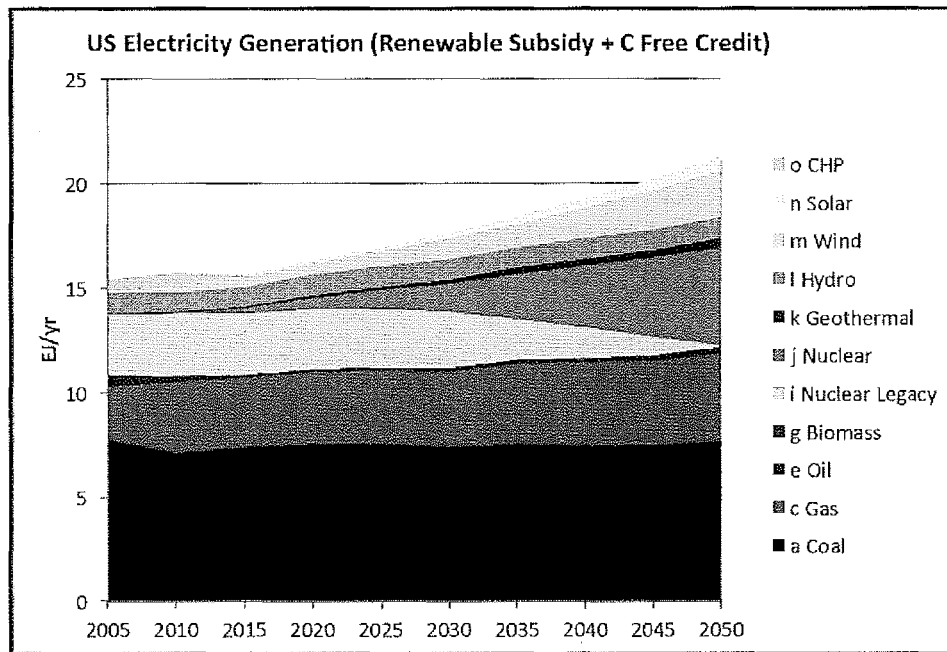


Figure 3. Electricity Generation in Expanded Subsidies Case

In the expanded subsidies case, coal remains the largest electricity generation technology providing almost 36 percent of electricity in the US in 2050 down from over 47 percent in 2015. Natural gas increases from 3.3 EJ/yr in 2015 to 4.2 EJ/yr in 2050; generating about 19.8% of electricity in 2050. In the expanded subsidies case, solar energy rises to 2.8 percent of electricity generated in 2050 and wind rises to 10.4 percent. Both wind and solar, though they increase, do not achieve the levels achieved in the business as usual case. In this case, nuclear electricity generation, as a percentage of overall generation, rises slightly from 20.5 percent in 2015 to 22.6 percent in 2050 (See table 5 below).

Table 5. Electricity Generation in Expanded Subsidies Case (2015 and 2050)

Technology	2015		2050	
	Electricity Generation (EJ/Yr)	Share (%)	Electricity Generation (EJ/Yr)	Share (%)
Coal	7.4	47.4	7.6	35.8
Natural Gas	3.3	21.2	4.2	19.8
Nuclear	3.2	20.5	4.8	22.6
Solar	0.0	0.0	0.6	2.8
Wind	0.5	3.2	2.2	10.4
Total	15.6	100	21.2	100

With a nuclear energy subsidy, packaged as a carbon-free production tax credit (PTC), nuclear energy electricity generation increase significantly, about 50 percent from 2015 to 2050, from 3.2 EJ/yr in 2015 to about 4.8 EJ/yr in 2050 (See Figure 4). This increase in nuclear electricity generation is accomplished at the expense of coal and natural gas, both of which reduce their relative contribution, and by lower increases in share by solar and wind; as compared to the reference case.

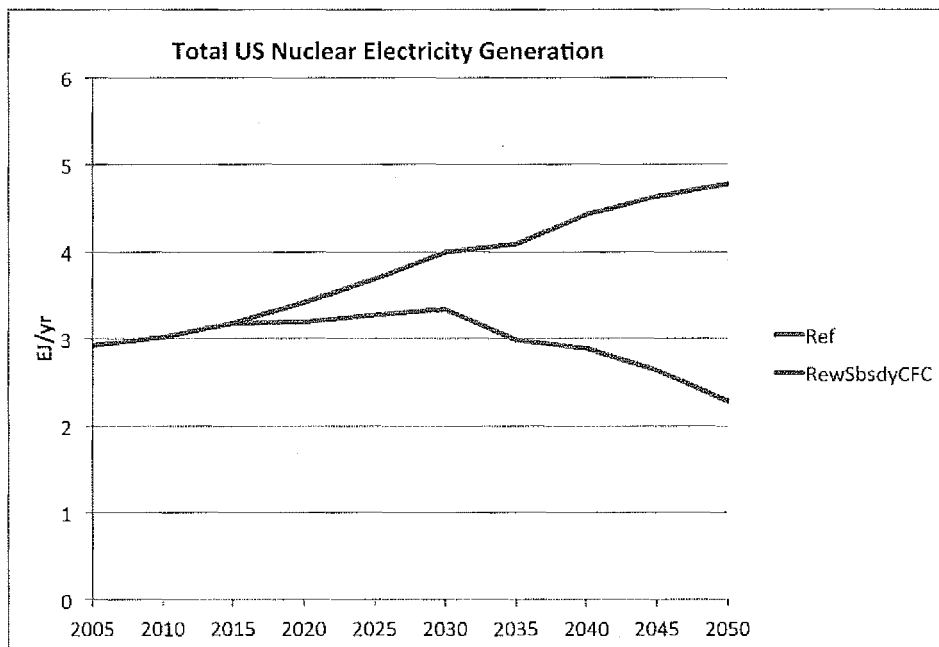


**Figure 4. Nuclear Electricity Generation in Expanded Subsidy Case**

To generate 4.8 EJ/year, would require about 150 GW of installed nuclear capacity in 2050; about 50 percent higher than exists in US today. To achieve this at least 50 GW of capacity will need to be constructed over the next 35 years. With retirements of many existing LWR between now and 2050 it would more likely require over 100 GW in new nuclear generating capacity. To achieve 50 GW of installed capacity in 35 years would require an average of 1.43 GW per year continuously for 35 years; about one large LWR per year for 35 years. To achieve 100 GW over a period of 35 years would require about three large plants per year, every year for 35 years; essentially equivalent to the effort that achieved 100 GW of installed nuclear capacity in the US from 1960 to 1985. The cost to the taxpayer for the PTC to achieve this level of growth would be large. The SEAB estimated that it would cost about \$213 million for a 1 GWe reactor per year.<sup>73</sup> Even if the PTC is applied for only the first six years of operation as was done with the 2005 Energy Policy Act the cost to deploy 100 GW would be on the order of \$130 billion.<sup>74</sup>

<sup>73</sup> Secretary of Energy Advisory Board (SEAB) Task Force Final Report on The Future of Nuclear Power, <https://energy.gov/seab/downloads/final-report-task-force-future-nuclear-power>, page 1.

<sup>74</sup> 100 one GWe reactors at \$213M per year for six years each

Presuming this large-scale construction program is accomplished, the impact on overall carbon emissions from the electricity sector is fairly modest (See Figure 5). This is because even though the amount of nuclear capacity increases significantly, there remains a significant port of electricity generation from coal and natural gas; 35.8 percent and 19.8 percent of US generation, respectively.

If nothing else, this case shows the power of production tax credits as an influence on technology decision making and therefore an effective policy lever for advocating nuclear energy. This validates the experience in the US in using PTC to spur renewable energy deployment as well as to spur deployment of nuclear energy as was done via the 2005 Energy Policy Act with its PTC for nuclear that resulted in deployment of the AP-1000s at Summer and Vogtle.

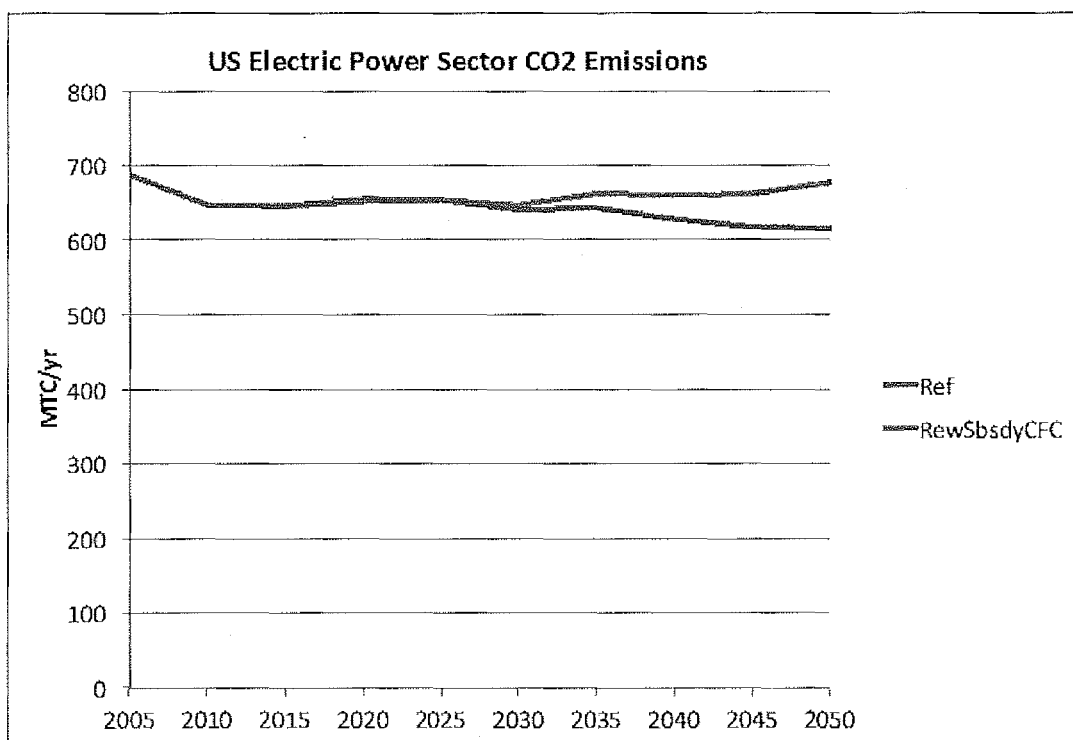


**Figure 5. CO2 Emissions from Electricity Generation in Expanded Subsidy Case**

The Clean Power Plan has as its goal the reduction in carbon emissions from the electricity generation section; specifically a 32 percent reduction from 2005 levels achieved by 2030. This equates in an emission rate of about 423 MT Carbon (1,551 MTCO<sub>2</sub>) per year by 2030. As can be seen in Figure 5, even with a carbon-free subsidy to promote nuclear electricity, carbon reductions do not achieve these levels; rather achieving about a 9 percent reduction but still remaining above 600 MT of carbon per year; a long way from achieving the desired goal. Even with a 50 percent increase in nuclear generating capacity; the relatively minor reduction in coal and natural gas generation results in carbon emissions remaining relatively high. To achieve the goal of the Clean Power Plan even higher levels of nuclear electricity generation buttressed by even higher levels of wind and solar and a lot less fossil-fueled electricity

generation will be required. These concepts are explored in the next series of scenarios; the Alternate Subsidy Cases.

### Alternate Expanded Subsidies Case

The expanded subsidy case above shows the difficulty in reaching the carbon reduction goals embodied in the Clean Power Plan. So the next questions to be explored are: Is it possible to achieve the CPP goals? What would it take to achieve the necessary reduction in carbon? In this section two different approaches to expanded subsidies are evaluated.

#### Alternate Expanded Subsidy Case 1 – Renewable Subsidies plus carbon taxes to achieve CPP goal

In the first instance the scenario evaluated is what would result if renewable subsidies and carbon taxes alone were used as the means of achieving carbon reduction goals with no specific nuclear energy subsidy or PTC provided. The logic here is to penalize fossil-fueled electricity production at a level high enough to drive carbon-emissions down to the required level, but no further.

To achieve the CPP emission goals, carbon-taxes will need to be invoked that force technology decision-making to less carbon intense technologies as well as introduce carbon capture and sequestration (CCS) (See Figure 6).

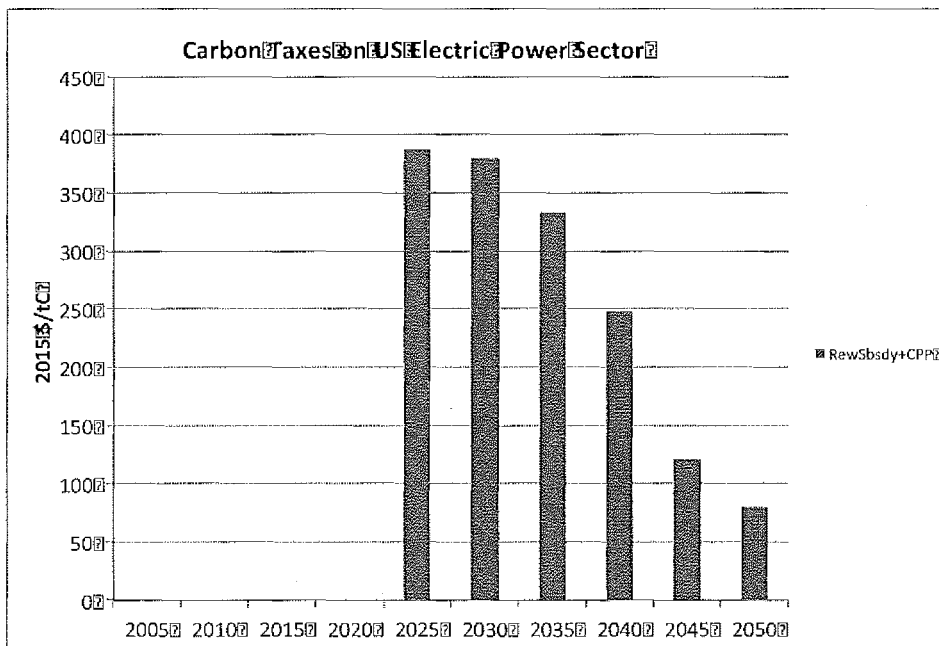


Figure 6. Carbon Taxes Needed to Achieve CPP Goals

In this case, total electricity generation grows from 15.6 EJ/yr in 2015 to 19.2 EJ/yr in 2050 (see Figure 9). Less electricity is generated in 2050 because it is more expensive than in the reference case due to the carbon-taxes driving out low-cost fossil-fueled options. As can be seen in Figure 9, a wide mix of technology options remain in use with a noticeable introduction of carbon capture and sequestration options.

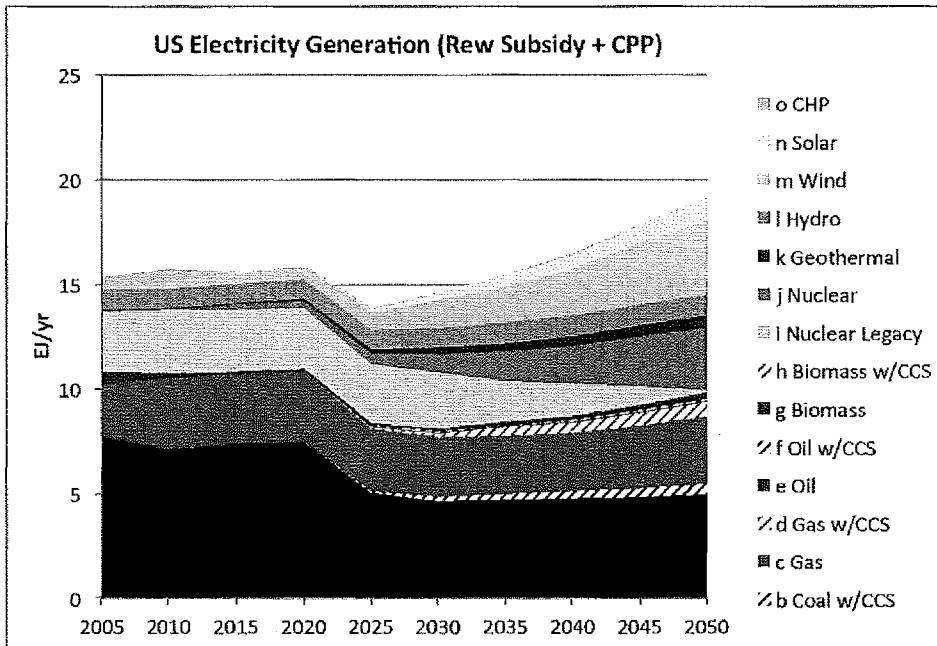


Figure 7. Electricity Generation with Carbon Tax to Achieve CPP Goal

In this scenario, coal’s share of electricity generation is reduced significantly with natural gas modestly declining by 2050; with coal still supplying over 28 percent and natural gas about 21 percent in 2050, portions of which operate in conjunction with CCS. In this alternate expanded subsidies case, solar energy rises to 5.7 percent of electricity generated in 2050 and wind increases significantly to 18.2 percent. In this case, nuclear electricity generation remains at a consistent level of generation at about 3.3 EJ/yr. As a percentage of overall generation, this represents a decrease from 20.5 percent in 2015 to about 16 percent in 2050 (See table 7 below).

Table 7. Electricity Generation in Alternate Expanded Subsidies Case 1 – Carbon Taxes to Meet CPP (2015 and 2050)

Technology	2015		2050	
	Electricity Generation (EJ/Yr)	Share (%)	Electricity Generation (EJ/Yr)	Share (%)
Coal	7.4	47.4	5.0	26.0
Coal w CCS	NA	NA	0.5	2.6
Natural Gas	3.3	21.2	3.3	17.2
Natural Gas w CCS	NA	NA	0.7	3.6
Nuclear	3.2	20.5	3.1	16.1
Solar	0.0	0.0	1.1	5.7
Wind	0.5	3.2	3.5	18.2
<b>Total</b>	<b>15.6</b>	<b>100</b>	<b>19.2</b>	<b>100</b>

Using carbon taxes, the impact on overall carbon emissions from the electricity sector is significant (See Figure 10). The CPP goal is achieved by 2030 and maintained thereafter. This is mainly due to a reduction in coal, the introduction of CCS technology, and the significant increases in wind and solar.

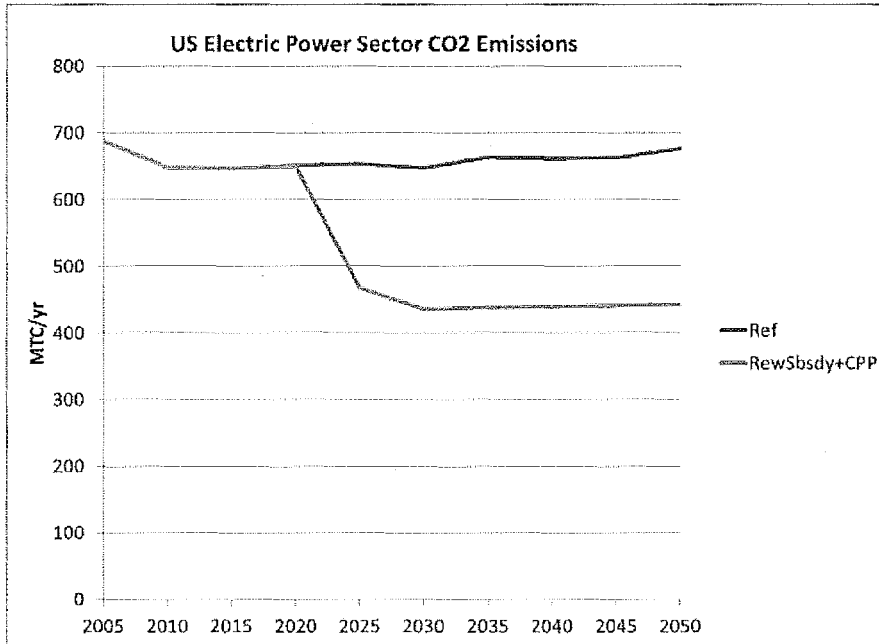


Figure 8. CO2 Emissions with Carbon Taxes

#### Alternate Expanded Subsidy Case 2 – Renewable Subsidies, Nuclear Subsidy, and Carbon Taxes to achieve CPP goal

In the second instance, the scenario explores what would result if renewable subsidies, a nuclear subsidy (the SEAB recommendation), and carbon taxes were all used as the means of achieving the CPP carbon reduction goals. The logic here is to provide a wider variety of policy tools so as to reduce carbon taxes yet still drive carbon-emissions down to the required level but no further.

To achieve the CPP emission goals, carbon-taxes will need to be invoked that force technology decision-making to less carbon-intensive technologies, but the level of carbon tax is reduced through the offering of a nuclear energy subsidy at the \$0.027/kWe-hr recommended by the SEAB (see Figure 11).



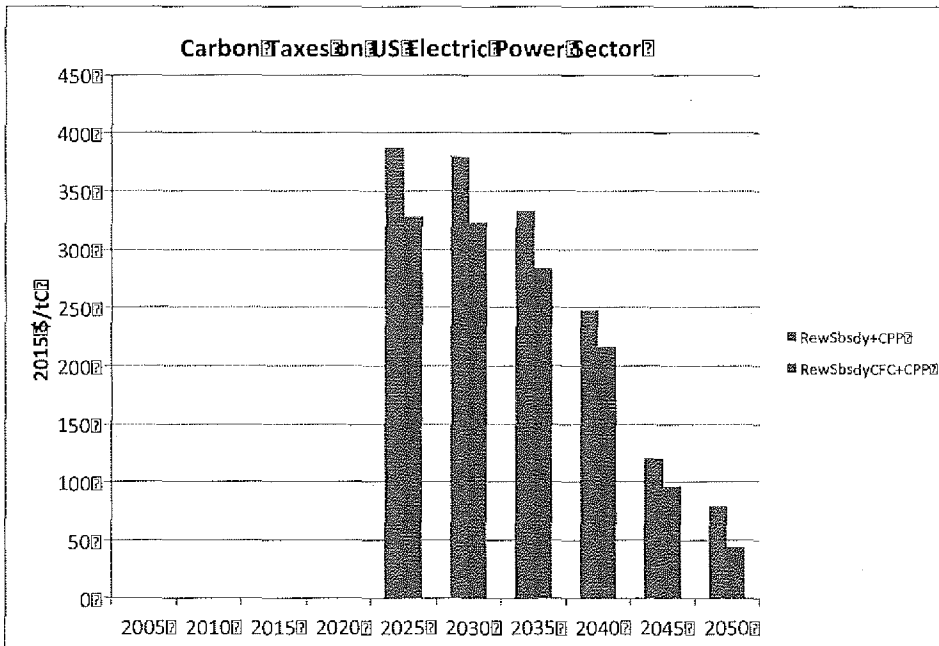


Figure 9. Carbon Taxes to Achieve CPP with (red) and without (blue) a Nuclear Subsidy

In this case, total electricity generation grows from 15.6 EJ/yr in 2015 to 20.6 EJ/yr in 2050 (see Figure 12). As can be seen in Figure 12, a wide mix of technology options remain in use, including CCS options.

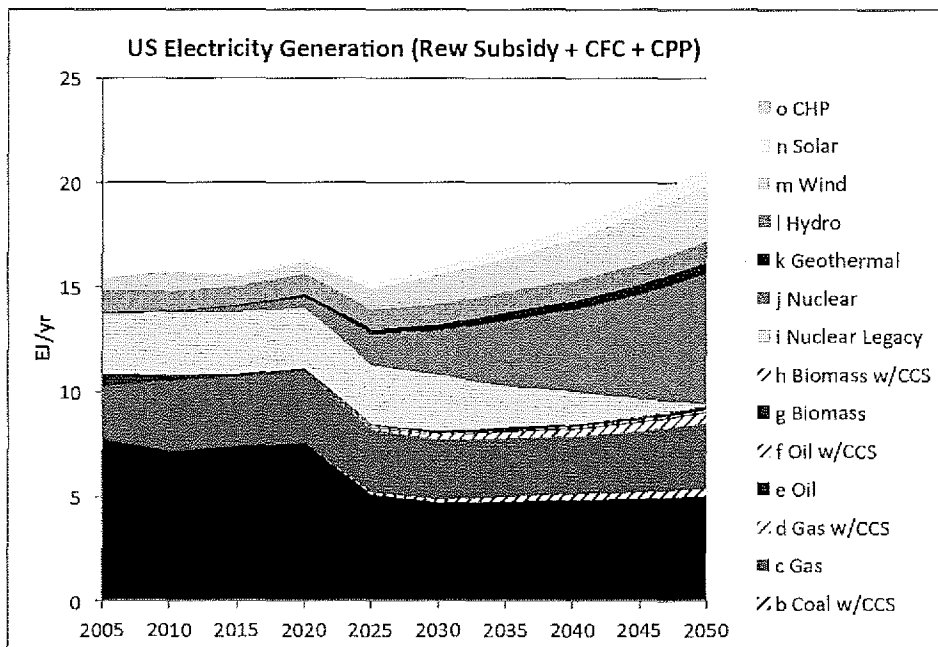


Figure 10. Electricity Generation with Carbon Tax and Nuclear Subsidy to Achieve CPP Goal

In this scenario, coal’s share of electricity generation is reduced significantly with natural gas modestly declining by 2050 with coal still supplying over 26 percent and natural gas about 17 percent in 2050; a portion of which operates in conjunction with CCS. In this alternate expanded subsidies case, solar energy rises to 3.9 percent of electricity generated in 2050 and wind increases to 13.1 percent. In this case nuclear electricity generation increases robustly from 3.2 EJ/yr in 2015 to about 6.4 EJ/yr on 2050; effectively doubling. This equates to 20.5 percent in 2015 to about 31 percent in 2050 as a percentage of overall generation (See Table 8 below).

**Table 8. Electricity Generation in Alternate Expanded Subsidies Case 2 – Carbon Taxes and Nuclear Subsidy to Meet CPP (2015 and 2050)**

Technology	2015		2050	
	Electricity Generation (EJ/Yr)	Share (%)	Electricity Generation (EJ/Yr)	Share (%)
Coal	7.4	47.4	5.1	24.8
Coal w CCS	NA	NA	0.3	1.4
Natural Gas	3.3	21.2	3.1	15.0
Natural Gas w CCS	NA	NA	0.5	2.4
Nuclear	3.2	20.5	6.4	31.1
Solar	0.0	0.0	0.8	3.9
Wind	0.5	3.2	2.7	13.1
<b>Total</b>	<b>15.6</b>	<b>100</b>	<b>20.6</b>	<b>100</b>

Using a nuclear subsidy to complement carbon taxes does allow the goals of the CPP to be met by 2030 (See Figure 13). The CPP goal is achieved by 2030 and maintained thereafter. This is mainly due to a reduction in coal, the introduction of CCS technology, and the expansion of wind, solar, and nuclear. In this case the nuclear subsidy results in a significant increase in nuclear at the expense of reduced increases in solar and wind. Carbon emission behavior in this scenario basically mimics the behavior see in the alternate expanded case scenario 1 (see Figure 10). The difference is in the relative mix of nuclear, solar, and wind technologies.

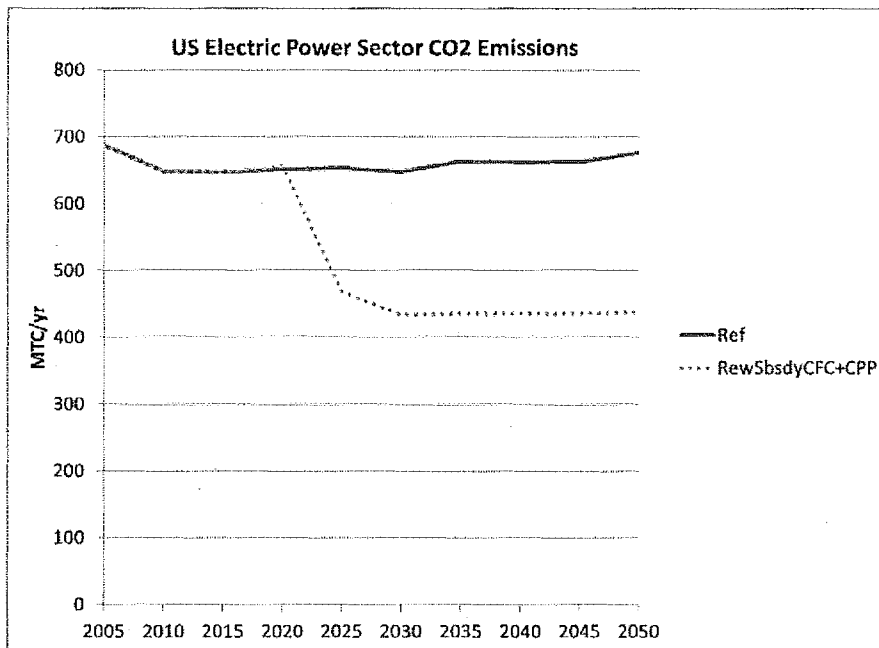


**Figure 11. CO2 Emissions with Carbon Taxes and Nuclear Subsidy**

What this scenario again highlights is the effectiveness of PTC as a policy tool in influencing technology decision-making. The use of PTC is a lever through which government can pick technology winners and losers; to exercise advocacy for particular technologies.

A look at the EIA analysis from the 2016 Annual Energy Outlook as compared to the Fuel Cycle Options analysis presented above shows that a nuclear-specific subsidy is required in order to encourage the growth of nuclear technology in the face of low cost alternative energy sources; i.e., natural gas. The analyses also show that achieving carbon reduction goals will require policy tools, tax credits and carbon taxes, to drive technology decision makers to choose carbon-free electricity sources and overcome the low cost of coal and natural gas. These analyses highlight several key points:

- *The high cost of advanced nuclear and the effect these costs have on deployment.*
- *The effectiveness of production tax credits as a policy tool to influence technology decision-making*
- *The need for more sophisticated modeling tools that can better model limits and potential ramifications of assumptions; for example, costs of tax credits and their ramifications on federal budgets and the likelihood of approval from political processes. Other aspects would be spent fuel inventories and their impact on repository loading, among others.*

### R&D program

The mission of NE is to support research, development, and demonstration activities to resolve the technical, cost, safety, waste management, proliferation resistance, and security challenges of increased use of nuclear energy.<sup>75</sup> The overall focus of NE R&D is maximizing the benefits of nuclear power by

<sup>75</sup> FY 2017 Congressional Budget Justification, Vol 3, page 409.

addressing the challenges of improving affordability of nuclear energy; management of nuclear waste; minimizing proliferation risks of nuclear materials; and further enhancing safety and incorporating lessons learned from Fukushima.<sup>76</sup>

Within this R&D focus, the Office of Nuclear Energy has developed several programs that are relevant to advanced reactors and their potential for commercial deployment. They are the Nuclear Technology Research and Development Program, the Nuclear Technology Demonstration and Deployment Program, and the Spent Fuel and Waste Disposition Program.

The following descriptions and analysis are based on a review of the Fiscal Year (FY) 2017 Budget Justification. It is noted that a reorganization of the Office of Nuclear Energy occurred after the FY17 budget was submitted. Therefore, the descriptions of programs will not precisely correlate to the nomenclature of the new organization. However, it is assumed that despite the reorganization that the underlying programs and justifications have not changed significantly. For the purposes of this report the following correlations are assumed:

- *The Nuclear Technology Research and Development program (NE-4) has assumed responsibility for the following sub-programs: Advanced Reactor Technologies, Material Recovery and Waste Form Development, Advanced Fuels, Used Nuclear Fuel Disposition R&D, Systems Analysis and Integration, and Fuel Resources.*
- *The Spent Fuel and Waste Disposition Program (NE-8) has assumed responsibility for the Used Nuclear Fuel Disposition R&D sub-program.*

#### **Advanced Reactor Technologies (ART) subprogram**

The Advanced Reactor Technologies (ART) subprogram supports the development of innovative reactor technologies that may offer improved safety, functionality and affordability with a goal to reduce long-term technical barriers for advanced nuclear energy systems.<sup>77</sup>

The ART program's goals are focused on high value research for long term concepts, R&D needs of promising mid-range concepts, and development of innovative technologies that benefit multiple advanced reactor concepts and stimulation of new ideas for transformational future concepts.<sup>78</sup>

#### **Material Recovery and Waste Form Development (MRWFD)**

The primary mission of the Material Recovery and Waste Form Development (MRWFD) subprogram is to develop advanced material recovery as well as advanced waste form development technologies that improve current fuel cycle performance with minimal processing, waste generation, and potential for material diversion.<sup>79</sup>

---

<sup>76</sup> FY 2017 Congressional Budget Justification, Vol 3, page 429.

<sup>77</sup> FY 2017 Congressional Budget Justification, Vol 3, page 436.

<sup>78</sup> FY 2017 Congressional Budget Justification, Vol 3, page 439.

<sup>79</sup> FY 2017 Congressional Budget Justification, Vol 3, page 445.

### **Advanced Fuels**

The mission of the Advanced Fuels subprogram is the development of advanced nuclear fuels for both existing light water reactors (LWR) and the entire spectrum of advanced nuclear energy systems. Advanced Fuels is pursuing two major paths: 1) the development of next generation LWR fuels with enhanced performance and accident tolerance, and 2) development over the long term of transmutation fuels with enhanced proliferation resistance and resource utilization.

### **Systems Analysis and Integration**

The Systems Analysis and Integration subprogram provides the critical capability needed to analyze complex fuel cycle system options, assess overall performance under various scenarios, and improve understanding of the interdependencies between various subsystems and associated technologies. The objective is to develop and implement analysis processes and tools and perform integrated fuel cycle evaluations to provide information that can be used to objectively and transparently inform decision makers about overall research and development (R&D) directions and to integrate activities through R&D efforts on common fuel cycle goals. A significant activity within this subprogram is the efforts to develop improved cost estimates with lower uncertainty for assessment of economic competitiveness of the most promising fuel cycles.<sup>80</sup>

### **Fuel Resources**

The Fuel Resources subprogram seeks to identify and implement actions the Department can take to assure that economic nuclear fuel resources remain available with priority in the near term on developing the technology for extraction of uranium from seawater.<sup>81</sup> The importance of this is making available a near-limitless supply of uranium that effectively caps the cost of fuel for nuclear reactors at whatever level can be achieved.

### **Used Nuclear Fuel Disposition R&D**

This subprogram supports R&D to identify alternatives and conduct scientific research and technology development to enable long term storage, transportation, and disposal of used nuclear fuel and wastes generated by existing and future nuclear fuel cycles.<sup>82</sup>

### **Analysis of the NE R&D Programs**

The Nuclear Technology Research and Development program, as the successor of the Reactor Concepts Research, Development and Demonstration (RD&D) program, has the mission of improving the competitiveness of nuclear energy with R&D for advanced reactors conducted within the Advanced Reactor Technologies (ART) subprogram. Specific activities of this subprogram are focused on fast reactor technologies, high temperature reactor technologies, advanced reactor generic technologies, activities in the supercritical CO<sub>2</sub> crosscut effort, support for development of an advanced reactor regulatory

---

<sup>80</sup> FY 2017 Congressional Budget Justification, Vol 3, page 452.

<sup>81</sup> FY 2017 Congressional Budget Justification, Vol 3, page 467.

<sup>82</sup> FY 2017 Congressional Budget Justification, Vol 3, page 456.

framework, and analyses to support deployment of a demonstration reactor.<sup>83</sup> Important work is also being done to advance the technology readiness level of HTGR fuels.

However, despite a stated intent of a focus on the affordability of nuclear energy, **a review of the specific activities of the ART subprogram reveals insufficient emphasis on the fundamental barrier of economics. There also appears to be no apparent emphasis on integration of advanced reactors into the emerging electricity grid with significant VRE. Activities to support deployment of a demonstration reactor are yet limited to studies and analyses with no decision on whether or not to proceed.**

The Systems Analysis and Integration subprogram has been conducting important work on economic analysis and cost estimates for reactor construction. **What is missing is a focus on multi-faceted analyses that address the nexus of policy, regulation, economics, and technology; the realm of the decision-maker of the buyer/user of reactor technology.** The lack of identity for this function in the new organization indicates a dwindling importance and could become a gap in capability if it continues. The ability to inform policy makers on the complex interactions of policy, regulation, economics and technology is key to performing an effective advocacy of nuclear energy; arguably one of the important mission elements of the Office of Nuclear Energy. One need look no further than the Office of Energy Efficiency and Renewable Energy (EERE) and its National Renewable Energy Laboratory (NREL) for an example of an effective advocacy function supported by a laboratory-based analysis function that analyzes and communicates the nexus of policy, regulation, economics, and technology. For example, the listed capabilities of NREL include: **understanding the impacts of markets and policies** on the deployment and use of renewable energy and energy efficiency (RE/EE) technologies; **projecting the impacts of RE/EE and conventional energy technologies**; **conducting technology systems analyses** to evaluate the technology attributes of RE/EE technologies; and **providing the foundation for energy analysis and decisions**, through the development of and dissemination of data and modeling tools.<sup>84</sup> Similar functions should be articulated and funded for NE-related national laboratories.

The importance of the Fuel Resources subprogram should be emphasized in that it sets an economic ceiling on the price of uranium as well as dispels the argument that there may be resources constraints on the expanded use of nuclear energy. While this line of argument has not been used recently, because of the static nature of nuclear capacity in the US, it is likely that nuclear energy critics will make the argument of lack of fuel resources, once it is understood that a significant increase in the use of nuclear energy is possible; as was voiced in the 1960s and 1970s. A superficial review of the IAEA/NEA publication "Uranium: Resources, Production, and Demand," also known as the "Redbook" provides a fairly low level of Reasonably Assured Resources (RAR).<sup>85</sup> Having the answer that there are essentially unlimited resources available from the sea at costs that do not significantly impact the cost of nuclear electricity would be an effective rebuttal to any potential concerns about the availability of fuel resources for advanced reactors.

---

<sup>83</sup> FY 2017 Congressional Budget Justification, Vol 3, page 437-438.

<sup>84</sup> [www.nrel.gov/analysis/capabilities.html](http://www.nrel.gov/analysis/capabilities.html), retrieved 5 Dec 2016

<sup>85</sup> [www.oecd-nea.org/ndd/pubs/2016/7301-uranium-2016.pdf](http://www.oecd-nea.org/ndd/pubs/2016/7301-uranium-2016.pdf), retrieved 9 Dec 2016

The objective of the UNF R&D subprogram suggests that it supports non-LWR advanced reactor deployment but **emphasis is on advanced, recycling fuel cycles that utilize advanced reactors and not on advanced reactors used in a once-through fuel cycle to generate electricity**, as would be the case if a HTGR or SFR was commercially deployed by 2040. There appears to be **little or no focus on non-LWR fuels requiring direct disposal as used fuels; not having undergone separation and recycling. There is no mention made of disposal of HTGR fuels or of SFR fuels; the two most likely candidates for commercial deployment.**

Overall, while NE's stated focus on economics is an indication that the importance of economics is recognized, it appears that program funding and its output, the real focus, is mainly focused on non-economic aspects, e.g., technical performance, safety, security, infrastructure, human capital development. **These other aspects, while important, miss the centrality of economics as the primary barrier to widespread deployment of nuclear energy, generally, and advanced reactors, specifically, in the future.**

### **A Word on Innovation and Technology Transfer**

The drive for innovation and invention and the transfer of technologies to the marketplace can be understood through either a technology-push model or through a technology-pull model; though, in reality it is not always this simple. Consider the case of energy generation technologies. In the US, where the users of technology are private enterprises with responsibilities to shareholders and the Securities and Exchange Commission, there must be a technology pull by the user driven by economics. Elsewhere, where users are governments or government-controlled enterprises, e.g., China, France, Korea, and Russia, there can be a technology-push for a new technology. Thus, **in the US with respect to advanced reactors, unless there is a technology pull by users driven by significant economic benefits, or a strong, sustained Federal policy-push for nuclear energy**, it is unlikely that they will be widely deployed commercially; other technology options are available and easier to deploy. Unless it can be monetized at the utility level, it will not be done.

The difficulty in the US is that the government previously operated on a technology push model with respect to nuclear energy driven by the scientific progress and infrastructure of World War II, the Cold War arms race, and the subsequent development of the nuclear Navy. Initially, with public utilities operating as de facto government-controlled corporations, a technology-push approach could be seen as governing and operative. Yet, the users of the technology, utilities and generation businesses have increasingly been moving to a technology-pull model as they have increasingly been deregulated; moving from public utilities to private businesses driven by profit motives and answering to shareholders and the Securities and Exchange Commission. This has relevance to the R&D program as they seek to find a ways to transition technologies from the laboratory to the marketplace. It has relevance to NE, as the nation's advocate for nuclear energy, to better understand the opportunities to understand and influence policy and the ability of policy to influence technology-decision makers. A central thesis of this report is that the economics of the market are the controlling factor in technology decision-making by energy generation enterprises and until and unless NE recognizes this and orients its R&D focus and methods to address this there is little likelihood that advanced reactors will be widely deployed commercially in the US.

## **SUMMARY AND CONCLUSIONS**

There are several strategic themes that will affect the electricity sector in the US over the next several decades and these will influence the extent to which advanced reactors could be commercially deployed. They include: decarbonization, electricity growth rate, natural gas supply and price, LWR retirements and solar and wind energy costs. Taken together, these indicate that over the next several decades it appears that nuclear energy and specifically advanced reactors will face significant headwinds that will minimize or even prevent widespread commercial deployment of new nuclear reactors even if the US moves to decarbonize its energy sector. Key among them are that low natural gas prices will likely continue to dominate the energy sector; and that solar and wind generating technologies look to continue their trends in reducing costs. Thus, the economic challenges facing advanced reactors look to remain in place with their significant influence on electricity generating technology decision-making.

In face of these trends, the question arises on what types of advanced reactors may be ready for commercial deployment by 2030. The main types being investigated currently are sodium fast reactors (SFR), high temperature gas-cooled reactors (HTGR), lead-cooled fast reactors (LFR), molten salt reactors (MSR), and light-water reactors that are small and medium sized (LWR SMR).

An independent analysis of commercial advanced reactor companies and associated designs was conducted and it was concluded that about a dozen different companies could potentially have designs available for commercial deployment by the 2030 timeframe. But, it is judged that only five (5) are actively and aggressively engaged in development with a view to having a design available for commercial deployment in the 2030 timeframe. Given current plans, technical maturity, and funding levels, it is likely that only LWR SMR concepts (e.g., NuScale, Holtec, mPower, and Westinghouse) will be available for commercial deployment by 2030. Advanced reactor concepts based on the most technically mature concepts, e.g., Terrapower, X-Energy, will likely only be available in 2035-2040 timeframe at the earliest.

However, even if and when these advanced reactor designs become available there remain significant barriers to their widespread commercial deployment. These barriers include economics, natural gas competition, the length and cost of regulatory approval, waste management issues, utility acceptance, and public acceptance and national will.

The most significant barrier to commercial deployment of advanced reactors is related to their economics and the uncertainties of costs to construct, operate, maintain, and decommission an advanced reactor, including fuel and waste management. Information gathered for this report indicates that no current advanced reactor concept is expected to provide an economic case that is significantly better than current LWR technologies. The apparent parity with LWR systems coupled with the large uncertainties in these cost estimates present a significant hurdle for advanced reactors to overcome; until costs of nuclear are competitive with all other electricity sources it is unlikely to be widely adopted.

Three sets of factors suggest their hopes that nuclear power will become a cost leader with respect to natural gas are unfounded: 1) the quickly increasing supply of natural gas and related transportation infrastructure, 2) the greater ease of construction, financing, operation, and decommissioning of natural gas plants compared to nuclear plants, and 3) the technological advantage of gas turbines over nuclear



turbines. Until costs of nuclear electricity are competitive with all other electricity sources it is unlikely to be widely adopted. Given the advantages described above, natural gas will likely remain an attractive technology option for utilities and a significant challenge for nuclear energy.

The long time and large costs associated with obtaining NRC Design Certification and licenses to construct and/or operate a nuclear reactor are barriers to commercial deployment of advanced reactors. With costs estimated on the order of \$500M-\$1,000M and requiring over a decade to complete, significant government support has enabled only a single LWR SMR to attempt the process; because this design builds on and rests on the commonality of its design with established LWR technology. With almost all experience and regulation in the US is based on LWR technology, shifting to a new technology will require new data, new training, new models, new regulations, guidelines, and standards. It is not a trivial undertaking and it will be an expensive and lengthy process for the first several advanced reactor designs. This uncertainty represents a significant barrier to commercial deployment of advanced reactors.

The inability of the US to commit to and follow a path for the disposal of used nuclear fuel remains a barrier for the deployment of advanced reactors. Given that the legal limit for commercial spent fuel in Yucca Mountain was set at 63,000 metric tons of heavy metal, there is already a need for a second repository or an amendment to the law to accommodate the fuel from existing reactors not to mention the new fuel types that would arise from widespread deployment of advanced reactors. How to address future fuels from different technologies has not yet been defined. The continued lack of a route to disposal remains a significant uncertainty for any utility to build new nuclear.

Electric utilities or electricity-generating companies are by their nature risk-averse enterprises because of their mandate to provide economic and reliable electricity. Thus, there is a high bar to any new generating technology being deployed. Unless it can be demonstrated over an adequate period of time that a new technology is safe, reliable, and economic it is unlikely to be chosen, absent a significant cost or monetized policy incentive.

Finally, the ever-present barrier to nuclear energy of adverse public opinion will exist for advanced nuclear technologies. Fukushima has done nothing to ease public concerns about nuclear energy. The public opposition to nuclear energy will likely be exacerbated by media highlighting fear of the new and unknown, the lack of a path to disposal for new fuels and waste types, and the unproven nature of the technology and economics. The increasing view of nuclear as an environmentally friendly zero carbon emission technology may help but absent a solid, widespread belief that advanced nuclear reactors are as safe or safer than current designs, this may not be enough. A significant and sustained effort to create the national will to move forward will be needed. This will require strong sovereign support that will need objective, informed, and persuasive advocates; one of which must be the DOE Office of Nuclear Energy.

A look at the EIA analysis from the 2016 Annual Energy Outlook and the Fuel Cycle Options analyses show that achieving carbon reduction goals will require a variety of policy tools, i.e., tax credits and carbon taxes, to drive technology decision makers to choose carbon-free electricity sources and overcome the low cost of coal and natural gas. They show that a nuclear-specific subsidy is required in order to encourage the growth of nuclear technology in the face of low cost alternative energy sources; i.e., natural

gas. However, a nuclear subsidy alone, even if it successfully increases installed capacity by 50 percent, is insufficient to meet carbon-reduction goals. To meet carbon reduction goals will require a mix of carbon-free technologies, including nuclear, at sufficient levels to significantly reduce the share of coal and natural gas.

With respect to NE's R&D programs, while NE's stated focus on economics is an indication that the importance of economics is recognized, it appears that program funding and its output, the real focus, is mainly focused on non-economic aspects, e.g., technical, education, infrastructure, human capital development. These other aspects, while important, miss the centrality of economics as the primary barrier to widespread deployment of nuclear energy, generally, and advanced reactors, specifically, in the future.

In summary, commercial deployment of advanced reactors faces significant challenges that can be briefly characterized as Competitiveness, Readiness, and Other Challenges. Taken together, they represent a high bar to be overcome. However, opportunities to overcome these challenges do exist.

A central thesis of this report is that the economics of the market are the controlling factor in technology decision-making by energy generation enterprises and until and unless NE recognizes this and orients its R&D focus and methods to address this there is little likelihood that advanced reactors will be widely deployed commercially in the US. Coupled with this is the need to understand and develop policy tools, like production tax credits, in order to overcome the economic hurdles and account for the non-economic benefits of nuclear energy.

## **RECOMMENDATIONS**

### **1. EMBRACE AND ENABLE NATIONAL ADVOCACY**

The Office of Nuclear Energy must embrace, encourage, and enable an advocacy role for nuclear energy. Without a strong expression of sovereign will there is little likelihood that advanced reactors will be overcome the significant challenges described in this report. The role of NE must be to inform and facilitate this sovereign support by developing alliances, mechanisms, messages, models, tools, and information that are objective, informed, and persuasive; unabashedly pro-nuclear. One particularly effective tool is the production tax credit. Tax credits have been used effectively as a policy tool for national advocacy for deployment of renewable energy sources as well as Generation III+ LWR. NE would do well to develop an understanding of the effects of their application; both on primary effect on deployment but also the secondary effects on budgets, taxation, politics, etc.

In many ways, the widespread commercial deployment of advanced reactors mirrors the commercial deployment of light water reactors at the dawn of the atomic age. In that era, sovereign will was expressed through the Atomic Energy Commission's Power Reactor Demonstration Program. This program laid the necessary groundwork for the successful and widespread commercial deployment of LWR in US. Commercial deployment of LWR in that era faced similar issues and challenges as do advanced reactor today.

There are some important differences between the 1960's and now that would need to be acknowledged and addressed including the rise of a popular anti-nuclear movement enabled by distributed social media; the reactor accidents that have occurred worldwide in Chernobyl, Three Mile Island, and most recently at Fukushima; and the deregulation of electricity generating markets with the attendant shift from technology-push to technology-pull.

For a modern incarnation of this type of sovereign support, look no further than the Office of Energy Efficiency and Renewable Energy (EERE) and its National Renewable Energy Laboratory (NREL) for an example of an effective advocacy function supported by a national laboratory; consider how effective their pro-renewable energy advocacy has been. They developed tools, models, data, expertise, and capacity and worked with industry groups and end users to develop the environment of policy, law, and regulation that has created a technology-pull for renewables that is revolutionizing electricity generation in the US over a relatively short time.

## **2. CONDUCT DEMONSTRATION(S)**

What has become evident by the conduct of this study is the fundamental need for a demonstration reactor to address the many barriers to commercial deployment of advanced reactors. A demonstration reactor would focus efforts to resolve technical, institutional and infrastructure issues such as licensing framework and regulation; create and mature fuel and services supply chains; allow for education and training of personnel; establish the economics, reliability, and safety of the technology; and create familiarity with buyers and the public.

In many ways, the barriers to widespread commercial deployment of advanced reactors mirror the issues facing the commercial deployment of light water reactors at the dawn of the atomic age. Therefore, any program to construct and operate an advanced demonstration reactor should look to the Atomic Energy Commission's Power Reactor Demonstration Program. This program existed between 1955 and 1963, and successfully subsidized the construction and operation of the first demonstration power reactors in the U.S.: a dozen 10-75 MW reactors that started service in the 1950s and three 200 MW-class reactors that started service in the early 1960s.<sup>86</sup> Commercial deployment of LWR in that era faced similar issues and challenges as do advanced reactor today. The path through these challenges was blazed through demonstration; a vital step to commercial deployment of any new reactor technology. Insights into how to shape and frame a new demonstration reactor program can be gleaned from a review of these past efforts.

Construction and demonstration of a demonstration reactor will likely be too expensive for industry to do alone so it would need to be a public-private partnership. Therefore, its purpose will also need to include demonstration of its ability to achieve US policy objectives such as demonstration of a sustainable fuel cycles.

---

<sup>86</sup> DOE FCO Report "Identification and Analyses of Fuel Cycle Economics Issues," September 30, 2014, p 23.

Because an important objective of any advanced demonstration reactor should include demonstration of public policy objectives such as sustainability it would make sense to ensure that the demonstration reactor technology chosen is compatible with the fuel cycle options that are most likely to be deployed in the future. Thus, **it would be beneficial to extend the results of the recent Evaluation and Screening Study of advanced fuel cycle systems to include a review of each potential advanced reactor concept to determine which demonstration reactor(s) would be most suitable for demonstration of important fuel cycle performance characteristics.** This technology-specific follow-on to the Evaluation & Screening Study would aid improved prioritization and coordination of NE R&D. The overarching context of sustainable fuel cycles could be used to evaluate the effect and required technologies to meet other R&D goals such as carbon reduction, economics, safety, suitability to integrate in smart grid with large VRE, etc. The capping of uranium costs as forecast by the Fuel Resources R&D program should also be incorporated as an input into the analysis of future fuel cycles and related advanced reactor technologies.

### **3. FACILITATE COMMERCIAL EFFORTS**

DOE has an array of nuclear energy R&D capabilities that would be very difficult and expensive to replicate commercially. Making these more readily available to industry to use in their effort to develop and deploy advanced reactors is necessary for progress to be made in the US. The role of DOE/NE-4 is to create tools, programs, facilities that provide equal opportunity for any/all commercial entities to advance their designs from lab to marketplace. This would include building and/or making available facilities capable of component testing, fast flux irradiations, hot cell/post-irradiation examination facilities, high performance computing, multi-physics models, and developing and disseminating the data needed to support modifying regulations, material qualifications, fuel enrichment increase, used fuel disposal qualification, and used fuel storage and transportation. Four recommendations are offered to improve NE support to commercial efforts:

#### **a. Construct and operate a fast neutron test reactor**

A key gap in US capabilities is a fast neutron irradiation capability; a fast neutron test reactor. A dedicated fast neutron irradiation capability is essential in order to allow for rapid innovation and certification of current and future advanced reactor designs. For example, materials capable of sustaining very high irradiation damage are a common need for many advanced reactors; the Terrapower TWR needs materials rated for up to 550 displacements per atom (dpa), compared to less than 100 dpa for LWR reactors. Currently, there are very few opportunities for fast neutron irradiation in the US and those that exist have relatively low fast neutron fluxes. This means that fast neutron irradiation damage experiments take a very long time to complete. The recent DOE study on Advanced Demonstration and Test Reactors succinctly makes these points:

*"...water-cooled materials test reactors (MTRs) produce damage rates (up to 10 dpa/yr) sufficient to support most thermal reactor development, but are already operating near full capacity. However, to attain peak doses typical of advanced fast reactors (200 to 500 dpa) using a water-cooled MTR would take 20 to 50 years. Advanced fast neutron reactor systems experience neutron damage rates that are significantly higher because the neutrons are typically not*

*thermalized and the magnitude of the fast neutron flux is much higher than for thermal systems.*<sup>87</sup>

There is also a need to replicate in-core interactions between materials and coolants in representative conditions, including neutron flux, temperatures, and pressures to allow for thorough understanding of all the complex physical and chemical interactions that can occur and develop over time; including radiation-induced changes. For many advanced reactor concepts this basic information does not exist. This understanding must also be continually improved upon over time to account for long-term conditions and mechanisms to be identified and understood. For example, thermal neutron irradiations in support of LWR are still routinely performed. Advanced reactor deployment will require this support as well.

High performance computer models are impressive but only as valid as the data they are developed with, which must come from physical experiment; especially when pushing the performance envelope into previously uncharted regions. A test reactor is a necessary complement to high performance computing.

Other benefits of a test reactor in the US would be to support and sustain: knowledge and expertise; creation of fast reactor fuel and waste management infrastructure and capabilities; licensing and regulatory development and oversight; commercial reactor research and development; and US influence in international reactor safety and safeguards activities.

Further, a fast test reactor would not only support commercial deployment of advanced reactors but would also provide an important national security capability enabling R&D on advanced reactors for defense purposes as well, e.g., advanced naval propulsion systems or very small, portable power generating systems. Therefore, it is recommended that DOE/NE reach out to its NNSA and DOD counterparts to explore potential collaborations to construct a fast test reactor in the US.

In summary, the lack of a dedicated fast neutron test reactor is a significant gap and hindrance to US advanced reactor R&D and their commercial deployment and it is recommended that DOE/NE pursue construction of a fast neutron test reactor project as soon as possible.

#### **b. Modifications to the Gateway for Accelerated Innovation in Nuclear initiative**

The Gateway for Accelerated Innovation in Nuclear (GAIN) initiative and the related voucher program is a good example of how DOE can facilitate commercial efforts to develop advanced reactors. Two recommendations are offered:

- To be more effective, though, the size of the awards may need to be increased because of the high costs associated with working in and with national laboratories.
- Another potential improvement would be to have a continuous open enrollment instead of a defined enrollment period once per year. Other federal programs that fund innovation have this feature, for example: the Army Research Laboratory Core Broad Agency Announcement (BAA) for

---

<sup>87</sup> Idaho National Laboratory, Advanced Demonstration and Test Reactor Options Study (Draft), March 2016, INL/EXT-16-37867, page xii.

Basic and Applied Scientific Research for 15 May 2012 – 31 March 2017,<sup>88</sup> the Defense Advanced Research Projects Agency (DARPA) Defense Sciences Office (DSO) Office-wide BAA,<sup>89</sup> and the U.S. Army Medical Research and Materiel Command Broad Agency Announcement for Extramural Medical Research.<sup>90</sup> Open enrollment would make GAIN more responsive to the businesses it is trying to serve, allowing them access to funds and facilities as needed for their schedules and deadlines.

**c. Establish the Correlation of Heavy Ion Irradiation and Neutron Irradiation, if possible**

In lieu of a fast neutron test reactor, one innovative method being pursued to increase the speed of irradiation damage is through the use of heavy-ion irradiation where damage rates can be significantly higher. For example, Terrapower, working with the University of Michigan, is using heavy ion irradiations for its in-core material development work. However, this technique is not yet widely accepted as equivalent to neutron irradiation. Until this equivalence is established, neutron irradiation damage will be needed to support NRC licensing as well as to eventually establish the correlation and equivalence of heavy-ion irradiation. A fast neutron test reactor would support this effort and bring it to a more rapid conclusion than otherwise possible. However, until a test reactor is available it would be useful for NE to work in a concerted effort with industry, academia, and the NRC to determine the equivalency (or not) of heavy ion irradiations with neutron irradiations. Showing this equivalency would enable development of other advanced materials and fuels in significantly more rapid timeframes than currently possible, thereby enabling more rapid innovation in advanced nuclear energy systems. In addition to working to construct a fast neutron test reactor, NE should consider creating a new High Impact Problem within the Nuclear Energy Advanced Modeling Systems program to address the use of heavy ions as a substitute for neutron irradiations and/or a Nuclear Energy University Program topic to address this.

**d. Waste Management R&D on advanced reactor used fuels**

The lack of a path forward for disposal of used nuclear fuels from advanced reactors is a source of uncertainty that could dissuade users from considering advanced reactors. To alleviate this, NE should ensure that R&D is conducted for the entire fuel cycle for advanced reactors including the management and disposal of the used fuels. Specifically, efforts should be initiated to address the potential for the direct disposal of once-through SFR fuels and HTGR fuels. Delineating a credible path forward to disposal for advanced reactor fuels is important to reduce the risks of their deployment.

Finally, supporting US-based commercial advanced reactor efforts is important even if the outlook for commercial deployment of advanced reactors is difficult in the US; there remains opportunity for deployment overseas where economic conditions, grid and market structure, and policy and regulatory environments are different and more amenable to these technologies. Therefore, it is important to continue development and support for US companies working on advanced reactors and their commercial deployment. Benefits for this include: ensuring safety and security of advanced reactors;

---

<sup>88</sup> [www.arl.army.mil/www/pages/8/W911NF-12-R-0011-04.pdf](http://www.arl.army.mil/www/pages/8/W911NF-12-R-0011-04.pdf), retrieved 30 Nov 2016

<sup>89</sup> [www.fbo.gov/index?s=opportunity&mode=form&id=028fd5d5bf74f32be40d0528a3b0e5ba&tab=core&\\_cvview=0](http://www.fbo.gov/index?s=opportunity&mode=form&id=028fd5d5bf74f32be40d0528a3b0e5ba&tab=core&_cvview=0), retrieved 30 Nov 2016

<sup>90</sup> [www.grants.gov/web/grants/view-opportunity.html?oppld=289274](http://www.grants.gov/web/grants/view-opportunity.html?oppld=289274), retrieved 30 Nov 2016

creating jobs for US workers, and retaining leadership and relevance in international non-proliferation and safety fora. Any overseas deployment will also help reduce uncertainty and thereby improve opportunities for domestic deployment, as well.

#### 4. BECOME ECONOMICALLY COMPETITIVE

Recognizing that there are significant inherent economic challenges to Generation IV advanced reactors based on their technology and regulatory context, there remains the need for advanced reactors to compete not just with Generation III+ reactors but also all other electricity generating technologies available in the marketplace, if they are to be widely deployed commercially.

Recommendations to accomplish this fall into two broad categories: hardware and software. More specifically, there is a need for technology breakthroughs (hardware) that allow nuclear energy to compete economically and there is a need for better understanding of the marketplace and technology decision-making by the end user (software) that, in turn, can be used to guide and prioritize R&D. Specific recommendations are:

##### a. AIM HIGH; GENERATION V

Third Way conducted an analysis of commercial advanced reactor development efforts:

*"Third Way has found that there are nearly 50 companies, backed by more than \$1.3 billion in private capital, developing plans for new nuclear plants in the U.S. and Canada."<sup>91</sup>*

While some of these businesses are not credible it still points out that there are a significant number of private enterprises engaged in development and deployment of advanced nuclear energy technologies. These businesses are working actively to develop Generation IV advanced reactors and SMR. In a sense, this can be considered as a "win" for the Generation IV program. Enough progress was made via governmental efforts and support to cause a significant commercial movement to emerge dedicated to profitably deploying these advanced reactor technologies. This movement is still nascent but it points out that maybe the goal of the NE R&D program could begin to shift to the next horizon; call it Generation V.

*"The greatest danger for most of us is not that our aim is too high and we miss it, but that it is too low and we reach it"*  
  
*- Michelangelo*

A shift to a new horizon is perhaps overdue. Consider that almost all the basic concepts of Generation IV designs were begun in the 1950-1960s. However, while the considerable body of work on Generation IV concepts has led to advanced reactor designs that are significant improvements over LWR in many aspects, they remain essentially equivalent to Generation II/III LWR technology in the very important attribute of economics, despite it having been a goal of Generation IV to improve the economics of nuclear energy. The economics of proposed Generation IV reactors remains a barrier to their deployment and it is unlikely that this will be overcome absent some form of national subsidy. The market reality of choosing

<sup>91</sup> [www.thirdway.org/report/the-advanced-nuclear-industry](http://www.thirdway.org/report/the-advanced-nuclear-industry), retrieved, 29 Oct 2016

technologies based on their cost will not change. Therefore, a goal for the next generation should be nuclear energy designs that are economically competitive with all other energy production technologies, e.g., natural gas, solar, and wind.

Considering all of the significant scientific advances and breakthroughs in nanotechnology, high performance computing, advanced manufacturing, and materials it may be possible to create truly revolutionary concepts that can fully compete economically with all other energy sources. Consider the possibilities with materials immune to irradiation, for reactors that don't need cooling, for direct power conversion systems that don't require turbines and heat exchangers. None of these may be technically achievable but there would be value in asking the questions and challenging the creativity of the American scientist and engineer to wrestle with them.

DOE/NE-4 could create a low-cost activity that involves competitions, grand challenges, and funded R&D to start researchers thinking about the next horizon in nuclear energy; one that breaks new ground in terms of how to harness the energy of the atom.

#### **b. ENHANCED ELECTRICITY GRID MODELING**

The projected large-scale increase in the deployment of variable renewable energy (VRE) sources, i.e., solar and wind highlights the need for improved analysis capabilities to guide future reactor development efforts. Designing in features that are compatible with expected grid performance requirements will tend to make these designs more attractive.

Current LWRs have limited ability to load-follow. But as VRE increase their role, advanced nuclear reactors will likely need to be able to load-follow where they increase or decrease their output to complement the output of VRE. Advanced reactors may be able to serve as rapid load-following buffers for the grid in order to allow maximum benefit from VRE while providing the maximum benefit of nuclear (always on baseload). The 2015 Quadrennial Technology Review makes this point:

*"Increased penetration of variable renewable energy systems such as wind and solar PV increases the need for flexible generation.... Such flexible generation generally also has greater value in electricity markets than baseload or variable supplies."<sup>92</sup>*

Thus, analyses could be conducted to explore the value of load-following as compared with other large-scale electricity storage technology options and others could define specific technical requirements, e.g., rates of change.

To enable these analyses, an enhanced grid modeling capability is needed to better understand the complex relationship between different energy technologies as they function on the US electricity grid given the significant projected growth of VRE. A **realistic grid simulator** would help understand and communicate the system performance and issues from increased use of VRE as well as to define requirements for advanced nuclear reactors that must function in this future grid. This would not require

---

<sup>92</sup> 2015 QTR Appendix 4K Hybrid Nuclear-Renewable Energy Systems, p 1.



developing a simulator from scratch; numerous organizations and companies have them. Examples of existing grid simulators are given in Attachment 4. Establishing relationships and working with other organizations that analyze and operate the grid would be beneficial as a way to exchange data and information. These organizations include the Pacific Northwest National Laboratory, Sandia National Laboratory, National Renewable Energy Laboratory, the Electric Power Research Institute, the Grid Modernization Laboratory Consortium<sup>93</sup>, the DOE Grid Tech Team<sup>94</sup>, the Center for Ultra-Wide-Area Resilient Electric Energy Transmission Networks (CURENT),<sup>95</sup> and the DOE Office of Electricity Delivery and Energy Reliability. In particular, CURENT has been developing a large-area testbed that may be suitable for evaluating the role and impact of advanced reactors in the future grid:

*"... the Large-Scale System Testbed is to represent large grids of the future, such as that of North America, at several resolution levels for both evaluation of new technologies and to drive research efforts. The success of the testbed enables a comprehensive evaluation of the impact of the changes and new technologies on the operation of future power grids. The models include different scenarios of generation mix and operating scenarios, wide-area measurements, new actuation technologies and new control strategies."<sup>96</sup>*

#### c. ENHANCED ANALYSIS CAPABILITIES

Understanding the role of advanced reactors in grids with significant amounts of variable energy sources as well as distributed sources (e.g., rooftop solar, electric vehicles) will likely require energy market clearing regulations to be modified to create an environment that this load-following capability would be economically beneficial to a utility. This highlights the intersection of regulation, policy, and technology in decision-making and the need to conduct sophisticated inter-disciplinary analyses to help understand technology decision-making in the context of changes in economic, policy, and regulatory drivers. The recent Summit on Improving the Economics of America's Nuclear Power Plants makes this point:

*"Much of the nation's electricity load has moved from traditional wholesale electricity markets with bilateral transactions and power pool agreements to independent system operator (ISOs)/regional transmission organization (RTOs), which operate/manage the transmission system independent of electricity generation to foster competition. This equitable access creates a large, dynamic, and complex system that must be better understood to avoid negative unintended consequences."<sup>97</sup>*

What market drivers can be identified to help influence decisions that support advanced reactors in future energy markets? How will proposed regulatory policy changes affect technology decision-making and

---

<sup>93</sup> <http://energy.gov/articles/launch-grid-modernization-laboratory-consortium>

<sup>94</sup> <http://energy.gov/under-secretary-science-and-energy/doe-grid-tech-team>

<sup>95</sup> <http://curent.utk.edu>

<sup>96</sup> <http://curent.utk.edu/research/erc-research-thrusts/>

<sup>97</sup> Idaho National Laboratory, Summit on Improving the Economics of America's Nuclear Power Plants, September 2016, INL/EXT-16-39257, page 4.

avoid unintended consequences? What level should the social costs of carbon be set at and what impact will they have on advanced reactor deployments? What form of regulation or policy would enable a technology-pull for advanced reactors in competitive markets? These and many other questions need answers supported by effective and sophisticated models and tools. To effectively answer these questions will require a greater understanding market forces, utility decision-making processes, and market regulation as well as advances in decision-making modeling tools.

Further, given that high costs are a consistent reason why nuclear energy is not selected by utilities and that uncertainty in costs is a major weakness of advanced nuclear reactors, developing a better understanding of costs would be valuable. Reducing the uncertainties in cost estimates could lead to alterations in modeling and decision-making. Continuing to improve the data and methods to provide a reliable life cycle cost estimate for all advanced reactors technologies that is suitable for use to compare reactor technologies as well as their performance against other energy generation technologies is needed.

Thus, a recommendation is to **create capabilities focused on the nexus of policy, regulation, economics, and technology**. Create tools, data, models, and results to support policy makers as they seek to understand and influence technology decision makers in private enterprises. An objective would be to make NE the go-to experts on the “software” aspects of advanced reactors in addition to their expertise on the hardware aspects. This will support and enable NE in its needed role as advocate for nuclear energy.

#### d. RELATIONSHIPS WITH OTHER ORGANIZATIONS

NE should enhance its relationships with the organizations in the US that do extensive work on modeling energy systems and their costs in order to ensure better input to their models with respect to nuclear energy. These include the Energy Information Administration, Electric Power Research Institute, and the National Renewable Energy Laboratory. Other organizations to consider include the Energy Modeling Forum at Stanford University<sup>98</sup>, the US Association for Energy Economics<sup>99</sup>, and Third Way<sup>100</sup>. DOE/NE efforts on improving knowledge and capability on nuclear energy economics should be matched with a goal that DOE/NE becomes the recognized source of expertise and capability in the field of nuclear energy economics. In strengthening these relationships, improving the data and information used, and the recognition of NE’s expertise and capabilities, there will be a wide spillover effect in support of nuclear energy advocacy.

**Disclaimer: This work was accomplished as part of contract GS-10F-0038Y/DE-DT0004091. It solely represents the views of the author and in no way represents the views, policies, and opinions of DOE or its staff.**

---

<sup>98</sup> <https://emf.stanford.edu>

<sup>99</sup> [www.usaee.org](http://www.usaee.org)

<sup>100</sup> [www.thirdway.org](http://www.thirdway.org)

## References

1. DOE Quadrennial Energy Review 2015 <http://energy.gov/epso/quadrennial-energy-review-qer>
2. DOE Quadrennial Technology Review 2015 [www.energy.gov/under-secretary-science-and-energy/quadrennial-technology-review](http://www.energy.gov/under-secretary-science-and-energy/quadrennial-technology-review)
3. Department of Energy, *Strategy for the Management and Disposal of Used Nuclear Fuel and High-Level Radioactive Waste*, January 2013  
<http://energy.gov/sites/prod/files/Strategy%20for%20the%20Management%20and%20Disposal%20of%20Used%20Nuclear%20Fuel%20and%20High%20Level%20Radioactive%20Waste.pdf>
4. Department of Energy, *Preliminary Evaluation of Removing Used Nuclear Fuel from Shutdown Sites*, September 30, 2016, FCRD- NFST-2016-000478, PNNL-22676 Rev. 8  
[http://energy.gov/sites/prod/files/2016/10/f33/Shutdown\\_Sites\\_Report\\_Sept2016\\_web.pdf](http://energy.gov/sites/prod/files/2016/10/f33/Shutdown_Sites_Report_Sept2016_web.pdf)
5. Energy Information Administration Annual Energy Outlook [www.eia.gov/forecasts/aeo/](http://www.eia.gov/forecasts/aeo/)
6. Idaho National Laboratory, *Advanced Demonstration and Test Reactor Options Study (Draft)*, March 2016, INL/EXT-16-37867, Revision 0
7. Nuclear Energy Institute, *Strategic Plan for Advanced Non-Light Water Reactor Development and Commercialization*, May 2016 [www.nei.org/Master-Document-Folder/Backgrounders/Reports-And-Studies/Advanced-Reactors-Strategic-Plan](http://www.nei.org/Master-Document-Folder/Backgrounders/Reports-And-Studies/Advanced-Reactors-Strategic-Plan)
8. Lawrence Berkeley National Laboratory, *Tracking the Sun VIII: The Installed Price of Residential and Non-Residential Photovoltaic Systems in the United States*, August 2015,  
<http://energy.gov/sites/prod/files/2015/08/f25/LBNL%20Tracking%20the%20Sun%20August%202015.pdf>
9. Department of Energy, *Wind Vision: A New Era for Wind Power in the United States*, March 2015, <http://energy.gov/eere/wind/maps/wind-vision>
10. Department of Energy, FY2017 Budget Request, Volume 3, Nuclear Energy,  
[http://energy.gov/sites/prod/files/2016/02/f29/FY2017BudgetVolume3\\_2.pdf](http://energy.gov/sites/prod/files/2016/02/f29/FY2017BudgetVolume3_2.pdf)
11. Idaho National Laboratory, *Nuclear Fuel Cycle Evaluation and Screening – Final Report*, October 8, 2014, FCRD-FCO-2014-000106, INL/EXT-14-31465,  
<https://fuelcycleevaluation.inl.gov/Shared%20Documents/ES%20Main%20Report.pdf>
12. Idaho National Laboratory, *Economic and Market Challenges Facing the U.S. Nuclear Commercial Fleet*, September 2016, INL/EXT-16-39951,  
<https://gain.inl.gov/Shared%20Documents/Economics-Nuclear-Fleet.pdf>
13. Idaho National Laboratory, *Summit on Improving the Economics of America's Nuclear Power Plants*, September 2016, INL/EXT-16-39257,  
<https://gain.inl.gov/Shared%20Documents/Convening%20Summit%20Final%20.pdf>
14. Energy Information Administration/Advanced Resources International, *World Shale Gas and Shale Oil Resource Assessment Technically Recoverable Shale Gas and Shale Oil Resources: An Assessment of 137 Shale Formations in 41 Countries Outside the United States*, June 2013,  
[www.eia.gov/analysis/studies/worldshalegas/pdf/overview.pdf](http://www.eia.gov/analysis/studies/worldshalegas/pdf/overview.pdf)
15. Pacific Northwest National Laboratory, *Nuclear Energy, Renewable Energy with Storage, and Climate Change Mitigation*, FCRD-FCO-2016-000501, September 16, 2016.

16. Secretary of Energy Advisory Board, *Final Report of the Task Force on the Future of Nuclear Power*, September 22, 2016, <https://energy.gov/seab/downloads/final-report-task-force-future-nuclear-power>



## Attachment 1 Task Statement of Work

### ATTACHMENT A.: Scope of Work

Task Statement: Conduct a quick independent review of the R&D portfolio of the Office of Nuclear Technology Research and Development (NE-4) and provide an assessment that can be used to as input for prioritization of the Office's R&D that is needed to meet the goals of the office in support of the Department of Energy's mission to achieve climate change objectives.

#### Deliverables:

- 1) A letter report describing the independent review that will be conducted and key questions the assessment will address. Due Date 10/28/16
- 2) Independent Review Report; Due 12/30/16

The CONTRACTOR will provide timely report input per the review schedule, support follow-up report reviews, and assist with finalizing the report as required. All activities shall be closely coordinated with the TechSource, Inc. PM and Task Leader.

Copies of UNCLASSIFIED deliverables will be furnished to TechSource, Inc. for its information. Contractor will include a brief status report of work performed for the period of each invoice.

Attachment 2 List of Companies Developing Advanced Reactors or LWR Small and Medium-sized Reactors (SMR)

Advanced Reactor Concepts	<a href="http://www.arcnuclear.com">www.arcnuclear.com</a>	SFR
Areva	<a href="http://www.aveva.com/EN/operations-2347/futur-reactors-generation.html">www.aveva.com/EN/operations-2347/futur-reactors-generation.html</a>	SFR, VHTR
CityLabs	None	VSMR
Dunedin	<a href="http://www.dunedinenergy.ca">www.dunedinenergy.ca</a>	VSMR
Flibe Energy	<a href="http://flibe-energy.com">http://flibe-energy.com</a>	MSR
GE-Hitachi	<a href="http://gehitachiprism.com">http://gehitachiprism.com</a>	SFR
Gen4 Energy	<a href="http://www.gen4energy.com">www.gen4energy.com</a>	LFR
General Atomics	<a href="http://www.ga.com/energy-multiplier-module">www.ga.com/energy-multiplier-module</a>	GFR
Holtec	<a href="https://smrllc.com">https://smrllc.com</a>	LWR SMR
Hybrid Power Technologies	<a href="http://hybridpowertechnologies.com/index.html">http://hybridpowertechnologies.com/index.html</a>	GFR
LakeChime	<a href="http://lakechime.com">http://lakechime.com</a>	LFR
mPower	<a href="http://www.bwxt.com/nuclear-energy/utility-solutions/smr/bwxt-mpower">www.bwxt.com/nuclear-energy/utility-solutions/smr/bwxt-mpower</a>	LWR SMR
Northern Nuclear	<a href="http://www.northernnuclear.ca/index.html">www.northernnuclear.ca/index.html</a>	VHTR
NuScale	<a href="http://www.nuscalepower.com">www.nuscalepower.com</a>	LWR SMR
Starcore Nuclear	<a href="http://starcorenuclear.ca/#!/welcome/">http://starcorenuclear.ca/#!/welcome/</a>	VHTR
TerraPower	<a href="http://terrapower.com">http://terrapower.com</a>	SFR
Terrestrial Energy	<a href="http://terrestrialenergy.com">http://terrestrialenergy.com</a>	MSR
Thorcon	<a href="http://thorconpower.com">http://thorconpower.com</a>	MSR
Transatomic Power	<a href="http://www.transatomicpower.com">www.transatomicpower.com</a>	MSR
Upower	<a href="http://www.upowertech.com">www.upowertech.com</a>	VSMR
Westinghouse	<a href="http://www.westinghousenuclear.com/New-Plants/Small-Modular-Reactor">www.westinghousenuclear.com/New-Plants/Small-Modular-Reactor</a>	LWR SMR, LFR
X-Energy	<a href="http://www.x-energy.com">www.x-energy.com</a>	VHTR

Attachment 3 Evaluation of Current Commercial Advanced Reactors

Company	Website	Reactor Type	When started	Planned Completion	Size (Mwe)	Size of Company/ Staffing	Hiring	Number and Quality of Partners	Engaged w NRC	Financial Strength/ Funding	Technical Maturity	Prior Experience in US	Amount of R&D to License / Innovativeness	Active R&D Underway	Total
NuScale	<a href="http://www.nuscalepower.com">www.nuscalepower.com</a>	LWR SMR	2000	2025	50	3	3	3	3	3	3	3	2	3	26
Holtec	<a href="https://smrlc.com">https://smrlc.com</a>	LWR SMR	2010	2025	160	3	3	3	3	2	2	3	2	3	24
TerraPower	<a href="http://terrapower.com">http://terrapower.com</a>	SFR	2006	2035	1150	3	3	3	2	3	2	2	2	3	23
mPower	<a href="http://www.bwxt.com/nuclear-energy/utilit">www.bwxt.com/nuclear-energy/utilit</a>	LWR SMR	2009	?	195	3	1	3	2	2	3	3	3	2	22
GE-Hitachi	<a href="http://gehitachi-prism.com">http://gehitachi-prism.com</a>	SFR	~1985	?	522	3	1	3	1	1	3	3	3	2	20
Westinghouse	<a href="http://www.westinghouse-nuclear.com/New">www.westinghouse-nuclear.com/New</a>	LWR SMR	?	?	225	3	1	2	2	1	3	3	3	2	20
X-Energy	<a href="http://www.x-energy.com">www.x-energy.com</a>	VHTR	2010	?	50	2	2	2	2	2	2	2	2	3	19
Areva	<a href="http://www.avea.com/EN/operations-2347/futur-reactors-generation.html">www.avea.com/EN/operations-2347/futur-reactors-generation.html</a>	SFR		2035		3	1	3	1	1	3	3	1	2	18
Transatomic Power	<a href="http://www.transatomicpower.com">www.transatomicpower.com</a>	MSR	2011	?	520	2	2	2	2	3	1	2	1	2	17
Areva	<a href="http://www.avea.com/EN/operations-2347/futur-reactors-generation.html">www.avea.com/EN/operations-2347/futur-reactors-generation.html</a>	VHTR		2035		3	1	3	1	1	2	3	1	1	16
Terrestrial Energy	<a href="http://terrestrialenergy.com">http://terrestrialenergy.com</a>	MSR		2029	190	2	1	2	1	2	1	2	1	3	15
General Atomics	<a href="http://www.ga.com/energy-mt-trioler-mod">www.ga.com/energy-mt-trioler-mod</a>	GFR	2008	2030	265	3	1	2		2	1	2	1	2	15
U-Battery	<a href="http://www.u-battery.com">www.u-battery.com</a>	VHTR	2008	2024	4	1	1	2	1	2	1	3	2	2	15
Advanced Reactor Concepts	<a href="http://www.arcnuclear.com">www.arcnuclear.com</a>	SFR	2006	?	100	1	1	1	1	1	2	3	3	1	14
Westinghouse	<a href="http://www.westinghouse-nuclear.com/New">www.westinghouse-nuclear.com/New</a>	LFR	?	?	?	3	1	1	1	1	1	1	1	2	12
Gen4 Energy	<a href="http://www.gen4energy.com">www.gen4energy.com</a>	LFR	2007	2030	25	1	1	2	1	2	1	1	1	2	12
Flibe Energy	<a href="http://flibe-energy.com">http://flibe-energy.com</a>	MSR	2011	?	?	1	1	1	1	1	1	2	1	1	10
Starcore Nuclear	<a href="http://starcorenuclear.ca/#/welcome">http://starcorenuclear.ca/#/welcome</a>	VHTR	2008	?	20	1	1	1	1	1	1	2	1	1	10
Thorcon	<a href="http://thorconpower.com">http://thorconpower.com</a>	MSR	2011	?	250	1	1	1	1	1	1	2	1	1	10
CityLabs	None	VSMR	?	?	?	1	1	1	1	1	1	1	1	1	9
Dunedin	<a href="http://www.dunedineenergy.ca">www.dunedineenergy.ca</a>	VSMR	?	?	6	1	1	1	1	1	1	1	1	1	9
Hybrid Power Technologies	<a href="http://hybridpowertechnologies.com/index.html">http://hybridpowertechnologies.com/index.html</a>	GFR	2005	?	785	1	1	1	1	1	1	1	1	1	9
LakeChime	<a href="http://lakechime.com">http://lakechime.com</a>	LFR	?	?	?	1	1	1	1	1	1	1	1	1	9
Northern Nuclear	<a href="http://www.northernnuclear.ca/index.html">www.northernnuclear.ca/index.html</a>	VHTR	?	?	36	1	1	1	1	1	1	1	1	1	9
Upower	<a href="http://www.upowertech.com">www.upowertech.com</a>	VSMR	?	?	?	1	1	1	1	1	1	1	1	1	9

## Attachment 4 Grid Simulation Models

### Government

- Pacific Northwest National Laboratory (PNNL)
  - [www.gridlabd.org](http://www.gridlabd.org)
  - [http://gridoptics.pnnl.gov/articles/m/o/d/Modeling\\_Simulation\\_and\\_Analysis\\_9a3f.html](http://gridoptics.pnnl.gov/articles/m/o/d/Modeling_Simulation_and_Analysis_9a3f.html)
  - [http://gridoptics.pnnl.gov/articles/o/p/e/Open-Source\\_Tools\\_fa67.html](http://gridoptics.pnnl.gov/articles/o/p/e/Open-Source_Tools_fa67.html)
- Sandia National Laboratory
  - <https://xyce.sandia.gov>

### Non-profit Organizations

- Center for Ultra-Wide-Area Resilient Electric Energy Transmission Networks (CURENT);
  - CURENT is a National Science Foundation Engineering Research Center that is jointly supported by the National Science Foundation and the Department of Energy. CURENT is led by the University of Tennessee, Knoxville. Partner institutions include: Northeastern University, Rensselaer Polytechnic Institute, and Tuskegee University
  - <http://curent.utk.edu>
- Electric Power Research Institute (EPRI)
  - <http://smartgrid.epri.com/SimulationTool.aspx>
- Independent System Operators
  - California ISO [www.caiso.com/market/Pages/NetworkandResourceModeling/Default.aspx](http://www.caiso.com/market/Pages/NetworkandResourceModeling/Default.aspx)
  - PJM [www.pjm.com/planning/resource-adequacy-planning/load-forecast-dev-process.aspx](http://www.pjm.com/planning/resource-adequacy-planning/load-forecast-dev-process.aspx)
  - Midwest ISO [www.misoenergy.org/Planning/Models/Pages/Models.aspx](http://www.misoenergy.org/Planning/Models/Pages/Models.aspx)
  - New England ISO [www.iso-ne.com/search?query=models](http://www.iso-ne.com/search?query=models)
  - Western Electricity Coordinating Council  
[www.wecc.biz/layouts/15/WopiFrame.aspx?sourcedoc=/Reliability/Approved-Dynamic-Models-June-2016.pdf&action=default&DefaultItemOpen=1](http://www.wecc.biz/layouts/15/WopiFrame.aspx?sourcedoc=/Reliability/Approved-Dynamic-Models-June-2016.pdf&action=default&DefaultItemOpen=1)

### Commercial

- GE Energy Consulting
  - [www.geenergyconsulting.com/practice-area/software-products](http://www.geenergyconsulting.com/practice-area/software-products)
- Siemens
  - <http://w3.siemens.com/smartgrid/global/en/products-systems-solutions/software-solutions/planning-data-management-software/planning-simulation/Pages/PSS-E.aspx>
- Power World Corporation
  - [www.powerworld.com/products/simulator/overview](http://www.powerworld.com/products/simulator/overview)
- Opal-RT Technologies
  - [www.opal-rt.com/product/emegasim-powergrid-real-time-digital-hardware-in-the-loop-simulator](http://www.opal-rt.com/product/emegasim-powergrid-real-time-digital-hardware-in-the-loop-simulator)
- Math Works
  - [www.mathworks.com/products/simpower/index.html?s\\_tid=gn\\_loc\\_drop](http://www.mathworks.com/products/simpower/index.html?s_tid=gn_loc_drop)





**Department of Energy**  
Washington, DC 20585

NOV 21 2019

Via email

Re: HQ-2019-01408-F

This is a final response to the request for information that you sent to the Department of Energy (DOE) under the Freedom of Information Act (FOIA), 5 U.S.C. § 552. You requested:

Copy of the work product (reports, memos, studies, plans, etc.) received to date from Contract DEDT0004091 awarded to Techsource.

Your request was assigned to the DOE's Office of Management (MA-64) and the Office of Nuclear Energy (NE) to conduct a search of their files for responsive documents. The search started on November 14, 2018, which is the cutoff date for responsive records.

DOE has identified three (3) documents responsive to your request. The documents are being released to you in their entirety.

The adequacy of the search, may be appealed within 90 calendar days from your receipt of this letter pursuant to 10 C.F.R. § 1004.8. Appeals should be addressed to Director, Office of Hearings and Appeals, HG-1, L'Enfant Plaza, U.S. Department of Energy, 1000 Independence Avenue, S.W., Washington, D.C. 20585-1615. The written appeal, including the envelope, must clearly indicate that a FOIA appeal is being made. You may also submit your appeal by e-mail to [OHA.filings@hq.doe.gov](mailto:OHA.filings@hq.doe.gov), including the phrase "Freedom of Information Appeal" in the subject line. (This is the method preferred by the Office of Hearings and Appeals.). The appeal must contain all the elements required by 10 C.F.R. § 1004.8, including a copy of the determination letter. Thereafter, judicial review will be available to you in the Federal District Court either (1) in the district where you reside, (2) where you have your principal place of business, (3) where DOE's records are situated, or (4) in the District of Columbia.

You may contact DOE's FOIA Public Liaison, Alexander Morris, FOIA Officer, Office of Public Information, at 202-586-5955 or by mail at MA-46/Forrestal Building 1000 Independence Avenue, S.W. Washington, D.C. 20585 for any further assistance and to discuss any aspect of your request. Additionally, you may contact the Office of Government Information Services (OGIS) at the National Archives and Records Administration to inquire about the FOIA mediation services they offer. The contact information for OGIS is as follows: Office of



Government Information Services, National Archives and Records Administration, 8601 Adelphi Road-OGIS, College Park, Maryland 20740-6001, e-mail at [ogis@nara.gov](mailto:ogis@nara.gov); telephone at 202-741-5770; toll free at 1-877-684-6448; or facsimile at 202-741-5769.

The FOIA provides for the assessment of fees for the processing of requests. See 5 U.S.C. § 552(a)(4)(A)(i); see also 10 C.F.R. § 1004.9(a). Your request was placed in the "other" category for fee purposes. Requesters in this category are entitled to two free hours of search time and 100 free pages. Since DOE did not exceed the two free hours of search time, no fees will be charged for processing your request.

If you have any questions about this letter, you may contact me or Ms. Jeniffer Pérez Santiago at:

MA-46/ Forrestal Building  
1000 Independence Avenue, S.W.  
Washington, DC 20585  
(202) 586-4933

I appreciate the opportunity to assist you in this matter.

Sincerely,



Alexander C. Morris  
FOIA Officer  
Office of Public Information

Enclosures

## INDEX

Request #: HQ-2019-01408-F-F

### Final response

**Copy of the work product (reports, memos, studies, plans, etc.) received to date from Contract DEDT0004091 awarded to Techsource.**

DOE has completed its search and has located three (3) documents responsive to your request.

- Three (3) documents are *being released in its entirety*.

## Part II. Summary of Search of Antineutrino Induced Lifetime

### Perturbations of Mn-54 Radionuclide

T. Ward (01.02.19)

Search studies were initiated to investigate neutrino induced lifetime perturbations of radionuclides, a possible new neutrino detection method that could be transformational physics. Grams of radioactive material could replace many tons of ordinary matter as detector material producing neutrino detection systems at costs orders of magnitude cheaper and smaller for use in monitoring nuclear reactor power levels and for national nuclear security surveillance. The discovery of a detectable level of lifetime perturbation induced by neutrinos with radioactive targets would greatly reduce the cost and complexity of neutrino detection for use in nuclear security applications. *This work was conducted under NE contract number DE-DT0004091.* The NE Office funded two experimental groups to try to measure the perturbations, a Sodium Iodide (NaI) gamma-ray detection system and a High Purity Germanium (HPGe) gamma-ray system. A Final Report on the NaI detector measurements was reported earlier (07.10.18) in the Part I report.

Here we report Part II final analysis of the Mn-54 study confirming the earlier detection limit and detailing all systematic errors including two new systematic errors not covered in the previous analysis, low frequency oscillations and ambient environmental electronic effects. The Mn-54 data were reanalyzed by determining systematic errors associated with: 1) energy calibration and background, 2) dead time corrections, 3) background spectra re-binning and subtraction, 4) pile-up corrections, 5) decay rate analysis of Region of Interest (ROI), 6) low frequency oscillations and 7) ambient environmental electronic effects.

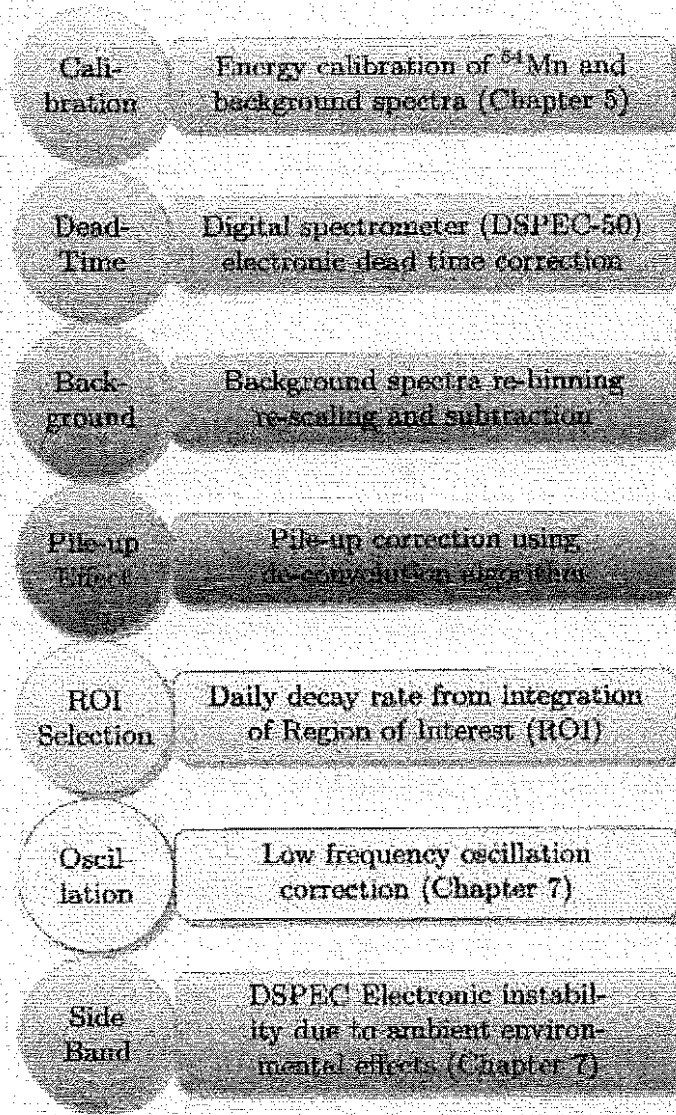
**High Purity Germanium (HPGe) Gamma-Ray Detection.** The Part I results of Koltick, Nistor, Heim and Liu measured the rate effects using HPGe detectors at HFIR. The 1-sigma upper limit for the three radioisotopes studied were reported earlier to be

Mn-54 (312d)	$<1.9 \times 10^{-5}$
Cs-137 (30.1 yr.)	$<1.73 \times 10^{-5}$
Ag-108m (434 yr.)	$<2.83 \times 10^{-5}$

The HPGe measurements using this new gamma-ray spectrum analysis methodology is state-of-art in terms of reducing total systematic errors to an unprecedented  $\pm 1.7 \times 10^{-5}$  level, an *uncertainty level 10-100 times lower* than many previous reported measurements of this type. The Cs-137 result included a positive-definite signal during reactor ON periods of  $\approx 3.5 \times 10^{-5}$ , a value according to first order theory would produce a positive-definite effect of  $\approx 30 \times 10^{-5}$  in Ag-108m decays. The Ag-108m null result of  $<2.8 \times 10^{-5}$  clearly indicates that some form of reactor background associated with ambient environmental electronic effects was not properly accounted for in the Part I Cs-137 analysis shown above. The final analysis of the Mn-54 decay was used for Dr. Liu's thesis (December 2018) that include reanalysis of the Mn-54 database and

new detailed studies of the low frequency oscillations in the data and electronic instabilities due to environmental effects.

**Reanalysis of Mn-54 Results.** The Ph. D. thesis work of Dr. Liu involved re-analysis of the Mn-54 database according to the data analysis flow diagram below:



Previous data analysis reported in Final Report I **only include analysis using the first five procedures.** As a result, a positive-definite result was observed in the Cs-137 data and the total statistical and systematic uncertainty in the Ag-108m data was almost a factor of two greater,

both anomalous results due possibly to the lack of the last two analysis paths shown above, the oscillation and side band analysis (details can be found in Chapter 7 of Liu Thesis).

**Summary of Final Report II.** Relative statistical and systematic uncertainties of new Mn-54 analysis: statistical uncertainties were typically  $\pm 0.7 \times 10^{-5}$  and systematic uncertainties of  $\pm 0.8 \times 10^{-5}$  for a combined total uncertainty at the 1-sigma 68% confidence level of  $\pm 1.5 \times 10^{-5}$ .

Because of the measurable Mn-54 half-life over the course of the experiment, the decay constant variation or decay curve fit provided another rate determining measurement in addition to ROI analysis of reactor ON and reactor OFF comparisons. One test is to compare the average rate variation without regard to reactor status, the result being the mean is less than the 1-sigma deviation, R is taken as the average rate variation in the ROI:

$$\frac{\delta R}{R} = (3.62 \times 10^{-6}) \pm (7.53 \times 10^{-6}),$$

consistent with a NULL result or zero value. The second test compares the reactor ON and reactor OFF residuals for segment analysis varying ON-OFF-ON and OFF-ON-OFF sequences for the entire data set which yielded for the average rate in ROI of

$$\frac{\delta R}{R} = (1.48 \times 10^{-5}) \pm (1.49 \times 10^{-5}),$$

again, consistent with no effect during the antineutrino exposure. The combined results establish the total uncertainty in the Mn-54 spectrum analysis at the 1-sigma 68% confidence level of

$$\frac{\delta R}{R} = \pm 1.5 \times 10^{-5}.$$

Similar uncertainty is expected for both Cs-137 and Ag-108m analysis improving upon the earlier analysis. The reanalysis of Cs-137 and Ag-108m are in process and will be reported later in Final Report III.

**Second Order Model Calculations.** The first order calculation used the Compton wavelength of the electron ( $\lambda_e$ ) which is commonly used in Fermi beta decay formulations and associated atomic effects. The second order calculation for  $\bar{\nu}e$  scattering requires the point-like classical electron radius given by  $r_e = \alpha_e \lambda_e$  where  $\alpha_e = 1/137.036$ , the fine structure constant. The  $\bar{\nu}e$  scattering cross-section is proportional to  $\sigma_{\bar{\nu}e} \propto (4\pi\alpha_e)r_e^2$  which results in a much smaller second order cross-section, consequently requiring a higher reactor flux to achieve a noticeable rate effect with a radioactive source. The maximum rate change remains the same for the atomic electron transitions,  $(\frac{\delta R}{R})_{\max} = 5.8 \times 10^{-4}$ , but longer lifetimes are required to off-set the corresponding smaller cross-section, so to see the maximum rate change effect in the HFIR reactor flux a half-life of  $t_{1/2} > 7700 \text{ yr}$  is required. The first order calculation yielded

$t_{1/2} > 650 \text{ yr}$  for the half-life to achieve the maximum effect in reducing the rate, therefore requiring a long-lived radioisotope such as Ag-108m (440 yr.) to test the first order model.

A beta-current device with a C-14 (5730yr.) radioactive target would be suitable for a second order measurement. Commercial beta-current devices such as a Tritium source produce currents of 50-250 nA ( $\approx 1 \times 10^{12} \text{ e}^-/\text{s}$ ) with an accuracy or uncertainty of about  $1 \times 10^{-4}$ . Reducing the uncertainty of a C-14 beta-current device to  $< 6 \times 10^{-5}$  provides a 5-sigma level measurement necessary for proof-of-principle of the concept for a rate effect of  $(\frac{\delta R}{R})_{\text{C-14}} = 3.9 \times 10^{-4}$ .

**Conclusion**. The current detection limits using HPGe systems preclude using gamma-ray detection methods to routinely monitor neutrino fluxes subject to second order perturbations. If the detection limit for neutrino perturbation of radioactive decay in second order is approximately  $1 \times 10^{-5}$  then it may be possible to use beta-current (nuclear battery) detectors to make practical precision measurements in the field.

In Part III we will summarize the reanalysis of the Cs-137 and Ag-108m results using the additional procedures or analysis paths, the oscillation and side band analysis (details can be found in Chapter 7 of Liu Thesis). The final set of analyzes for the three radioisotopes will be published in a series of papers in a peer-reviewed journal.



## Perturbation on $^{108m}\text{Ag}$ Decay Rate Induced by Reactor Antineutrinos

Preliminary Data Analysis and Results

Date: June 11<sup>th</sup>, 2018

Jonathan Nistor and Jordan Heim

### I. Ag-108 Data Collection:

Data collection has been ongoing since source installation on 21-Nov-2017. The 0.45 uCi Ag-108 disk source was affixed to the detector's nylon source holder on 21-Nov-2017--- after which the environmental enclosure was resealed and front shield wall reinstalled. Primary data collection commenced the following week on 29-Nov-2017, when the enclosure and HPGe crystals returned to thermal equilibrium. At this stage, HFIR has been at full power for 34 days (during cycles 476 and 477), with refueling outages spanning 44 days in aggregate. For reference, the HFIR operating forecast for the next few cycles is presented below:

a.	11/14/18 – 12/08/17	Cycle 476	24 days** (Completed)
b.	12/08/17 – 01/09/18	EOC 476	32 days (Completed)
c.	01/09/18 – 02/02/18	Cycle 477	24 days (Completed)
d.	02/02/18 – 02/20/18	EOC 477	18 days (Completed)
e.	02/20/18 – 03/16/18	Cycle 478	24 days (Completed)
f.	03/16/18 – 05/01/18	EOC 478	46 days (Completed)
g.	05/01/18 – 05/25/18	Cycle 479	24 days (Completed)
h.	05/25/18 – 06/12/18	EOC 479	18 days (Completed)

The measurement campaign consists of 24-hour real-time collection intervals on the Ag-108 source. The data collected are in the form of differential energy spectra from ~4 keV up to 3.7 MeV. One such differential energy spectrum obtained during this collection period is shown in Figure 1. During a 24-hour period, a total of  $7.4 \times 10^8$  counts are collected with an associated statistical uncertainty of roughly 3.7 parts in  $10^5$ .



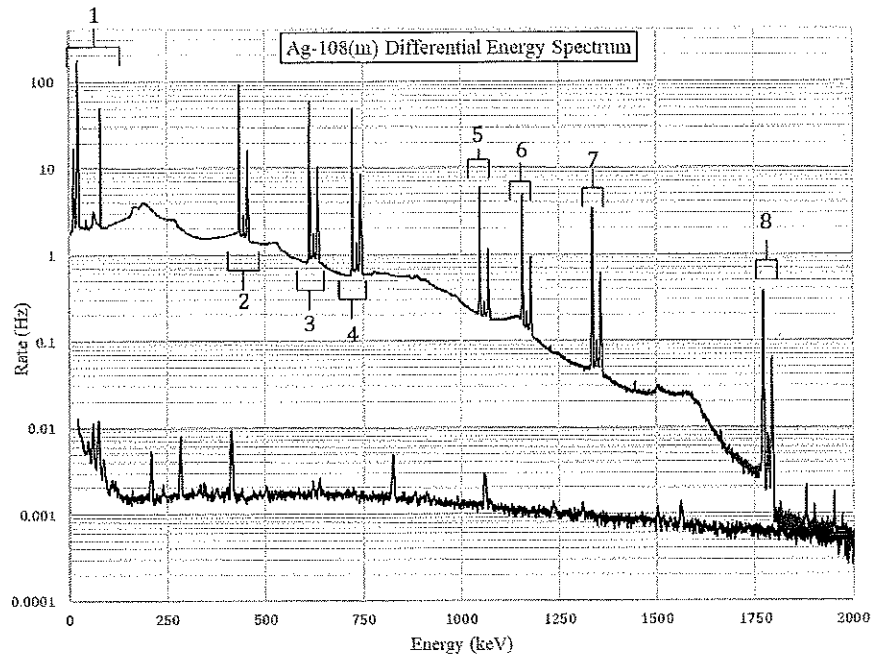


Figure 1: The Ag-108 differential Energy Spectrum is shown in red. The HFIR gamma backgrounds are shown in black.

Table 1: The prominent photon lines in the collected  $^{108}\text{Ag}$  energy spectra.

	Line Energy[ref] (keV)	Line Identification
	21.02	$K\alpha_2$ (Ag x-ray)
	21.177	$K\alpha_1$ (Ag x-ray)
	23.791	$K\beta_3$ (Ag x-ray)
	23.819	$K\beta_1$ (Ag x-ray)
	24.299	$K\beta_2$ (Ag x-ray)
	69.25	$^{108m}\text{Ag}$ IT Ge escape peak
	79.131	$^{108m}\text{Ag} \rightarrow ^{108}\text{Ag}$ IT
$E_1$	433.937	$^{108m}\text{Ag} \rightarrow ^{108}\text{Pd}$ EC
$E_2$	614.276	$^{108m}\text{Ag} \rightarrow ^{108}\text{Pd}$ EC
$E_3$	722.907	$^{108m}\text{Ag} \rightarrow ^{108}\text{Pd}$ EC
	2204.059	$^{214}\text{Bi}$ $\gamma$ -ray
	2614.511	$^{208}\text{Tl}$ $\gamma$ -ray

The key features of the spectrum are dominated by the decay of Ag-108m to Pd-108 via electron capture. This decay mode results in three nuclear de-excitation photons being emitted through a cascade to the ground state of Pd-108. The electron vacancy from the decay additionally results in prominent  $K\alpha$  and  $K\beta$  x-rays (also in coincidence with the de-excitation gamma rays). These lines and their corresponding energies are presented in Table 1.

Additionally, the internal transition (IT) of Ag-108m to its ground state is evidenced in the spectrum by the presence of the 79.131 keV gamma-ray line. The key features of the energy spectrum are broken up into 8 regions as shown in Figure 1. Region 1 refers to the low energy portion of the spectrum and is depicted in Figure 2, along with the higher energy portion of the differential energy spectrum.

A description of these regions is as follows:

- Region 1: The  $K_{\alpha,\beta}$  x-rays from the decay to Pd-108 via electron capture. Also present is the IT de-excitation photon. (Refer to Figure 2)
- Region 2: The E1 gamma-ray from the EC decay and pileup from Region 1 x-rays
- Region 3: The E2 gamma-ray from the EC decay and pileup from Region 1 x-rays
- Region 4: The E3 gamma-ray from the EC decay and pileup from Region 1 x-rays
- Region 5: E1 + E2 geometric summing from cascade + pileup x-rays
- Region 6: E1 + E3 geometric summing from cascade + pileup x-rays
- Region 7: E2 + E3 geometric summing from cascade + pileup x-rays
- Region 8: E1 + E2 + E3 geometric summing from cascade + pileup x-rays

The corresponding energies of these pileup lines can be found in Table 2.

Table 2: Geometric & random pileup lines, and escape peaks in energy spectra.

	Line Energy[ref] (keV)	Line Identification
	69.25	$^{108m}\text{Ag}$ IT Ge escape peak
	424.06	E1 Ge escape peak
	604.40	E2 Ge escape peak
	713.03	E3 Ge escape peak
$E_1 + E_2$	1048.21	Summing from cascade
$E_1 + E_3$	1156.84	Summing from cascade
$E_2 + E_3$	1337.18	Summing from cascade
$\Sigma = E_1 + E_2 + E_3$	1771.12	Summing from cascade
$\Sigma + E_1$	2205.06	Random Summing
$\Sigma + E_2$	2385.40	Random Summing
$\Sigma + E_3$	2494.03	Random Summing

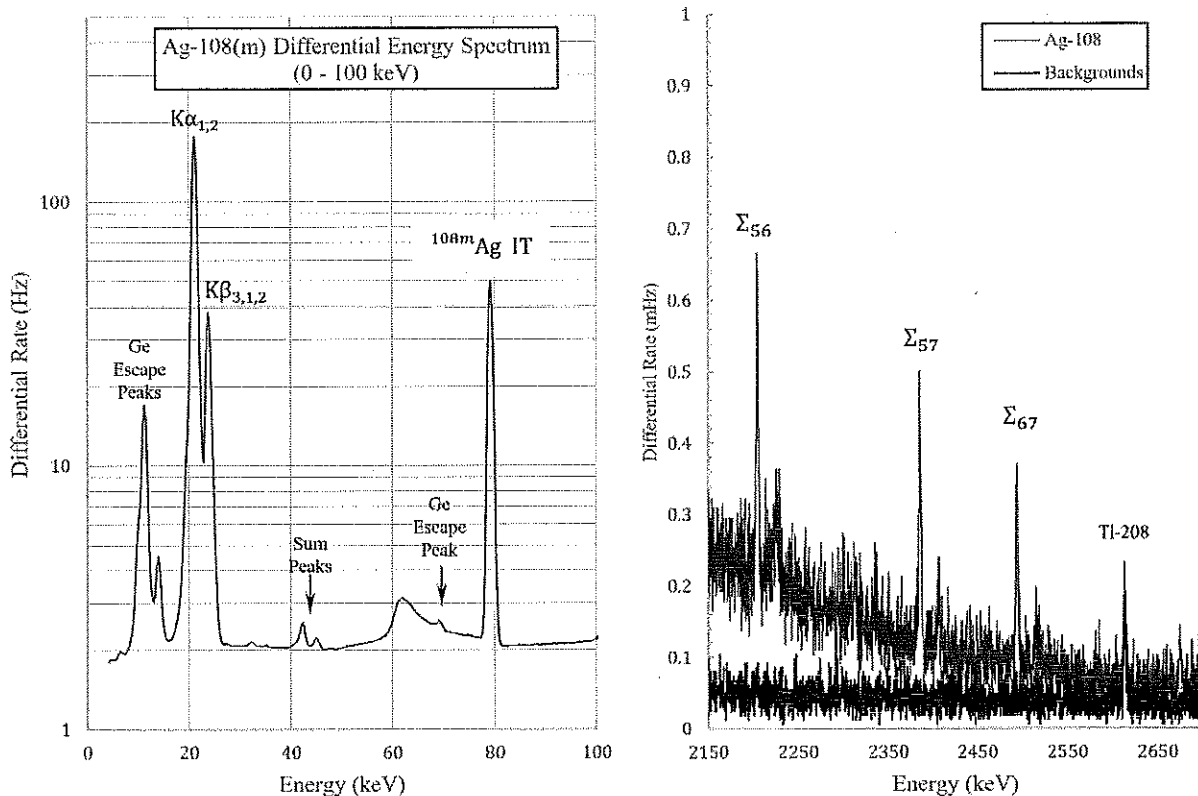


Figure 2: (left) Low energy portion of the Ag-108m differential energy spectrum. (Right) Higher energy portion of the Ag-108m energy spectrum in red, HFIR background spectrum in black.

## II. Analysis Procedures:

The analysis procedures for the current Ag-108m study follow closely those conducted for Cs-137. Each daily spectrum is energy calibrated from the well-defined, known lines (a subset of those given in Tables 1 and 2). These calibrations are used to perform a re-binning followed by a bin-by-bin subtraction of the two archetypal background spectra obtained for Reactor-off and Reactor-on periods. A deconvolution is not performed to the background-subtracted spectra since random summing is effectively constant during the duration of the experiment. Finally, a fixed region of interest (ROI) is integrated to obtain the total daily counts associated with the primary EC and IT photon lines.

### [1] Line Fitting and Energy Calibrations

Peak fitting algorithms have been constructed for each line presented in Tables 1 and 2. A fit is performed to an n-th order polynomial (that approximates the underlying continuum) and a Gaussian distribution (that represents the energy deposited by the incident photon). A  $\chi^2$  minimization is performed using the Levenberg–Marquardt algorithm weighted by Poisson statistics of each bin. The parameters most relevant for calibration purposes are the line centroid, line resolution, and the standard 1s error associated with both. Figure 3 shows the daily centroids of the 433.94 keV photon from the EC decay (shown in black).

The centroids and their corresponding energies (13 data points for each daily spectrum) are used to perform a linear calibration  $E = a + bX$ , as depicted in Figure 4. The daily calibration parameters ( $a$  and  $b$ ) are plotted in Figure 5.

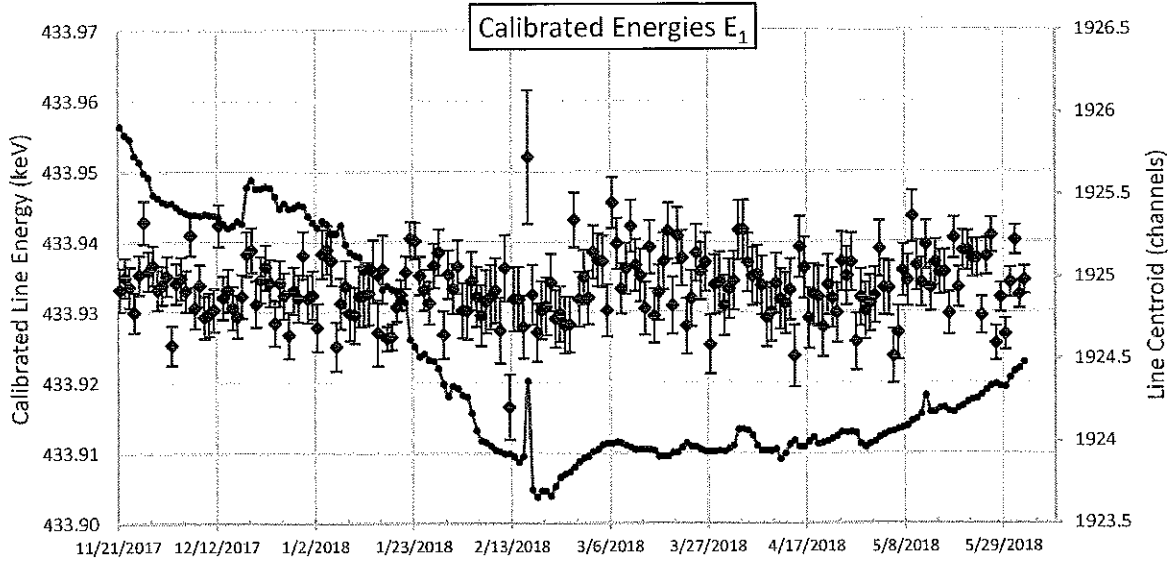
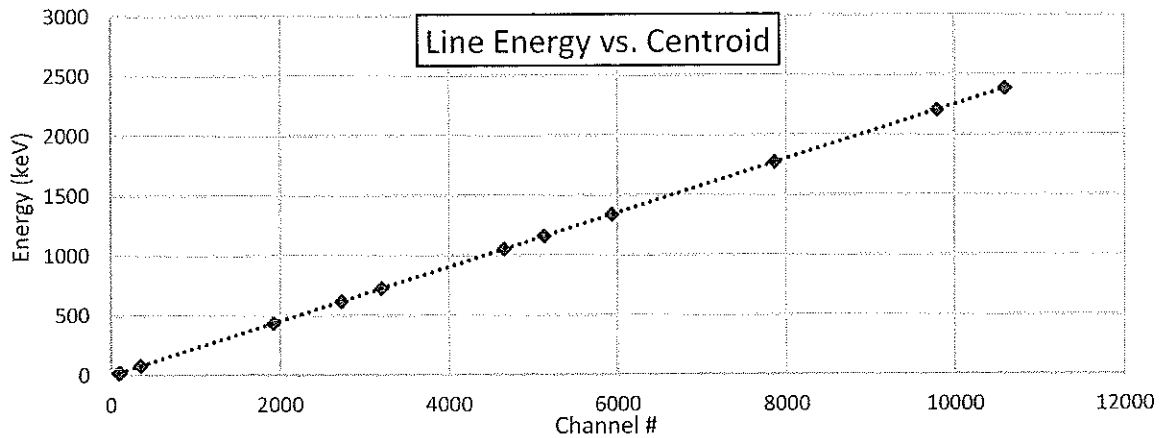


Figure 3 Determined Centroid and calibrated line energy for the 433.94 keV gamma photon.



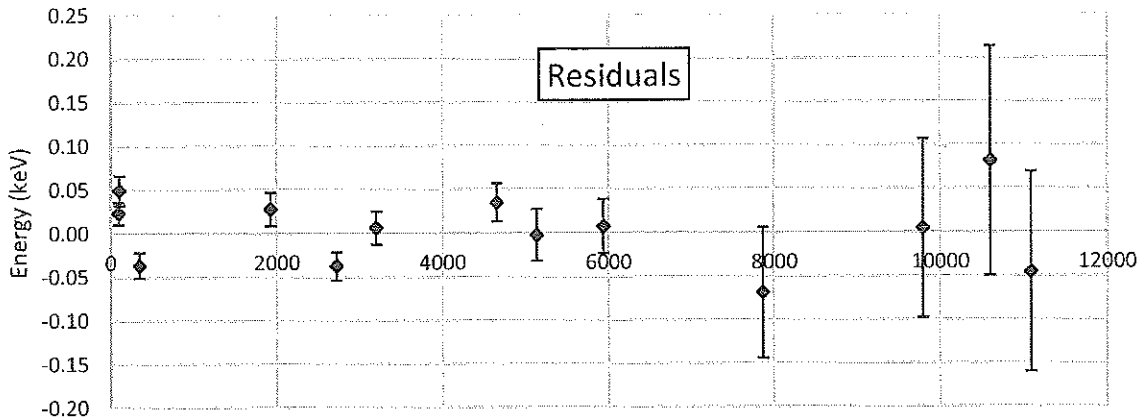


Figure 4: Linear energy calibration for one daily spectrum. The uncertainties on line energy are taken to be the resolution  $\sigma$  divided by the  $\sqrt{N}$  (where  $N$  is the number of counts in the peak).

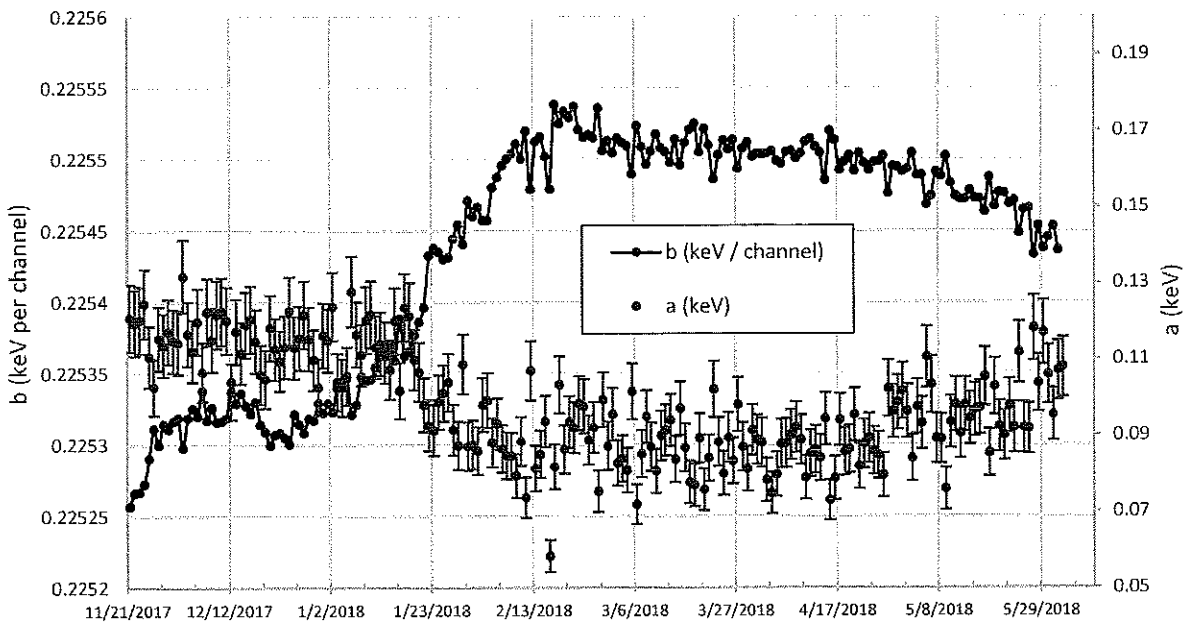


Figure 5: Daily calibration parameters

[Remarks]

1. It is evident that centroid stability is significantly degraded as compared to the performance of the system during the Cs-137 phase. This can be primarily attributed to greater variability in the HPGc crystal temperature, although the reason for the elevated temperature fluctuations is not entirely clear.

2. Nevertheless, energy calibrations effectively remove all drift in line energy over time. For example, see the calibrated line energies for the E1 photopeak (red points in Figure 3).

## [2] Background Subtraction

The daily energy calibrations are used to re-bin the archetypal on/off background spectra. Unlike for the Cs-137 data set, the backgrounds were not scaled by the upper energy portion of the spectra. Unlike the Cs-137 spectra, the Ag-108 spectra has counts that populate all the channels of the differential energy spectrum. This is due to the many coincidences that occur from the E1,E2,E3 photon cascade. Moreover, these photons are coincident with the x-rays produced from the electron capture. The resulting K-shell vacancy produces a series of x-rays as the electrons transition to the ground state.

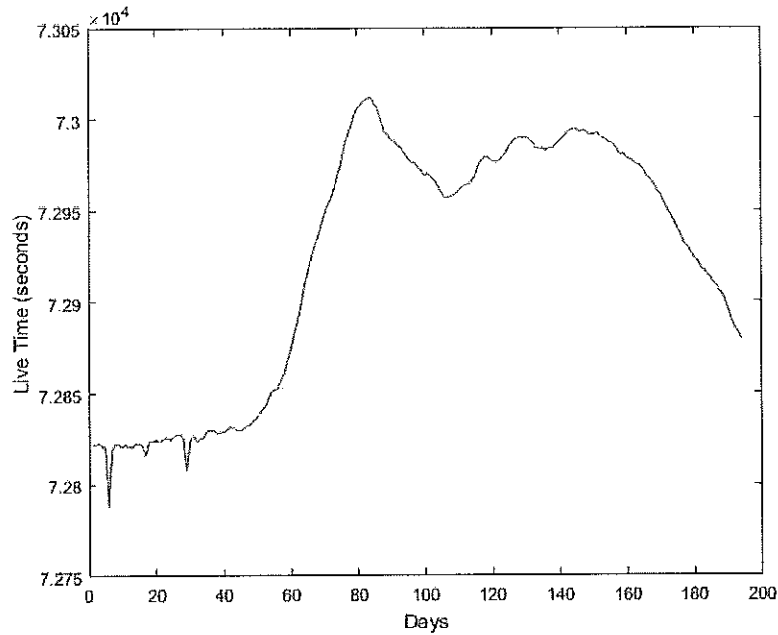
The upper energy portion of the Ag-108 spectrum (as shown in Figure 2) demonstrates how populated this region is with counts originating from the source (as opposed to the backgrounds). As such, it would be inappropriate to use this region for background scaling purposes. Instead, fluctuations in reactor power are used to estimate fluctuations in total background rates.

Figures 8 and 9 show the rebinned background spectrum, and the background-subtracted Ag-108 spectrum (integrated over 194 days). Of note is how effectively the Tl-208 peak is removed.

## [3] Region of Interest (ROI) Integration

The ROIs around each of the primary photon lines are integrated by fixing the energy bounds of the ROI. This is accomplished by using the daily energy calibrations to determine the proper bin edges of the ROI.

Figure 6 shows the ROI count rates vs. time for the E1, E2, and E3 principle gamma-ray photons produced in the electron capture decay mode. It is evident that there are common anomalies in the count rates among all the ROIs. These features appear to arise from an incorrect livetime computation by the DSPEC. As can be seen in the plot below, the livetime exhibits an inverse correlation to the features observed in the ROI count rates. It may be that the digital spectrometer incorrectly assesses the true deadtime of the system for the Ag-108 source. The solid angle subtended by detector is approximately 35%, which means that roughly a third of all counts registered are pile-up events. The larger number of distorted pulses processed by the DSPEC could account for increased error in dead time determinations.



#### [4] Ratio of Decay Modes

One way to eliminate potential uncertainties introduced by the livetime clock (among other things), is to consider the ratio of different portions of the spectrum. As detailed in the accompanied note, the ratio of the EC decay mode to the IT decay mode will manifest any fluctuations in the decay rate:

$$\frac{\Delta r}{r} \equiv \frac{r_{\text{off}} - r_{\text{on}}}{r_{\text{off}}} = \frac{\delta \lambda}{\lambda}$$

Figure 7 shows the daily ratios (top plot) and the aggregated ratios by reactor cycle (bottom plot). Aggregating all the reactor-on data together, and similarly the reactor-off data, the total fractional change is:

$$\frac{\Delta r}{r} = (-0.71 \pm 3.17) \times 10^{-5}$$

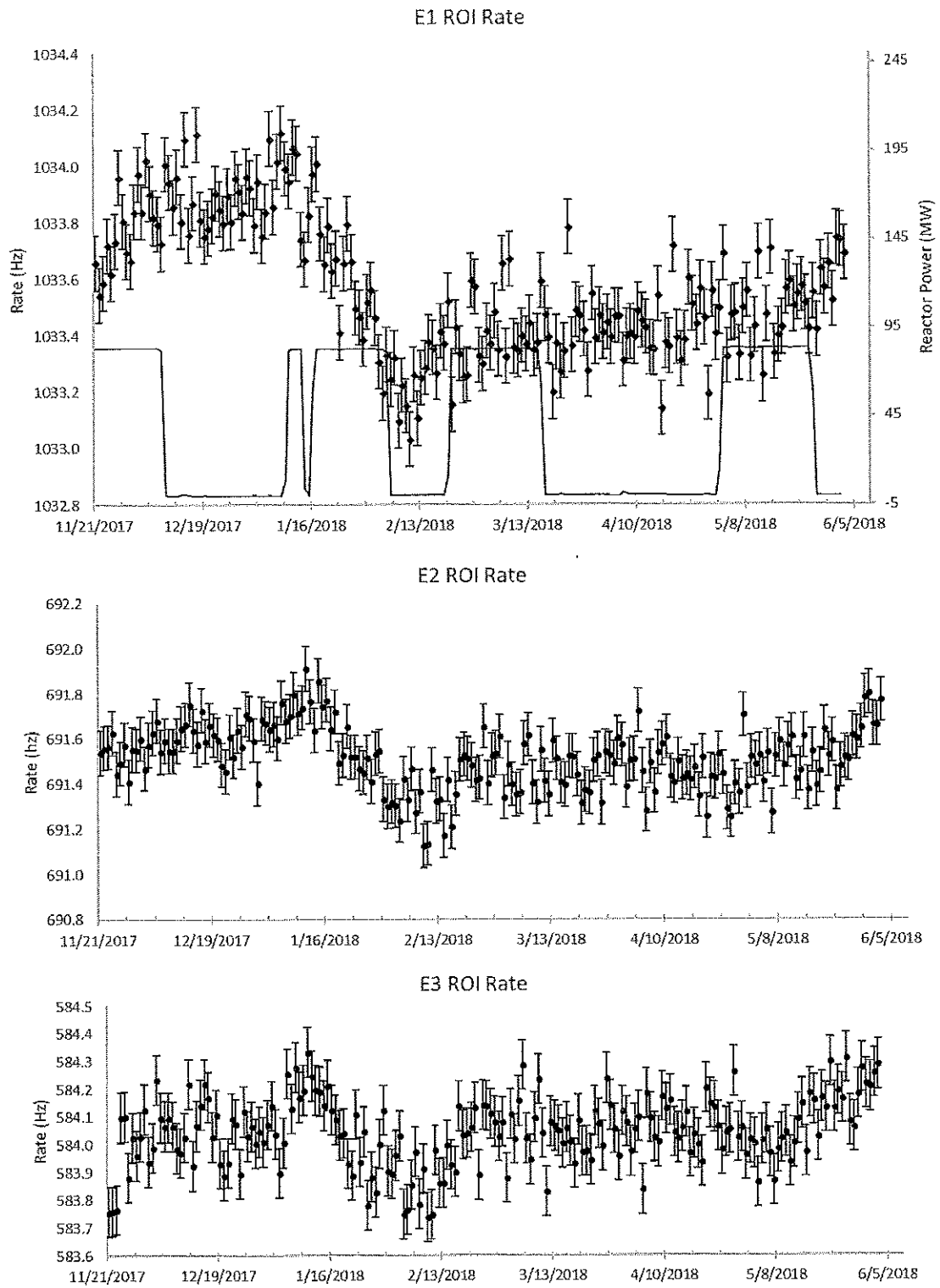


Figure 6: ROI count rates for the three principle gamma photons produced in the electron capture decay mode.



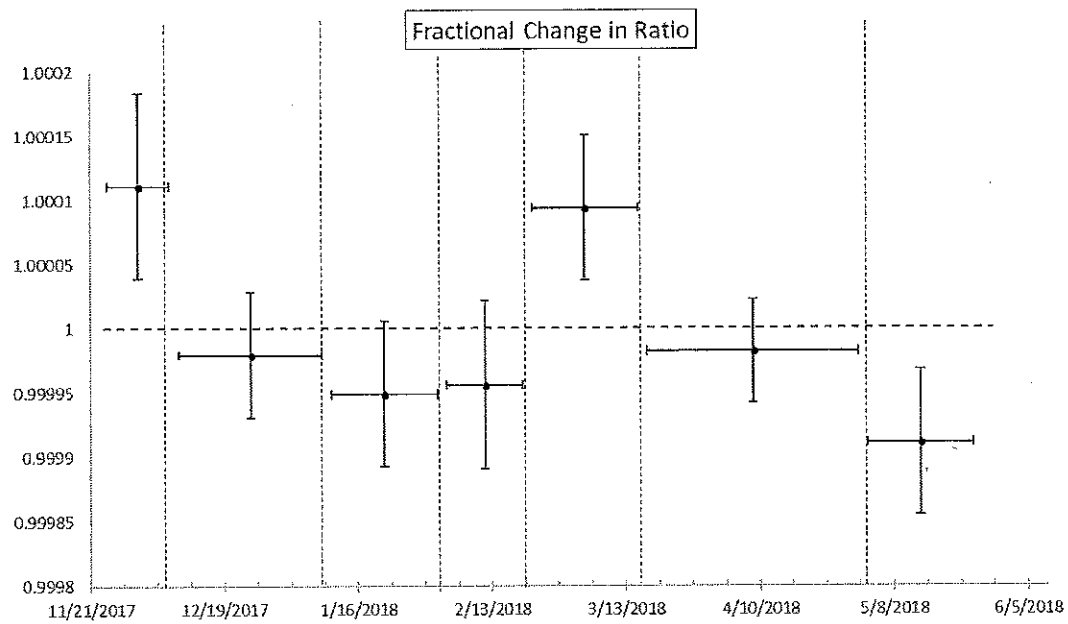
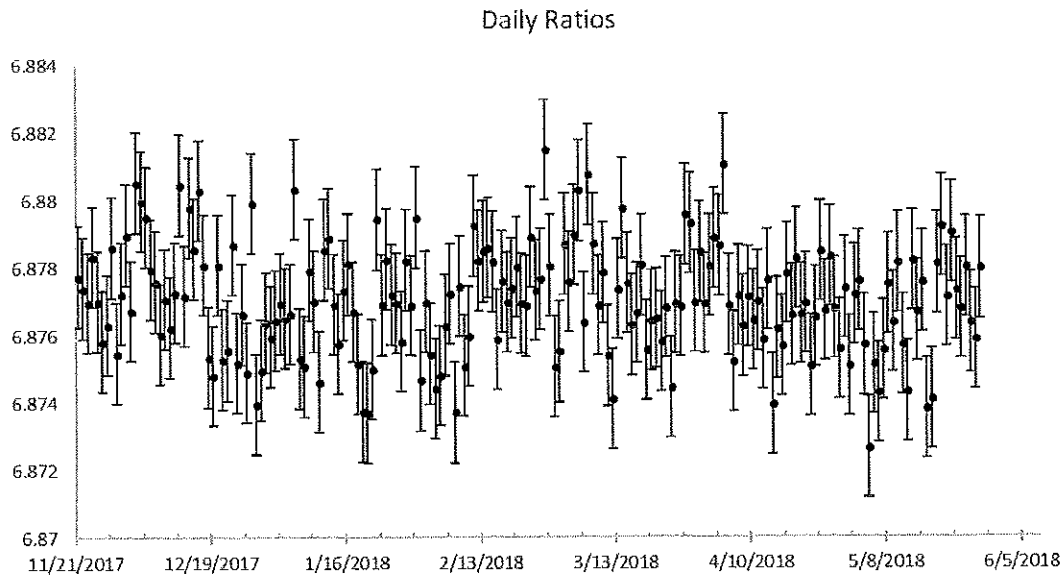
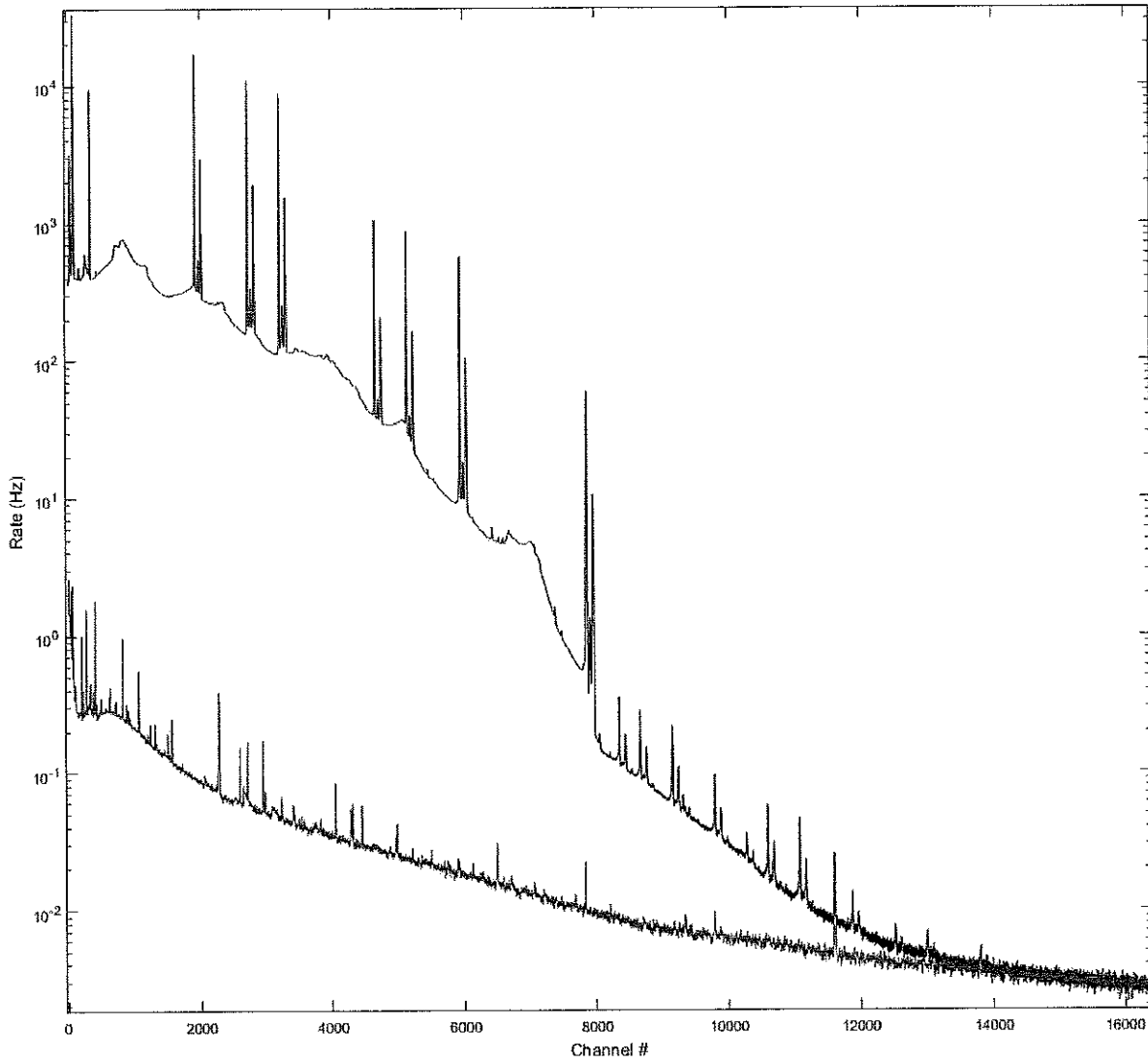


Figure 7: Scatter plot of the ratios of the integrated counts in the EC ROIs over the IT ROI, binned according to reactor status



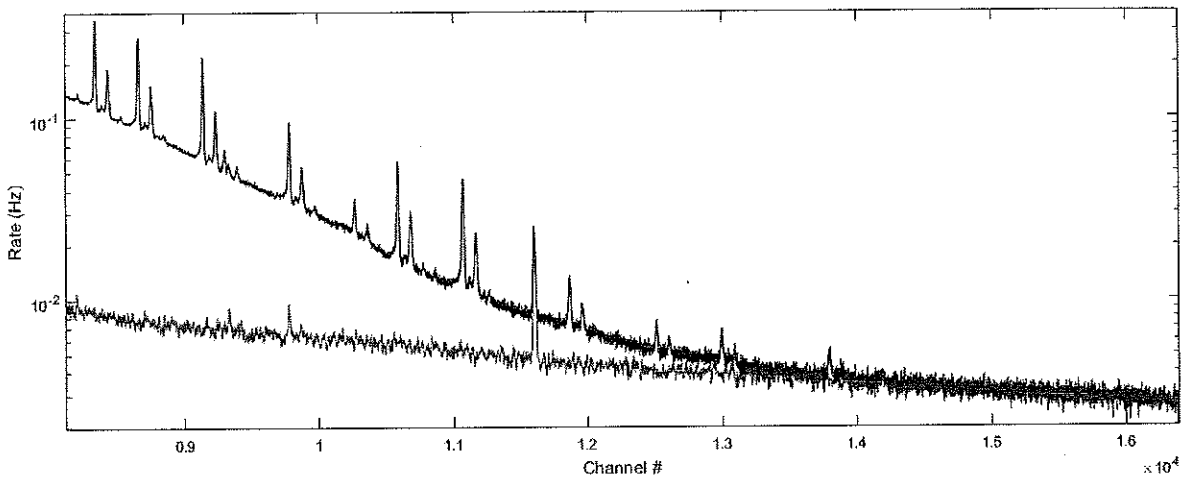


Figure 8: Integrated Ag-108 energy spectrum (black) and re-binned background spectrum (red) for the full 194 days of data collection. The bottom plot shows the prominent Tl-208 peak at channel # 11,600 (approximately)

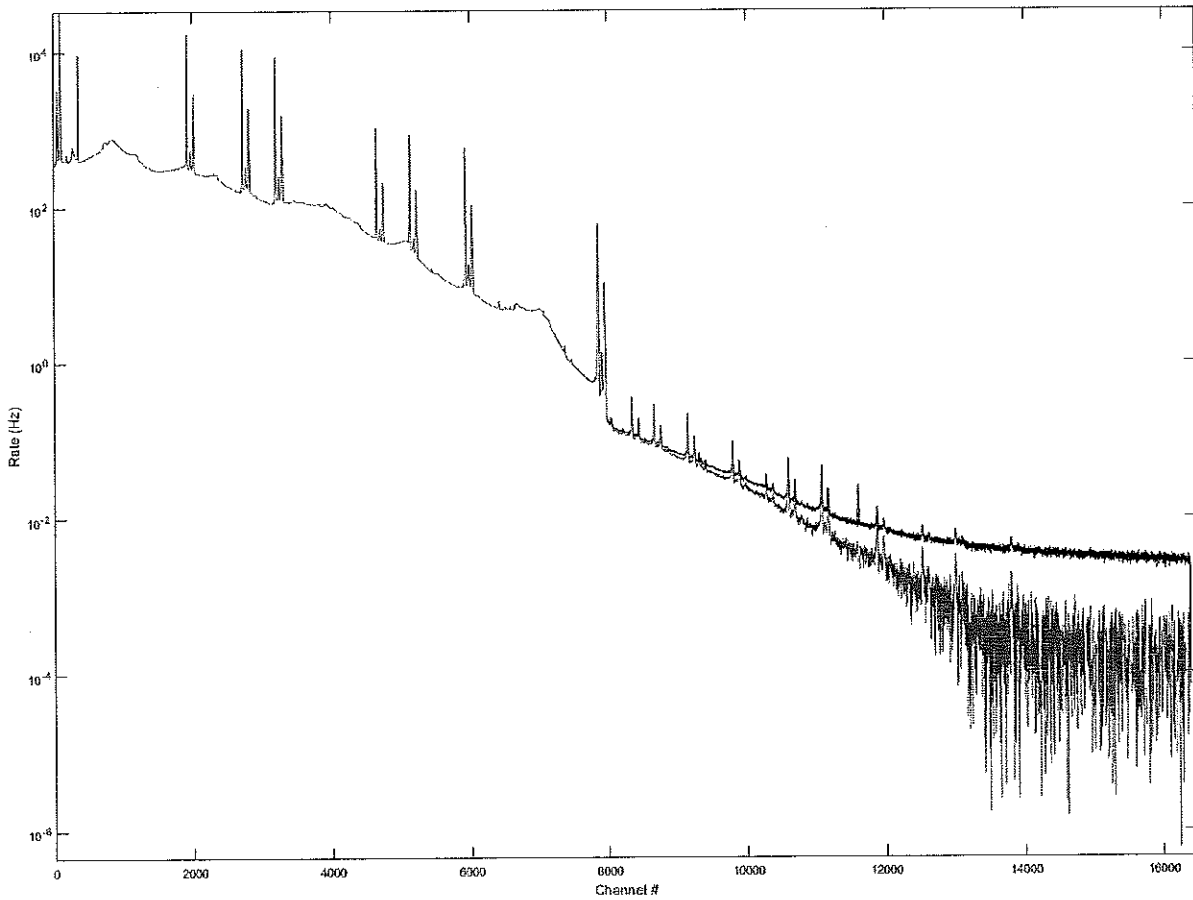


Figure 9: The background subtracted Ag-108 energy spectrum (blue) and subtracting the re-binned backgrounds.

## Summary of Searches for Antineutrino Induced Lifetime Perturbations of Radionuclides

T. Ward (07.02.18)

Search studies were initiated by NE to investigate neutrino induced lifetime perturbations of radionuclides, a possible new neutrino detection method that could be transformational physics. Nanograms of radioactive material could replace many tons of ordinary matter as detector material producing neutrino detection systems orders of magnitude cheaper and smaller for use in monitoring nuclear reactor power levels and for national nuclear security surveillance of nuclear reactors, radioactive sources and nuclear weapons tests. The discovery of a detectable level of lifetime perturbation induced by neutrinos with radioactive targets would greatly reduce the cost and complexity of neutrino detection for use in nuclear security applications. The NE Office funded two experimental groups to try to measure the perturbations, a Sodium Iodide (NaI) gamma-ray detection system and a High Purity Germanium (HPGe) gamma-ray system.

**Sodium Iodide (NaI) Gamma-Ray Detection.** Fischbach and Barnes measured the rate effects at HFIR using NaI detectors. They reported null measurements with 2-sigma 90% upper confidence limits for the following radioisotopes:

Mn-54 (312d)	$< 1.19 \times 10^{-4}$
Na-22 (2.602 yr.)	$< 9.54 \times 10^{-5}$
Co-60 (5.271 yr.)	$< 4.83 \times 10^{-5}$

Overall the NaI measurement, analysis and results are quite exceptional. These low systematic error measurements using NaI detectors are among the most precise gamma decay measurements made to date. The limits set are a factor of 10 lower than many previous reported measurements.

**High Purity Germanium (HPGe) Gamma-Ray Detection.** Koltick, Nistor, Heim and Liu measured the rate effects using HPGe detectors at HFIR. The 2-sigma 90% confidence level upper limit for the three radioisotopes studied were determined to be

Mn-54 (312d)	$< 3.80 \times 10^{-5}$
Cs-137 (30.1 yr.)	$< 3.47 \times 10^{-5}$
Ag-108m (434 yr.)	$< 5.67 \times 10^{-5}$

The HPGe measurements using new gamma-ray spectrum analysis methodology is state-of-art in terms of reducing total systematic errors to an unprecedented  $\pm 1.7 \times 10^{-5}$  level, an uncertainty level 10-100 times lower than many previous reported measurements of this type.

**Conclusion.** The current detection limits listed above preclude using gamma-ray detection methods to monitor neutrino fluxes. If the detection limit for neutrino perturbation of radioactive decay is of the order of  $1 \times 10^{-6}$  then it may be possible to use beta-current (nuclear battery) detectors to make the measurements.

**Report of the  
Independent Scientific Review Panel  
on the Search for  
Electron Antineutrino Induced Perturbation  
in Beta Decay**

Compiled and Edited by Dr. Thomas Ward  
Science and Technical Advisor to Office of Nuclear Energy



**TECHSOURCE<sup>®</sup>**  
A Science & Engineering Consultancy

20251 Century Boulevard  
Germantown, Maryland 20874

**29 June 2018**

**Report of the  
Independent Scientific Review Panel  
on the Search for  
Electron Antineutrino Induced Perturbation  
in Beta Decay**

Compiled and Edited by Dr. Thomas Ward  
Science and Technical Advisor to Office of Nuclear Energy



**TECHSOURCE<sup>®</sup>**  
A Science & Engineering Consultancy

20251 Century Boulevard  
Germantown, Maryland 20874

**29 June 2018**

## TABLE OF CONTENTS

Acronyms .....	3
<b>1 Executive Summary .....</b>	<b>4</b>
<b>2 Introduction .....</b>	<b>4</b>
2.1 Chronological Review and Assessment .....	5
2.1.1 Phase I HPGe Measurement .....	6
2.1.2 NaI Measurements and Results .....	7
2.1.3 Phase II HPGe Measurements .....	8
<b>3 Conclusion .....</b>	<b>20</b>
<b>4 References .....</b>	<b>20</b>

## LIST OF FIGURES

Figure 1. Derivative of Photopeak Rate Mn-54 .....	8
Figure 2. Variance of Three Regions Reactor ON/OFF for Mn-54 Source .....	9
Figure 3. Cs-137 Residual Photopeak Counts Best-fit Exponential Decay Curve with the Error Bars Indicating the Statistical Uncertainty on the Daily Count Rates.....	9
Figure 4. Binned Residual Cs-137 Photopeak Counts for the Region of Interest from 640 keV to 680 keV for Reactor ON and Reactor OFF .....	10
Figure 5. Antineutrino-radioactive Nucleus Scattering Inducing a Neutrino Schwinger Anomalous Magnetic Moment in First Order .....	13
Figure 6. An EM Antineutrino Interaction with a Weak Interaction Z-vertex in which the Spin-flip Changes Chirality of the Antineutrino and Flips the Spin of the K-electron in the Process .....	14
Figure 7. The Ag-108 Differential Energy Spectrum is Shown in Red while the HFIR Gamma Backgrounds are Shown in Black .....	16
Figure 8. Illustrates the (left) Low Energy Portion of the Ag-108m Differential Energy Spectrum and the (Right) Higher Energy Portion of the Ag-108m Energy Spectrum in red, HFIR Background Spectrum in Black.....	18
Figure 9. Fractional Change in the IT to EC Photopeak Modes of Ag-108m.....	19

## LIST OF TABLES

Table 1. Model Predictions for Various Radioisotopes at HFIR .....	11
Table 2. The Prominent Photon Lines in the Collected <sup>108</sup> Ag Energy Spectra.....	16
Table 3. Geometric and Random Pileup Lines, and Escape Peaks in Energy Spectra .....	17

## ACRONYMS

Ag-108m	Silver-108m
Co-60	Cobalt-60
Cs-137	Cesium-137
Ge	Germanium
HFIR	High Flux Isotope Reactor
HPGe	High Purity Germanium
Mn-54	Manganese-54
Na-22	Sodium-22
NaI	Sodium Iodide
NE	Office of Nuclear Energy
ORNL	Oak Ridge National Laboratory
SME	Subject Matter Expert
USDOE	U.S. Department of Energy



## **1 Executive Summary**

The panel is very favorably impressed with the high degree of care and ingenuity that has gone into this work. The experiment and the analysis were completed using a very careful and well-thought-out method. The measurement of small effects is in general difficult. So is the presentation of the results of such measurements. The difficulties are magnified if the existence of an effect would challenge what has been conventional wisdom in the field. In particle physics and gravitational-wave astrophysics there is now a convention of requiring 5-sigma for a new particle or a new effect. The statistics of this experiment are presumably under control however the systematic errors in measurements of this type are not necessarily negligible and judgment is required, there is no simple recipe.

The analysis of reactor-on and reactor-off spectra and accompanying de-convolutions are of critical importance. There are many factors influencing Germanium (Ge) detector counting and it appears many were considered by the authors, however the key to the result of this analysis is evaluation of all possible systematic errors. The systematic error determined in the Manganese (Mn-54) decay measurement of  $\pm 1.5 \times 10^{-5}$  is extraordinary by current High Purity Germanium (HPGe) forensics standards, yet the compelling Cesium-137 (Cs-137) result of  $(3.4 \pm 1.7) \times 10^{-5}$  must be considered inconclusive. The small change could easily be accounted for by unknown systematic errors associated with background subtraction or reactor operation. A definitive 5-sigma result is required, perhaps the Silver (Ag-108m) study that is predicted to produce a >5-sigma result will provide the answer, after all “extraordinary claims require extraordinary evidence or proof”.

*Preliminary results of the Ag-108m study determined an upper limit at  $(2.5 \pm 1.0) \times 10^{-5}$ , this result combined with those of Cs-137 and Mn-54 place a limit for any effect much below all previously reported studies. Although one cannot rule out an effect at lower perturbation levels, the current limit precludes a practical application of such an effect if it exists.*

## **2 Introduction**

In March 2014, a Sodium Iodide (NaI) gamma-ray study of antineutrino induced perturbations in the beta decay of Mn-54 was initiated at the High Flux Isotope Reactor (HFIR) at Oak Ridge National Laboratory (ORNL). The study was conducted by Professors Ephraim Fischbach and Virgil Barnes of Purdue University, Dr. Thomas Grunfeld and graduate research students Jordon Heim and Jonathan Nistor. The Office of Nuclear Energy (NE), U.S. Department of Energy (USDOE) was presented an unsolicited funding proposal in July 2014 for continuance of the work at HFIR. Dr. Thomas Ward reviewed the proposal for NE and though skeptical of the extraordinary claims, he approved it for initial funding provided an independent scientific review panel could be established to follow the work in progress. Initial funding for continuance of the NaI work and the review panel was acquired in August 2014.

Extraordinary claims from several dozen studies reported that solar neutrinos or electron antineutrinos from reactors interacting with radioactive targets could cause beta decay lifetime perturbations of 0.1%. The possibility of such an effect at that level opens a variety of forensic applications to monitor antineutrino flux from a variety of sources of interest in nuclear nonproliferation.

An independent review panel was assembled in September 2014 and consisted of five members:

- 1) Professor Guy Emery, Bowdoin College, subject matter expert (SME) in atomic and nuclear physics,
- 2) Professor John Rasmussen, UC Berkeley and LBL, SME nuclear structure and decay,
- 3) Professor Hugon Karwowski, University North Carolina and TUNL, SME experimental neutrino physics,
- 4) Professor David Koltick, Purdue University, SME nuclear detection methods, and
- 5) Dr. Thomas Ward, TechSource, Inc., the coordinator and facilitator for the panel.

The charge to the SME panel was to assess and review the scientific progress of the project, to make recommendations to further enhance the scientific and experimental quality of the study and to point out possible areas of systematic error that needed to be addressed to produce a precision measurement. The initial response of the panel to previous reported claims was skepticism since “extraordinary claims require extraordinary evidence or proof” and credible evidence was lacking in most previous reports. However, the possibility of detecting neutrino transmutation in beta decay is of fundamental theoretical and experimental importance as well as possible applications as a monitor for national nuclear security purposes. A determination of an upper limit can provide a meaningful result in the search for lifetime perturbations in weak interactions and as a test of beta decay in the standard model.

## **2.1 Chronological Review and Assessment**

Over the course of six months, from October 2014 to April 2015, the panel reviewed the existing published reports and the NaI experimental set-up and analysis procedures of the HFIR Mn-54, Sodium-22 (Na-22) and Cobalt-60 (Co-60) Study. There were immediate concerns that the NaI measurements lacked energy resolution in addition to possible large systematic uncertainties in natural and reactor background subtraction, temperature and pressure variation effects on energy calibration stability, pile-up, dead time correction and photopeak analysis. Source strength of several microcurie were required to produce high count rates ( $>10$  kHz) and dead-time ( $>15\%$ ) to reduce the statistical uncertainty to  $<1 \times 10^{-5}$ . The NaI experiment had a goal to establish a low systematic uncertainty of a  $<2 \times 10^{-4}$  allowing for a 5-sigma result with a 0.1% signal, a value reported in many previous experiments. In March 2015, it was the recommendation of the panel

to pursue the possibility of using high-purity Germanium (HPGe) detectors to make measurements because of added benefits of reduced systematic errors:

- 1) higher energy resolution,
- 2) precise energy calibrations,
- 3) dead-time correction,
- 4) exacting measurement of sum peak and accidental coincidence pile-up, and
- 5) background subtraction

all of which were thought to be determined with higher precision than with NaI detectors. It was estimated that systematic uncertainties might be reduced to the level of  $(1-10)\times 10^{-5}$ . The NaI detector group wanted to continue their NaI measurements at HFIR which would take another year to complete both measurements and analysis. Additionally, the Fischbach group did not have the HPGe equipment to field an additional experiment. The NaI experiment was funded through June 2016.

#### **Phase I HPGe Measurement**

Over the spring and summer of 2015, Dr. Thomas Ward met with the review panel members in Indiana, Maine, North Carolina and California and they finalized a plan to use HPGe detectors to make precision measurements with sources Mn-54, Co-60 and Cs-137 at HFIR. In April 2015, the detector SME, Professor Koltick, was asked if he could field the necessary HPGe detector systems needed for such a study from his equipment pool. His answer was yes but with the caveat that new cooling systems and electronic data acquisition equipment would be needed in addition to construction of a detector bay to house two HPGe detectors, one for source measurement and the other for background measurement. A proposal and budget was submitted to NE in April 2015 and approved for immediate start in May 2015. Eventually four Ph.D. graduate students, Jonathan Nistor, Jordan Heim, Haoyu Wang and Jay Liu were assigned to the project. Mr. Nistor and Mr. Heim continued to work with the NaI group during its data collection and analysis stages while they designed, built and commissioned the HPGe detector shielding bays for operation at HFIR. Mr. Wang was assigned the electronics and data acquisition system and Mr. Liu the data analysis software. It was decided that measurements would be made with Mn-54 and Cs-137 sources only. The first phase HPGe measurements with the Mn-54 source at HFIR began August 2015 and concluded mid-January 2016. A data total of 28 days reactor ON and 103 days reactor OFF were accumulated in preliminary measurements [Koltick and Liu, 2016a]. These data were simply analyzed for energy line shifts, energy resolution and decay curve analysis for the 835 keV line, a procedure commonly used in some forensic studies. A simple Gaussian shape fit to the photopeak yielded an average energy resolution of  $\delta E/E = 8.9 \times 10^{-4}$  and a preliminary upper limit to the change in the decay constant using only the deadtime correction of  $\Delta\lambda/\lambda < 3 \times 10^{-3}$ . *The panel noted that this value was obtained without corrections due to background or pileup indicating that precision measurements must account for small but finite time-dependent photopeak energy shifts, photopeak shape analysis, background subtraction and pileup corrections.* **The Phase I final**

**time domain analysis of the Mn-54 decay curve** with 72 days reactor ON data yielded a limit in the change in the decay constant of  $\Delta\lambda/\lambda < 1.4 \times 10^{-4}$ , indicating the difficulty of making lifetime change measurements with only photopeak decay curve analysis and decay curve fitting. This result was in good agreement with the NaI result detailed below. *The panel recommended precision spectral data analysis for Phase II to account for Compton, reactor and room backgrounds, deadtime correction, accidental and sum coincidence pileup and photopeak shape to reduce systematic errors another order of magnitude.*

### **NaI Measurements and Results**

The final report of the NaI measurements was submitted June 2016 [Barnes, et. al., 2016]. In the Phase I study three sources were studied: Mn-54, Co-60 and Eu-152. The Phase I study was conducted at HFIR between March 15 to March 30, 2014 with 8 days of reactor ON and 8 days reactor OFF. The Phase I results were used to tune-up the experiment and work out operational problems. The reported results were obtained from the Phase II study which took place at HFIR from August 2014 to March 2015 (218 days) and used sources of Na-24, Mn-54 and Co-60. The ORTEC detectors and data acquisition system came with the MAESTRO software program that provides for best fit for the photopeak centroid, full width at half max, full width a fifth max of the peak. Corrections for rate dependent distortions due to deadtime and pileup must be considered. The MAESTRO/digiBASE system corrects for the dead time but cannot account for pileup effects. The pileup correction was accounted for by a correction factor that brought the photopeak decay curve into agreement with the reported half-life. Time domain analysis that included a lifetime factor ( $\epsilon$ ) due to possible antineutrino interactions with the source provided limits set by the systematic uncertainty obtained from the difference between reactor-ON and reactor-OFF. In this manner they reported null measurements with 3-sigma 95% upper confidence limits:

Na-22	$< 1.43 \times 10^{-4}$
Mn-54	$< 1.79 \times 10^{-4}$
Co-60 of	$< 7.24 \times 10^{-5}$ .

Overall the NaI measurement, analysis and results are quite exceptional. At face value these very low systematic error measurements using NaI detectors are among the most precise decay curve lifetime measurements made to date using NaI detectors. However, as noted, the time domain analysis using the photopeak difference procedure did not consider a full spectral analysis of the backgrounds (Compton, pile-up, room and reactor backgrounds) only the photopeak region of interest (ROI). The analysis relied upon commercial deadtime correction software and the introduction of an algorithm to account for rate dependent systematic error effects such as the pileup known to exist within the spectra. The rate dependent effects need to be directly determined from spectral analysis to reduce the systematic errors, another order of magnitude which could prove very difficult with the poor energy resolution of NaI detectors.

## Phase II HPGe Measurements

Two aspects of the Phase II study were a) Spectral photopeak analysis of Mn-54 decay rate variation with reactor ON and reactor OFF, and b) Spectral photopeak analysis of Cs-137 decay rate variation with reactor ON and reactor OFF.

**Mn-54 Spectral Analysis.** Preliminary analysis results from the August 2015 to January 2016 run was reported in November 2016 [Koltick and Liu, 2016a]. Non-linearity in the energy response of  $6 \times 10^{-4}$  over the full 2650 keV spectrum would present problems in background and pile-up corrections for the photopeak. A non-linear calibration correction was developed and used to analyze the photopeak. At the level of precision demanded by this experiment the photopeak's cannot be treated as simple Gaussian shapes. The true shape of the photopeak contains a plethora of complex physics and no model exists that can account or it. Analysis of the 835 keV Mn-54 photopeak can be made, provided the environment and background conditions are stable, using a simple Gaussian shape that is proportional to the true rate. Therefore, differences in reactor ON and reactor OFF can be used to observe any effects of antineutrino interactions on the decay.

Figure 1 shows the derivative of the photopeak rate showing the region of most interest.

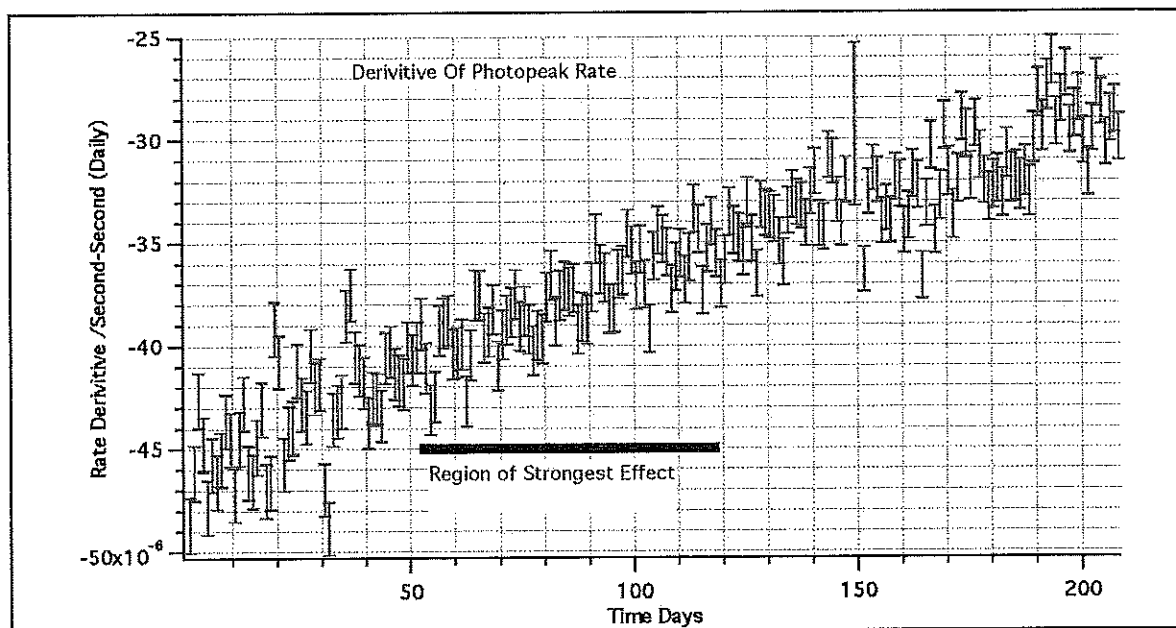
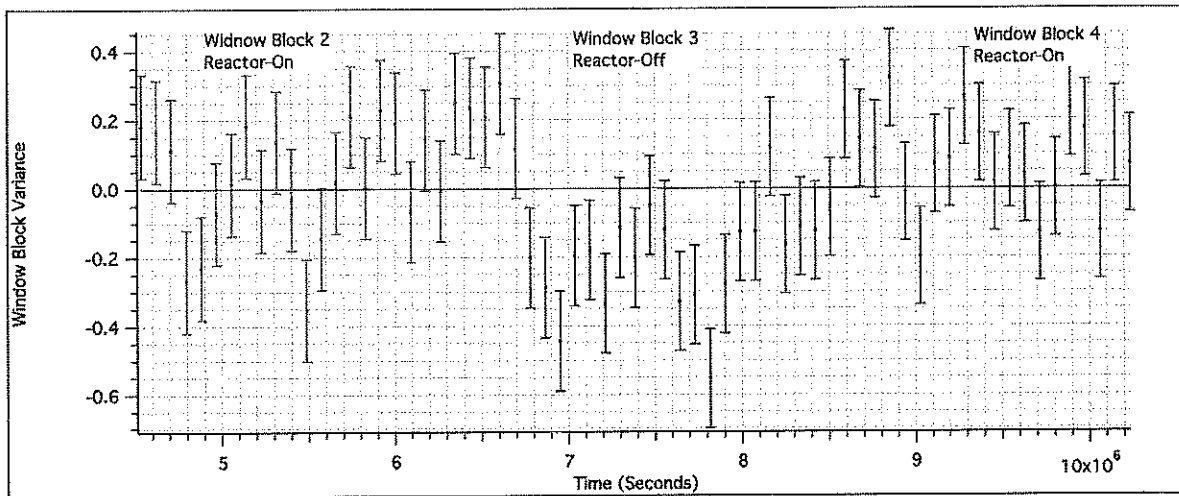


Figure 1. Derivative of Photopeak Rate Mn-54

Figure 2 shows variance in the three windows, Block 2 reactor ON, Block 3 reactor OFF and Block 4 reactor ON. The rate change for the reactor OFF is negative and could perhaps indicate that there may be reactor background or pile-up in the reactor ON spectra that was unaccounted for in the procedure.



**Figure 2. Variance of Three Regions Reactor ON/OFF for Mn-54 Source**

The residual rate difference between reactor OFF-ON is  $\Delta R/R = -0.015 \pm 0.030 \text{ Hz}$  which yields a systematic error or limit to the decay rate change of  $\Delta\lambda/\lambda < 2.0 \times 10^{-5}$  at the 67% confidence level. This systematic error is the limit at which these rate change measurements can be made using HPGe gamma-ray analysis. It is important to note that the sign of the rate change between reactor OFF-ON is wrong since it implies that the lifetime is sped up.

*Cs-137 Spectral Analysis.* The detail of the Cs-137 study were reported in the Project Overview, July 2017 [Nistor and Heim, 2017]. The study was conducted at HFIR from 11 March 2016 to 01 July 2016 and from 13 November 2016 to 26 May 2017. In total over 264 days of data were collected for 87 days reactor ON and 167 days reactor OFF. During a 24-hour period a total of  $6.2 \times 10^8$  counts are collected with a statistical uncertainty of about  $4 \times 10^{-5}$ . Over the course of 87 days a total of  $5.39 \times 10^{10}$  counts are accumulated in the reactor ON spectra.

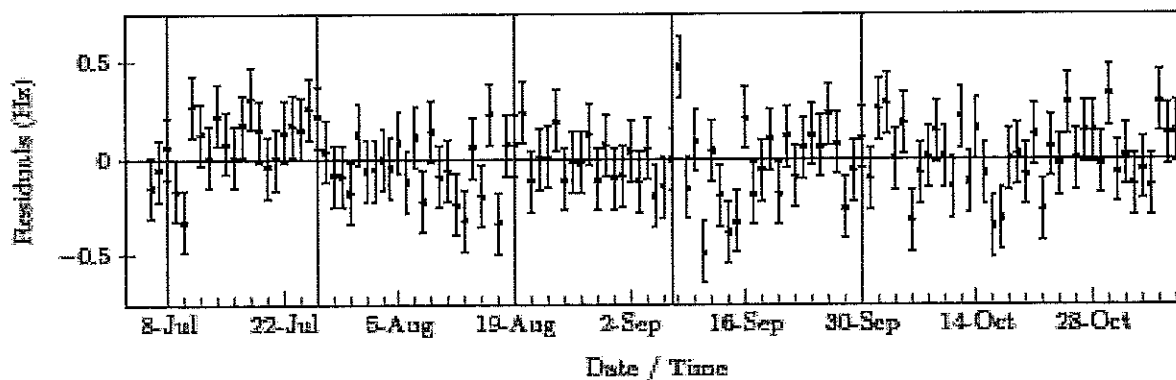


**Figure 3. Cs-137 Residual Photopeak Counts Best-fit Exponential Decay Curve with the Error Bars Indicating the Statistical Uncertainty on the Daily Count Rates**

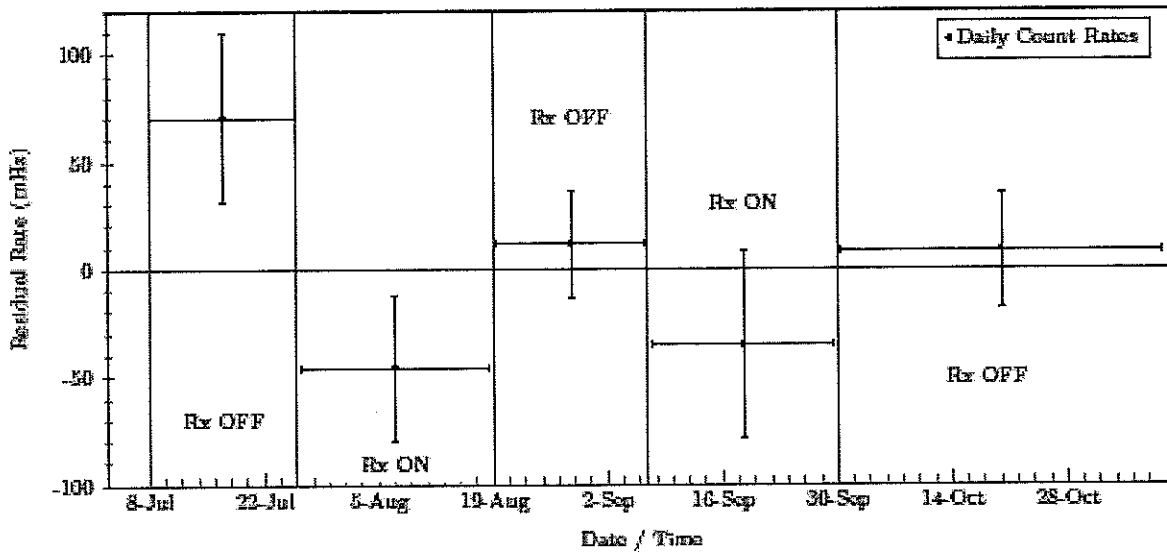
To investigate the effects from a possible novel interaction of reactor antineutrinos with the Cs-137 radioactive source, we write the interaction rate as:

$$\delta R = \phi_{\bar{\nu}} \sigma_{\bar{\nu}} N. \quad (1)$$

where  $\sigma_{\bar{\nu}}$  is the effective cross-section,  $\phi_{\bar{\nu}}$  the reactor antineutrino flux and N the number of radioactive target nuclei in the source. Rewriting Eq. 1, the fractional change in count rate from reactor OFF-ON is given by

$$\frac{\delta R}{R} = \frac{\phi_{\bar{\nu}} \sigma_{\bar{\nu}}}{\lambda} \quad (2)$$

The data from Figure 3 can be binned and a comparison of the residuals from reactor ON to reactor OFF can be made as shown in Figure 4.



Note: The uncertainty on each datum is taken as the residual error of each daily run added in quadrature.

**Figure 4. Binned Residual Cs-137 Photopeak Counts for the Region of Interest from 640 keV to 680 keV for Reactor ON and Reactor OFF**

The difference in reactor OFF-ON was found to be

$$\delta R = Off - On = 0.0638 \pm 0.0331 Hz \quad (3)$$

which yields from Eq. 1 a cross-section of  $\sigma_{\bar{\nu}} \approx 9 \times 10^{-27} cm^2$  and a rate change of

$$\frac{\delta R}{R} = (3.37 \pm 1.74) \times 10^{-5}. \quad (4)$$

This value is to be compared with the model developed in this study [Ward 2015-18],

$$\frac{\delta R}{R} = \frac{\delta \lambda}{\lambda} = 2.5 \times 10^{-5}. \quad (5)$$

The positive-definite result, Eq. 4, is a 2-sigma (95% CL) result and is to be considered compelling but inconclusive since unknown and unaccounted for systematic errors of the order of  $> 1 \times 10^{-5}$  are possible as evidenced in the Mn-54 study. What is required is a radioactive source test that results in  $> 5$ -sigma result. According to the model, Ag-108m (434 year) fits the bill as tabulated in Table 1. Current Phase III experiments using Ag-108m source are underway at HFIR and the final results should become available in June 2018.

**Table 1. Model Predictions for Various Radioisotopes at HFIR**

Radioisotope	$\phi_{\max} (\bar{\nu}_e cm^{-2} sec^{-1})$	$\delta \lambda (1 \times 10^{-5})$
Mn-54 (312.12d)	$2.36 \times 10^{15}$	-0.07
Cs-137 (30.1 yr.)	$6.71 \times 10^{13}$	-2.5
Ag-108m (434 yr.)	$4.65 \times 10^{12}$	-29.7
Bi-208 (368,000 yr.)	$5.32 \times 10^9$	-58.1

*Physics Model of Anomalous Neutrino Scattering Interactions.* Neutrinos are produced in weak interactions and to first order interact only weakly and gravitationally. A new theoretical approach to the detection of neutrinos involve **EM neutrino scattering** and sterile neutrino production from **radioactive targets**, targets that already possess a weak interaction vertex by being radioactive. Therefore, **neutrino absorption is not considered**, only scattering processes with a radioactive nucleus, a neutrino scattering process that is EM in nature.



In this new paradigm, sterile neutrino production does not require mass mixing to produce a fourth-generation neutrino, rather a simple process of EM chiral spin-flip scattering or oscillation between active and sterile Dirac neutrinos. The sterile neutrino is forbidden to interact weakly due to chiral coupling and lack of weak charge. Recent experimental evidence of neutrino detection has been reported using radioactive targets as opposed to non-radioactive “ordinary” target material, i.e., water and liquid scintillator detectors. *The interaction of a neutrino with ordinary matter requires the propagation of a weak interaction vertex and a cross-section of the order of  $1 \times 10^{-44} \text{ cm}^2$ .*

In an EM scattering process, the Dirac neutrino (anti-neutrino) performs a chiral oscillation ( $\nu_L \rightarrow \nu_R, \bar{\nu}_R \rightarrow \bar{\nu}_L$ ) from active to sterile type by scattering with the orbital electron of the weak interaction vertex of a radioactive nucleus undergoing weak decay. The EM spin-spin scattering of the active neutrino ( $\nu_L, \bar{\nu}_R$ ) with the atomic electrons of the weak interaction vertex follows from the **Dirac neutrino having an anomalous magnetic moment** by possessing both mass and spin. The resulting magnetic dipole-dipole interaction flips the spin of both the incoming neutrino (chiral oscillation) and the orbital electron taking part at a weak interaction vertex. The EM scattering cross-section is calculated to be approximately 6 millibarns ( $\approx 6.3 \times 10^{-27} \text{ cm}^2$ ). The neutrino chiral scattering process produces a small perturbation of the decay rate, a finite measurable change in the electron density of the radioactive nucleus resulting in a maximum decay rate change of the order of  $\frac{\Delta R}{R} \leq 6 \times 10^{-1}$ . Radioactive targets of a few hundred nanogram are sufficient neutrino detector target material to measure the effect compared to several tons for ordinary non-radioactive targets used for the usual detection method.

Neutrinos acquire mass in the SM and through neutrino mass mixing oscillations. The neutrinos can be maximally mixed (50/50) between electron, muon and tau flavors. The mixed neutrino masses are:  $m_\nu^e = (83.7 \pm 27) \text{ meV}$ ,  $m_\nu^\mu = (92.4 \pm 27) \text{ meV}$  and  $m_\nu^\tau = (144.0 \pm 27) \text{ meV}$ . The mixed electron neutrino wave function is composed of 50% electron, 44% muon and 6% tau. Only Dirac neutrinos were considered since Majorana neutrinos violate lepton number in weak and EM interactions and Dirac neutrinos can exhibit both left and right chirality in EM processes.

The anomalous magnetic moment of the neutrino is attributed to self-energy interaction with the neutral current (NC) of a radioactive nucleus and **EM field of the nucleus**. The  $\gamma - Z^0$  self-energy and polarization effects arising from the virtual emission and absorption of **light quanta** with the creation of virtual electron-positron pair from the one-loop interaction as shown in Figure 5. The NC is a lepton scattering process unlike the charged current (CC,  $W^\pm$ ) neutrino absorption-emission process. The neutrino anomalous magnetic moment is designated the Schwinger exchange moment with  $\delta\mu_\nu^{Schw} = \frac{\alpha_e}{2\pi}$  and another factor of  $\frac{1}{2}$  due to  $\nu_e$  mass mixing.

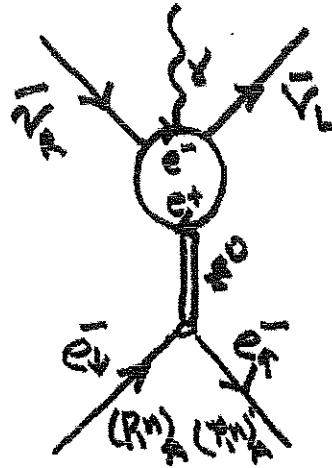
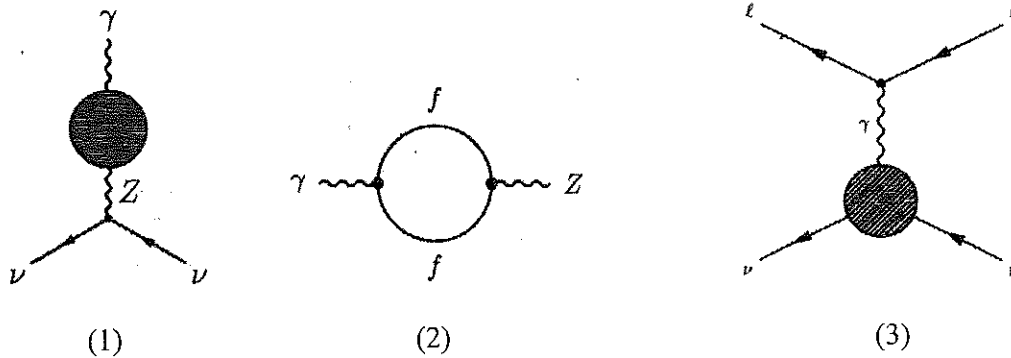


**Figure 5. Antineutrino-radioactive Nucleus Scattering Inducing a Neutrino Schwinger Anomalous Magnetic Moment in First Order**

The Figure 5 diagram is composed of variations of three components: (1) Neutral current  $\gamma - Z^0$  vertex of a radioactive nucleus, (2) the self-energy term with virtual  $e^+e^-$  loop, and (3) the lepton scattering magnetic dipole-dipole interaction.



The Dirac neutrino magnetic moment with induced Schwinger anomalous magnetic dipole moment is calculated to be

$$\mu_{\nu}^{Schw} = \frac{m_{\nu}}{m_e} \left( \frac{\alpha_e^2}{2\pi} \right) \left( \frac{1}{2} \right) \mu_B = 6.8 \times 10^{-13} \mu_B \quad (6)$$

Where the anomalous dipole moment is  $(\alpha_e/2\pi)$ , the factor  $\frac{1}{2}$  arises from the maximal mass mixing of the neutrino flavors and the coupling to the radioactive nucleus orbital electron magnetic field is  $\alpha_e$ . This estimate should be good to within  $(m_e/m_\mu < 0.005)$ , the muon magnetic dipole contribution due to the neutrino mass mixing.

The EM scattering of the antineutrino with the radioactive nucleus (weak interaction vertex) involves the electron magnetic field of the Z-boson vertex as shown below in Figure 6 where the magnetic dipole-dipole (neutrino-electron) scattering flips the spin of the neutrino and the spin of the electron in the process, an EM spin-flip process. The Dirac neutrino changes chirality in the process going from a right-handed antineutrino to a left-handed one, from active to sterile type.

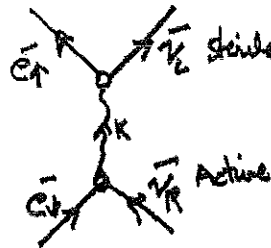


**Figure 6. An EM Antineutrino Interaction with a Weak Interaction Z-vertex  
in which the Spin-flip Changes Chirality of the Antineutrino and  
Flips the Spin of the K-electron in the Process**

The coupling constant for the scattering of the antineutrino with the electron and nuclear field taking part at the Z-boson vertex is  $(\frac{\alpha_e}{4\pi})^2$ , allowing us to calculate the EM scattering cross-section where the range of the interaction is given by the Compton wavelength of the electron at the nucleus or Z-boson vertex,

$$\sigma_{scat} = (\frac{\alpha_e}{4\pi})^2 (4\pi\lambda_e^2) = 6.3mb \quad (7)$$

For example, EM scattering with the atomic electron scatters the bound 1S (K-shell) electron taking part in the weak interaction process into the continuum states via the spin-flip process. This scattering reduces the electron density at the nucleus slowing down the decay rate by a small but finite maximum amount  $\Delta R = \frac{\alpha_e}{4\pi} = 0.0581\%$ . This value must be corrected by the fractional amount of the  $K(\square 90\%)$  or  $L(\square 10\%)$  shell electron occupancy which takes part in the scattering interaction.

The source radioactivity

$$A(dps) = N(atoms)\lambda, \quad (8)$$

relates to the cross-section and maximum effective antineutrino flux for the maximum decay rate change (0.0581%) of a radioactive source given by

$$\delta A(dps/cm^2) = N(atoms/cm^2) \times \sigma_{\nu_e}(cm^2) \times \phi_{MAX}(\bar{\nu}_e cm^{-2} sec^{-1}), \quad (9)$$

upon rearranging to yield

$$\frac{\alpha_e}{4\pi} \lambda(sec^{-1}) \square \sigma_{\nu_e}(cm^2) \times \phi_{MAX}(\bar{\nu}_e cm^{-2} sec^{-1}) \quad (10)$$

with  $\lambda = \frac{\ln 2}{t_{1/2}(sec)}$ ,  $\alpha_e^{-1} = 137.036$  and  $\sigma_{\nu_e} = 6.319 \times 10^{-27} cm^2$ .

Examples of the model predications for the cases examined here are given in Table 1 above.

**Phase III. Note added 06.20.18: Search for Perturbation on <sup>108m</sup>Ag Decay Rate Induced by Reactor Antineutrinos**

Data collection began on 21 Nov 2017. The 0.45 uCi Ag-108m disk source was counted for a total of 82 reactor days ON and 114 days Reactor OFF. The measurement campaign consists of 24-hour real-time collection intervals on the Ag-108m source. The data collected are in the form of differential energy spectra from ~4 keV up to 3.7 MeV. One such differential energy spectrum obtained during this collection period is shown in Figure 7. During a 24-hour period, a total of  $7.4 \times 10^8$  counts are collected with an associated statistical uncertainty of roughly 3.7 parts in  $10^5$ .

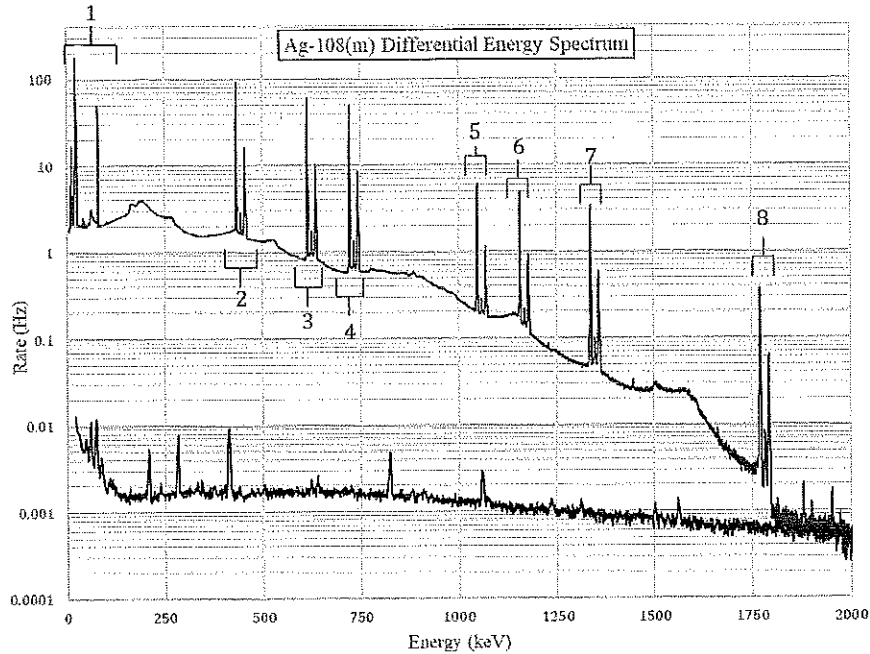


**Figure 7. The Ag-108 Differential Energy Spectrum is Shown in Red while the HFIR Gamma Backgrounds are Shown in Black**

The key features of the spectrum are dominated by the decay of Ag-108m to Pd-108 via electron capture. This decay mode results in three nuclear de-excitation photons being emitted through a cascade to the ground state of Pd-108. The electron vacancy from the decay additionally results in prominent  $K\alpha$  and  $K\beta$  x-rays (also in coincidence with the de-excitation gamma rays). These lines and their corresponding energies are presented in Table 2.

**Table 2. The Prominent Photon Lines in the Collected  $^{108}\text{Ag}$  Energy Spectra**

	Line Energy[ref] (keV)	Line Identification
	21.02	$K\alpha_2$ (Ag x-ray)
	21.177	$K\alpha_1$ (Ag x-ray)
	23.791	$K\beta_3$ (Ag x-ray)
	23.819	$K\beta_1$ (Ag x-ray)
	24.299	$K\beta_2$ (Ag x-ray)
	69.25	$^{108m}\text{Ag}$ IT Ge escape peak
	79.131	$^{108m}\text{Ag} \rightarrow ^{108}\text{Ag}$ IT
$E_1$	433.937	$^{108m}\text{Ag} \rightarrow ^{108}\text{Pd}$ EC
$E_2$	614.276	$^{108m}\text{Ag} \rightarrow ^{108}\text{Pd}$ EC
$E_3$	722.907	$^{108m}\text{Ag} \rightarrow ^{108}\text{Pd}$ EC
	2204.059	$^{214}\text{Bi}$ $\gamma$ -ray
	2614.511	$^{208}\text{Tl}$ $\gamma$ -ray

Additionally, the internal transition (IT) of Ag-108m to its ground state is evidenced in the spectrum by the presence of the 79.131 keV gamma-ray line. The key features of the energy spectrum are broken up into 8 regions as shown in Figure 7. Region 1 refers to the low energy portion of the spectrum and is depicted in Figure 8, along with the higher energy portion of the differential energy spectrum.

A description of these regions is as follows:

- Region 1:** The  $K_{\alpha,\beta}$  x-rays from the decay to Pd-108 via electron capture. Also present is the IT de-excitation photon. (Refer to Figure 3.)
- Region 2:** The E1 gamma-ray from the EC decay and pileup from Region 1 x-rays
- Region 3:** The E2 gamma-ray from the EC decay and pileup from Region 1 x-rays
- Region 4:** The E3 gamma-ray from the EC decay and pileup from Region 1 x-rays
- Region 5:** E1 + E2 geometric summing from cascade + pileup x-rays
- Region 6:** E1 + E3 geometric summing from cascade + pileup x-rays
- Region 7:** E2 + E3 geometric summing from cascade + pileup x-rays
- Region 8:** E1 + E2 + E3 geometric summing from cascade + pileup x-rays

The corresponding energies of these pileup lines can be found in Table 3.

**Table 3. Geometric and Random Pileup Lines, and Escape Peaks in Energy Spectra**

	Line Energy[ref] (keV)	Line Identification
	69.25	$^{108m}\text{Ag}$ IT Ge escape peak
	424.06	$E_1$ Ge escape peak
	604.40	$E_2$ Ge escape peak
	713.03	$E_3$ Ge escape peak
$E_1 + E_2$	1048.21	Summing from cascade
$E_1 + E_3$	1156.84	Summing from cascade
$E_2 + E_3$	1337.18	Summing from cascade
$\Sigma = E_1 + E_2 + E_3$	1771.12	Summing from cascade
$\Sigma + E_1$	2205.06	Random Summing
$\Sigma + E_2$	2385.40	Random Summing
$\Sigma + E_3$	2494.03	Random Summing

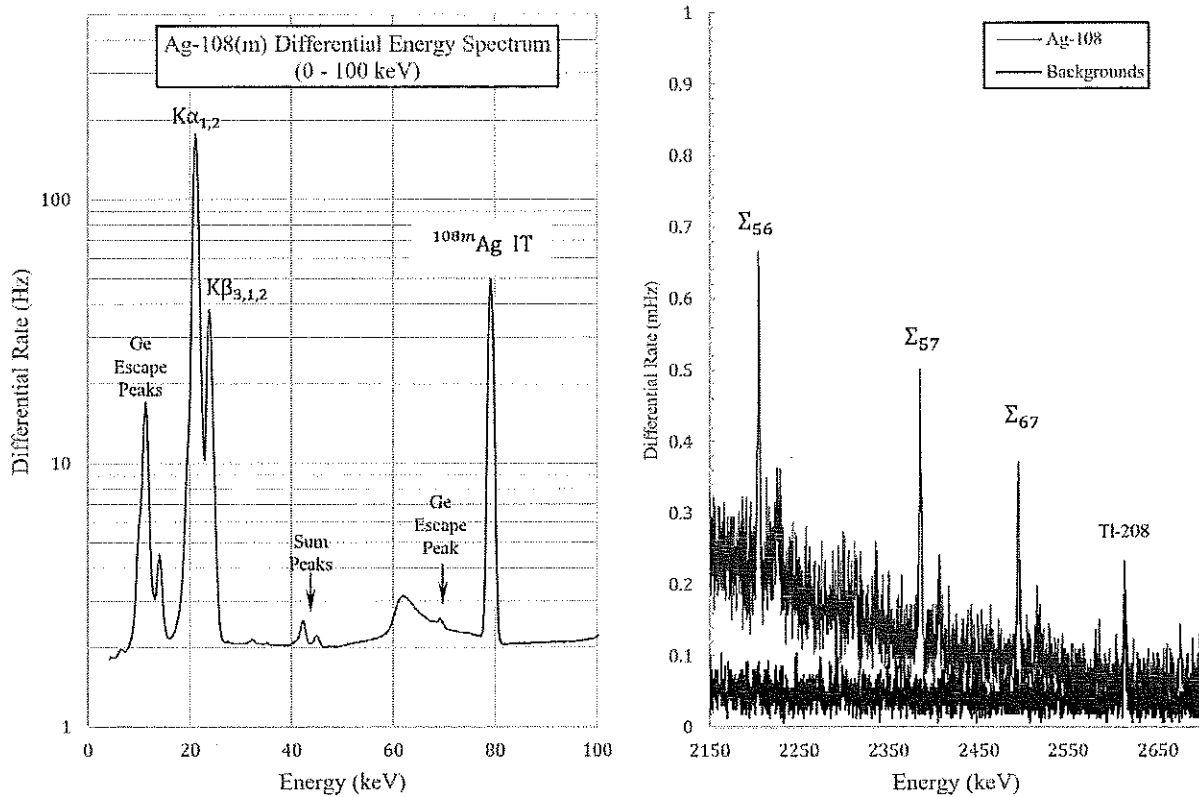


**Figure 8. Illustrates the (left) Low Energy Portion of the Ag-108m Differential Energy Spectrum and the (Right) Higher Energy Portion of the Ag-108m Energy Spectrum in red, HFIR Background Spectrum in Black**

The analysis procedures for the current Ag-108m study follow closely with those conducted for Cs-137. Each daily spectrum is energy calibrated from the well-defined, known lines (a subset of those given in Tables 2 and 3). These calibrations are used to perform a re-binning followed by a bin-by-bin subtraction of the two archetypal background spectra obtained for reactor OFF and Reactor ON periods. A deconvolution is not performed to the background-subtracted spectra since random summing is effectively constant during the duration of the experiment. Finally, a fixed ROI is integrated to obtain the total daily counts associated with the primary EC and IT photon lines.

The ROIs around each of the primary photon lines are integrated by fixing the energy bounds of the ROI. This is accomplished by using the daily energy calibrations to determine the proper bin edges of the ROI. One way to eliminate potential uncertainties introduced by the live time clock (among other things), is to consider the ratio of different portions of the spectrum. The ratio of the EC decay mode to the IT decay mode will manifest any fluctuations in the decay rate:

$$\frac{\Delta r}{r} \equiv \frac{r_{\text{off}} - r_{\text{on}}}{r_{\text{off}}} = \frac{\delta \lambda}{\lambda}$$

Figure 9 shows the daily ratios (top plot) and the aggregated ratios by reactor cycle (bottom plot). Aggregating all the reactor ON data together, and similarly the reactor OFF data, the total fractional change is:

$$\frac{\Delta r}{r} = (-0.71 \pm 3.17) \times 10^{-5}$$

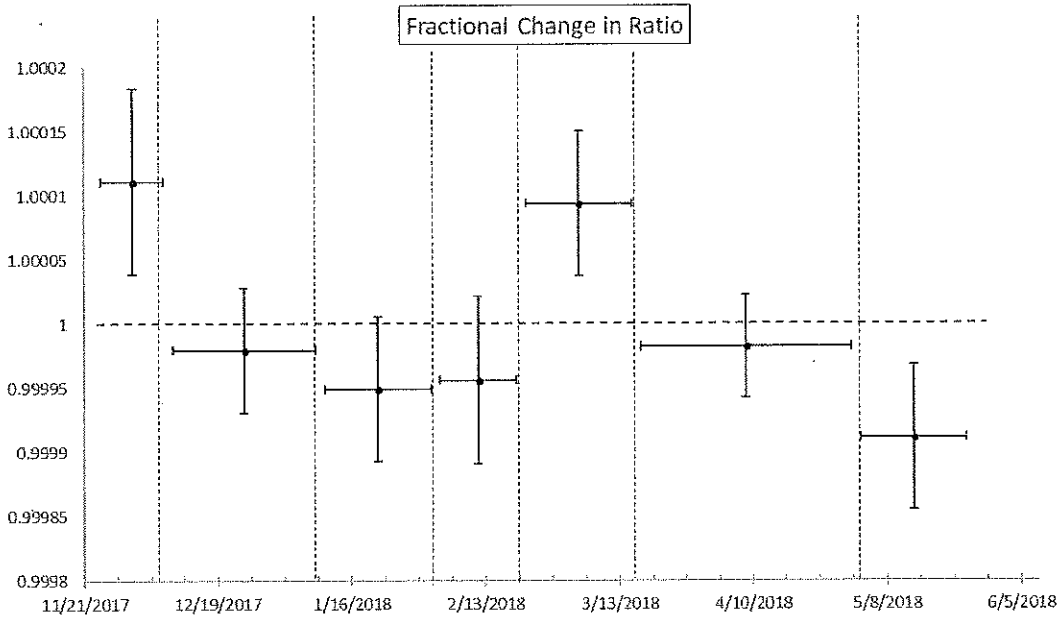


**Figure 9. Fractional Change in the IT to EC Photopeak Modes of Ag-108m**

As a further example, the E3 (722 keV) ROI for the reactor ON minus reactor OFF was

$$\frac{\Delta r}{r} = (-0.98 \pm 2.43) \times 10^{-5}$$

A value typical of the EC ROI analysis yielding for Ag-108m decay an upper limit to the systematic uncertainty of

$$\frac{\Delta r}{r} = \pm 2.82 \times 10^{-5}$$

The 3-sigma 95% confidence level upper limit for the three radioisotopes studied are

Mn-54 (312d)	$\pm 5.1 \times 10^{-5}$
Cs-137 (30.1 yr.)	$\pm 5.2 \times 10^{-5}$
Ag-108m (434 yr.)	$\pm 8.5 \times 10^{-5}$



### **3 Conclusion**

These limits preclude the practical application of this methodology using gamma-ray analysis however, the use of beta current measurements with a factor of 10 or lower accuracy ( $<1 \times 10^{-6}$ ) can be used to search for antineutrino induced perturbations.

### **4 References**

Barnes, et. al, **Search for Perturbations of Nuclear Decay Rates Induced by Reactor Electron Antineutrinos**, 30 June 2016, **Final Report of NaI Measurements**, arXiv.1606.09325.

Koltick and Liu, 2016a, **Obtaining Background Free Gamma-ray Decay Spectra**.

Koltick and Liu, 2016b, **Preliminary limits on Antineutrino Interactions on Electron Capture in Mn-54 Decay**.

Nistor and Heim, 2017, **Perturbations of Nuclear Decay Rates Induced by Reactor Antineutrinos**.

Ward, 2015, **Sterile Neutrino Theory, Detection and Application**.